AICS

RIKEN Advanced Institute for Computational Science

ANNUAL REPORT

FY2017

AICS Research Activities

RIKEN Center for Computational Science

AICS was renamed R-CCS in 2018. This reports the activities of AICS in FY 2017.

RIKEN AICS
Annual Report FY2017
AICS Research Activities

February 28, 2019

Preface

Welcome to the AICS Annual Report for 2017.

Our institute, RIKEN AICS, is the Japanese flagship research institution in computational science and is meant to be the center of excellence for various simulation fields such as weather and climate, cosmology, biology, physics, chemistry, engineering etc. We also focus on computer science such as processor design and system software as well as fundamental technologies including programming framework and visualization. By achieving outstanding results through strong collaborations between computer scientists and computational scientists, AICS wants to be a world hub for computer and computational sciences.

The K computer started full service in September 2012. In many areas, we see many great results. Many projects that use the K computer would be difficult or impossible to do elsewhere. In addition AICS research teams have developed common computing techniques for utilization of the K computer and coded the very efficient parallelized application program packages. Now the K computer is being used in many different fronts and extending the boundaries of computational science. As you see in this report, our AICS research teams made a great contribution to produce many of these exciting results.

The K computer has established massively parallel computation in Japan. The K computer also enhanced the resolution both in precision and the system size significantly through massively parallel computation. In addition, capacity computing opened the possibility of prediction in complex and non-linear/chaotic phenomena. We are now tackling highly complex scientific and social problems with inherent uncertainties and unpredictability. The way to deal with such uncertainty is to simultaneously run multiple ensembles, using many different combinations of parameters, and thus be able to explore the solution. The K computer significantly enhanced the capacity computing in addition to the capability computing.

Supercomputer has become a fundamental technology which supports the society today, and pioneers the society of tomorrow. Continued development of world top-class supercomputer is vital for the world leadership in science and technology. AICS is charged with the development of the post K computer. The flagship 2020 project division is developing a world ' s top-class supercomputer, " post K " launching in around 2021 to spearhead the quest for knowledge of human kind, and contribute to the world at large.

Our aim is to balance various factors, such as power consumption, computational performance, user convenience, and ability to produce ground-breaking results. Post K supercomputer will be characterized by its all-round capabilities compared to any other system in the world in the 2020 ' s. The post K will extend the fields pioneered by the K computer and also challenge new areas. We are very looking forward to the post K supercomputer.

We hope you enjoy reading all the wonderful advances made by AICS.

AICS has been renamed RIKEN-Center for Computational Science (R-CCS). With the new leadership, R-CCS has started a new era as the world ' s leading center of high-performance computing. We appreciate your continued support.

Kimihiko Hirao, Director

Organization

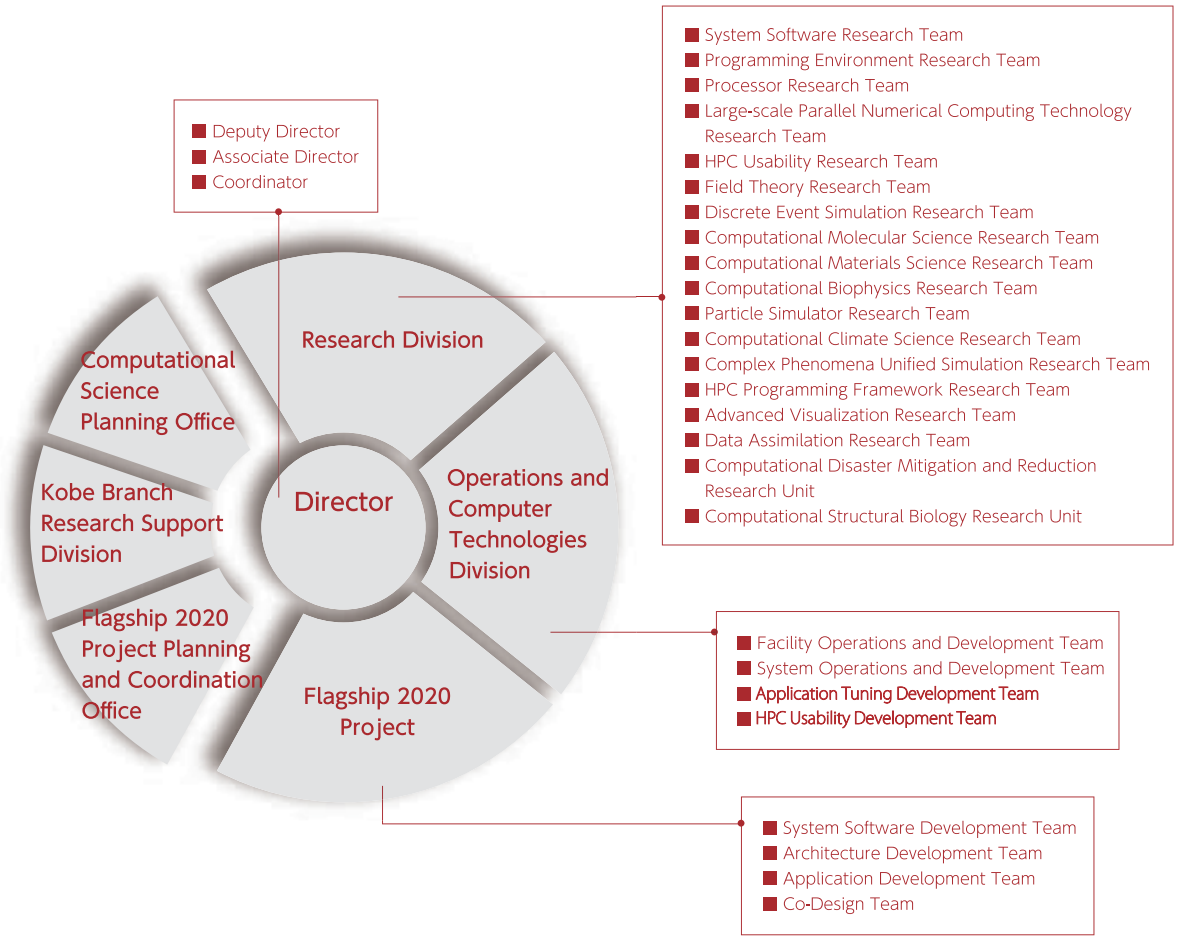

Contents

Part I

Research Division

Chapter 1

System Software Research Team

1.1 Members

Yutaka Ishikawa (Team Leader)

Masamichi Takagi (Senior Scientist)

Atsushi Hori (Research Scientist)

Balazs Gerofi (Research Scientist)

Yoshiyuki Morie (Research Scientist)

Masayuki Hatanaka (Research & Development Scientist)

Takahiro Ogura (Research & Development Scientist)

Tatiana Martsinkevich (Postdoctoral Researcher)

The system software research has been conducted in cooperation with the following members of the System Software Development Team in the Flagship 2020 project.

1.2 Research Activities

The system software team focuses on the research and development of an advanced system software stack not only for the "K" computer but also for toward exa-scale computing. We have been mainly focusing on scalable high performance communication and file I/O libraries and/or middlewares. The former research topics, sharing virtual address space and IHK/McKernel light-weight kernel, have been almost taken over by the System Software Development Team, but the research results are shown here.

1.3 Research Results and Achievements

1.3.1 Persistent Collectives

Collective communication latency is a major concern, as it has become longer with the increase of scale of parallel computers. Overlapping computation and communication is one effective method for hiding communication delay. Recent networks have offloading functionality, so non-blocking communication is more important. Although non-blocking collective communication exists as an overlapping method, it requires generating a command sequence every time a non-collective communication is issued. In contrast, persistent non-blocking collective communication can be separated into the initialization and the collective communication body, so the initialization can be removed from the loop. In such a persistent non-blocking collective communication, the sequence of communication commands is generated at the time of initialization. The communication command sequence is then reused for each collective communication instead of the sequence needing to be re-generated. Moreover, if the sequence can be offloaded to a network device, then more efficient execution is possible without

using CPU cycles. Although some implementations of persistent non-collective communication exist, there is no implementation of persistent non-collective communication that uses the offload functionality.

The offloading functionality was added to the Tofu2 interconnect on the FX100 supercomputer, a successor to the K computer. In this paper, an offloaded persistent non-collective broadcast for the Tofu2 interconnect is implemented. We will report the performance improvement from offloading persistent non-blocking collective communication on a real machine.

Tofu2 has a framework for hardware-driven distributed execution of communication commands called session mode CQ (SMCQ). As shown in Figure 1.1, SMCQ consists of a transmit order queue (TOQ) and three

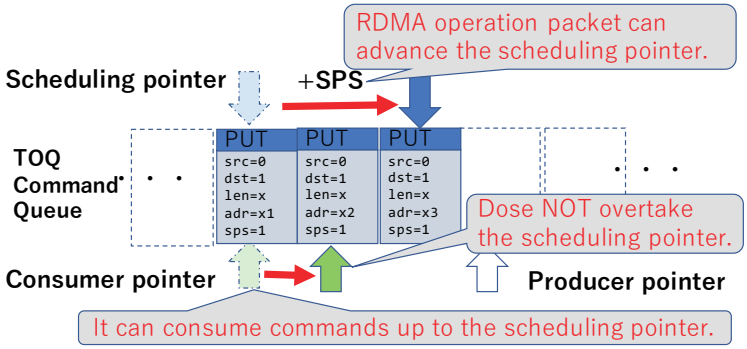

Figure 1.1: Overview of session mode CQ.

pointers: the producer, consumer, and scheduling pointers. The TOQ descriptor has the information for RDMA communication such as command type, source, destination, and session progress step (SPS) field. The producer pointer points to the end of command sequences enqueued by the application. The consumer pointer indicates the end of commands executed. When an RDMA engine processes an incoming RDMA operation packet, the scheduling pointer can be advanced by the SPS fields of the packet. Therefore, the progress of the command processing in SMCQ is driven by incoming packets and does not need the help of the CPU.

1.3.1.1 Offloaded Persistent Broadcast

We implemented the offloaded persistent broadcast for FX100[6,7]. This implementaion targets the Trinaryx3 algorithm used in the K computer. This is an algorithm for improving the communication bandwidth by

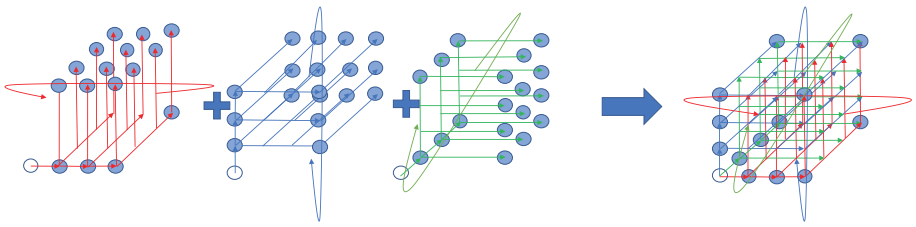

Figure 1.2: Overview of Trinaryx3.

mapping multiple pipeline paths for the torus network. The Trinaryx3 algorithm is an extension of the Trinary algorithm in which broadcast data are divided into three fragments, each of which is transmitted using the Trinary algorithm. The three pipeline paths of the trinary tree are mapped to the 3D torus in Figure 1.2. Each pipeline communication is offloaded and executed by SMCQ.

Figure 1.3 shows the performance of an offloaded persistent non-blocking broadcast on the FX100. The offloaded persistent non-blocking broadcast is better than the non-blocking broadcast because the persistent non-blocking collective is able to complete creating the sequence of communication commands and exchanging the remote memory information at MP_Bcast_init(). Figure 1.4 shows the execution times of MPI_Bcast_init and MPI_Start. MPI_Bcast_init is relatively expensive and should not be repeated. Also, the cost of MPI_Start is sufficiently small, indicating that offloading is effective.

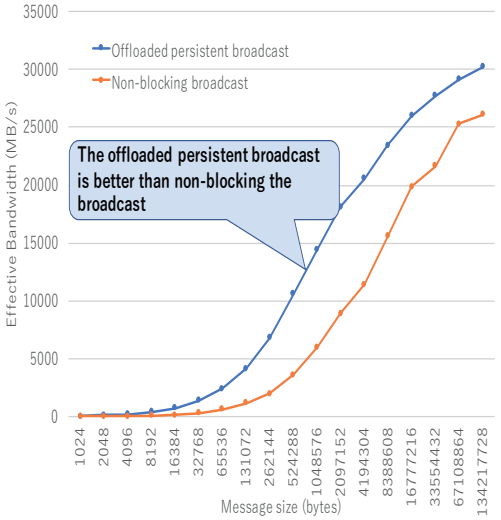

Figure 1.3: Effective bandwidth (MB/s) (12 processes).

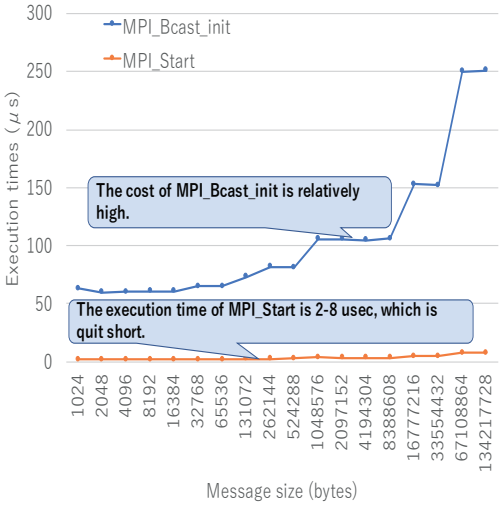

Figure 1.4: Execution times of MPI_Bcast_init and MPI_Start (μs) (12 processes).

1.3.1.2 Offloaded Persistent Neighborhood alltoall

This implementation targets 2D Cartesian Halo exchange pattern[3]. It uses four SMCQs (one SMCQ per `MPI_Sendrecv` exchange) in the pattern.

Figure 1.5 shows the communication latency on `FX100` for four types of persistent *neighbor alltoall* collective implementation. In this figure, the horizontal axis shows the message size in the halo exchange and the vertical axis shows the elapsed time from `MPI_Start` to `MPI_Wait`. The `NAAP`, the offload version, is 60% better than `P2PP` at 8 bytes message size.

Name	*init*	*start*	*test*
NAAP	Tofu2 API	Tofu2 API	Tofu2 API
P2PP	MPI_{Send|Recv}_init	MPI_Startall	MPI_Testall
P2PN	*n/a*	MPI_I{send|recv}	MPI_Testall
NAAN	*n/a*	MPI_Ineighbor_alltoall	MPI_Test

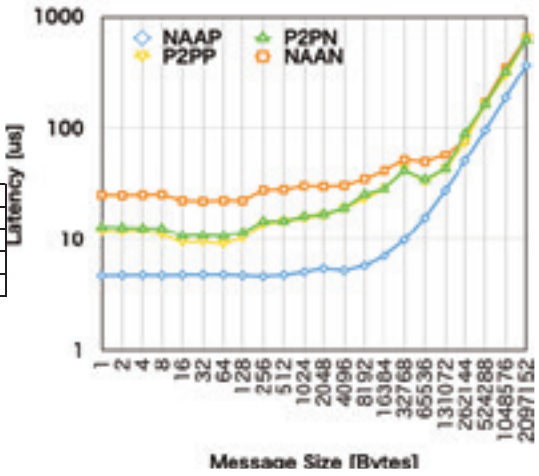

Figure 1.5: Latency Benchmark of Persistent Neighborhood All-to-All

1.3.2 Data Transfer Framework

This section describes the progress in the work on the Data Transfer Framework. The framework targets multi-component applications in which components are loosely coupled via files written using PnetCDF file I/O library. By using the DTF such components can silently replace file I/O with direct sending of data between the components and thus, improve the performance of the application.

```
[INFO]
ncomp=2  ! number of components
comp_name="rdr"  ! component name
comp_name="wrt"
ioreq_distrib_mode="range"  !divide by dim length
buffer_data=0
[FILE]
filename="restart.nc"
writer="wrt"  !component that writes to the file
reader="rdr"  !component that reads from the file
iomode="memory"  !enable direct transfer
```

Figure 1.6: DTF configuration file

1.3.2.1 Introduction

Multi-component workflows, where one component performs a particular transformation with the data and passes it on to the next component, is a common way of performing complex computations. Using components as building blocks we can apply sophisticated data processing algorithms to large volumes of data. Because the components may be developed independently, they often use file I/O and the Parallel File System to pass data. However, as the data volume increases, file I/O quickly becomes the bottleneck in such workflows. In this work, we propose an I/O arbitration framework called DTF to alleviate this problem by silently replacing file I/O with direct data transfer between the components. DTF treats file I/O calls as I/O requests and performs I/O request matching to perform data movement. Currently, the framework works with PnetCDF-based multi-component workflows. It requires minimal modifications to applications and allows the user to easily control I/O flow via the framework's configuration file.

1.3.2.2 Overview

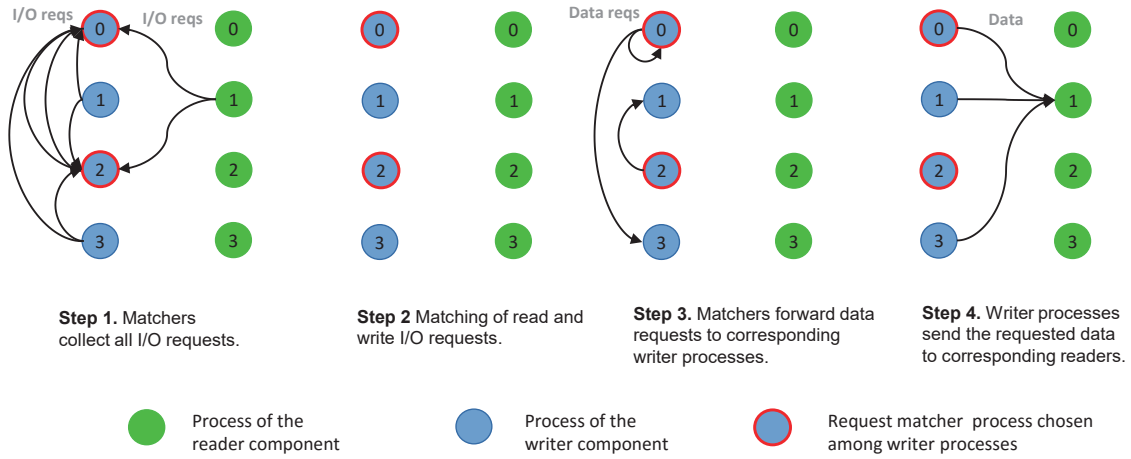

Figure 1.7: I/O request matching. Request matchers are marked with a red shape outline. For simplicity, only one reader process is showed to have read I/O requests.

The DTF aims to provide users of multi-component workflows with a tool that would allow them to quickly switch from file I/O to direct data transfer without needing to cardinally change the source code of the components.

First, the user must provide a simple configuration file that describes the file dependency in the workflow (example in Figure 1.6). It only needs to list the files that create a direct dependency between two components, i.e. if the components are coupled through this file. The DTF intercepts PnetCDF calls in the program and, if the file for which the call was made is listed in the configuration file as subject to the data transfer, the DTF handles the call accordingly. Otherwise, PnetCDF call is executed normally.

In order to transfer the data from one component to another, we treat every PnetCDF read or write call as an *I/O request*. The data transfer is performed via what we call *the I/O request matching*. First, designated processes, called *I/O request matchers*, collect all read and write requests for a given file. Then, each matcher finds out who holds the requested piece of data by matching each read request against one or several write

```
/*Initialize DTF*/
dtf_init(dtf_inifile, "wrt");
/*Create file*/
ncmpi_create("restart.nc",...);
<...>
 /*Write some data*/
ncmpi_put_vara_float(...);
/*Write some more data*/
ncmpi_put_vara_float(...);
/*Perform I/O request matching*/
dtf_transfer("restart.nc");
/*Close the file*/
ncmpi_close(...);
/*Finalize DTF*/
dtf_finalize();
```

Figure 1.8: Component writing to file

```
/*Initialize DTF*/
dtf_init(dtf_inifile, "rdr");
/*Open the file*/
ncmpi_open("restart.nc",...);
<...>
/*Read all data at once*/
ncmpi_get_vara_float(...);
/*Perform I/O request matching*/
dtf_transfer("restart.nc");
/*Close the file*/
ncmpi_close(...);
/*Finalize DTF*/
dtf_finalize();
```

Figure 1.9: Component reading from file

requests. Finally, the matcher instructs the processes who have the data to send it to the corresponding process who requested it. All the inter-process communication happens using MPI. We note that here we differentiate between the PnetCDF non-blocking I/O requests and the DTF I/O requests, and we always assume the latter unless stated otherwise.

The I/O patterns of the component that writes to the file and the component that reads from it may be drastically different, however, dynamic I/O request matching makes DTF flexible and allows it to handle any kind of I/O patterns transparently for the user.

The three main API functions provided by the DTF are the following:

- `dtf_init(config_file, component_name)` - initializes the DTF. The user must specify the path to the DTF configuration file and state the name of the current component which should match one of the component names in the configuration file;
- `dtf_finalize()` - finalizes the DTF;
- `dtf_transfer(filename)` - invokes the data transfer for file *filename*;

A simplified example of a writer and reader components is presented Figures 1.8 and 1.9, as well as their common DTF configuration file (Figure 1.6). To enable the direct data transfer it was enough to add three lines of code to each component — to initialize, finalize the library and to invoke the data transfer — and provide a simple configuration file.

1.3.2.3 Perfromance evaluation

Next, we show how the DTF performs with a real world workflow application — SCALE-LETKF. SCALE-LETKF is a real-time severe weather prediction application that combines weather simulation with assimilation of weather radar observations. It consists of two components — SCALE and LETKF — that are developed independently. SCALE is a numerical weather prediction application based on the ensemble simulation; LETKF performs data assimilation of real-world observation data together with simulation results produced by SCALE. In each iteration, SCALE writes the simulation result to the Parallel File System (PFS) using the Parallel NetCDF API. The files are subsequently read by LETKF. After LETKF finishes assimilating the observation data, the output is written to files which become the input for SCALE in the next iteration.

In the chosen test case LETKF assimilates the data from a Phased Array Weather Radar with a resolution of 500 m. The number of processes participating in one ensemble simulation is fixed to nine processes in all tests, the total number of processes per component is nine multiplied by the number of ensembles.

The size of the history and restart file in one ensemble is constant, we change the total amount of I/O by varying the number of ensembles from 25 to 100. Table 1.1 contains the information about the amount of data written and read in each configuration. In all tests, every ensemble process in SCALE writes 363 MB of data, out of which LETKF process requires only about one quarter. A SCALE process generates 255 write requests, LETKF process — 31 read request.

The results show that the DTF helps to improve the total execution time of SCALE-LETKF (Figure 1.10) by cutting on the I/O time. In the largest execution with 100 ensembles, the I/O time was improved by a factor of 3.7 for SCALE and 10 for LETKF.

Table 1.1: Cumulative I/O amount in SCALE-LETKF

Number of ensembles	Total write size (GB)	Total read size (GB)
25	79.78	18.97
50	159.56	37.94
75	239.35	56.91
100	319.13	75.88
Per process	363 MB	86.3 MB

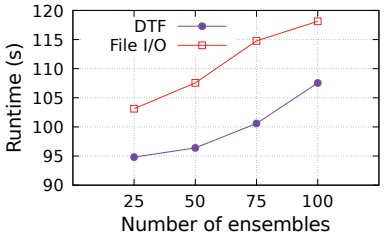

Figure 1.10: Runtime

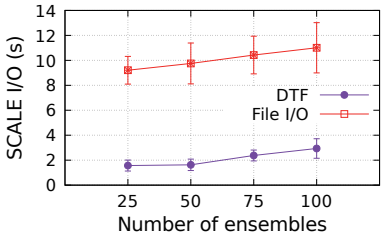

Figure 1.11: SCALE I/O

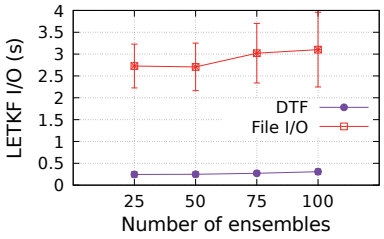

Figure 1.12: LETKF I/O

For more details on the design of the DTF and more experimental results please refer to [5].

1.3.3 Sharing Virtual Address Space

The two most common parallel execution models for CPUs today are multiprocess and multithread. The multiprocess model allows each process to own a private address space, and the multithreaded model shares all address space by default. We propose a new implementation of the third model, called *Process-in-Process (PiP)*, where multiple processes are mapped into a single virtual address space. Thus, each process still owns its private storage but can directly access the storage of other processes in the same virtual address space. The idea of address-space sharing is not new. What makes PiP unique, however, is that its design is completely in user space, making it a portable and practical approach for large supercomputing systems.

PiP allows multiple parallel tasks to execute the same or different programs in a shared virtual address space environment while maintaining privatized variable sets. The PiP task does not follow the definition of conventional process or thread. For instance, PiP tasks share the same virtual address space whereas processes have isolated virtual address space; two PiP tasks can execute arbitrary programs in parallel in the same virtual address space, whereas threads must be derived from the same program. Moreover, a process or PiP task always starts its execution from the `main()` function, but a thread starts its execution from an arbitrary function. PiP defines a special task called *root process* that owns the virtual address space and spawns multiple tasks executing in the same VAS as of the root, and the model is thereby named *Process-in-Process*.

Table 1.2: Experimental platform information

Name	CPU	# Cores	Clock	Memory	OS
Wallaby	Xeon E5-2650 v2	8×2(×2)	2.6 GHz	64 GiB	CentOS 7.3 (and McKernel)
OFP	Xeon Phi 7250	68(×4)	1.4 GHz	96(+16) GiB	CentOS 7.2
Albireo	ARM Cortex A57	8	2.0 GHz	16 GiB	CentOS 7.3
The K Computer	SPARC64 VIIIfx	8	2.0 GHz	16 GiB	XTCOS

Table 1.2 shows the hardware and software environments where PiP is being tested to run on. We design two execution modes in the PiP implementation;

Process Mode: In this mode, the OS kernel thread and its stack can be created by calling the Linux `clone()` system call. In this mode, PiP tasks behave like normal processes regarding PID, termination, file descriptors, and signal handling.

Thread Mode: In this mode, the `pthread_create()` POSIX function is used and PiP tasks behave like threads regarding TID, termination, file descriptors, and signal handling. Again, PiP provides the variable

privatization even in this thread execution mode.

Figure 1.13 compares the time to spawn null tasks by using PiP, Pthread, `fork()&exec()`, `vfork()&exec()`, and `posix_spawn()` on the machines listed in Table 1.2. As shown in this figure, the PiP spawning times are mostly the same as those with creating processes.

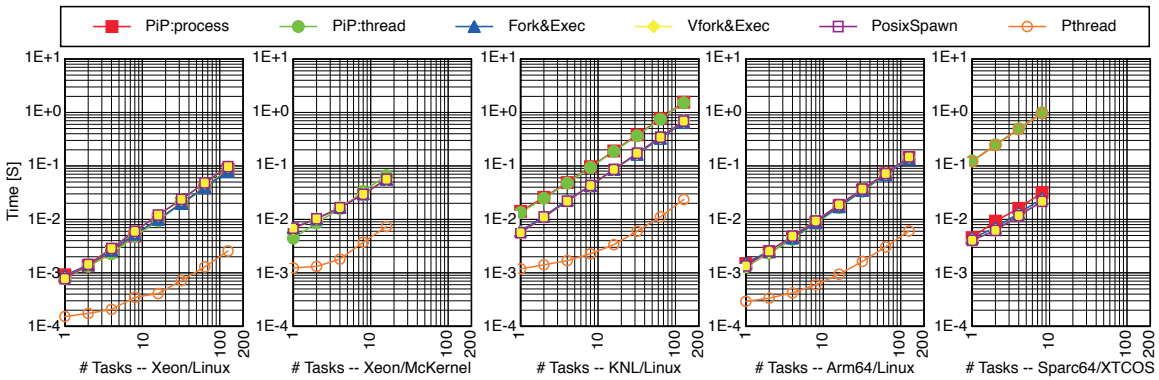

Figure 1.13: Task spawning time on four platforms

1.3.3.1 DOE-MEXT Collaboration

To prove the efficiency of PiP, MPICH is prototyped to utilize PiP. This work has been done in the context of DOE-MEXT research collaboration. The modifications in the prototyped PiP-aware MPICH are; 1) Hydra process manager to spawn MPI processes as PiP tasks, 2) enhanced PT2PT rendezvous protocol to have only one memory copy for intra-node communication, 3) single-copy MPI datatype communication, and 4) modified `MPI_Win_allocate_shared` to have shared memory regions.

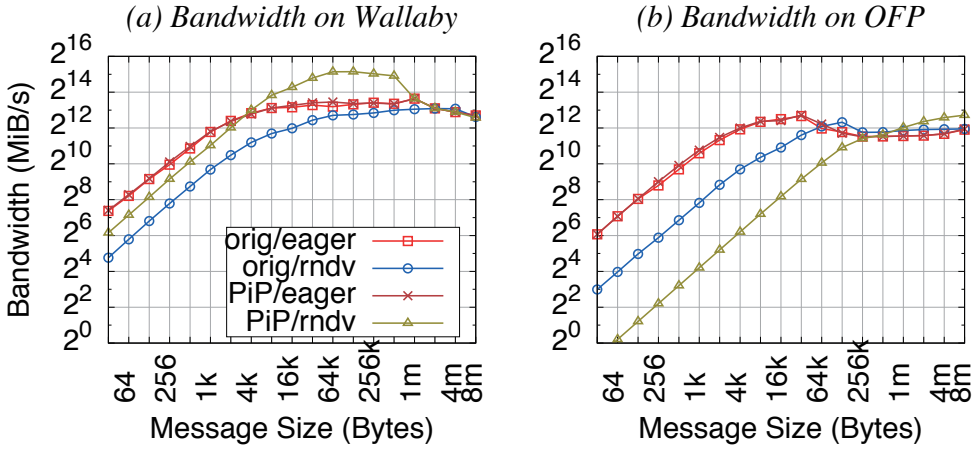

Figure 1.14: Intel MPI Benchmark PingPong Performance Improvement

In [4], a variety of PiP micro-benchmark and macro-benchmark results are reported. Figure 1.14 shows one of them, the PingPong bandwidth differences between the original MPICH and PiP-aware MPICH. As shown in this figure, PiP succeeds to boost the bandwidth, especially on the Xeon processor. Among the evaluation results, it should be noted that PiP can be used for in-situ applications for having better communication performance between simulation program and in-situ program.

1.3.3.2 CEA-Riken Collaboration

It is known that new parallel execution models, where virtual address space is shared among tasks and each task has a privatized variable set, can implement efficient intra-node communications and save memory. MPC developed by CEA is very similar to PiP in terms of providing the new execution model.

To have deeper knowledge on MPC and PiP, the source codes are shared and investigated on both sides. MPC allocator, which is another malloc library developed in the MPC project, can be used in PiP in which an allocated memory region by a task cannot be freed by the other task. This problem is already solved in MPC. In this first project year of the collaboration between CEA and Riken, MPC and PIP focused on the evaluation of the tools on each side, and proposing collaborations axes on the MPC allocator. The investigation of embedding MPC allocator into PiP reveals that the current MPC allocator cannot be embedded into PiP without source code changes, which have been identified.

1.3.4 IHK/McKernel

This Section describes recent research results related to IHK/McKernel. Specifically, results of large scale evaluation will be provided in Section 1.3.4.1, published in [1]. An introduction to the PicoDriver fast-path device driver framework is given in Section 1.3.4.2, published in [2]. Finally, results of characterizing hardware performance variation across various hardware platforms using lightweight OS kernels are presented in Section 1.3.4.3, published in [8].

1.3.4.1 Large Scale Evaluation on Oakforest-PACS

We performed large scale evaluation of the IHK/McKernel lightweight multi-kernel operating system using up to 2,048 compute nodes of Oakforest-PACS. Without striving for completeness we provide some of the results we obtained.

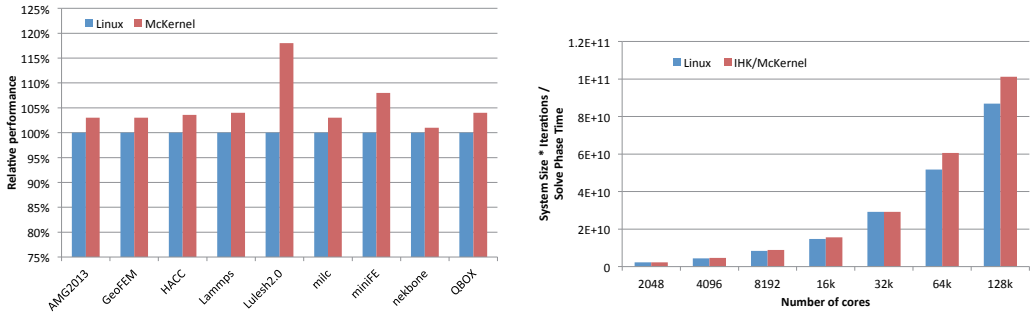

(a) Single node experiments

(b) AMG2013 scaling experiments

Figure 1.15: Single node and AMG2013 scaling results.

Figure 1.15a shows single node experiments as a baseline for further measurements. The figure shows relative performace obtained on McKernel compared to Linux. As seen, McKernel outperforms Linux on all benchmarks achieving up to 18% on the Lulesh benchmark.

The rest of the results presented here show select scaling measurements for the AMG2013, miniFE and CCS-QCD mini-applications, shown in Figure 1.15b, Figure 1.16a, and Figure 1.16b, respectively. As shown, McKernel outperforms Linux on these benchmarks by up to 21%, 3.5X and 38%, respectively. For further information on scaling results and their analysis, refer to [1].

1.3.4.2 PicoDriver: Fast-path Device Drivers for Multi-kernel Operating Systems

Standalone lightweight kernel operating systems in high-end supercomputing have a proven track record of excellent scalability. However, the lack of full Linux compatibility and limited availability of device drivers in LWKs have prohibited their wide-spread deployment. Multi-kernels, where an LWK is run side-by-side with Linux on many-core CPUs, have been proposed to address these shortcomings. In a multi-kernel system the LWK implements only performance critical kernel services and the rest of the OS functionality is offloaded to Linux. Access to device drivers is usually attained via offloading. Although high-performance interconnects are commonly driven from user-space, there are networks (e.g., Intel's OmniPath or Cray's Gemini) that require

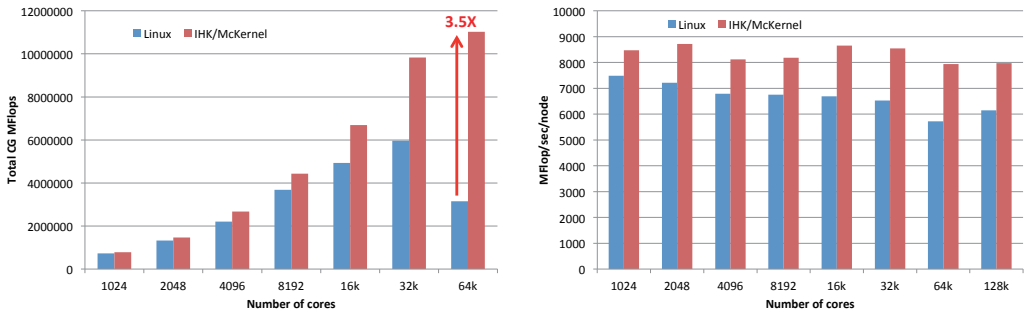

(a) miniFE scaling experiments (b) CCS-QCD scaling experiments

Figure 1.16: MiniFE and CCS-QCD scaling results.

device driver interaction for a number of performance sensitive operations, which in turn can be adversely impacted by system call offloading.

We have recently proposed *PicoDriver* [2], a novel device driver architecture for multi-kernels, where only a small part of the driver (i.e., the performance critical piece) is ported to the LWK and access to the rest remains transparent via Linux. Our solution requires no modifications to the original Linux driver, yet it enables optimization opportunities in the lightweight kernel. We demonstrated that on 16,384 Intel Knight's Landing (KNL) CPU cores (interconnected by OmniPath network) we can outperform Linux by up to 30% on various mini-applications.

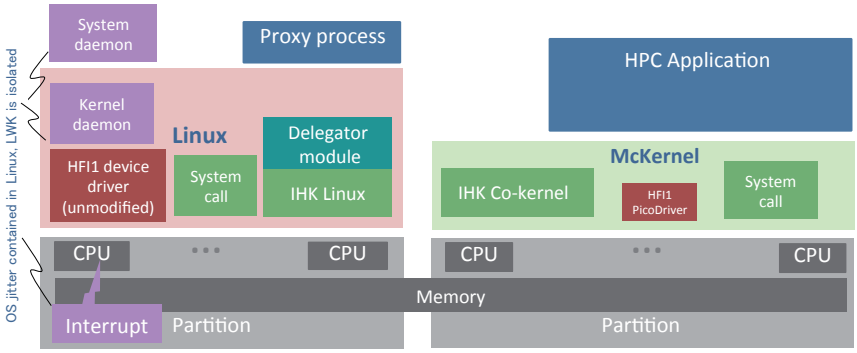

Figure 1.17: Overview of the IHK/McKernel architecture with the HFI1 *PicoDriver*.

Figure 1.17 shows the overall structure of *PicoDriver*. As seen, McKernel contains a small HFI *PicoDriver* while Linux hosts the original driver provided by Intel. McKernel, for instance, has no facilities such as the Linux device model, the VFS layer or `/proc` and `/sys` pseudo file systems. McKernel also doesn't provide mechanisms for bottom half processing (e.g., tasklets or workqueues, often used in device drivers. However, it is not our intention to provide these mechanisms, but instead we strive to implement an LWK optimized version of the fast-path code. The HFI1 driver amounts to about 50K source lines of code (SLOC), but from this codebase, less than 3K SLOC is related to the routines that is in our interest, which demands a significantly lower development effort than if we were to port the entire driver. As the figure indicates, we emphasize again that the Linux device driver remains completely unmodified. For more details on design and implementation, refer to [2].

For brevity, we include only two application results in this document, shown in Figure 1.18. The figure shows normalized performance to Linux on up to 256 compute nodes of Oakforest-PACS. As seen, McKernel with the HFI1 *PicoDriver* ourperforms Linux by up to 30% on these applications.

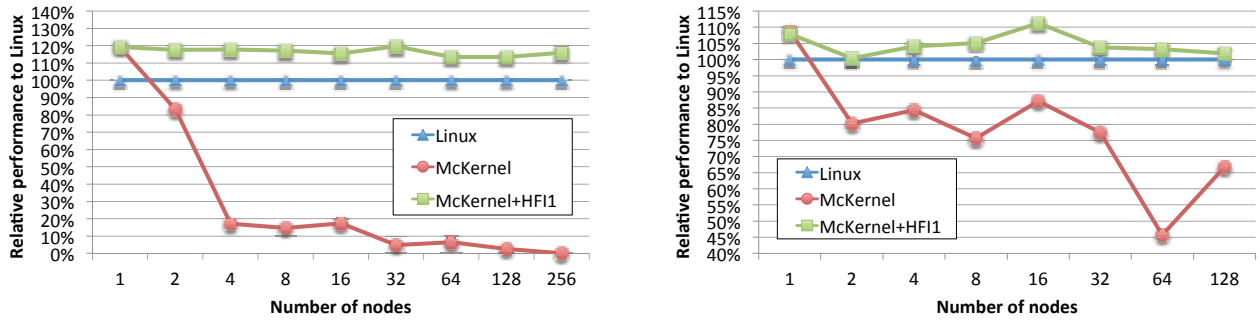

(a) UMT2013 (b) HACC

Figure 1.18: Performance results for UMT2013 and HACC.

Table 1.3: **Summary of architectures.**

Platform/ Property	Intel Ivy Bridge	Intel KNL	Fujitsu FX100	Cavium ThunderX	IBM BG/Q
ISA	x86	x86	SPARC	ARM	PowerISA
Nr. of cores	8	64+4	32+2	48	16+2
Nr. of SMT threads	2	4	N/A	N/A	4
Clock frequency	2.6 GHz	1.4 GHz	2.2 GHz	2.0 GHz	1.6 GHz
L1d size	32kB	32kB	64kB	32kB	16kB
L1i size	32kB	32kB	64kB	78kB	16kB
L2 size	256kB	1MB x 34	24MB	16MB	32MB
L3 size	20480kB	N/A	N/A	N/A	N/A
On-chip network	?	2D mesh	?	?	Cross-bar
Process technology	22nm	14nm	20nm	28nm	45nm

1.3.4.3 Hardware Performance Variation: A Comparative Study using Lightweight Kernels

Imbalance among components of large scale parallel simulations can adversely affect overall application performance. Software induced imbalance has been extensively studied in the past, however, there is a growing interest in characterizing and understanding another source of variability, the one induced by the hardware itself. This is particularly interesting with the growing diversity of hardware platforms deployed in high-performance computing (HPC) and the increasing complexity of computer architectures in general. Nevertheless, characterizing hardware performance variability is challenging as one needs to ensure a tightly controlled software environment.

Recently, we have proposed to use lightweight operating system kernels to provide a high-precision characterization of various aspects of hardware performance variability [8]. Towards this end, we have developed an extensible benchmarking framework and characterized multiple compute platforms (e.g., Intel x86, Cavium ARM64, Fujitsu SPARC64, IBM Power) running on top of lightweight kernel operating systems. Our initial findings show up to six orders of magnitude difference in relative variation among CPU cores across different platforms.

We used a number of different platforms to characterize, Table 1.3 shows a summary of these architectures.

Our benchmark suite currently consists of eight benchmark kernels and four sub-kernels. We selected our kernels from well-known algorithms such as DGEMM and SHA256, Mini-Apps, and micro benchmarks. For more details on the execution and evaluation of the benchmarks refer to the paper. For demonstration purpose, we present two of our measurement results here for SHA256 and the DGEMM kernel.

We found that the different architectures exhibited diverse behaviour for the SHA256 benchmark, shown in Figure 1.19. Despite the same L1 cache size and associativity, we observed no L1 data misses on the ThunderX platform but approximately 150k misses on the Intel Ivy Bridge platform. We decided to include the results as-is because we consider cache implementation details also micro-architecture-specific. Another reason is that the number of L1 misses on Ivy Bridge show little variation themselves. The wide base of the violins on FX100 and ThunderX already indicate that a lot of cores experience no variation at all, while Ivy Bridge performs

significantly worse and KNL shows an order of magnitude more variation still.

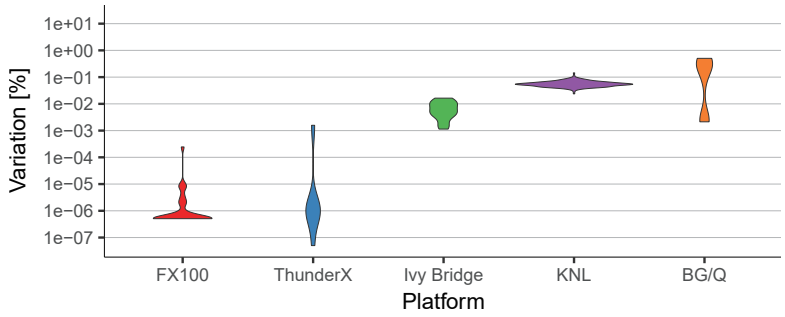

Figure 1.19: Hardware performance variation under the SHA256 benchmark.

We expected the BlueGene/Q to be among the lowest variation platforms but our measurements do not reflect that. At this point we can only speculate that the 16 KiB L1 data cache and the only 4-way set associativity of the L1 instruction cache have influence on the performance variation. We reduced the cache fill level to 80 % so that auxilary data such as stack variables have the same cache space in 32 KiB and 16 KiB caches, but we could not measure lower cache miss number of lower performance variation.

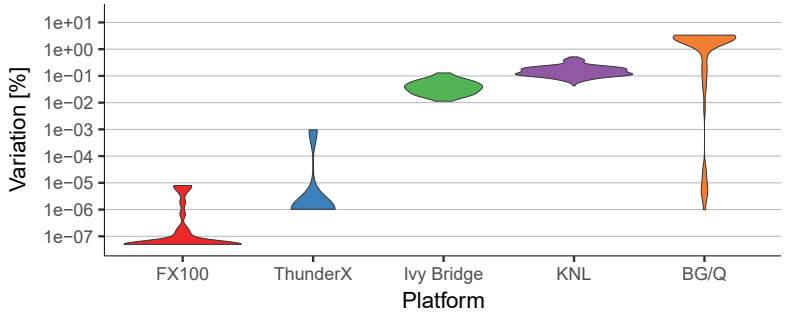

Figure 1.20: Hardware performance variation under the DGEMM benchmark.

Figure 1.20 shows results for the DGEMM benchmark, which measures floating point operations. This benchmark confirms the low variation of the FX100 and ThunderX platforms and the rather high variation of the Ivy Bridge, KNL and BlueGene/Q platforms. We saw high numbers of cache misses on the Ivy Bridge platforms and therefore reduced the cache pressure to 70 % fill level. We saw stable or even zero cache miss numbers for all cores of the Ivy Bridge platform, but variation did not improve.

1.3.5 Utility Thread Offloading Interface

The number of cores per node in HPC system has increased to hundreds. This abundance makes it possible to partition core resource and run different kinds of tasks in different partitions to increase application performance by parallelism and increase isolation between them by partitioning. Typical example of this technique is to run helper threads in a dedicated partition, such as MPI asynchronous progress threads and glibc asynchronous I/O threads. However, the resource management part of the technique is done manually. And thus it puts too much burden on user and the management is not portable across different systems or system settings. To respond to this situation, we introduce a standard abstract interface, called Utility Thread Offloading Interface (UTI). It focuses on the system where resource is divided into two partitions for two kinds of tasks, i.e., compute tasks and helper tasks, and focuses on the shared resource management with those two. It is designed as the first step toward the system-wide, shared resource management with multiple kinds of tasks and multiple partitions.

This is on-going work and the followings were done during this fiscal year.

1. Revision of the UTI API. This work was done in collaboration with Intel, Sandia National Lab and incorporating the feedbacks of Argonne National Lab. and CEA.
2. Prototype implementation of UTI kernel functions in IHK/McKernel.
3. Prototype implementation of UTI user-level library for IHK/McKernel.

4. Implementation of asynchronous progress thread using UTI in MPICH.

The first two topics are explained in the followings.
UTI API The API consists of C functions and macros. The usage steps are described in the followings.

1. A runtime library (e.g. MPI library) creates a hint description object by calling `uti_attr_init()` and write the hints using the abstract expression, by using `UTI_ATTR_*` macros. The hints include preferred CPU locations and thread behaviors relating to the scheduling policy.

2. The runtime library passes the hints to kernel and lets it create a helper thread (or utility thread) by calling `uti_pthread_create()`. The created thread is pthread-compatible.

3. Kernel finds the optimal CPU location and scheduling policy using the hints.

IHK/McKernel implementation The implementation is divided into the following four functions.

- Thread creation

  1. A runtime library uses special system call to modify the behavior of `clone()` and then calls `clone()` to create a utility thread (call it mck-uti-thread)
  2. mck-uti-thread enters kernel mode and sends a context switch request with its user-context to Linux and waits for the system call request or exit request described below
  3. A `mcexec` worker thread takes the request (call this thread lin-uti-thread)
  4. lin-uti-thread creates a `ptrace` tracer process and loads the context. `ptrace` is used for the hook described below.
  5. The tracer process attaches to lin-uti-thread

- System call offload to McKernel

  1. The tracer process hooks a system call and sends a system call request to McKernel if it is one of the system calls which modify McKernel objects (e.g. `mmap, munmap, brk, futex`).
  2. mck-uti-thread waiting in kernel mode takes the request and perform the system call for lin-uti-thread

- Signal

  1. McKernel relays a signal to mck-uti-thread to Linux
  2. A `mcexec` worker thread sends the signal to lin-uti-thread

- Exit

  1. The tracer process detects the exit of lin-uti-thread and sends an exit request to McKernel
  2. mck-uti-thread waiting in kernel mode takes the request and calls the exit function

1.4 Schedule and Future Plan

We continue to enhance performance and functionality of our system software stack for K, FX100, Post-K, and other manycore architectures, such as Intel Xeon Phi.

1.5 Publications

[1] Gerofi, B., Riesen, R., Takagi, M., Boku, T., Ishikawa, Y., and Wisniewski, R. W., "Performance and Scalability of Lightweight Multi-Kernel based Operating Systems," In 2018 IEEE International Parallel and Distributed Processing Symposium (IPDPS), May 2018.

[2] Gerofi, B., Santogidis, A., Martinet, D., and Ishikawa, Y., "PicoDriver: Fast-path Device Drivers for Multi-kernel Operating Systems," In 2018 ACM Symposium on High-Performance Parallel and Distributed Computing (HPDC), June 2018.

[3] Hatanaka, M., Takagi, M., Hori, A., and Ishikawa, Y., "Offloaded MPI Persistent Collectives using Persistent Generalized Request Interface," In EuroMPI/USA 2017, Sept. 2017.

[4] Hori, A., Si, M., Gerofi, B., Takagi, M., Dayal, J., Balaji, P., and Ishikawa, Y., "Process-in-process: Techniques for practical address-space sharing," In HPDC '18: The 27th International Symposium on High-Performance Parallel and Distributed Computing, June 2018. (Karsten Schwan Best Paper Award)

[5] Martsinkevich, T., Gerofi, B., Lien, G.-Y., Nishizawa, S., keng Liao, W., Miyoshi, T., Tomita, H., Ishikawa, Y., and Choudhary, A., "DTF: An I/O Arbitration Framework for Multi-component Data Processing Workows," In 2018 International Supercomputing Conference (ISC), June 2018.

[6] Morie, Y., Hatanaka, M., Takagi, M., Hori, A., and Ishikawa, Y., "Prototyping of Offloaded Persistent Broadcast on Tofu2 Interconnect," In SC'17 poster, Nov. 2017.

[7] Morie, Y., Hatanaka, M., Takagi, M., Hori, A., Ishikawa, Y., and Nanri, T., "Evaluation of Prototyping Persistent Collective Communication on FX100," In IPSJ SIG Technical Report, vol. 2018-HPC-163, Feb. 2018. (In Japanese)

[8] Weisbach, H., Gerofi, B., Kocoloski, B., Hartig, H., and Ishikawa, Y., "Hardware Performance Variation: A Comparative Study using Lightweight Kernels," In 2018 International Supercomputing Conference (ISC), June 2018.

Chapter 2

Programming Environment Research Team

2.1 Members

Mitsuhisa Sato (Team Leader)

Yuetsu Kodama (Senior Research Scientist)

Hitoshi Murai (Research Scientist)

Miwako Tsuji (Research Scientist)

Masahiro Nakao (Research Scientist)

Jinpil Lee (Postdoc Researcher)

Tetsuya Odajima (Postdoc Researcher)

Manabu Yagi (Postdoc Researcher)

Hidetoshi Iwashita (Research Associate)

Masahiro Yasugi (Senior Visiting Researcher)

Hitoshi Sakagami (Senior Visiting Researcher)

Brian Wylie (Visiting Researcher)

Christian Feld (Visiting Researcher)

Kengo Nakajima (Senior Visiting Researcher)

Tomoko Nakashima (Assistant)

Hiroko Takahashi (Assistant)

2.2 Research Activities

Our team conducts researches and developments on parallel programming models and language to exploit full potentials of parallelism in large-scale distributed memory systems such as the K computer and increase productivity of parallel programming.

In 2017FY, in order to archive these objectives above, we carried out the following researches:

(1) We continued working on the development and improvement of XcalableMP(XMP) programming languages. XcalableMP is a directive-based language extension, designed by XcalableMP Specification Working Group (XMP Spec WG) including some members from our team as a community effort in Japan. It allows users to develop parallel programs for distributed memory systems easily and to tune the performance by having minimal and simple notations. In this year, we continued the improvement of Coarray functions in Fortran for the K computer and others.

(2) As an extension of XcalableMP to exascale computing, we are proposing a new programming model, XcalableACC, for emerging accelerator clusters, by integrating XcalableMP and OpenACC. This research is funded by JST CREST project on post-petascale computing. As we continued working on the language design and the compiler development of XcalableACC, we have been evaluating the performance using several benchmark program and actual application such as QCD. In this year, by additional funding of SPPEXA project which is an international collaboration with French and Germany, we have been working on MUST verification tool to XMP for correctness checking of user applications.

(3) As the post-K computer will be a large-scale multicore-based system, we are investigating programming models for manycore-based parallel systems as XcalableMP 2.0. We focus especially on the integration of dynamic tasking with PGAS programming model. In this year, We have been working on the performance evaluation on the prototype implementation.

(4) Co-design for HPC is a bidirectional approach, where a system would be designed on demand from applications, and applications must be optimized to the system. We are working on the design of tools for co-design, including the SCAMP profiler for the network of large scale systems.

(5) In order to exploit the full performance of large-scale systems, we had been proposed a multi SPMD programming model, which use multiple programming models across different architectural levels and had been developed a software to realize the proposed programming model by adopting a scientific workflow environment and a PGAS language called XcalableMP (XMP). we continued the improvement such as fault tolerant features, and the evaluation using applications. This work has been carried out under the collaboration of MDLS, France.

(6) We conducted several collaborations on the performance evaluation with JSC, University of Tsukuba, Kyusyu Institute of Technology and other groups. As for performance tuning tools, We continue the collaboration with JSC for g a tuning tool Scalasca, which is being developed by JSC, for the K computer. In this year, we carried out the performance study on NEST brain simulator developed by JSC, using Scalasca.

In addition to the research activities, we conducted promotion activities to disseminate our software. To promote XcalableMP as a means for parallelization of programs, we made the XcalableMP workshop, seminars or tutorial as follows:

- The 5th XcalableMP workshop (Oct. 31)
- Tutorials on XMP (at CEA, France in September, at Kashiwa in September, at U. Kyushu, Fukuoka, in February). Tutorials consist of both classroom and hands-on learning

In this year, our team has organized the following workshop and mini-symposiums in SIAM Parallel Processing Symposium held in Waseda, Japan:

- Workshop on PGAS programming models: Experiences and Implementations (PGAS-EI), HPC Asia 2017 workshop, Tokyo, Japan.
- PP18 mini-symposium on “Emerging Programming Models for Extreme-Scale Computing”
- PP18 mini-symposium on “Research Compiler Infrastructure for High Performance Computing”

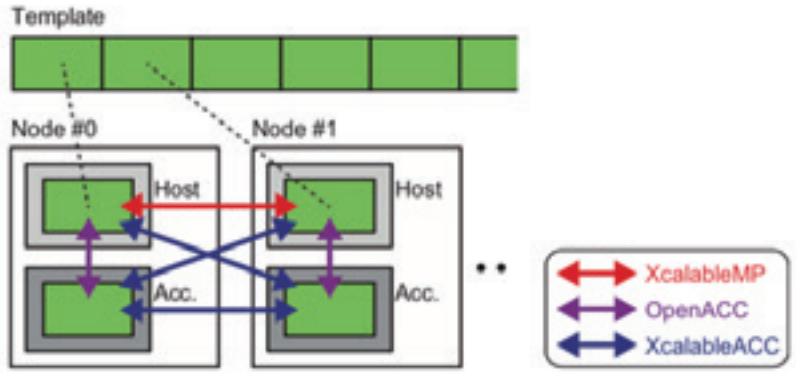

Figure 2.1: XcalableACC Concept

```
1 typedef struct Quark {
2   double v[4][3][2];
3 } Quark_t;
4 typedef struct Gluon {
5   double v[3][3][2];
6 } Gluon_t;
7 Quark_t v[NT][NZ][NY][NX], tmp_v[NT][NZ][NY][NX];
8 Gluon_t u[4][NT][NZ][NY][NX];
9
10 #pragma xmp template t[NT][NZ]
11 #pragma xmp nodes n[NODES_T][NODES_Z]
12 #pragma xmp distribute t[block][block] onto n
13 #pragma xmp align v[i][j][*][*] with t[i][j]
14 #pragma xmp align tmp_v[i][j][*][*] with t[i][j]
15 #pragma xmp align u[*][i][j][*][*] with t[i][j]
16 #pragma xmp shadow v[1:1][1:1][0][0]
17 #pragma xmp shadow tmp_v[1:1][1:1][0][0]
18 #pragma xmp shadow u[0][1:1][1:1][0][0]
19 ..
20 int main(){
21 ..
22 #pragma acc enter data copyin(v, tmp_v, u)
```

Figure 2.2: Declaration of distributed arrays for Lattice QCD

2.3 Research Results and Achievements

2.3.1 XcalableACC for Lattice QCD

Accelerated clusters, which are distributed memory systems equipped with accelerators, have been used in various fields. For accelerated clusters, programmers often implement their applications by a combination of MPI and CUDA (MPI+CUDA). However, the approach faces programming complexity issues. To solve these issues, we develop the XcalableACC (XACC) language, which is a hybrid model of XcalableMP (XMP) and OpenACC. XACC enables programmers to develop applications on accelerated clusters with ease.

Fig. 2.1 shows an XACC concept where execution units are called "node" all of which execute the same program via the SPMD execution model. Each node consists of a host and some accelerators (For simplicity, Fig. 2.1 shows only one accelerator). A distributed array is declared using a "template", which is a dummy array that represents a global index space. Fig. 2.1, a green square in each node is a part of the distributed array.

The XACC programming model uses XMP, OpenACC and XACC directives. XMP directives declare distributed arrays, divide loop statements and transfer data among host memory. OpenACC directives transfer the distributed arrays between host memory and accelerator memory on the same node and calculate the loop statements divided by XMP on accelerators. XACC directives transfer data among accelerator memories or between accelerator memory and host memory on different nodes.

2.3.1.1 Implementation of Lattice QCD

To evaluate XACC performance and productivity, we implemented a lattice quantum chromodynamics (Lattice QCD) application. Fig. 2.2 shows how to declare distributed arrays of the quark and gluon. In lines 1-8, the quark and gluon structure arrays are declared. The NT, NZ, NY and NX are the numbers of TZYX axis elements. In lines 10-18, distributed arrays are declared where the macro constant values NODES_T and NODES_Z indicate the number of nodes on the T and Z axes. Thus, the program is parallelized on T and Z axes. In lines 16-18, the shadow directives add halo regions to the arrays because each quark and gluon element is affected by its neighboring orthogonal elements. In line 22, the enter data directive transfers the distributed arrays from host memory to accelerator memory.

```
1 void WD(Quark_t v_out[NT][NZ][NY][NX], const Gluon_t u
      [4][NT][NZ][NY][NX], const Quark_t v[NT][NZ][NY][
      NX])
2 {
3 #pragma xmp align v_out[i][j][*][*] with t[i][j]
4 #pragma xmp align u[*][i][j][*][*] with t[i][j]
5 #pragma xmp align v[i][j][*][*] with t[i][j]
6 #pragma xmp shadow v_out[1:1][1:1][0][0]
7 #pragma xmp shadow u[0][1:1][1:1][0][0]
8 #pragma xmp shadow v[1:1][1:1][0][0]
9  ...
10 #pragma xmp loop (t,z) on t[t][z]
11 #pragma acc parallel loop collapse(4) present(v_out, u, v)
12  for(int t=0;t<NT;t++)
13   for(int z=0;z<NZ;z++)
14    for(int y=0;y<NY;y++)
15     for(int x=0;x<NX;x++){
```

Figure 2.3: A portion of Wilson-Dirac operator(1)

```
1 #pragma xmp reflect(v) width(/periodic/1:1,/periodic/1:1,0,0) orthogonal acc
2 #pragma xmp reflect(u) width(0,/periodic/1:0,/periodic/1:0,0,0) orthogonal acc
3 WD(tmp_v, u, v);
4 #pragma xmp reflect(tmp_v) width(/periodic/1:1,/periodic/1:1,0,0) orthogonal acc
5 WD(v, u, tmp_v);
```

Figure 2.4: A portion of Wilson-Dirac operator(2)

Fig. 2.3 shows a part of the Wilson-Dirac operator code, which is a main kernel in Lattice QCD. All arguments in WD() are distributed arrays. In XMP and XACC, distributed arrays which are used as arguments must be redeclared in function to pass their information to a compiler. Thus, the align and shadow directives are used in WD(). In line 10, the loop directive parallelizes the outer two loop statements. In line 11, the parallel loop directive parallelizes all loop statements.

Fig. 2.4 shows how to call WD(). The reflect directives are inserted before WD() in order to update own halo region. In line 2, "1:0" in width clause means only the lower halo region is updated because only it is needed in WD(). The u is not updated before the second WD() function because values of u are not updated in WD(). Moreover, the "orthogonal" clause is added because diagonal updates of the arrays are not required in WD().

2.3.1.2 Performance evaluation

This section evaluates the performance of XACC on the Lattice QCD code. For comparison purposes, those of MPI+CUDA and MPI+OpenACC are also evaluated. For performance evaluation, we use the HA-PACS/TCA system which consists of 64 compute nodes and 256 GPUs

Fig. 2.5 shows the performance results that indicate the time required to solve one CG iteration as well as the performance ratio values that indicate the comparative performance of XACC and other languages. When the performance ratio value of a language is greater than 1.00, the performance result of the language is better than that of XACC. Fig. 2.5 shows that the performance ratio values of MPI+CUDA are between 1.04 and 1.18, and that those of MPI+OpenACC are between 0.99 and 1.04. Moreover, Fig. 2.5 also shows that the performance results of both MPI+CUDA and MPI+OpenACC become closer to those of XACC as the number of nodes increases.

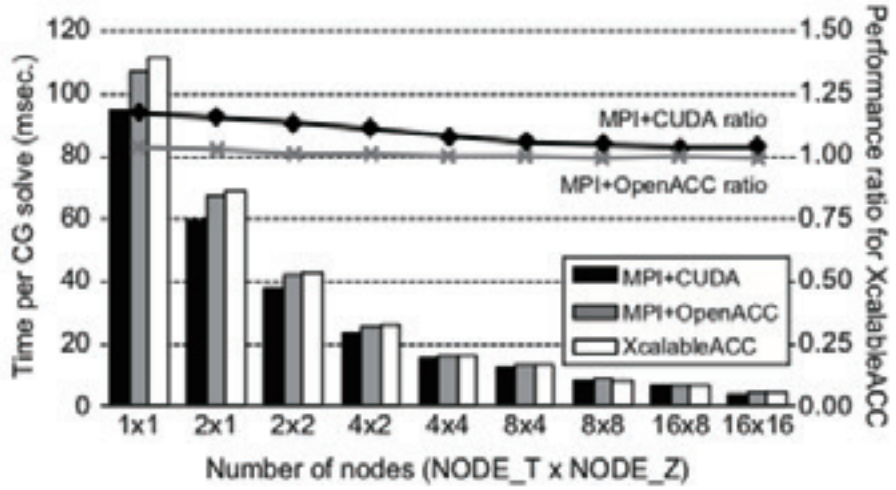

Figure 2.5: Performance results

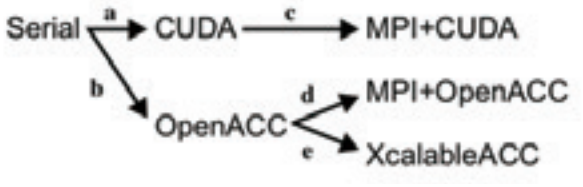

Figure 2.6: Application development order on accelerated cluster

2.3.1.3 Productivity evaluation

We developed three Lattice QCD codes using MPI+CUDA, MPI+OpenACC, and XACC. Fig. 2.6 shows our procedure for developing each code where we first develop the code for an accelerator from the serial code, and then extend it to handle an accelerated cluster. As one of metrics for productivity, Delta Source Lines of Codes (DSLOC) is proposed. The DSLOC indicates how the codes change from a corresponding implementation. The DSLOC is the sum of three components: how many lines are added, deleted and modified. When the DSLOC is small, the programming costs and the possibility of program bugs will be small as well. We use the DSLOC to count the amount of change required to implement an accelerated cluster code from a serial code.

Table I shows the DSLOC where lowercase characters correspond to Fig. 2.6. The DSLOC of XACC (b+e) is smaller than MPI+CUDA (a+c) and MPI+OpenACC (b+d). The difference between XACC and MPI+CUDA is 420.0%, and that between XACC and MPI+OpenACC is 39.4%.

2.3.1.4 Conclusion

In this study, we evaluated performance and productivity of XACC through the implementation of the Lattice QCD code. For comparison purposes, we also implemented the Lattice QCD code using MPI+CUDA and MPI+OpenACC. We began by evaluating all performance on the HA-PACS/TCA system using up to 64 compute nodes and 256 GPUs. The results showed that performance results of XACC is almost equal to those of MPI+CUDA and MPI+OpenACC when large numbers of compute nodes are used. Next, we evaluated productivity using the DSLOC metric. The result indicates that XACC provides the best productivity of all.

2.3.2 XcalableMP 2.0 for task-parallelism in distributed memory systems

XcalableMP (XMP) is a Partitioned Global Address Space (PGAS) style of language for describing large-scale scientific code for parallel systems with distributed memory architecture.

Currently, we are working on the next version of XcalableMP specification, called XcalableMP 2.0. The important topics for XcalableMP 2.0 might include the support for manycore clusters, that is multitasking with integrations of PGAS model and synchronization models for dataflow/multitasking executions. For this issue, we propose an extension by a new directive called tasklet to describe multithreaded and dataflow programming

	a	b	c	d	e	a+c	b+d	b+e
DSLOC	552	22	280	201	138	832	223	**160**
Add	137	20	185	140	134	322	160	**154**
Delete	73	0	0	0	0	73	0	**0**
Modify	342	2	95	61	4	437	63	**6**

Table 2.1: Delta-SLOC of Lattice QCD implementations

```
#pragma xmp tasklet [clause[, clause] ... ] [on { node-ref | template-ref } ]
  (structured-block)

#pragma xmp taskletwait [on { node-ref | template-ref } ]

#pragma xmp tasklets
  (structured-block)

  where clause is :
    {in | out | inout} (variable[, variable] ... ])
```

Figure 2.7: Syntax of the `tasklet`, `taskletwait`, and `tasklets` directives in XMP.

model. We expect this model will enables less overhead of synchronization eliminating expensive global synchronization, overlap between computation and communication in manycore, and light-weight communication by RDMA in PGAS model.

2.3.2.1 OpenMP and XMP Tasklet Directive

Although OpenMP originally focuses on work sharing for loops as the `parallel for` directive, OpenMP 3.0 introduces task parallelism using the `task` directive. It facilitates the parallelization where work is generated dynamically and irregularly as in recursive structures or unbounded loops. The `depend` clause on the `task` directive is supported from OpenMP 4.0 and specifies data dependencies with dependence-type `in`, `out`, and `inout`. Task dependency can reduce the global synchronization of a thread team because it can execute fine-grained synchronization between tasks through user-specified data dependencies.

To support task parallelism in XMP as in OpenMP, the `tasklet` directive [1] is proposed. Fig. 2.7 describes the syntax of the `tasklet`, `tasklets`, and `taskletwait` directives for the multi-tasking execution in XMP. The `tasklet` directive generates a task for the associated structured block on the node specified by the `on` clause, and the task is scheduled and immediately executed by an arbitrary thread in the specified node if there is no task dependency. If it has any task dependencies, the task execution is postponed until all dependencies are resolved. These behaviors occur when these tasks are surrounded by `tasklets` directive. The `taskletwait` directive waits on the completion of the generated tasks on each node.

2.3.2.2 Multi-tasking Execution Model in XcalableMP between nodes

In OpenMP, the task dependency in a node depends on the order of reading and writing to data based on the sequential execution. Therefore, the OpenMP multi-tasking model cannot be applied to describe the dependency between tasks running in different nodes since threads of each nodes are running in parallel. In OmpSs, interactions between nodes are described through the MPI task that is executing MPI communications. Task dependency between nodes is guaranteed by the completion of MPI point-to-point communication in tasks. While this approach can satisfy dependencies between nodes, it may cause further productivity degradation because it forces users to use a combination of two programming models that are based on different description formats. Therefore, we propose new directives for communication with tasks in XMP, and they enable users to write easily the multi-tasking execution for clusters by only using language constructs.

[1] There is the `task` directive in XMP, it is different from OpenMP's one.

```
int A[3], B;
#pragma xmp nodes P(3)
#pragma xmp template T(0:2)
#pragma xmp distribute T(block) onto P
#pragma xmp align A[i] with T(i)

#pragma xmp tasklets
{
#pragma xmp tasklet out(A[0]) on P(1)
   A[0] = 0;       /* taskA */
#pragma xmp tasklet gmove in(A[0]) out(A[1])
   A[1] = A[0];   /* taskB */
#pragma xmp tasklet gmove in(A[1]) out(B) on P(2:3)
   B = A[1];       /* taskC */
}
```

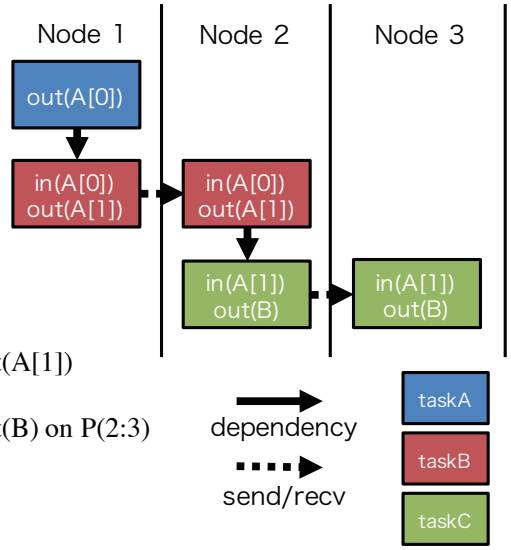

Figure 2.8: Example of the `tasklet` and `tasklet gmove` directives.

We propose two new directives, `tasklet gmove` and `tasklet reflect` directives to describe interactions between nodes in tasks by point-to-point communication for the inter-node data dependency, and these communications are synchronized only between sender and receiver of communication in each task.

The `tasklet gmove` directive copies the variable of the right-hand side (rhs) into the left-hand side (lhs) of the associated assignment statement for local or distributed data in tasks. If the variable of the rhs or the lhs is the distributed data, this directive may execute communication. The communication is detected and performed automatically by the XMP runtime system. This directive must be executed by all nodes in the current executing node set specified by the `on` clause. When `in`, `out`, or `inout` clause presents on the `tasklet gmove` directive, the generated task have each data dependency in a node similar to the `tasklet` directive.

Fig. 2.8 shows an example of the `tasklet` and `tasklet gmove` directives. In this example, array *A[]* of length 4 is distributed to 2 nodes as equal-size contiguous blocks; therefore, node 1 and 2 can deal with indices 0 to 1 and 2 to 3, respectively. This code has three tasks, taskA and taskB are executed on node 1, and taskB and taskC are executed on node 2, that these execution nodes are specified by the `on` clause. There are flow dependency between taskA and taskB by *A[0]*, and taskB and taskC by *B*. After the execution of taskA, taskB on node 1 sends *A[0]* to node 2 which is determined by the execution nodes set by the `on` clause. In node 2, taskB receives *A[0]* from node 1 in *B*. When finishing the receive operation in taskB, taskC is immediately started on node 2 because the flow dependency by *B* is satisfied.

The `tasklet reflect` directive is a task-version of reflect operation. It updates halo regions of the array specified to `array-name` in tasks. In this directive, data dependency is automatically added to these tasks based on the communication data because the boundary index of the distributed data is dynamically determined by XMP runtime system.

2.3.2.3 Preliminary Performance Evaluation on Oakforest-PACS

We have designed a simple code translation algorithm from the proposed directives to XMP runtime calls with MPI and OpenMP. The `tasklets` directive is converted to OpenMP `parallel` and `single` directives. The execution node is determined by the `on` clause that is translated to an `if` statement. The `tasklet gmove` and `tasklet reflect` directives are converted to MPI_Send/Recv() and these MPI functions are executed in OpenMP tasks with data dependency specified by users. However, in case of the MPI blocking call such as MPI_Send/Recv() in these codes, the deadlock may occur depending on the task scheduling mechanism by the combination of MPI and OpenMP. To prevent this problem, we used the MPI asynchronous communications such as MPI_Isend/Irecv(), MPI_Test(), and the OpenMP `taskyield` directive.

We have evaluated the performance on our Oakforest-PACS. We select the Flat and Quadrant mode for KNL. While the Intel Xeon Phi 7250 has 68 cores, 64 cores usage per a node is recommended in this system. As our benchmark program, we used Blocked Cholesky factorization program which calculates a decomposition of a Hermitian, positive-definite blocked matrix as into the product of a lower triangular matrix and its conjugate

transpose. We implemented tow versions in different parallelization approaches: "Parallel Loop" and "Task", in MPI and OpenMP. The "Parallel Loop" version is the conventional barrier-based implementation described by work sharing for loops by the `parallel for` directive and independent tasks using the `task` directive without the `depend` clause. Although this version of the blocked Cholesky factorization is applied the overlap of the communication and computation at the process level, it performs the global synchronization in work sharing. The "Parallel Loop" version of Laplace equation solver is not include the overlap of the communication and computation. The "Task" version is implemented using our proposed model by task dependency using the `depend` clause instead of global synchronization.

We measured the performance using from one to 32 nodes, 1 process per node, 64 cores per process, and 1 thread per core. As problem size of these benchmarks, the matrix size is 32768 × 32768 and the block size is 512 × 512 in double precision arithmetic. The matrix is distributed by two-dimensional block-cyclic data distribution in blocked Cholesky factorization and two-dimensional block data distribution in Laplace equation solver.

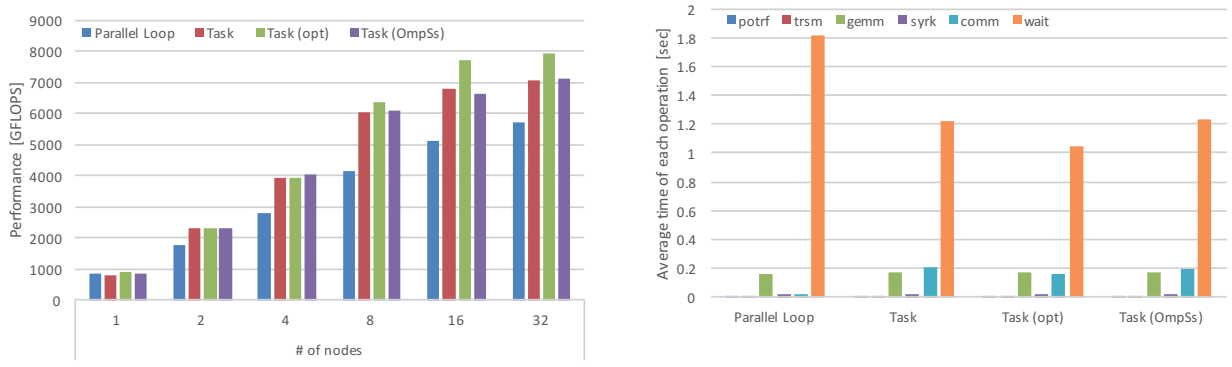

(A) Performance

(B) Breakdown at 32 nodes execution

Figure 2.9: Performance and breakdown of the blocked Cholesky factorization on Oakforest-PACS system.

Figs. 2.9 show the performance and breakdown of the blocked Cholesky factorization on the Oakforest-PACS. The breakdown indicates the average time of each operations performed on all threads because tasks executed on threads differ each time the program is executed. The "wait" in breakdown represents the waiting time of the thread including the global synchronization. In Fig. 2.9 (A), the "Task" version show better performance than the barrier-based implementations, "Parallel Loop" version. The reason why "Task" version outperforms "Parallel Loop" version is that the global synchronization spends more cost in work sharing of loops and among tasks as the "wait" shown in Fig. 2.9 (B). The relative performances of "Task" version against the barrier-based implementation, "Parallel Loop" version, is 123%.

2.3.2.4 Communication Optimization for Many-core Clusters

In the version reported in the previous subsection, the communication are executed in MPI_THREAD_MULTIPLE as MPI thread-safety level since tasks executed on threads may communicate simultaneously. Our basic performance analysis of point-to-point communication using OSU Micro-Benchmarks indicates that the performance of multi-threaded communication with MPI_THREAD_MULTIPLE degrades when increasing the number of threads, compared to a single-threaded communication.

According to the observation above, we optimize the communication by delegating all communications to the communication thread. To delegate the communication to a single thread, we make a global queue accessible by all threads so that the tasks enqueues the communication requests into its queue and wait for the communication completion. Meanwhile, the communication thread dequeues the requests for communication to perform the requested communications, and check the communication completion, respectively. The communication thread executes only the communication, and the other threads perform computation tasks.

In Figs. 2.9 (A),"Task (opt)" version are higher than that of the multi-tasking execution with MPI_THREAD_MULTIPLE. The reason is that the communication time is reduced compared with the "Task" version as shown in Figs. 2.9 (B). The relative performance against the barrier-based implementation, "Parallel Loop" in Figs. 2.9, are improved to 138% and 141%, respectively.

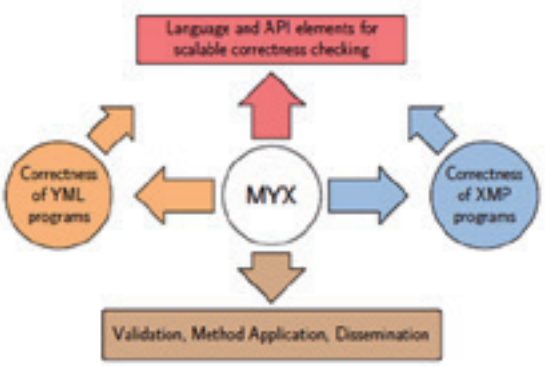

Figure 2.10: Overview of MYX collaboration

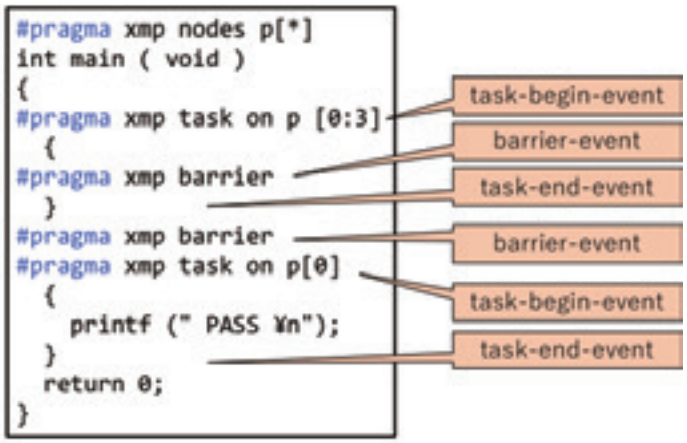

Figure 2.11: Example of XMPT Events

In near future, we expect the performance of MPI_THREAD_MULTIPLE will also be improved as the design and implementation is getting matured for parallel manycore system. Currently, we are investigating a lower-level communication API for efficient one-sided communication of PGAS operations in multithreaded execution environment.

2.3.3 SPPEXA MXY project

MYX (MUST correctness checking for YML and XMP programs) is an international collaboration for correctness checking of exascale parallel programs.

MUST was originally developed by RWTH Aachen as a tool for checking MPI programs, and extended to support emerging PGAS and workflow programming models. Fig. 2.10 shows the overview of MYX collaboration.

In this collaboration, we defined and implemented the XMPT interface, which is an XMP tools interface modeled after the OpenMP tools interface, OMPT. The definition of XMPT will finally be included in the XMP specification

According to XMPT, the XMP runtime notifies an interested tool about any encountered directive as XMPT events, which are designed to be used by correctness as well as performance analysis as shown in Fig. 2.11.

For correctness analysis, XMPT enables productivity improvements in programming for Exascale by means of scalable correctness checking of XMP-programs, such as one-sided communications and global data accesses, by analyzing the semantics expressed by the XMP control flow directives and identifying semantic issues. For performance analysis, XMPT enables tracing tools like Score-P to log event information and use the data to visualize the performance of execution.

On the other hand, we had proposed a multi SPMD programming framework, where multiple SPMD programs are integrated into a workflow. In our implementation of the multi SPMD programming framework, YML had been employed to realize a workflow programming model, and XMP had been supported to describe

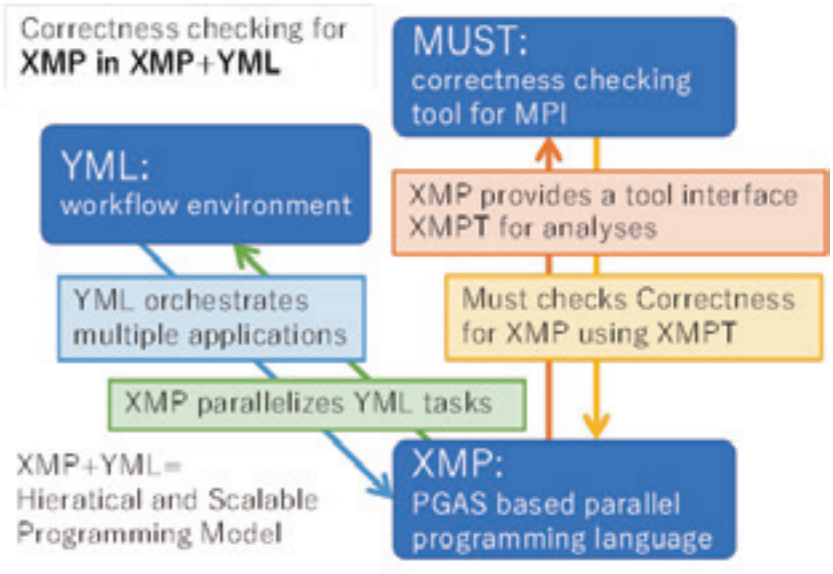

Figure 2.12: Correctness Checking for XMP in XMP/YML

the tasks of the workflow. In order to incorporate XMP checked by MUST into the XMP/YML multi SPMD programming framework, we have investigated how to apply MUST correctness checking to the worker programs invoked by a master scheduler program.

2.3.4 Performance study of NEST on K computer using Scalasca

The group on NEST, a brain simulator for Neuronal sciences is engaged in performance analysis of the simulator (5th-generation kernel, in the development community's terminology) and collaborating, under the MOU with Juelich Supercomputing Centre (JSC), with scientists and Ph.D. students from the ICT group at RIKEN, the computational neuroscience division and JSC at Juelich Research Center in Germany.

To collect the performance data at scale, up to 82,944 nodes that K computer provides, we've chosen Scalasca as our tool for investigation (the porting work of Scalasca to K computer is a collaboration work between the Application Support division at JSC and Programing environment research group and it has been actively maintained).

As a first step toward the goal of this project, we've collected data by running the well-studied neuronal-network model without instrumentation to use as a base-line date and the new 5th-gen kernel at the time of the experiment, demonstrated its newly implemented and introduced algorithms and data structures improve the expected good scalability up to the full-node scale of K computer. This set of data is used in the original research paper entitled "Extremely scalable spiking neural network simulation code: from laptops to exascale computers", in Frontiers in Neuroinformatics [1] and the press release on the results were published by the Human Brain Project [2].

Next, we manually instrumented NEST to minimize the sizable overhead incurred if automatic instrumentation by compiler is chosen, and collected and analyzed the profile data set. (about 20% of execution time increase due to manual instrumentation) From the data, we've determined the MPI communication cost is about 1% of wall-clock time even in an experiment where neurons scattered across the 82,944 nodes.

Another finding from the profile data is that the computing cost increase with the increase the number of nodes involved. We plan to come back to this and investigate when the stable simulation code base which includes the 5th generation kernel is released.

2.4 Schedule and Future Plan

We have been developing a production-level XcalableMP compiler and make it available for the K computer's users as well as the users of conventional clusters.

[2] https://www.humanbrainproject.eu/en/follow-hbp/news/an-algorithm-for-large-scale-brain-simulations/

Towards exascale computing, there are two major approaches, manycore and GPU. We are already working on XcalableACC as a solution for accelerator-based system, which has been explored in the JST CREST project.

As well as dissemination of the current version of XcalableMP, we are now moving forward to the next version, XcalableMP 2.0, which includes new features such as the integration of dynamic tasking with PGAS programming model for large-scale manycore systems, especially for the post-K.

And, for the coming Post-Moore era, we will start a study on parallel programming models for the architecture of the Post-Moore. As a first step, we will expoit the programming models for FPGA cluster as one of the candidates for such architecture.

2.5 Publications

2.5.1 Journal Articles

[1] Jakob Jordan, Tammo Ippen, Moritz Helias, Itaru Kitayama, Mitsuhisa Sato, Jun Igarashi, Markus Diesmann, Susanne Kunkel: "Extremely Scalable Spiking Neuronal Network Simulation Code: From Laptops to Exascale Computers", Front. Neuroinform. 2018 (2018)
[2] M. Yagi, K. Seki, Y. Matsumoto, D. C. Delcourt, and F. Leblanc (2017), Global Structure and Sodium Ion Dynamics in Mercury's Magnetosphere With the Offset Dipole, Journal of Geophysical Research: Space Physics, Vol 122, Issue 11, pp. 10,990-11,002.

2.5.2 Conference Papers

[1] Hitoshi Murai, Masahiro Nakao, Hidetoshi Iwashita, Mitsuhisa Sato. "Preliminary Performance Evaluation of Coarray-based Implementation of Fiber Miniapp Suite using XcalableMP PGAS Language," Second Annual PGAS Applications Workshop (PAW), CO, USA, Nov. 2017.
[2] Masahiro Nakao, Hitoshi Murai, Hidetoshi Iwashita, Akihiro Tabuchi, Taisuke Boku, Mitsuhisa Sato. "Implementing Lattice QCD Application with XcalableACC Language on Accelerated Cluster," IEEE Cluster 2017, HI, USA, Sep. 2017.
[3] Akihiro Tabuchi, Masahiro Nakao, Hitoshi Murai, Taisuke Boku, Mitsuhisa Sato: Implementation and Evaluation of One-sided PGAS Communication in XcalableACC for Accelerated Clusters. CCGrid 2017: 625-634
[4] Masahiro Nakao, Hitoshi Murai, Taisuke Boku, Mitsuhisa Sato. "Linkage of XcalableMP and Python languages for high productivity on HPC cluster system," Workshop on PGAS programming models: Experiences and Implementations, Tokyo, Japan, Jan. 2018.
[5] Akihiro Tabuchi, Masahiro Nakao, Hitoshi Murai, Taisuke Boku, Mitsuhisa Sato: Performance evaluation for a hydrodynamics application in XcalableACC PGAS language for accelerated clusters. HPC Asia Workshops 2018: 1-10
[6] Hidetoshi Iwashita, Masahiro Nakao, Hitoshi Murai, Mitsuhisa Sato. "A Source-to-Source Translation of Coarray Fortran with MPI for High Performance," HPC Asia 2018, Tokyo, Japan, Jan. 2018.
[7] keisuke Tsugane, Jinpil Lee, Hitoshi Murai, Mitsuhisa Sato: Multi-tasking Execution in PGAS Language XcalableMP and Communication Optimization on Many-core Clusters. HPC Asia 2018: 75-85
[8] Masahiro Nakao, Hitoshi Murai, Taisuke Boku, Mitsuhisa Sato. "Performance Evaluation for Omni XcalableMP Compiler on Many-core Cluster System based on Knights Landing," IXPUG Workshop Asia 2018, Tokyo, Japan, Jan. 2018.
[9] Joachim Protze, Christian Terboven, Matthias S. Muller, Serge Petiton, Nahid Emad, Hitoshi Murai, Taisuke Boku, "Runtime Correctness Checking for Emerging Programming Paradigms," First International Workshop on Software Correctness for HPC Applications, 2017.

2.5.3 Invited Talks

[1] Mitsuhisa Sato, "FLAGSHIP 2020 Project: Development of "Post-K" and ARM SVE", GoingARM workshop at ISC 2017, Germany.
[2] Mitsuhisa Sato, "FLAGSHIP 2020 Project: Development of "Post-K" and ARM SVE", GoingARM workshop at ISC 2017, Germany.
[3] Mitsuhisa Sato, "Update of FLAGSHIP 2020 Project: the Post-K and ARM SVE", 3rd US-Japan Joint Institute for Fusion Theory Workshop on Innovations and co-designs of fusion simulations towards extreme scale computing, Kashiwa, Japan.

[4] Mitsuhisa Sato, "Update of FLAGSHIP 2020 Project", BoF SC17: Arm User Experience: Testbeds and deployment at HPC centers, Denver, US.
[5] Mitsuhisa Sato, "How does PGAS "collaborate" with MPI+X?", Keynote of GAS Applications Workshop (PAW) 2017 at SC17, Denver, US.
[6] Mitsuhisa Sato, "Trends and Challenges on Programming Models for Extreme-Scale Computing", Keynote of mini-symposium "Emerging Programming Models for Extreme-Scale Computingg" at SIAM Parallel Processing in SIAM conference on Parallel Processing 2017, Waseda, Japan.
[7] Yuetsu Kodama,"Preliminary Performance Evaluation of Application Kernels using Arm SVE with Multiple Vector Lengths", Going Arm @ Supercomputing 2017, 2017/11.

2.5.4 Posters and Presentations

[1] Miwako Tsuji "YML, XMP and Fault Tolerance for post-peta, exascale and beyond", First French-Japanese-German Workshop on programming and computing for Exascale and beyond
[2] Miwako Tsuji, Jeff Vetter, Mitsuhisa Sato, "Exascale co-design and performance modeling tools", IEEE Cluster/Workshop on Japan-USA Collaboration for Extreme-scale System Software (DOE/MEXT)
[3] Miwako Tsuji, Yuetsu Kodama "Performance evaluation with Arm HPC tools for SVE", ARM HPC Workshop by RIKEN AICS and Linaro
[4] Miwako Tsuji, Mitsuhisa Sato, "An extension of the fault tolerant multi-SPMD programming environment for large scale systems and MPI-IO", HPCAsia2017 Poster,2018
[5] Miwako Tsuji, "Fault Tolerance Features of a Multi SPMD Scientific Workflow Programming Model", SIA MPP18, 2018
[6] Hitoshi Murai, XcalableACC PGAS Language for Accelerated Clusters and XMPT Tool Interface, SPPEXA Workshop Japan 2017,2017.
[7] Hitoshi Murai and Jinpil Lee, PGAS Programming Models and Coarray, 2017 JLESC Summer School, 2017.
[8] Hitoshi Murai, Programming Languages & Tools for Higher Performance & Productivity, ARM HPC Workshop by RIKEN AICS and Linaro, 2017.
[9] Masahiro Nakao, Hitoshi Murai, Hidetoshi Iwashita, Akihiro Tabuchi, Taisuke Boku, Mitsuhisa Sato. "Productivity and Performance of XcalableACC Language for Acceralated Clusters," The 7th AICS International Symposium, Kobe, Hyogo, Japan, Feb, 2017.
[10] Masahiro Nakao, Hitoshi Murai, Akihiro Tabuchi, Taisuke Boku, Mitsuhisa Sato. "Performance Evaluation of NICAM-DC-MINI using XcalableACC on Accelerated Cluster," HPC Asia 2018 Poster, Tokyo, Japan, Jan. 2018.
[11] Miwako Tsuji, Mitsuhisa Sato. "An extension of the fault tolerant multi-SPMD programming environment for large scale systems and MPI-IO," HPC Asia 2018 Poster, Tokyo, Japan, Jan. 2018.

2.5.5 Patents and Deliverables

- Omni XcalableMP compiler ver. 1.3 (registered as an R-CCS-supported software)

Chapter 3

Processor Research Team

3.1 Members

Kentaro Sano (Team Leader)

Tomohiro Ueno (Postdosctoral Researcher)

3.2 Research Activities

We are researching parallel-computing models and architectures for high-performance computing, considering future computing technologies. To achieve high-performance computing with a large-scale system such like the K computer and its successor, called post-K computer, we need to use a huge number of networked computing nodes in a way that they cooperate with each other by communicating data. However, the overall performance is usually degraded by considerable overhead required for global communications and synchronization among the nodes. One of our research goals is to achieve highly-efficient parallel computing based on the data-flow model, where we can restrict performance degradation by localizing communication and synchronization even in the case of large-scale processing with a huge number of computing nodes.

The data-flow model is one of the major examples of non von Neumann architectures that most of today's computers are based on. The data-flow model is based on data-driven execution which is usually programmed in a single-assignment language to describe data dependency, while von Neumann architecture is based on control-driven execution to execute operations with a sequential flow of control which is programmed in traditional imperative languages. In the data-flow model, there is a flow of data values through a network of primitive operations, flowing from operations that produce those values to ones that consume them as operands. An operation is triggered when all its operands become available, and the operation results are output to other operations that consume them. Since these data-flow and operation-triggering take place simultaneously all over the network, fine-grain parallelism can naturally be exploited by performing many operations in parallel.

Although the data-flow concept itself is not new and various data-flow architectures including static and dynamic ones had been researched particularly in 1980s, nowadays the advancement of field-programmable gate arrays (FPGAs) allows us to revive it as feasible and promising solution to scalable high-performance computing. In the case where a data-flow graph of operations connected in a network is implemented as a pipelined circuit with a custom structure, we can naturally exploit massive parallelism with low global-synchronization overhead in a large-scale system. This means that we can built highly scalable systems for high-performance computing with the data-flow model. In the case where we implement the data-flow concept as a software-based task scheduler, we can expect more efficient parallel computation with existing machines.

Toward such high-performance computing with the data-flow model, we are developing data-flow accelerators where custom-computing circuits are implemented on FPGAs for target applications, design tools or compilers to automatically generate the data-flow circuits from software-like codes of computational description, and system software to effectively use these platforms by managing resources and scheduling tasks in a system based on the data-flow model.

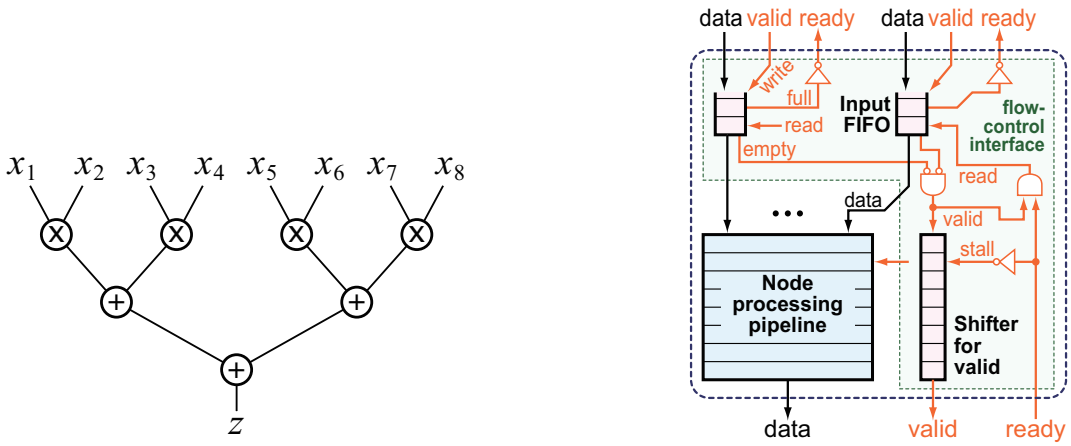

a) Example of a data-flow graph. b) Hardware structure of a data-flow node.

Figure 3.1: Data-flow graph and its node with flow-control interface.

3.2.1 Data-flow accelerators with custom computing circuits on FPGAs

As the semiconductor scaling technology goes into sub-10nm, profound difficulties become tangible in terms of transistors per cost, limitation of power density, and latency of data-movement. These restrictions make it much more difficult for the conventional microprocessor architectures, such as multi-core CPUs and many-core accelerators including GPUs, to scale their performance substantially because they are not designed to efficiently utilize hardware resources of sub-10nm devices for performance. To make matters worse, these conventional architectures are latency-sensitive in scaling performance, and therefore, it also becomes more difficult to scale a system with many chips connected at relatively higher latency for data movement among chips.

Under the circumstance, FPGA-based reconfigurable data-flow computing is attracting attention as a promising solution for efficient and scalable computation with sub-10nm chips connected at high data-movement latency. FPGA is a semiconductor device where circuits can be reconfigured by a designer after manufacturing. FPGA contains an array of programmable logic blocks with registers, on-chip memories (called block RAMs), DSP blocks, and various I/O blocks. Using the available hardware resources on FPGA, we can construct various hardware structures with an architecture customized to individual application. This hardware customizability can bring efficient computation where switching and data movement are achieved with less redundancy. In addition to this excellent nature of reconfigurability, state-of-the-art FPGA devices are now being given hard macros including floating-point DSP blocks (FP-DSPs), high-bandwidth memory controllers, and high-speed serial transceivers, which are advantageous to high-performance computing.

The key to obtain high-performance out of hardware customizability is pipelining, where more stages can perform more operations with a data stream even with a limited bandwidth. So far, a number of studies have been reported on successful FPGA-based stream computing. For FPGA-based stream computing, usually computation in a loop body is expanded to a data-flow graph (DFG), and then converted to a pipelined datapath containing a lot of operators. By streaming data from a memory to the pipeline, we execute data-flow computing with an FPGA.

So far, we have been developing an FPGA-based accelerator with a stream computing model for a wide range of applications including high-performance computing [1][3][4][5][7]. The on-chip accelerator system is composed of *FPGA shell* and *a user-designed core*. The FPGA Shell is an fixed part of hardware system containing peripherals such as PCI-Express (PCIe) interface, scatter-gather DMAs, DDR3 memory controllers, and performance counters, which are unchanged for different applications. In the user-designed core, a pipelined circuit customized for a target application is implemented for its stream computing. The circuit is designed based on the DFG of a loop kernel. For example, the DFG of the following computation:

$$z = (x_1x_2 + x_3x_4) + (x_5x_6 + x_7x_8). \tag{3.1}$$

is given by Fig.3.1a, where each node corresponds to a floating-point operator. To achieve the data flow control for triggering the operation when all its inputs become ready, we designed the template hardware structure of each DFG node, which is shown in Fig.3.1b. The structure is composed of the node processing pipeline for the node operation, and the flow-control interface.

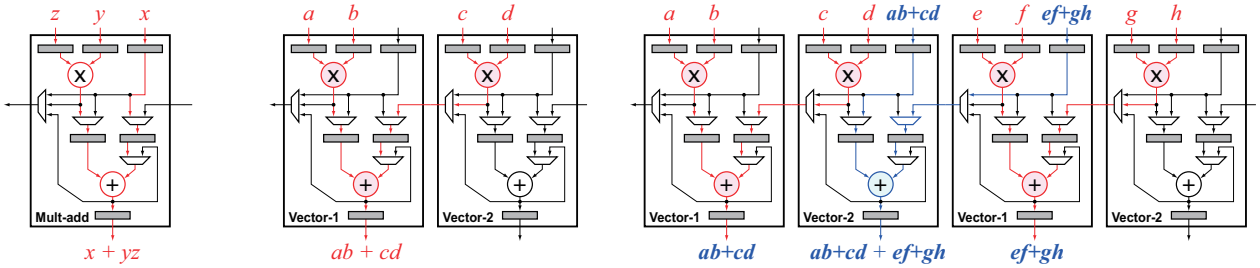

a) Multiply-add (MA). b) Scalar product of 2x2 (SP2x2). c) Scalar product of 4x4 (SP4x4).

Figure 3.2: Floating-point DSP block (FP-DSP) structure of Arria10 FPGA, and its modes; Multiply-add, Scalar product of 2x2, and Scalar product of 4x4.

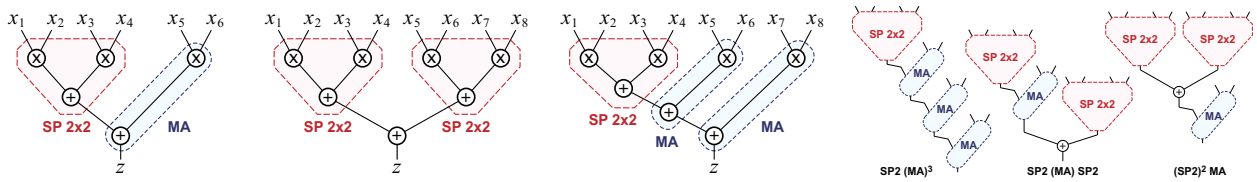

a) SP3x3 as SP2(MA). b) SP4x4 as $(SP2)^2$. c) SP4x4 as $SP2(MA)^2$. d) Three combinations for SP5x5.

Figure 3.3: Various assignment for grouped operators.

3.2.2 Data-flow hardware compiler for custom computing with FPGA

One classical way to design circuits is to write codes in hardware description language (HDL) such like Verilog-HDL and VHDL, to make register-transfer level (RTL) description of the hardware. However, in terms of productivity, such a way is not suitable for users who program their own codes for their target applications. Therefore, high-level synthesis (HLS) compilers have been researched and developed so that users can perform computation with FPGAs just by writing abstract description of computation in a software-like abstract format.

We are also developing our own compiler for users to generate a data-flow computing circuit just by writing formulae, which fits the user-designed core in the accelerator system [1][3][4][16][18][19]. We refer to the compiler as a stream processor generator, *SPGen*. SPGen builds a DFG from the input codes with single-assignment formulae, maps nodes in the DFG into hardware resources on FPGA, and then generates Verilog-HDL codes to describe RTL structures with hardware modules and wires for their connection.

In our research, we formulate an optimization problem in mapping DFG nodes onto hardware resources [16][18]. When constructing a stream computing pipeline with a given DFG, there is a design space where we have to explore especially for optimal assignment of operators to hardware resources on an FPGA. This is because the assignment influences the achievable performance due to difference in:

[1] resource utilization,

[2] the number of pipeline stages, and

[3] the sizes of inserted delay nodes.

For 1), we should reduce the hardware size as much as possible by efficiently assigning DFG nodes to resources, so that we can put more stream-processing elements (SPEs) on an FPGA. It is known that we can increase computing performance with more operators pipelined even for the same memory bandwidth.

In particular, in the case that the latest FPGAs such as Arria10 and Stratix10 are used, we should take care of the modes of FP-DSPs because the operator utilization of FP-DSP depend on the modes. Fig.3.2 shows the structure and modes of the FP-DSP in ALTERA Arria10 FPGAs [M.Langhammer2015]. Fig.3.2a is a simplified block diagram of a single FP-DSP, where a floating-point multiplier and an adder are cascaded with pipeline registers and multiplexers. The FP-DSP has three inputs of x, y, z and one output r in addition to the chain-in and the chain-out that are connected to the adjacent FP-DSPs. The FP-DSP has several modes. In *a single-operation (SO) mode*, FP-DSP is used as a single multiplier or adder, resulting in 50% utilization of the operators in an FP-DSP. On the other hand, in *the multiply-add (MA) mode*, both the multiplier and the adder

in FP-DSP are combined and fully used for a multiplication-and-then-addition operation, as shown in Fig.3.2a. Obviously, we can reduce the number of used FP-DSPs by using MA mode instead of using only SO mode.

By using *scalar-product (SP) modes* of Figs.3.2b and c, we can reduce consumption of not only FP-DSPs, but also logic elements and registers. SP modes are for an inner product of n-dimensional vectors, such as a 4-D vector product. We refer to a mode for n-D vector product as SPnxn. Fig.3.2b shows the block diagram of two adjacent FP-DSPs for SP2x2 mode. Here, the FP-DSPs are configured differently with Vector-1 and Vector-2 structures, respectively. The chain-out from the second FP-DSP is connected to the chain-in of the first FP-DSP to form the reduction of the two multiplication results. Fig.3.2c shows the block diagram of four adjacent FP-DSPs for SP4x4 mode, where the reduction tree of Fig.3.1a is implemented with the adders and the general-purpose routing from the outputs to the inputs of FP-DSPs. By forming such operators grouped into a big pipeline, we can also reduce the area of flow-control interface in Fig.3.1b per operator.

Furthermore, we can reduce pipeline stages of a DFG by using MA and SP modes. This is because these MA and SP mode has totally less stages than SO modes, and we can skip latency of the input FIFOs in flow-control interfaces by removing wrappers. Considering the negative effect caused by the prologue and epilogue in pipelining, a shorter pipeline is favorable for higher utilization. Simultaneously, the delay nodes that are inserted into a DFG get smaller because the delay difference to be adjusted is also expected to be smaller.

Thus, we have an grouping problem in mapping DFG nodes onto hardware, and it has a combinational space to be explored. However, finding an optimal solution by hand is a difficult task, which results in low productivity, particularly when a DFG is large. To automate the process for higher productivity, we are developing an algorithm and a tool to explore the design space for DFG nodes to be appropriately grouped and mapped onto FP-DSPs on FPGA.

Hereafter, we refer to the operators of MA and SPs as *big operators*. Moreover, we refer to the operators in the found subgraph that is assigned to MA of SP modes of FP-DSP as *grouped operators*. Now we are developing an algorithm trying to find as many larger subgraphs as possible in a given DFG to be replaced with less big operators than the grouped operators in the subgraphs. We search replaceable subgraphs by matching big operators in the following order:

$$\text{SP8x8} \rightarrow \text{SP7x7} \rightarrow \cdots \rightarrow \text{SP2x2} \rightarrow \text{MA}.$$

This is because the expected reduction of FP-DSPs and pipeline stages decreases in this order of big operators.

In general, SPnxn operators, such that $n \geq 3$, are generated by using several SP2x2 and MA operators. For example, the big operator of SP3x3 is composed of single SP2x2 and single MA as shown in Fig.3.3a. Besides, the big operators of SP4x4-8x8 have multiple sorts of DFGs because of the way to combine SP2x2 and MA operators. For example, SP4x4 operator has two sorts of DFGs. To generate SP4x4 operator, the elementary operators, i.e. SP2x2 and MA, are selected so that the total number of multiplier is 4. One kind of DFG is composed of two SP2x2 operators as shown in Fig.3.3b. Combination of two SP2x2 operators with an adder generates a single SP4x4 operator. On the other hand, the other DFG of SP4x4 is composed of a single SP2x2 and two MA operators as shown in Fig.3.3c. Connection of the SP2x2 and MAs in the order of SP2(MA)^2 also constructs a single SP4x4 operator with another structure of DFG. SP5x5 also has three variants of DFG as shown in Fig.3.3d. Similarly, bigger operators like SP6x6 and SP8x8 have more variants with smaller operators combined in a DFG.

In our developed algorithm, we are trying to pick up subgraphs containing more and bigger operators as possible. For example, we prefer Fig.3.3b than Fig.3.3d for a subgraph of SP4x4. We will evaluate difference in area and operating frequency of generated hardware among differently grouped operators.

3.2.3 Hardware-based bandwidth compressor

High-performance computing with the data-flow model requires sufficient bandwidth to feed data streams into hardware from external memories and/or network interfaces to connect multiple semiconductor devices. If available bandwidth is lower than required bandwidth, operators in data-flow circuits are not sufficiently utilized resulting in degraded sustained performance. However, it is not easy to drastically increase the bandwidth of off-chip I/O pins for memory interfaces and network interfaces. Even if it is possible, it would require more cost and power consumption to obtain higher off-chip bandwidth.

To enhance sustained bandwidth without physical improvement, we have proposed hardware-based data compression of numerical data [2][5][6], which performs high-throughput on-the-fly lossless compression of a floating-point data stream. With data compression, we can enhance sustained bandwidth by encoding more data into a channel at the same bandwidth. This means that the physical bandwidth can efficiently be utilized

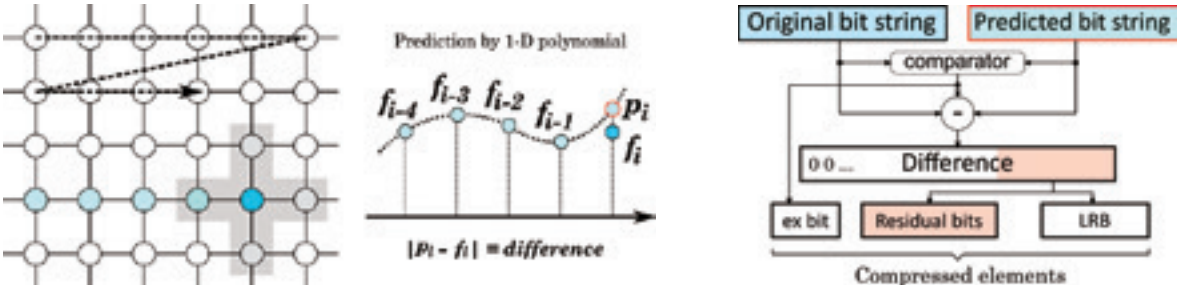

a) Prediction assuming numerical continuity. b) Compression algorithm.

Figure 3.4: Compression algorithm.

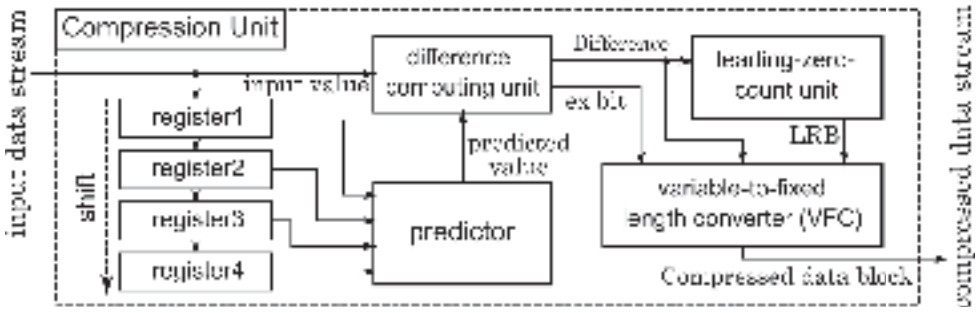

Figure 3.5: Block diagram of data compression hardware.

with compressed data streams where redundancy is reduced. If the data are compressed to $1/r$ of the original size at the compression ratio of r, we can send r times more data at the same bandwidth.

For compression, we rely on numerical continuity in a data stream as shown in Fig.3.4a. We generate a data stream by traversing n-dimensional grid. Since such data on a grid are intermediate results of numerical simulation with partial differential equations as government equations, we can assume that they have some continuity. In this research, we assume polynomial continuity that can be used to predict the next element of the data stream with several last elements. Fig.3.4a shows an example of 3rd order polynomial prediction using the three data values: f_{i-4} to f_{i-1}.

Since the difference between the predicted value and the original value become closer to zero if the data stream well follows the assumed continuity, we can encode the difference with less bits. Fig.3.4b shows the algorithm of our prediction-based compression, where we encode the non-zero part of the difference, called residual bits, with the exchange-bit (ex-bit), the residual bits, and the length of residual bits (LRB). The ex-bit and LRB have a fixed bit length of 4 bits, while the length of the residual bits is variable. When the residual bits have only 4 bits, the original 32-bit floating-point value is expressed with 8 bits resulting in the compression ratio of $r = 32/(4 + 4) = 8$.

Fig.3.5 shows the structure of the hardware-based data compressor. The hardware is pipelined and takes several clock cycles, however, such latency doesn't affect the overall performance of stream computation as long as the throughput is maintained. We designed the hardware achieving high-throughput processing.

So far we have applied the hardware-based compressor only to 32-bit single-precision floating-point data streams. To improve its applicability, we modified the compressor for various data types including double, single, half-precision floating-point data, and investigated the compression ratio and the circuit area. In addition to clarification of the relationship between data types and the compression performance/hardware area, we improved the design of the compressor by introducing the partial-prediction mechanism for double-precision floating-point data, so that its circuit area is reduced.

3.3 Schedule and Future Plan

From the research activities on the data-flow computing system so far, the following items are achieved:

[1] Custom computing hardware for stream computing with FPGA based on the data-flow computing model.

[2] Data-flow hardware compiler for custom computing with FPGA, and the formulation of an optimization problem in mapping DFG to hardware.

[3] Hardware-based bandwidth compressor and its improvement.

For the first achievement, we are now extending it to multiple FPGA chips connected by a dedicated network. For the second, we are developing more sophisticated algorithms for design space exploration, and a compiler front-end for existing software language like C. For the third, we are planning to apply the bandwidth compression to various computing problems running on FPGAs.

3.3.1 Articles

[1] Kohei Nagasu, Kentaro Sano, Fumiya Kono, and Naohito Nakasato, "FPGA-based Tsunami Simulation: Performance Comparison with GPUs, and Roofline Model for Scalability Analysis," Journal of Parallel and Distributed Computing, Vol.106, pp.153-169, DOI:10.1016/j.jpdc.2016.12.015, 2017.
[2] Tomohiro Ueno, Kentaro Sano, and Satoru Yamamoto, "Memory Bandwidth Compressor for FPGA-based High-Performance Custom Stream Computation," ACM Transactions on Reconfigurable Technology and Systems (TRETS), Vol.10, No.3, Article No.18, DOI:10.1145/3053688 (22 pages), May, 2017.
[3] Kentaro Sano and Satoru Yamamoto, "FPGA-based Scalable and Power-Efficient Fluid Simulation using Floating-Point DSP Blocks," IEEE Transactions on Parallel and Distributed Systems (TPDS), Vol.28, Issue.10, pp.2823-2837, DOI:10.1109/TPDS.2017.2691770, Oct 2017.
[4] Kentaro Sano, Shin Abiko, and Tomohiro Ueno, "FPGA-based Stream Computing for High-Performance N-Body Simulation using Floating-Point DSP Blocks," Proceedings of the International Symposium on Highly-Efficient Accelerators and Reconfigurable Technologies (HEART), Article No.16, DOI:10.1145/3120895.3120909 (6 pages), June, 2017.
[5] Antoniette Mondigo, Tomohiro Ueno, Daichi Tanaka, Kentaro Sano*, and Satoru Yamamoto, "Design and Scalability Analysis of Bandwidth-Compressed Stream Computing with Multiple FPGAs," Proceedings of the International Symposium on Reconfigurable Communication-centric Systems-on-Chip (ReCoSoC), USB Stick(paper#s4p1, 8 pages), July, 2017.
[6] Tomohiro Ueno*, Kentaro Sano, and Takashi Furusawa, "Performance Analysis of Hardware-Based Numerical Data Compression on Various Data Formats," Proceedings of the Data Compression Conference (DCC), pp.345-354, March, 2018.
[7] Antoniette Mondigo, Tomohiro Ueno, Daichi Tanaka, Kentaro Sano, and Satoru Yamamoto, "High-Performance Scalable Stream Computing with Multiple FPGAs," 2017 年ハイパフォーマンスコンピューティングと計算科学シンポジウム予稿集 (HPCS2017), poster paper#P4-4 (1 page), June 5-6, 2017.

3.3.2 Invited Talks

[8] 佐野 健太郎, "ポストムーア時代のデータフローアーキテクチャと FPGA による高性能計算," 第 19 回イノベーション協創研究会 (日立中央研究所), March 15, 2017.
[9] 佐野 健太郎, "FPGA による高性能データフロー計算システムの研究開発と数値流体力学計算への応用," CAE 計算環境研究会第 10 回シンポジウム (帝京大学霞が関キャンパス), Dec 4, 2017.
[10] 佐野 健太郎, "FPGA を用いた高性能計算の可能性とデータフロープログラミング," 第 17 回 PC クラスタシンポジウム (秋葉原コンベンションホール), Dec 15, 2017.
[11] Kentaro Sano, "Data-flow HPC with custom hardware on FPGA cluster," SIAM Conference on Parallel Processing for Scientific Computing (PP18), Waseda University, Tokyo, Japan, March 10, 2018.
[12] Kentaro Sano, "Data-Flow Hardware Optimization by Design Space Exploration," 3rd International Workshop on FPGA for HPC (IWFH), Akihabara, Tokyo, Japan, March 12, 2018.
[13] Kentaro Sano, "The path toward reconfigurable high-performance computing," 5th Workshop on Japan-USA Collaboration for Extreme-scale System Software, Akihabara, Tokyo, Japan, March 13, 2018.

3.3.3 Papers (non-reviewed)

[14] 安孫子 慎, 佐野健太郎, 上野 知洋, "浮動小数点 DSP 搭載 FPGA を利用したストリーム計算に基づく高性能多体問題シミュレーション専用計算機," 電子情報通信学会リコンフィギャラブルシステム研究会 信学技法, Vol.117, No.46, pp.87-92, May, 2017.
[15] 田中 大智, Antoniette Mondigo, 佐野 健太郎, 山本 悟, "密結合 FPGA クラスタによる並列流体計算の通信性能評価," 第 31 回数値流体力学シンポジウム講演論文集, CDROM(paper No. C01-3, 1 page), Dec 12, 2017.

[16] 長州 航平, 佐野 健太郎, 山本 悟, ”FPGA を利用した津波シミュレーション専用計算機の資源割当て最適化と性能評価,” 第 31 回数値流体力学シンポジウム講演論文集, CDROM(paper No. C01-2, 1 page), Dec 12, 2017.
[17] 田中 大智, Antoniette Mondigo, 佐野 健太郎, 山本 悟, ”密結合 FPGA クラスタのための直接網の設計と評価,” 電子情報通信学会リコンフィギャラブルシステム研究会 信学技法, Vol.117, No.379, pp.71-76, Jan, 2018.
[18] 長洲 航平, 佐野 健太郎, ”FPGA によるデータフロー計算機におけるハードウェア資源割当て最適化,” 電子情報通信学会リコンフィギャラブルシステム研究会 信学技法, Vol.117, No.379, pp.145-150, Jan, 2018.
[19] 李 珍泌, 上野 知洋, 佐藤 三久, 佐野 健太郎, ”FPGA 向けストリームプロセッサ生成のための C 言語フロントエンドの開発,” 第 163 回ハイパフォーマンスコンピューティング研究発表会 情報処理学会研究報告, Vol.HPC163, (7 pages), Feb, 2018.

3.3.4 Other publications

[20] 佐野 健太郎, ”今どきコンピュータ科学計算の基礎知識,” CQ 出版 Interface 2017 年 6 月号 スパコン技術研究コーナ, pp.168-173, April, 2017.
[21] Kentaro Sano, ”Accelerating Simulation of Tsunamis,” Intel Design Solutions (日本語:佐野 健太郎, ”津波のシミュレーションの高速化”, デザイン・ソリューション), 4 pages, Mar, 2017.

Chapter 4

Large-scale Parallel Numerical Computing Technology Research Team

4.1 Members

Toshiyuki Imamura (Team Leader)

Yiyu Tan (Research Scientist)

Yusuke Hirota (Postdoctoral Researcher)

Yoshiharu Ohi (Postdoctoral Researcher)

Daichi Mukunoki (Postdoctoral Researcher/Visiting Researcher, Tokyo Women Christian University)

Tetsuya Sakurai (Senior Visiting Researcher, University of Tsukuba)

Daisuke Takahashi (Senior Visiting Researcher, University of Tsukuba)

Yoshio Okamoto (Visiting Researcher, The University of Electro-Communications)

Franz Franchetti (Visiting Researcher, Carnegie Mellon University)

Takeshi Fukaya (Visiting Researcher, Hokkaido University)

Sarah Huber (Visiting Researcher, Bergische Universtät Wuppertal)

Martin Galgon (Visiting Researcher, Bergische Universtät Wuppertal)

Andreas Marek (Visiting Researcher, Max-Plank Computing & Data Facility)

Doru Adrian Thom Popovich (Student Trainee, Carnegie Mellon University)

Masaaki Aoki (Student Trainee, Kobe University)

Masatoshi Takayanagi (Student Trainee, Yamanashi University)

Ryota Kayanuma (Student Trainee, The University of Electro-Communications)

Koichiro Watanabe (Student Trainee, The University of Electro-Communications)

Haruka Yamada (Intern, University of Tsukuba)

Aya Motohashi (Assistant)

4.2 Research Activities

The Large-scale Parallel Numerical Computing Technology Research Team conducts research and development of large-scale, highly parallel and high-performance numerical software for K computer. Simulation programs require various numerical techniques to solve systems of linear equations, to solve eigenvalue problems, to compute and solve non-linear equations, and to do fast Fourier transforms. In addition, since 2016 we have started to investigate Tensor decomposition and its accelerations on some emerging devices.

From the previous research experiences, we completely understand that it must be essential to select appropriate algorithms and develop software packages by assembling numerical libraries based on the significant concepts of high parallelism, high performance, high precision, resiliency, and scalability. Our primary mission is to develop and deploy highly-parallelized and scalable numerical software framework on the K computer, namely KMATHLIB. It comprises several components to solve specific problems such as

- systems of linear equations,
- eigenvalue problems,
- singular value decomposition,
- fast Fourier transforms,
- higher order data (Tensor) decomposition, and
- nonlinear equations.

The K- and post-K- related issues are also our challenging works such as

- communication reducing and avoidance,
- cooperation with advanced development devices,
- fault detection (soft-error), and
- precision-aware computing (higher-or-reduced/variable-or-mixed accuracy).

We are going to complete our mission through a tighter collaboration among computational science (simulation), computer science (hardware and software), and numerical mathematics. Our final goal is to establish fundamental techniques to develop numerical software libraries for next-generation supercomputer systems based on active cooperation within AICS.

4.2.1 Communication avoiding optimization

Following the research activities in FY2016-2017, we conducted the studies regarding **communication avoiding** techniques to improve the solver performance. They are mainly done under three frameworks;

[1] K Grant-in-Aid, especially for, eigenvalue solver,

[2] flagship 2020 project cooperating with the architecture team, and

[3] collaboration between Japan Atomic Energy Agency.

4.2.1.1 CA Conjugate Gradient method on a large-scale plasma simulation code

Through collaboration with Dr. Yasuhiro Idomura from Japan Atomic Energy Agency, several huge-scale plasma CFD simulations for future exascale computing are studied. In these CFD simulations, the implicit solver for solving a system of the linear equations based on the Krylov subspace method dominates computational time, and it has numerical difficulties and less parallel scalability. We examined the feasibility of Communication Avoiding CG (CACG) methods, including s-step CG, pipeline CG, and a matrix power kernels (MPK) to address this problem.

Since FY2016, we have been developing the Chebyshev Basis CG (CBCG) method as one of CACG methods, and we have investigated an appropriately preconditioned CBCG method, namely P-CBCG. In the numerical simulation code, we computed complex multi-phase flows consisting of gas and multi-component liquid, and so on. Since a system of linear equations to be solved shows an ill-condition property, we expect that the P-CG

solver improves the convergence. In the numerical experiment by using the P-CACG method and the P-CBCG method, we observed proper strong scaling when a benchmark code was tested on an ICEX system and a KNL system. However, the results obtained on both systems show a different tendency, which is also confirmed on the K computer system (the cost model follows $1/s$ perfectly on the K computer, here, s refers to the number of bases). We need to clarify such performance degradation on present systems concerning the network latency and network bandwidth. The research progresses regarding the CACG methods and CA-preconditioners were presented at ScalA@17 [9], AESJ Spring meeting [20], SIAM PP 18 [28] and [31], and SCAsia 2018 [11]. Moreover, the other type of iterative method for sparse eigensolver was reported at ParCo 2017 [7], SCAsia 2018 [12], and IPSJ SIGHPC [22].

4.2.1.2 2.5D PDGEMM

For a seamless transition to the emerging system, the post-K computer, we are developing a new parallel matrix multiplication routine (so-called PDGEMM in PBLAS) that can achieve **proper strong scaling** on the post-K computer using the 2.5D algorithm with the help of **communication avoidance**. The 2.5D algorithm requires a 2.5D matrix distribution stacking a matrix with a 2D distribution over a 3D process grid. To support the compatibility with the conventional PDGEMM, which computes matrices distributed as a 2D distribution on a 2D process grid, our implementation was designed to perform a matrix redistribution between 2D and 2.5D distributions before and after the computation (2D-compatible 2.5D-PDGEMM).

From FY2015 to FY2017, we have developed prototype implementations based on the Cannon's algorithm and the SUMMA algorithm, furthermore, evaluated the performance using up to 16384 nodes of the K computer. The results showed that our implementations outperformed conventional 2D-PDGEMMs including the PBLAS PDGEMM even when the matrix redistribution cost between 2D and 2.5D distributions was included. For example, we observed that our implementation (with stack size c=4) achieved an approximately 3.3-fold speed increase in the case of 16,384 nodes (matrix size: n=32,768) when compared with the 2D implementation (some of the results were reported in the previous Annual report for FY2016-17).

In FY2017-18, we first presented the result in a technical paper in IPSJ SIGHPC [13] and a poster at ISC 2017 [15]. Besides, we have created a performance model, which can explain the observed performance on the K computer, and estimated the latency costs in the MPI communications and the performance on 65536 nodes on the K computer. We presented the result in a paper submitted to PPAM 2017 [5], and a talk at SIAM PP18 [29].

4.2.2 New scheduling policy based on a Batched BLAS

Since 2012, we have been developing the EigenExa library towards and beyond post-peta-scale computer systems. EigenExa is a parallel numerical library to solve large-scale standard eigenvalue problems. The performance results were reported, for example at JSST2017 [8], JLESC [17], EPASA 2018 [25], and SIAM PP18 [30]. It outperforms ScaLAPACK on the K computer. However, we have positioned a performance bottleneck in the divide-and-conquer part, which comes from a static and sequential scheduling policy in the present implementation.

We proposed a new parallel divide-and-conquer algorithm based on an execution schedule by using batched kernels to solve real-symmetric tridiagonal eigenvalue problems on manycore systems. Our scheduling policy reschedules the sequence of tasks at the same level of the task tree and aggregates multiple tasks which call same BLAS routine into a group of batch operations (see Fig. 4.1). The new algorithm increases **parallelism** and requires **less global synchronizations** than the conventional scheduling which was implemented in the previous codes. We compared the performance of the solver based on our new algorithm by using two manycore processors (Intel Xeon Phi Knight Corner and Knight Landing) and a general multicore processor (Intel Xeon E5). The obtained results show that the solver with the algorithm is comparable to the Intel MKL on a Xeon E5 and outperforms the Intel MKL and PLASMA on the two Xeon Phi systems (See Fig. 4.2). The idea and results were presented at PPAM2017 [4].

4.2.3 Block Jacobi eigensolver

Under the collaboration framework with Prof. Yusaku Yamamoto from the University of Electro-Communications, his Ph.D. candidate, Mr. Shuhei Kudo, and our team have investigated the parallel one-sided blocked Jacobi method. Especially in FY2017-2018, Mr. Kudo implemented a singular value decomposition method

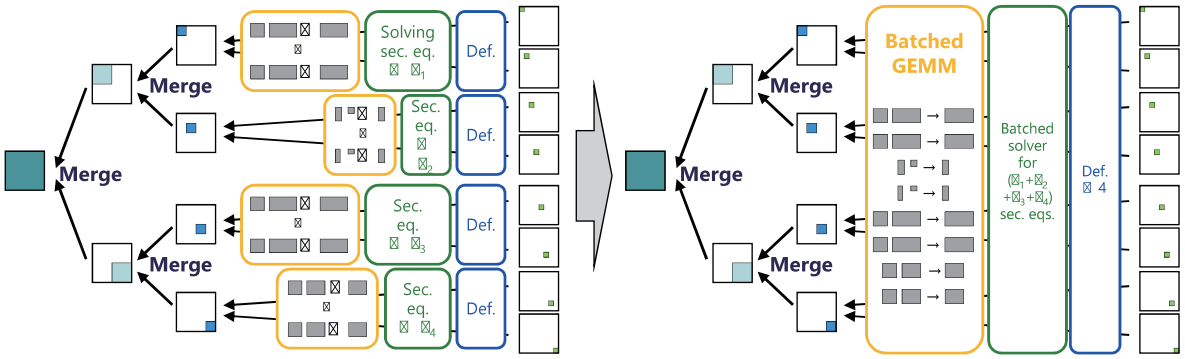

Figure 4.1: New task scheduling based on a Batched BLAS

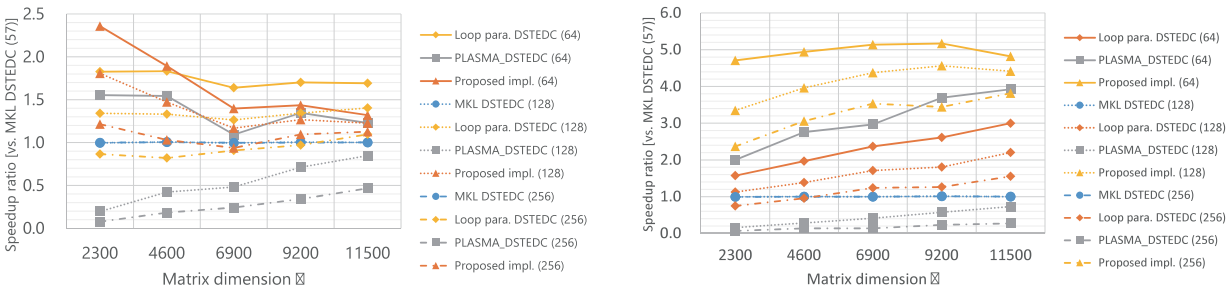

Figure 4.2: Performance improvement of the DC algorithm based on the BatchedBLAS (Left: Inversion of a Frank matrix, Right: random matrix)

for distributed-memory environments, and we obtained better performance improvement compared with the ScaLAPACK's implementation.

Both the eigen and the singular value decomposition based on the Jacobi method work accurately but slow due to their large number of iterations. The 2D blocking data distribution for the blocked Jacobi method is a crucial idea to reduce both communication volume and counts rather than the simple 1D blocking. It has the critical features of **communication avoidance** and also improves the **parallelim** that were argued in previous subsections. Mr. Kudo proposed the novel AllReduce-type algorithm for the one-sided blocked Jacobi (OSBJ) method, which was expected to improve the total performance due to the improvement of parallelization on the matrix-matrix multiplication. Kudo's implementation exhibited excellent parallel performance while it was still an early experimental version. The Fig. 4.3 presents a strong scalability result using up to 12,288 nodes in the K computer, in which the experimental system achieved about two-fold or more performance improvement over the ScaLAPACK's implementation.

4.2.4 Sparse tensor decomposition

With the explosion of data, scalable and fast solutions for mining and analyzing massive amounts of data are becoming essential. Tensor decomposition has recently become popular in data analytics due to its ability to identify possible relations and predicting missing elements among high-dimensional data. Nowadays, it has been used in many applications, such as computer vision, signal processing, healthcare data analysis, recommender systems, and machine learning. In many of these applications, the tensor representation of data is high-dimensional and sparse, and the number of non-zero entries is vast. For example, a tensor-based on Amazon review text has dimensions of 4.8 million $\times$ 1.7 million $\times$ 1.8 million and contains 1.7 billion non-zero entries. Therefore, efficient tensor decompositions are indispensable for analyzing such huge datasets. In this research, the SPLATT, a sparse tensor decomposition toolkit based on the CANDECOMP/PARAFAC decomposition (CPD), is introduced and evaluated on the K computer, and its scalability and computation efficiency are

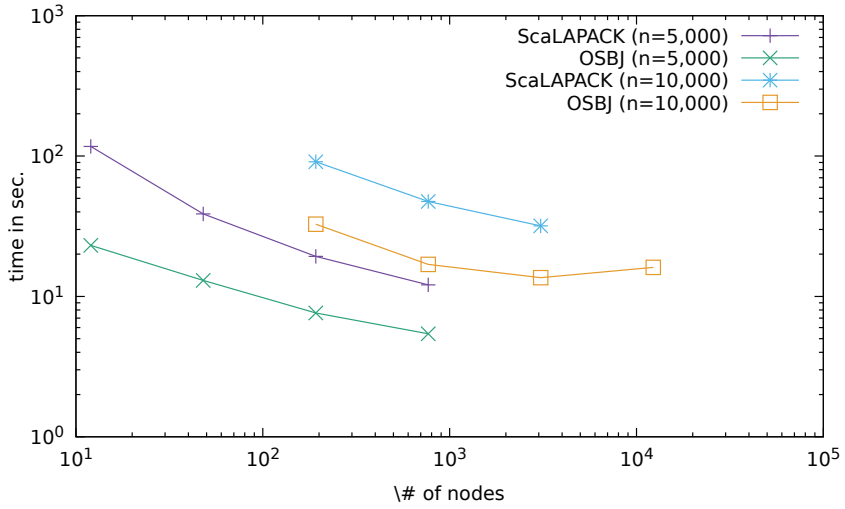

Figure 4.3: The strong scalability of SVD using our implementation and ScaLAPACK's PDGESVD on K-computer

investigated. Fig. 4.4 presents the average time taken by each iteration and the MPI communication volume when the test dataset is Amazon-Reviews. Fig. 4.4a indicates that the system scalability looks good. From Fig. 4.4b, as the number of the computation nodes is increased, the average MPI communication is decreased significantly. The related results were presented at the Tensor-Network workshop hosted by our team [18], SIAM PP 18 [27], and ATAT 2018 [32].

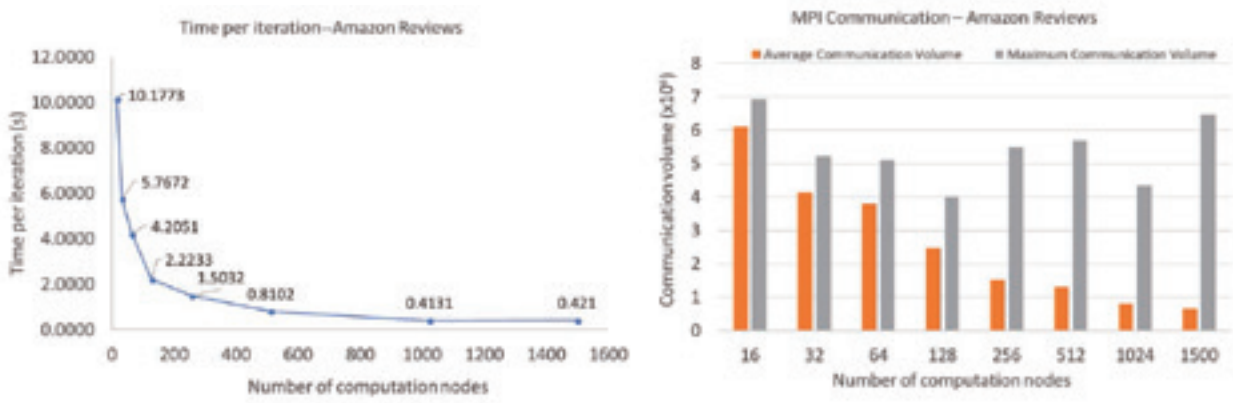

(a) Time taken by each iteration (b) MPI communication

Figure 4.4: Performance of SPLATT tested by the Amazon-Reviews

4.2.5 Energy efficient FPGA-based matrix multiplier

Matrix multiplication is the fundamental building block of numerical linear algebra, and dramatically affects the high-performance computing (HPC) applications. Even now, how to improve the performance of matrix multiplication at hardware and software level is still an open problem although many methods have already been developed to speed up computation through parallel programming in supercomputers or cluster systems. Unfortunately, because of the power wall and memory wall, performance and power improvements due to technology scaling and instruction level parallelism in general-purpose processors have ended. Moreover, the

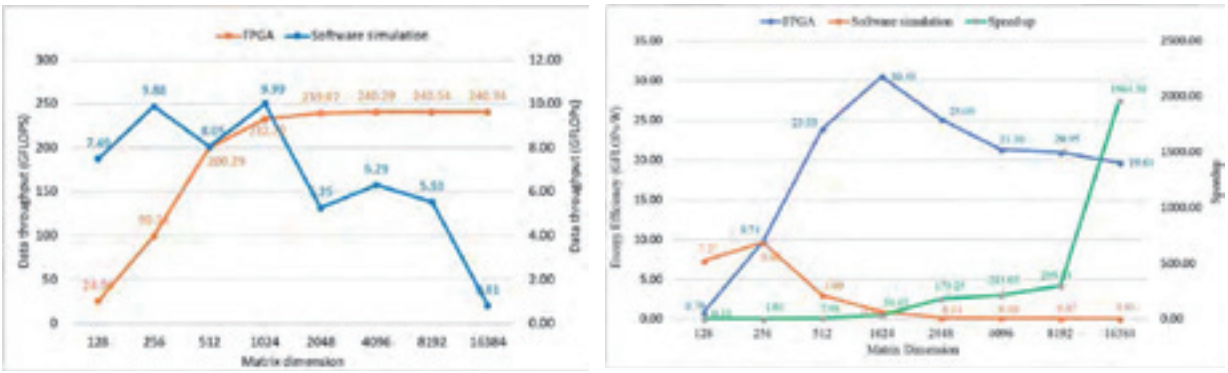

(a) Data throughput (b) Energy efficiency

Figure 4.5: Performance of the FPGA-based matrix multiplier

guiding metric to evaluate the performance of computing systems is evolved from computing power (FLOPs: floating-point operations per second) to energy efficiency (computing power/power consumption: FLOPs/W) at post-Moore's era. How to reduce power consumption while increasing performance is one of the core concerns in future HPC systems. It is well known that heterogeneous systems with hardware specialization in the form of GPUs, FPGAs, and ASICs, offer a promising path toward major leaps in processing capability while achieving high energy efficiency. In this research, an FPGA-based matrix multiplier, which is design by using OpenCL, is presented to improve energy efficiency. Fig. 4.5 shows the data throughput and energy efficiency of the proposed matrix multiplier in the case of different matrix scales. When data are single precision floating-point, and matrix dimension is 16,384×16,384, the matrix multiplier implemented by the FPGA board DE5a-NET achieves 240GFLOPs in data throughput and 19.64 GFLOPs/W in energy efficiency, which are about 300 times and 2000 times over the software simulation carried out on a PC with 32 GB DDR4 RAMs and an AMD processor Ryzen 7 1700 running at 3.0 GHz, respectively. The related results were published at IEEE ICECS [10], and presented at JLESC [16].

4.2.6 Other activities

In the year of FY2017-2018, the following studies were also done and published by the team:

[1] Perfect Matched Layer (PML) for 2D vorticity analysis (Trans. JSIAM [1]),

[2] Real-time sound rendering processor (Applied Science [2]),

[3] Re-design of modernized API for numerical linear algebra (ParCo2017 [6]),

[4] Double-double data format (iWAPT2017 [3]),

[5] HOTRG (High-order Tensor Renormalization Group) (SIAM PP18 [26]), and

[6] Three dimensional parallel FFT (IPSJ SIGHPC [19] and [24]).

4.3 Schedule and Future Plan

Some of the technology trends towards the post-K computer have become clear in the FY, and we recognized that some of the optimization technologies studied on manycore architecture are of significance in the second phase of the team activities. For a short-term research milestone, we would like to focus on following topics and accelerate our research activities in FY2018-2021 when the post-K computer is expected to be launched in regular operations.

- 'Communication avoiding' algorithm:
  We continue to investigate the communication avoiding algorithms and methods in any view of numerical linear algebra.

- ‘Reproducible and maintainable numerical software framework’:
  During the first phase (FY2012-2016), we developed a common framework to plugin OSS software, namely, KMATHLIB-API. However, we recognized that a more flexible and customizable mechanism was required for future systems by combining the features of modern programming languages and run-time systems. Therefore, we would like to collaborate with the system software and architecture development team and the compiler development team.

- ‘Precision-and-power aware computing’:
  We have studied high-precision numerical software, for example, QP-BLAS and QP-Eigen, under a collaboration with JAEA. Recently, we recognized that another critical issue came from power consumption. As calculation with reduced precision and a wider SIMD instruction set are prominent technologies for energy saving, in addition, taking advantage of an FPGA or a similar customizable precision would be another direction of future numerical software, thus, precision-and-power aware computing is an essential theme of the team.

4.4 Publications

4.4.1 Articles

[1] Daijiro Sonoda, Yoshiharu Oi, and Tomoya Tatsuno, ‘Implementation of a Fictitious Absorbing Layer for Two-Dimensional Vorticity Equations Based on the Perfectly Matched Layer,’ Transactions of Japan Society of Industrial and Applied Mathematics, Vol. 27, No.2, pp. 84–111, 2017 (*written in Japanese*, 園田 大二郎，大井祥栄，龍野智哉, 2 次元渦度方程式への Perfectly Matched Layer に基づく仮想吸収層の実装, 日本応用数理学会論文誌，日本応用数理学会)
[2] Tan Yiyu, Yasushi Inoguchi, Makoto Otani, Yukio Iwaya, and Takao Tsuchiya, ‘A Real-Time Sound Field Rendering Processor,’ Applied Science, 2018, 8, 35.
[3] Susumu Yamada, Toshiyuki Imamura, Takuya Ina, Narimasa Sasa, Yasuhiro Idomura, and Masahiko Machida, ‘Quadruple-Precision BLAS Using Bailey’s Arithmetic with FMA Instruction: Its Performance and Applications’, 2017 IEEE International Parallel and Distributed Processing Symposium Workshops, IPDPS Workshops 2017, Orlando / Buena Vista, FL, USA, May 29 – June 2, 2017, pp. 1418–1425, 2017.
[4] Yusuke Hirota, and Toshiyuki Imamura, Parallel Divide-and-Conquer Algorithm for Solving Tridiagonal Eigenvalue Problems on Manycore Systems, Parallel Processing and Applied Mathematics — 12th International Conference, PPAM 2017, Lublin, Poland, September 10–13, 2017, Revised Selected Papers, Part I, Lecture Notes in Computer Science, Vol. 10777, pp. 623–633, 2017.
[5] Daichi Mukunoki, and Toshiyuki Imamura, ‘Implementation and Performance Analysis of 2.5D-PDGEMM on the K Computer’, Parallel Processing and Applied Mathematics — 12th International Conference, PPAM 2017, Lublin, Poland, September 10–13, 2017, Revised Selected Papers, Part I, Lecture Notes in Computer Science, Vol. 10777, pp. 348–358, 2017.
[6] Toshiyuki Imamura, Daichi Mukunoki, Yusuke Hirota, Susumu Yamada, and Masahiko Machida, ‘Design Towards Modern High Performance Numerical LA Library Enabling Heterogeneity and Flexible Data Formats’, Parallel Computing is Everywhere, Proc. of the International Conference on Parallel Computing, ParCo 2017, 12–15 September 2017, Bologna, Italy, pp. 97–106, 2017.
[7] Susumu Yamada, Toshiyuki Imamura, and Masahiko Machida, ‘Communication Avoiding Neumann Expansion Preconditioner for LOBPCG Method: Convergence Property of Exact Diagonalization Method for Hubbard Model’, Parallel Computing is Everywhere, Proc. of the International Conference on Parallel Computing, ParCo 2017, 12–15 September 2017, Bologna, Italy, pp. 27–36, 2017.
[8] Yusuke Hirota, and Toshiyuki Imamura, ‘Performance Analysis of a Dense Eigenvalue Solver on the K Computer,’ Proc. the 36th JSST Annual International Conference on Simulation Technology, 25–27 October 2017, Tokyo, Japan, pp. 232–235, 2017.
[9] Yasuhiro Idomura, Takuya Ina, Akie Mayumi, Susumu Yamada, K. Matsumoto, Yuuichi Asahi, and Toshiyuki Imamura, ‘Application of a communication-avoiding generalized minimal residual method to a gyrokinetic five dimensional eulerian code on many core platforms,’ Proc. the 8th Workshop on Latest Advances in Scalable Algorithms for Large-Scale Systems, ScalA@SC 2017, Denver, CO, USA, November 13, 2017, pp. 7:1–7:8, 2017.
[10] Yiyu Tan, and Toshiyuki Imamura, ‘An energy-efficient FPGA-based matrix multiplier’, Proc. 24th IEEE International Conference on Electronics, Circuits and Systems, ICECS 2017, Batumi, Georgia, December 5–8, 2017, pp. 514–517, 2017

[11] Yasuhiro Idomura, Takuya Ina, Akie Mayumi, Susumu Yamada, and Toshiyuki Imamura, 'Application of a Preconditioned Chebyshev Basis Communication-Avoiding Conjugate Gradient Method to a Multiphase Thermal-Hydraulic CFD Code', Supercomputing Frontiers — 4th Asian Conference, SCFA 2018, Singapore, March 26-29, 2018, Proceedings, Lecture Notes in Computer Science, Vol. 10776, pp. 257–273, 2018

[12] Susumu Yamada, Toshiyuki Imamura, and Masahiko Machida, 'High Performance LOBPCG Method for Solving Multiple Eigenvalues of Hubbard Model: Efficiency of Communication Avoiding Neumann Expansion Preconditioner,' Supercomputing Frontiers — 4th Asian Conference, SCFA 2018, Singapore, March 26-29, 2018, Proceedings, Lecture Notes in Computer Science, Vol. 10776, pp. 243–256, 2018

4.4.2 Oral talks and Poster presentations

[13] Daichi Mukunoki, and Toshiyuki Imamura,'Implementation and Performace evaluation of a distributed parallel matrix-product base on a 2.5D algorithm using K computer', IPSJ SIG Technical Report (High Performance Computing), Vol. 2017-HPC-159, No. 1, pp. 1–6, April 2017 (*in Japanese*).

[14] Yoshiharu Ohi,'Performance evaluation of time-integral method by using Parareal approach,' Numerical Analysis Symposium 2017 (NAS2017) (*in Japanese*).

[15] Daichi Mukunoki, and Toshiyuki Imamura, 'Implementation and Evaluation of 2.5D Matrix Multiplication on K Computer', ISC High Performance (ISC 2017), research poster session, Jun. 2017.

[16] Yiyu Tan, 'Exploiting Acceleration of Numerical Linear Algebra,' 7th JLESC workshop, Urbana, Illinois, July 2017.

[17] Toshiyuki Imamura, 'HPC Libraries for Solving Dense Symmetric Eigenvalue Problems,' 7th JLESC workshop, Urbana, Illinois, July 2017.

[18] Yiyu Tan, 'SPLATT: a Software Toolkit for Sparse Tensor,' Research meeting 'Tensor-network computing (TN) and Tensor-based numerical software,' RIKEN AICS, 3–4 August 2017.

[19] Masaaki Aoki, Yusuke Hirota, Toshiyuki Imamura, and Mitsuo Yokokawa, 'Research on the scalability of KNL by using FFT kernels,' IPSJ SIG Technical Report (High Performance Computing), Vol. 2017-HPC-161, No. 16, pp. 1–7, September 2017 (*in Japanese*).

[20] Akie Mayumi, Hiyoyasu Idomura, Takuya Ina, Susumu Yamada, and Toshiyuki Imamura, 'Evaluation of Convergence property of Preconditioned Chebyshev Basis CG method for Multiflow simulation code JUPITER,' 2017 Spring meeting of Atomic Energy Society of Japan, September 2017(*in Japanese*).

[21] Toshiyuki Imamura, and Tetsuzo Usui, 'Porting and Optimization of Numerical Libraries for Arm SVE,' Arm HPC Workshop by RIKEN AICS and Linaro, Akihabara, Dec. 2017.

[22] Susumu Yamada, Toshiyuki Imamura, and Masahiko Machida, 'Exact-diagonalization for Hubbard model using LOBPCG method; Communication avoiding Neumann expansion preconditioner for solving multiple eigenvalues,' IPSJ SIG Technical Report (High Performance Computing), Vol. 2017-HPC-162, No. 4, pp. 1–6, December 2017 (*in Japanese*).

[23] Daichi Mukunoki, 'Review on Implementation technology of Numerical libraries for next-generation computer systems,' JSIAM seminar, Hongo, University of Tokyo, December 2017.

[24] Masaaki Aoki, Toshiyuki Imamura, Mitsuo Yokokawa, and Yusuke Hirota, 'Performance Evaluation of multi-dimensionally-distributed 3D FFT on manycore processor systems', IPSJ SIG Technical Report (High Performance Computing), Vol. 2018-HPC-163, No. 29, pp. 1–7, February 2018 (*in Japanese*).

[25] Toshiyuki Imamura, Yusuke Hirota, and Takeshi Fukaya, 'Overview of the EigenExa project, past, present and future,' International Workshop on Eigenvalue Problems: Algorithms; Software and Applications, in Petascale Computing (EPASA2018), Tsukuba, Mar. 2018.

[26] Haruka Yamada, Akira Imakura, Toshiyuki Imamura, and Tetsuya Sakurai, 'A Parallel Implementation Technique of HOTRG for the 3D Cubic Lattice Ising Model', SIAM PP18, Tokyo, Mar. 2018

[27] Yiyu Tan, and Toshiyuki Imamura, 'The SPLATT Toolkit on the K Computer,' SIAM PP18, Tokyo, Mar. 2018

[28] Yasuhiro Idomura, Takuya Ina, Akie Mayumi, Susumu Yamada, K. Matsumoto, Yuichi Asahi, and Toshiyuki Imamura: 'Performance Evaluation of a Modified Communication-Avoiding Generalized Minimal Residual Method on Many-Core Platforms', SIAM PP18, Tokyo, Mar. 2018

[29] Daichi Mukunoki, and Toshiyuki Imamura, 'Performance Analysis of 2.5D-PDGEMM on the K Computer', SIAM PP18, Tokyo, Mar. 2018

[30] Toshiyuki Imamura, Yusuke Hirota, Susumu Yamada, and Masahiko Machida, 'Communication Avoiding Approach for Reduction to Tri-Diagonal, Bi-Diagonal, and Hessenberg Forms,' SIAM PP18, Tokyo, Mar. 2018

[31] Akie Mayumi, Yasuhiro Idomura, Takuya Ina, Susumu Yamada, and Toshiyuki Imamura: 'Performance Property of Preconditioned Chebyshev Basis CG Solver for Multiphase CFD Simulations', SIAM PP18, Tokyo, Mar. 2018

4.4.3 Invited Talks

[32] Toshiyuki Imamura, and Yiyu Tan, 'Review of Tensor-decomposition toolkit on K Computer,' 2018 Conference on Advanced Topics and Auto Tuning in High-Performance Scientific Computing (ATAT2018), March 26–27, 2018, National Cheng Kung University, Tainan, Taiwan.

4.4.4 Software

[33] EigenExa, `http://www.aics.riken.jp/labs/lpnctrt/en/projects/eigenexa/`.
[34] KMATH_EIGEN_GEV, `http://www.aics.riken.jp/labs/lpnctrt/en/projects/kmath-eigen-gev/`.
[35] KMATH_RANDOM, `http://www.aics.riken.jp/labs/lpnctrt/en/projects/kmath-random/`.
[36] KMATHLIB_API, `http://www.aics.riken.jp/labs/lpnctrt/en/projects/kmathlib-api`.
[37] KMATH_FFT3D, `http://www.aics.riken.jp/labs/lpnctrt/en/projects/kmath-fft3d/`.
[38] ASPEN.K2, `http://www.aics.riken.jp/labs/lpnctrt/en/projects/aspen-k2/`.
[39] MUBLAS-GEMV, `http://www.aics.riken.jp/labs/lpnctrt/en/projects/mublas/`.
[40] SLFP, `http://www.aics.riken.jp/labs/lpnctrt/members/mukunoki/slfp-0.0.1.tgz`.

Chapter 5

HPC Usability Research Team

5.1 Members

Hiroya Matsuba (Team Leader)

Motohiko Matsuda (Research Scientist)

5.2 Research Activities

The mission of the HPC Usability Team is to develop a software platform that contributes to increasing the number of uses of K computer. This team focuses on infrastructure providers, such as utility companies, as potential new users of supercomputers, expecting that simulation of infrastructure facilities will provide valuable information for its operation. For example, if a simulator of a cooling facility is available, the operator can search for an energy-efficient combination of parameters such as a temperature of cooling water, power of pumps, and positions of valves. Simulation is especially valuable because it enables operators to test parameters that are impossible to apply to the real facilities because of safety reasons.

The main obstacle in conducting facility simulations is difficulty in modeling the target facility. Complicated facilities are often composed of many components. They have to be modeled in various ways. For example, some simple parts, like a heat exchanger, may be modeled as a single dimension (1D) component. Such 1D modeling is valid if it is enough to model its overall behavior with a simple differential equation, ignoring the the size, shape or structure of the parts. On the other hand, other parts may require 3D modeling with a precise modeling of the fluid flow, for example. In the worst case, the facility may contain black boxes of which even operators of the facility do not know the operating principle. In such a case, models must be created using observed data. Building models with such various modeling techniques requires deep knowledge of both mechanical and computer engineering. In addition, methods to combine the models are also needed to make a complete facility simulator from the models.

The HPC Usability Research Team is working to tackle the difficulties to create such complex simulators. To achieve this, both of the followings are important.

- Develop an easy method to make simulation models of components of facilities.
- Develop an easy method to combine different simulators.

For the easy modeling of components, we are planning to create a new domain-specific language that covers a wide variety of modeling methods such as DAE (differential algebraic equations), PDE (partial differential equations), particle simulations, agent simulations, and so on. Although different modeling method must be handled by different simulators, we still assume it possible to provide a similar user interface for different simulators. Providing different simulators with a similar user interface is valuable because it contributes to reducing the learning costs of users. For the easy combination of simulators, we are planning to develop a quick coupler. The coupler is software that picks up values from a working simulator and passes the values as input for another simulator to realize the combined simulation. Although the concept of the coupler was already introduced many year ago, it is hard to implement in a standard computer language like C/Fortran because developers have to manually specify which value of a model corresponds to which value of another model. In order to simplify this task, we aim to develop a generalized coupler that is easily applicable to all

models developed with our domain specific language mentioned above. The coupler will also connect simulators with machine learning frameworks. This is necessary when we have to develop simulation models of black box components from observed data, or when we develop an artificial intelligence that learns simulation results.

To reach the research objectives described above, we are planning to conduct our research with the following two steps. The first step is to find a particular facility to simulate and create a simulation model for that facility by ourselves. By experiencing the difficulties in creating the simulator, we, at first, develop a minimal set of a software platform that simplifies our tasks. After establishing the first platform, the second step is to find several additional targets and expand our platform so that it can be applied to the additional ones. This process enables us to develop a software platform that is both practical and general.

In this fiscal year, which is the first fiscal year of this team, we made the following progress.

- We have selected the cooling facility of K computer as our first modeling target and developed an initial version of the simulation model in collaboration with the Operations and Computer Technologies Division.
- We have invented a technique to efficiently conduct facility simulation for machine learning, especially for reinforcement learning, in collaboration with Hitachi, Ltd.

The details of these accomplishments are described in the following sections.

5.2.1 Simulation of K Computer Cooling Facilities

As the modeling target of our first example case, we selected the cooling facility of K computer. That facility is suitable as the modeling target especially because various kinds of information is available from the facility. Such information is collected by sensors installed in this fiscal year by the Operations and Computer Technologies Division (details may be reported in a later chapter of this report). Such data enables us to evaluate how accurately our simulation model reflects the actual behavior of the facility.

For overall modeling of the whole facility, we decided to use Modelica language [A]. Modelica is a domain specific language for modeling complex systems that are described with DAEs. Because Modelica is component-based language, users usually can implement models of complex systems just by connecting basic components, many of which are prepared in a standard library, with GUI.

An initial version of our model of the cooling facility is shown in Figure 5.1. This is a screenshot of a Modelica tool called Dymola [B]. Each icon in this figure is a Modelica component. Such a component is implemented either by just using a component in the standard library, by writing the Modelica language, or by connecting other components. As shown in this figure, Modelica models usually define relations between components with a few scalar values. Such modeling method is often called 1D modeling.

The 1D modeling includes coarse approximations. For example, in the model of Figure 5.1, it is assumed that cooling towers exchange heat between cooling water and the atmosphere ideally. However, in fact, because the cooling towers are located on the roof of the facility building, wind direction dramatically affects the efficiency of heat exchange.

In order to improve the accuracy of the model, we will have to make more precise models for some parts of the facility, such as the cooling tower. This case shows why we are going to develop a domain specific language that is applicable to various modeling methods. When we want some parts of a facility to be simulated more precisely than 1D modeling, we have to develop their models with different methods, such as the 3D fluid flow and heat transfer. 3D modeling is technically possible by using appropriate software like OpenFOAM, but learning both Modelica and OpenFOAM is a tedious task for model developers because they provide quite different programming models. A domain specific language that covers a wide variety of modeling method with similar user interface will help reduce such learning costs.

References

[A] Modelica: https://www.modelica.org/
[B] Dymola: https://www.3ds.com/products-services/catia/products/dymola/

5.2.2 Efficient Execution of Simulations for Reinforcement Learning

Reinforcement learning is a machine learning technology in which a software agent learns how to react to various situations in a given environment. We expect that this technology may be used to develop artificial intelligence (AI) for facility operations. For example, by trying various options to react to an emergency situation and by leaning the resulting situation, the AI will eventually be able to take better actions.

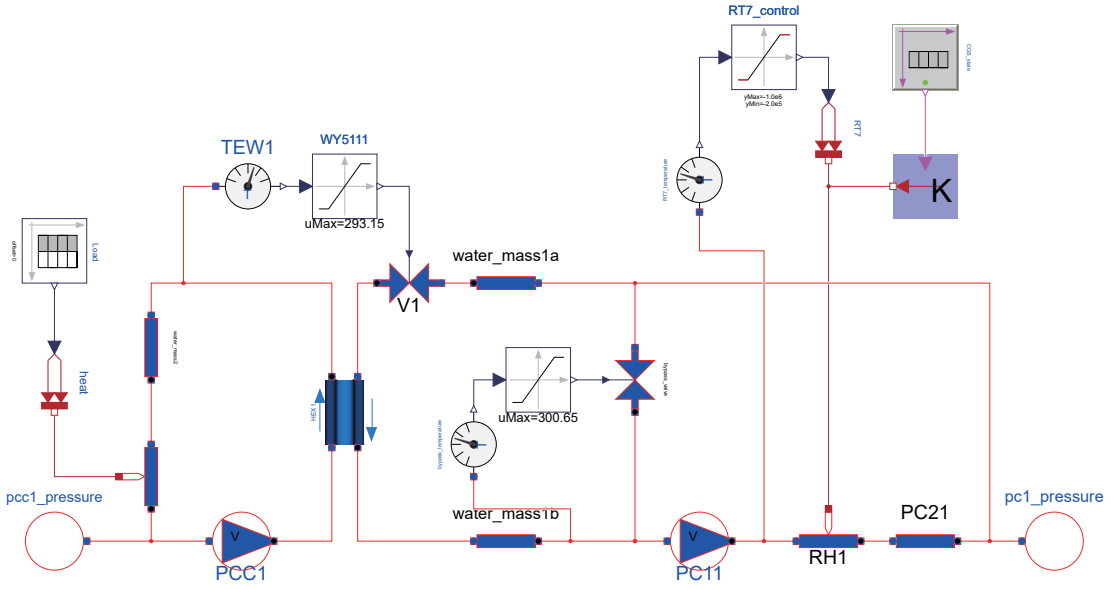

Figure 5.1: K Computer Cooling Model

In order to develop the AI that can take appropriate actions in such emergency situations, the AI has to have the experiences to handle the situation before the incident happens. However, it is impossible to allow AI to do trial and error in a real infrastructure facility because most infrastructure facilities should be kept in healthy and safe conditions. Simulation is used to provide a virtual environment where AI can make many mistakes and learn how to handle the situations.

We have developed a simulation system that consists of a Modelica simulator, called JModelica [C], and a machine learning framework, called ChainerRL [D]. Using this software environment, we also have developed a method to improve efficiency of simulation execution by eliminating redundant execution of simulations. This work has been done in a collaborative research project with Hitachi, Ltd. We have filed a patent regarding this efficient execution [1].

References

[C] JModelica: https://jmodelica.org/
[D] ChainerRL: https://github.com/chainer/chainerrl

5.2.3 Other Activities

We have done much engineering effort on K computer, mainly for setting up an environment for machine learning frameworks to run. We have also set up Modelica simulator on K computer.

As for the machine learning frameworks, we have set up TensorFlow [E] and Chainer [F]. Both have Python interfaces, but the core part of the frameworks is written in the C or C++ language. So, executable binaries for K computer had to be created. As for TensorFlow, many recent build tools are required, most of which is not installed on the login nodes of K computer. Therefore, we decided to cross-compile the software. By installing a GCC based cross-compiler, which can generate binary files for K computer, onto a standard x86 server with a recent Linux distribution, and by setting up the compilation tool to use the cross-compiler, SPARC executable files of TensorFlow were successfully created. Because Chainer requires only common compilation tools, we were able to compile them natively on the computing nodes of K computer using GCC.

For the Modelica simulator, we set up JModelica on K computer. JModelica also has a Python interface on the native libraries written in C/C++. We have successfully compiled this software on the computing nodes of

K computer using native GCC, although we had to manually download and install many Python modules that JModelica depends on.

Due to lack of the functionalities of GCC to generate executable files with the HPC-ACE extension of the SPARC architecture, the performance of all the software mentioned above is not optimal for K computer.

References

[E] TensorFlow: https://www.tensorflow.org/
[F] Chainer: https://chainer.org/

5.3 Schedule and Future Plan

We will start designing our DSL, which is the main part of our future research products, in the fiscal year 2018. We will also continue the modeling of the cooling facilities of K computer so that our simulator show some information that is beneficial for the operation of K computer.

5.4 Publications

5.4.1 Patents

[1] M. Mase, T. Sakurai, and H. Matsuba, "Simulation execution method and computer system", Joint application by Riken and Hitachi, Ltd., March, 2018

5.4.2 Invited Talks

[2] H. Matsuba, "Software platform for decision-making simulations (in Japanese)", Automatic Tuning Research Group Academic Session 18, Tokyo, Feb. 23, 2018

5.4.3 Presentations

[3] H. Matsuba, "How to find interesting research goals (in Japanese)", Summer United Workshops on Parallel, Distributed and Cooperative Processing (panelist), Akita, Jul. 26, 2017
[4] H. Matsuba, "A case of data analysis for efficient operation of datacenters", 2018 AICS International Symposium, Kobe, Feb. 7, 2018

Chapter 6

Field Theory Research Team

6.1 Members

Yoshinobu Kuramashi (Team Leader)

Yoshifumi Nakamura (Research Scientist)

Hiroya Suno (Research Scientist, Joint Position with the Nishina Center for Accelerator-based Research)

Eigo Shintani (Research Scientist)

Yuya Shimizu (Postdoctoral Researcher)

Ken-Ichi Ishikawa (Visiting Scientist, Hiroshima University)

Shoichi Sasaki (Visiting Scientist, Tohoku University)

Takeshi Yamazaki (Visiting Scientist, University of Tsukuba)

Shinji Takeda (Visiting Scientist, Kanazawa University)

6.2 Research Activities

Our research field is physics of elementary particles and nuclei, which tries to answer questions in history of mankind: what is the smallest component of matter and what is the most fundamental interactions? This research subject is related to the early universe and the nucleosynthesis through Big Bang cosmology. Another important aspect is quantum properties, which play an essential role in the world of elementary particles and nuclei as well as in the material physics at the atomic or molecular level. We investigate nonperturbative properties of elementary particles and nuclei through numerical simulations with the use of lattice QCD (Quantum ChromoDynamics). The research is performed in collaboration with applied mathematicians, who are experts in developing and improving algorithms, and computer scientists responsible for research and development of software and hardware systems.

Lattice QCD is one of the most advanced case in quantum sciences: interactions between quarks, which are elementary particles known to date, are described by QCD formulated with the quantum field theory. We currently focus on two research subjects: (1) QCD at finite temperature and finite density. We try to understand the early universe and the inside of neutron star by investigating the phase structure and the equation of state. (2) First principle calculation of nucleon form factors. Proton and neutron, which are called nucleon, consist of three quarks. We investigate their internal structure and low energy properties by the measurement of various form factors.

Successful numerical simulations heavily depend on an increase of computer performance by improving algorithms and computational techniques. However, we now face a tough problem that the trend of computer architecture becomes large-scale hierarchical parallel structures consisting of tens of thousands of nodes which individually have increasing number of cores in CPU and arithmetic accelerators with even higher degree of parallelism: we need to develop a new type of algorithms and computational techniques, which should be different from the conventional ones, to achieve better computer performance. For optimized use of K computer

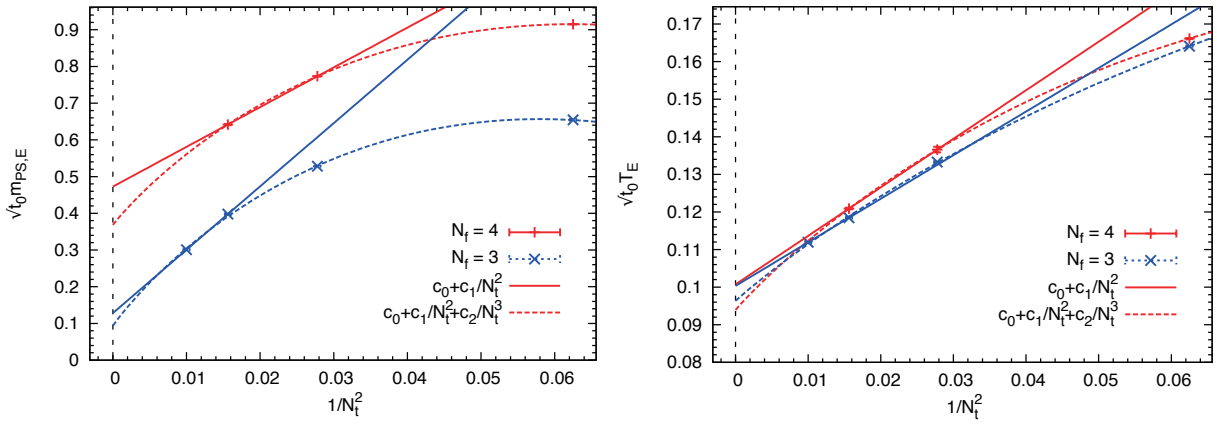

Figure 6.1: Continuum extrapolation of the critical point $\sqrt{t_0}m_{\rm PS,E}$ (left) and $\sqrt{t_0}T_{\rm E}$ (right) with $\sqrt{t_0}$ the Wilson flow scale. Red and blue symbols denote 4 and 3 flavor cases, respectively.

our research team aims at (1) developing a Monte Carlo algorithm to simulate physical system with negative weight effectively and (2) improving iterative methods to solve large system of linear equations. These technical development and improvement are carried out in the research of physics of elementary particles and nuclei based on lattice QCD.

6.2.1 QCD at finite temperature and finite density

Establishing the QCD phase diagram spanned by the temperature T and the quark chemical potential μ in a quantitative way is an important task of lattice QCD. We have been working on tracing the critical end line in the parameter space of temperature, chemical potential and quark masses in 4, 3 and 2+1 flavor QCD using the $O(a)$-improved Wilson quark action and the Iwasaki gauge action. We have determined the critical end point at zero chemical potential $\mu = 0$ in 3 flavor case. Our strategy is to identify at which temperature the Kurtosis of physical observable at the transition point on several different spatial volumes intersects. This method is based on the property of opposite spatial volume dependence of the Kurtosis at the transition point between the first order phase transition side and the crossover one. We have carried out a systematic study of the critical end point changing the temporal lattice size from $N_t = 4$ to 10 in 3 flavor case, which corresponds to change the lattice spacing. In Fig. 6.1 (left and right panels) we show the continuum extrapolation of the critical pseudoscalar meson mass $m_{\rm PS,E}$ and the critical temperature $T_{\rm E}$ normalized by $\sqrt{t_0}$, where $\sqrt{t_0}$ denotes the Wilson flow scale. We also make the same study in 4 flavor case for comparison. We observe that the critical temperature seems to follow the $O(a^2)$ scaling property both in 3 mad 4 flavor cases. On the other hand, $\sqrt{t_0}m_{\rm PS,E}$ shows significantly large scaling violation and its continuum extrapolation gives different values for 3 and 4 flavor cases: rather close to zero for the former and sufficiently deviated from zero for the latter. The origin of the difference between 3 and 4 flavor cases and ,especially, whether $m_{\rm PS,E}$ in 3 flavor case may vanish in the continuum limit are intriguing theoretical issues. Currently we are performing a simulation at finer lattice spacing to investigate the possibility that $m_{\rm PS,E}$ may vanish in the continuum limit.

6.2.2 Nucleon form factors

Nucleon form factors are good probes to investigate the internal structure of the nucleon which is a bound state of quarks. Study of their properties requires nonperturbative method and much effort has been devoted to calculate them with lattice QCD since 1980's. Unfortunately, the current situation is that we are still struggling for reproducing the well-established experimental results, e.g., the electric charge radius and the axial vector coupling. This means that we have not yet achieved proper treatment of a single hadron in lattice QCD calculation. The left panel of Fig. 6.2 shows a summary plot of the electric charge radius calculated with lattice QCD as of 2014. We focus on two major systematic uncertainties in the current lattice QCD simulations: one is heavier quark masses than the physical values and the other is finite spatial volume effects. In order to get rid of them we have carried out calculation of the nucleon form factors on a $(10.8\ {\rm fm})^4$ lattice at the physical point in 2+1 flavor QCD. Thanks to the large spatial volume we can get access to small momentum transfer region up to $q^2 = 0.013\ {\rm GeV}^2$. The right panel of Fig. 6.2 plots our results for the electric charge radius, whose

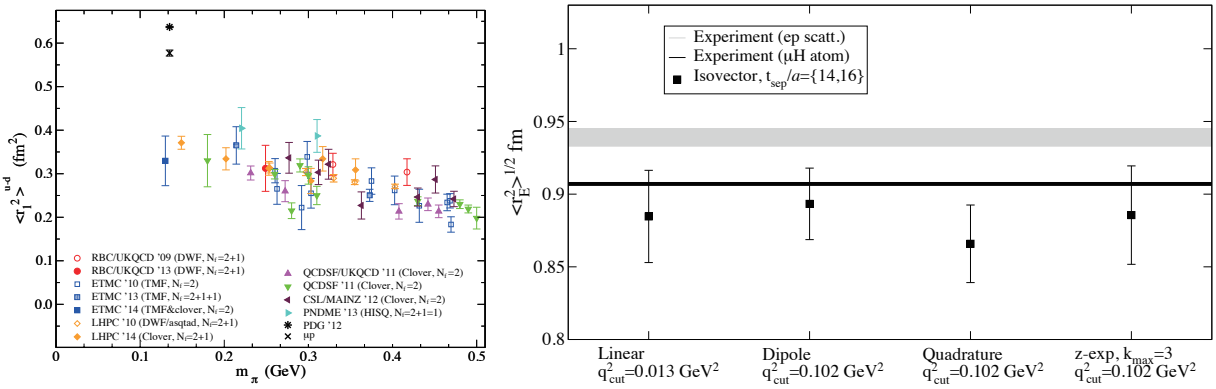

Figure 6.2: Summary plot of lattice QCD results for electric charge radius presented in the international conference of "Lattice 2014" (left) and our result on a $(10.8\ \mathrm{fm})^4$ lattice at the physical point in 2+1 flavor QCD (right). Experimental results for *e-p* scattering and muonic hydrogen spectroscopy are represented by "$*$" and "$\times$" symbols in the left panel and gray and black horizontal bands in the right panel.

four data represent four types of analyses to extract the electric charge radius from the form factor. Comparing the left and right panels in Fig. 6.2 our results show a remarkable improvement. We are now trying further reduction of the magnitude of the error.

6.2.3 Tensor network scheme in path-integral formalism

The Monte Carlo simulation of lattice gauge theory is quite powerful to study nonperturbative phenomena of particle physics. However, when the action has an imaginary component like the θ term, it suffers from the numerical sign problem, which is failure of importance sampling techniques. The effect of the θ term on the non-Abelian gauge theory, especially quantum chromodynamics (QCD), is important, because it is related to a famous unsolved problem, "strong CP problem". The difficulty is also shared with the finite density lattice QCD. So development of effective techniques to solve or by-pass the sign problem leads to a lot of progress in the study of the QCD phase diagram at finite temperature and density. The tensor network scheme is a promising theoretical and computational framework to overcome these difficulties. So far we have developed the Grassmann version of the tensor renormalization group (GTRG) algorithm in the tensor network scheme, which allows us to deal with the Grassmann variables directly. The GTRG algorithm was successfully applied to the analysis of the phase structure of one-flavor lattice Schwinger model (2D QED) with and without the θ term showing that the algorithm is free from the sign problem and the computational cost is comparable to the bosonic case thanks to the direct manipulation of the Grassmann variables. This was the first successful application of the tensor network scheme to a Euclidean lattice gauge theory including the relativistic fermions in path-integral formalism. Toward the final target of 4D QCD we are currently working on three research subjects in the tensor network scheme: (i) non-Abelian gauge theories, (ii) higher dimensional (3D or 4D) models, and (iii) development of computational techniques for physical observables. In 2017 we have succeeded in applying the tensor network scheme to three dimensional finite temperature Z_2 gauge theory. The left panel of Fig. 6.3 shows the N_σ dependence of the specific heat as a function of $1/\beta$ at $N_\tau = 3$, where N_σ and N_τ denote the spatial and temporal extent of the lattice, respectively, and $1/\beta$ is proportional to temperature. We observe the clear peak structure at all the values of N_σ and the peak height $C_{\max}(N_\sigma)$ grows as N_σ increases. We can determine the critical exponent ν from the finite size scaling behavior of the peak position $\beta_c(N_\sigma)$. In the right panel of Fig. 6.3 we plot the N_σ dependence of $\beta_c(N_\sigma)$ at $N_\tau = 3$. The solid curve represents the fit result obtained with the fit function of $\beta_c(N_\sigma) = \beta_c(\infty) + BN_\sigma^{1/\nu}$ for $N_\sigma \in [512, 4096]$, which gives $\beta_c(\infty) = 0.711150(4)$ and $\nu = 0.99(4)$. The value of the critical exponent is consistent with $\nu = 1$ in the universality class of the two dimensional Ising model as expected by the Svetitsky-Yaffe conjecture. Next step may be an application of the tensor network scheme to non-commutative gauge theories.

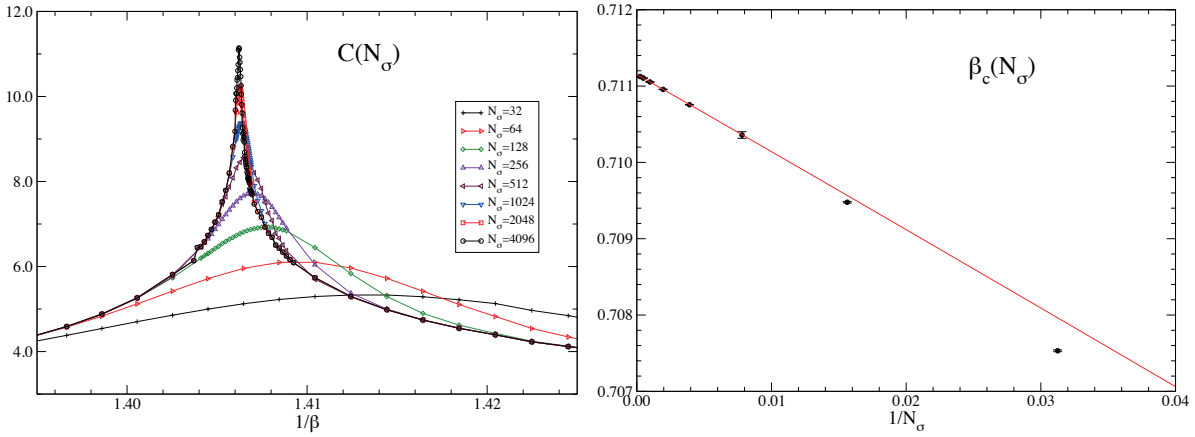

Figure 6.3: N_σ dependence of specific heat as a function of $1/\beta$ (left) and scaling property of $\beta_c(N_\sigma)$ (right).

6.3 Schedule and Future Plan

6.3.1 QCD at finite temperature and finite density

We are performing a systematic study of the critical end point in 4 flavor QCD in comparison with 3 flavor case. We also investigates whether or not $m_{\mathrm{PS,E}}$ in 3 flavor QCD vanishes in the continuum limit.

6.3.2 Nucleon form factors

We are trying to reduce the statistical error of the nucleon form factors on a $(10.8\ \mathrm{fm})^4$ lattice at the physical point. After that we plan to investigate the cutoff effect.

6.3.3 Tensor network scheme in path-integral formalism

As stated above, there are three important subjects in research and development of tensor network scheme in path-integral formalism: (i) non-Abelian gauge theories, (ii) higher dimensional (3D or 4D) models, and (iii) development of computational techniques for physical observables. Future research keeps to follow these three directions.

6.4 Publications

6.4.1 Articles

[1] Takeshi Yamazaki and Yoshinobu Kuramashi, "Relation between scattering amplitude and Bethe-Salpeter wave function in quantum field theory", Phys. Rev. D 96 (2017) ref. 114511.

[2] Xiao-Yong Jin, Yoshinobu Kuramashi, Yoshifumi Nakamura, Shinji Takeda and Akira Ukawa, "Critical point phase transition for finite temperature 3-flavor QCD with non-perturbatively $O(a)$-improved Wilson fermions at $N_t = 10$", Phys. Rev. D 96 (2017) ref. 034523.

[3] Yuya Shmizu and Yoshinobu Kuramashi, "Berezinskii-Kosterlitz-Thouless transition in lattice Schwinger model with one-flavor of Wilson fermion", Phys. Rev. D 97 (2018) ref. 034502.

[4] Daisuke Kadoh, Yoshinobu Kuramashi, Yoshifumi Nakamura, Ryo Sakai, Shinji Takeda and Yusuke Yoshimura, "Tensor network formulation for two-dimensional lattice $N = 1$ Wess-Zumino model", JHEP 1803 (2018) ref. 141.

[5] Yusuke Yoshimura, Yoshinobu Kuramashi, Yoshifumi Nakamura, Ryo Sakai and Shinji Takeda, "Calculation of fermionic Green functions with Grassmann higher-order tensor renormalization group", Phys. Rev. D 97 (2018) ref. 034502.

[6] Taisuke Boku, Ken-Ichi Ishikawa, Yoshinobu Kuramashi and Lawrence Meadows, "Mixed precision solver scalable to 16000 MPI processes for lattice quantum chromodynamics simulations on the Oakforest-PACS system", arXiv:1709.08785 [physics.comp-ph].

[7] Yasumichi Aoki, Taku Izubuchi, Eigo Shintani and Amarjit Soni, "Improved lattice computation of proton decay matrix elements", Phys. Rev. D 96 (2017) ref. 014506.

[8] V. G. Bornyakov et al., "Flavour breaking effects in the pseudoscalar meson decay constants", Phys. Lett. B767 (2017) p. 366.

[9] T. Haar et al., "Applying polynomial filtering to mass preconditioned Hybrid Monte Carlo", Comput. Phys. Commun. 215 (2017) p. 113.

[10] A. J. Chambers et al., "Nucleon structure functions from lattice operatorproduct expansion", Phys. Rev. Lett. 118 (2017) ref. 242001.

[11] A. J. Chambers et al., "Electromagnetic form factors at large momenta from lattice QCD", Phys. Rev. D 96 (2017) ref. 114509 .

[12] R. Sakai, S. Takeda and Y. Yoshimura, "Higher order tensor renormalization group for relativistic fermion systems", Prog. Theor. Exp. Phys. (2017) 063B07.

6.4.2 Conference Papers

[13] Natsuki Tsukamoto, Ken-Ichi Ishikawa, Yoshinobu Kuramashi, Shoichi Sasaki, and Takeshi Yamazaki for PACS Collaboration, "Nucleon structure from 2+1 flavor lattice QCD near the physical point", EPJ Web Conf., 175 (2018) ref. 06007.

[14] Taku Izubuchi, Yoshinobu Kuramashi, Christoph Lehner and Eigo Shintani, "Lattice study of finite volume effect in HVP for muon g-2", EPJ Web Conf. 175 (2018) ref. 06020.

[15] Renwick Hudspith, Randy Lewis, Kim Matlman and Eigo Shintani, "α_s from the hadronic vacuum polarisation", EPJ Web Conf. 175 (2018) ref. 10006.

[16] Xiao-Yong Jin, Yoshinobu Kuramashi, Yoshifumi Nakamura, Shinji Takeda and Akira Ukawa, "Continuum extrapolation of critical point for finite temperature QCD with $N_f = 3$", arXiv:1710.08057 [hep-lat].

[17] R. Sakai, D. Kadoh, Y. Kuramashi, Y. Nakamura, S. Takeda, and Y. Yoshimura, "Application of tensor network method to two-dimensional lattice $N = 1$ Wess-Zumino model", EPJ Web Conf. 175 (2018) ref. 11019.

[18] Takeshi Yamazaki, Ken-Ichi Ishikawa, Yoshinobu Kuramashi for PACS Collaboration, "Comparison of different source calculations in two-nucleon channel at large quark mass", EPJ Web Conf., 175 (2018) ref. 05019.

[19] S. Takizawa et al., "A scalable multi-granular data model for data parallel workflows", HPC ASIA 2018, Proceedings of the International Conference on High Performance Computing in Asia-Pacific Region (2018) p. 251-260.

6.4.3 Invited talks

[20] Yoshinobu Kuramashi, "Lattice QCD approach to proton puzzle", 2018 Annual (73th) Metteing of the Physical Society of Japan, Tokyo University of Science, Noda, Japan, March 22-25, 2018.

[21] Eigo Shintani, "Lattice QCD study of nucleon EDM", RCNP Workshop on Fundamental Physics Using Neutrons and Atoms, RCNP, Osaka, Japan, July 4-5, 2017.

[22] Eigo Shintani, "Lattice study of finite size effect in the leading order of hadronic contribution to muon $g-2$", First Workshop of the Muon g-2 Theory Initiative, Q Center, Chicago, USA, June 3-6, 2017.

[23] Eigo Shintani, "Lattice calculation of matrix element on proton decay", International Workshop on Baryon & Lepton Number Violation 2017, Case Western University, Cleveland, Ohio, USA, May 15-18, 2017.

[24] Takeshi Yamazaki, "Binding energy of light nucleus from lattice QCD", QCD Downunder 2017, Novotel Cairns Oasis Resort, Australia, July 10-14, 2017.

[25] Takeshi Yamazaki, "Study of nucleon structure from lattice QCD", The Forth Project Report Meeting of the HPCI System Including K computer, KOKUYO Hall, Tokyo, Japan, November 2, 2017.

[26] Takeshi Yamazaki, "Relation between scattering amplitude and Bethe-Salpeter wave function in quantum field theory", Multi-Hadron Systems from Lattice QCD, University of Washington, Seattle, USA, February 5-9, 2018.

[27] Takeshi Yamazaki, "A new calculation method of scattering phase shift with Bethe-Salpeter wave function in lattice QCD", 2018 Annual (73th) Metteing of the Physical Society of Japan, Tokyo University of Science, Noda, Japan, March 22-25, 2018.

[28] Sinji Takeda, "Tensor networks in particle physics", Tensor Networks 2017, AICS, Kobe, Japan, August 3, 2017.

6.4.4 Posters and Presentations

[29] Yoshinobu Kuramashi for PACS Collaboration, "A large scale simulation of 2+1 flavor lattice QCD", The 35th International Symposium on lattice field theory (Lattice 2017), Palacio de Congresos de Granada, Spain, June 19-24, 2017.

[30] Eigo Shintani, "Lattice study of finite volume effect in HVP for muon $g-2$", The 35th International Symposium on lattice field theory (Lattice 2017), Palacio de Congresos de Granada, Spain, June 19-24, 2017.

[31] Takeshi Yamazaki, Ken-ichi Ishikawa, Yoshinobu Kuramashi for PACS Collaboration, "Comparison of different source calculations in two-nucleon channel at large quark mass", The 35th International Symposium on lattice field theory (Lattice 2017), Palacio de Congresos de Granada, Spain, June 19-24, 2017.

[32] S. Takeda, "Cost reduction of tensor renormalization group algorithm by projective truncation technique", 2018 Annual (73th) Metteing of the Physical Society of Japan, Tokyo University of Science, Noda, Japan, March 22-25, 2018.

[33] S. Takeda, "Continuum extrapolation of critical point for finite temperature QCD with $N_f = 3$", The 35th International Symposium on lattice field theory (Lattice 2017), Palacio de Congresos de Granada, Spain, June 19-24, 2017.

Chapter 7

Discrete-Event Simulation Research Team

7.1 Members

Nobuyasu Ito (Team Leader)

Yohsuke Murase(Research Scientist)

Naoki Yoshioka (Research Scientist)

Shih-Chieh Wang (Postdosctoral Researcher)

Daigo Umemoto (Postdosctoral Researcher)

Tomio Kamada (Guest Researcher)

Takeshi Uchitane (Guest Researcher)

7.2 Research Activities

Computer simulations are now essential for all fields of science and engineering, and indispensable to our society. They extend our ability in theoretical and mathematical description, and accelerate the global development. When a problem is challenged with computer simulation, mathematical models to describe it are prepared and solved with appropriate parameters and conditions using computers. There are two kinds of simulation models: "continuous" models using continuous functions and differential equations, and "discrete" models using discrete objects and case-wise evolution rules. The continuous models are used in, for example, flow simulations with hydrodynamic equations like Navier-Stokes and Euler, electromagnetic simulations with the Maxwell's equations, and elementary-particle simulations with field theoretic models like lattice QCD, Computers calculate and simulate discretized approximation model of these continuous models, and the calculations are often characterized by enormous number of repetitions of regular processing patterns.

The discrete models are used in, for example, particle simulations with event-driven dynamics and discrete-element models, and traffic and processing simulations with agent, queueing, automata and network models. Computers judge whether conditions are fulfilled or not and determine next states, that is, discrete-events.

One characteristic feature of discrete-event simulations is their variety both in model parameters and behaviors. Different parameters of discrete models often result in qualitatively quite different behaviors. For example, two particles just pass through when they do not collide with each other, but they will be scattered to different orbits when they collide. A automaton reacts specifically when their inputs satisfy its activation condition. A system with such discrete elements will behaves unpredictable way. This feature is much different from the case of "continuous" simulations which are often characterized by continuous change in behaviors when input parameters are slightly modified.

Another feature of discrete-event simulations is its network structure. Relations between elements are often characterized by graphs and the graphs have usually nonuniform. For example, in a system of hard particles, colliding particles are connected and noncolliding ones are not. The connection changed at every collision.

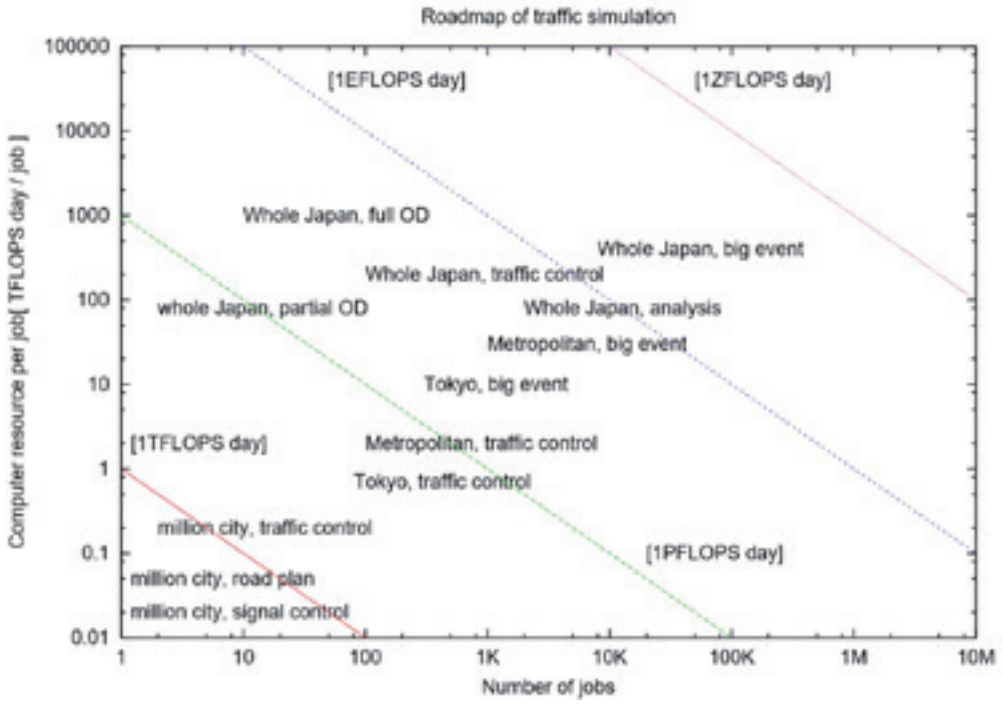

Figure 7.1: Roadmap of traffic simulations.

Another example is human relations. Some are friendly connected, and some are competing. Such human relations are known to be characterized by a small-world structure.

Figure 7.1, 7.2 and 7.3 show roadmaps of social simulations[1]. They show estimated computer resources estimated to be necessary to solve some social challenges. The horizontal axis shows typical number of simulations to solve a challenge, and the vertical axis shows resources for one simulation of the challenge. They are plotted with logarithmic scale and therefore lines $y = -x$ show total resources for the challenge.

These features are typically observed in simulations of particle, magentic, biological and medical systems and also of social systems, for example, traffic, economy and social relationship. The Discrete-event simulation research team(DESRT) have been elucidating future applications of the K and future supercomputers to such social simulation. It is observed that computer applications to social issues will be more feasible when Peta-flops computer becomes popular. It is exactly the situation now we are. And this trend will be the more important when Exa- and Zeta-flops machines are available.

7.2.1 Parameter-space explorer: OACIS and CARAVAN

Discrete-event simulations usually require simulations for many parameters. We can design, submit and analyze a few to tens of parameters by hand, but it is hard for thousands or more, although millions of simulations are often necessary. Furthermore, next parameters are often determined based of simulation results with previous parameters. So a naive map-reduce type execution is not always useful. So we need some application tools to remedy the situation.

The DESRT has been developing job management tools named OACIS and CARAVAN to challenge the huge-parameter space. The name OACIS is an abbreviation of "Organizing Assistant for Comprehensive and Interactive Simulations"[2]. The OACIS and CARAVAN are not only to help crawling in parameter space, but also to connect various applications.

The OACIS have been released for public use as an AICS software, and the CARAVAN is now being tested with its prerelease version. Both of these two tools are used with user's simulation and analysis softwares. A user register one's simulation and analysis softwares togather with their input parameters and available host computers to these tools, then the tools control submitting and analyzing jobs.

Each simulation and each analysis for many parameters will be properly processed by computers if they are specified correctly, but error will easily be introduced by human side. In this sense, supercomputers are de-

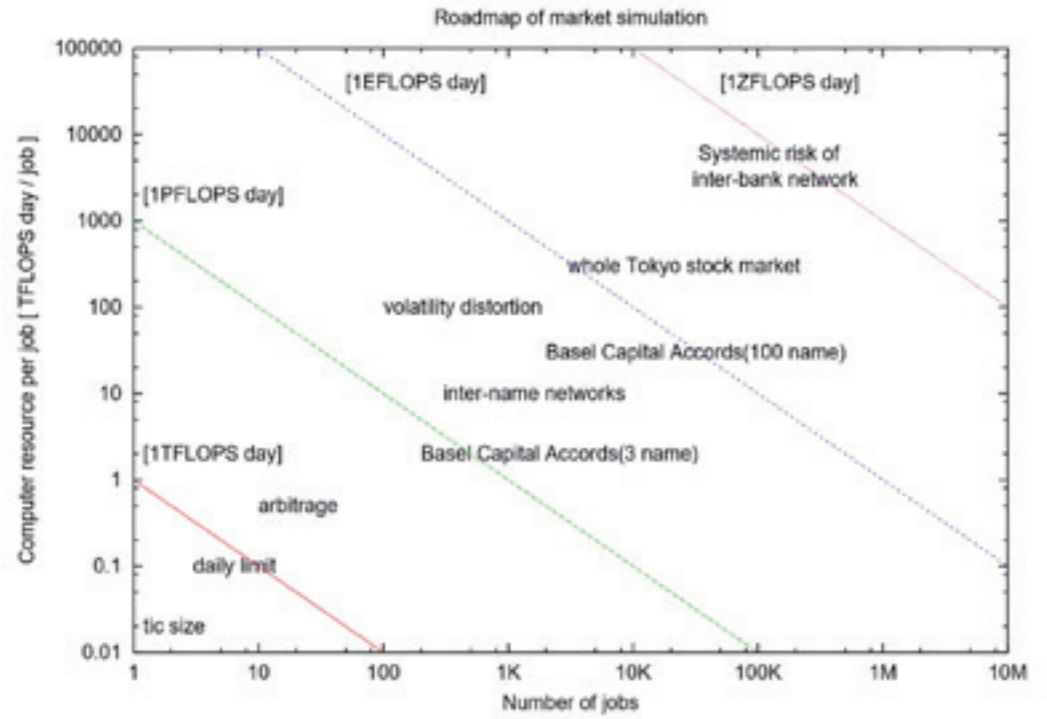

Figure 7.2: Roadmap of market simulations.

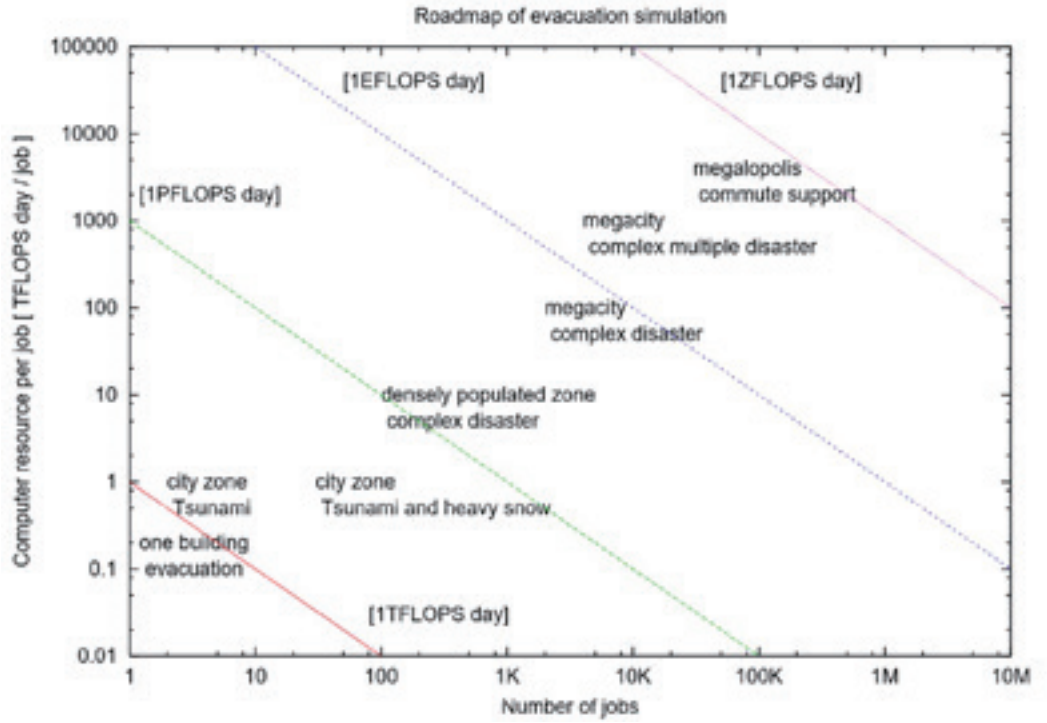

Figure 7.3: Roadmap of evacuation simulations.

manding not only greater programming skill but also more reliable operation and smarter decision of simulation parameters. The OACIS and CARAVAN are designed to solve this demand. A difference of the two tools is number of jobs and/or parameter sets. The OACIS is designed for jobs up to $10^6 \sim 10^7$ different parameters, and the CARAVAN to 10^9 and more.

The OACIS, a job management tool for simulations and analyses are designed and developped in DESRT. It is coded using Ruby, Ruby-on-rail framework and MongoDB. After installation, users register their applications for simulations and analyses, and their computers from PC to supercomputers like K to the OACIS. Then they can design and order executions of simulations and analyses on its web-browser front end. The ssh connection is used to operate the registered remote computers and Job states are supervised by the OACIS. Current prototype transfers output files of simulations and analysis to the local computer operating the OACIS from remote computers. The results and historical data are preserved in local computer using MongoDB.

Applications and users of the OACIS have been growing in and out of AICS. As an example, the OACIS is applied to the RoboCupRescue Simulation[3]. In the RoboCupRescue Simulation, many teams made up and delivered their agent application for a specified rescue task, and the OACIS is used to rate their efficiency.

In this year 2017, improvement debugging, and user support have been continued. The CARAVAN is coded with a PGAS language X10 implemented to the K computer. A preliminary version was released in this year.

7.2.2 Social modeling and simulations

The DESRT has a perspective to challenge the social complexity by combining three major components: traffic, economics and social relations, and we have been committed to develop those models and simulations with the K computer, collaborating with many research groups in Kobe University, Ritsumeikan University, the University of Tokyo, the National Advanced Institute of Industrial Science and Technology, and IBM Japan. This collaboration named "CASSIA" had been supported by JST, CREST. In this year 2017, we extended and updated this collaboration and started a new research project named "PostK-MultiSESIM" supported by MEXT as "Exploratory Challenges on Post-K computer(Studies of multi-level spatiotemporal simulation of socioeconomic phenomena)".

7.2.2.1 Traffic model: Macroscopic fundamental diagram

Car traffic are typical traffic mode, and its simulations have been applied to reduce jam, pollution and accidents. There are many car-traffic models, and they have a lot of degree of freedom and parameters. Road network and traffic rules are complicated, and set of origin and destimation(OD set), is not well determined. Only for a single straight road, models and their behavior are established. But beyond this simple situation, reproduced traffic depends highly on a model used for simulations.

Traffic on a single straight road is characterized by a relation of car density ρ and car flux$f$, which is called as a "fundamental diagram(FD)". In low density, car flux is proportional to car density with a coefficient corresponding to a speed limit. In high density, flux decreases with density. Such unimodal $f(\rho)$ characterizes the traffic.

It has been proposed that a similar fundamental diagram may exist in traffic of urban network[1], and it is called as a "macroscopic fundamental diagram(MFD)". So we have studied a density-flux relation on a simple road network with models and simulations[4]. The road network we studied is N roads from a crossing coming back to the same crossing(left in Fig. 7.1). All of N roads have the same length, L. For this simplest road networks, two kinds of traffic models are analysed. One is to replace each road with a nonlinear register obeying a FD, that is,

$$f(\rho_i) = \begin{cases} v\rho_i & \text{if } \rho_i \le \rho_{\mathrm{P}} \\ w(1-\rho_i) & \text{if } \rho_{\mathrm{P}} \le \rho_i < 1 \end{cases} \tag{7.1}$$

where ρ_i denotes car density of a road $i (i = 1, 2, \cdots, N)$ with speed limit v, $\rho_{\mathrm{P}} \equiv 1/v$ and $w \equiv (1 - 1/v)^{-1}$. And density ρ_i develops obeying a evolution equation,

$$\frac{\mathrm{d}\rho_i}{\mathrm{d}t} = \frac{1}{N-n}\sum_{j=1}^{N} f(\rho_j) - f(\rho_i), \quad n = \sum_{i=1}^{N} \delta_{f(\rho_i),1}, \tag{7.2}$$

[1] N. Geroliminis and C. F. Daganzo, Transp. Res. B vol.42, p.759 (2008)

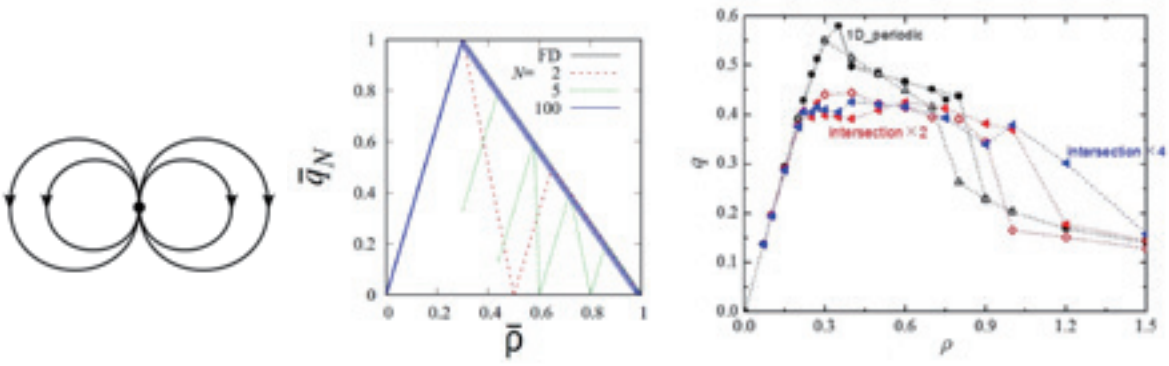

Table 7.1: A road network with $N = 4$ is shown(left). MFD of a nonlinear register model(middle) and of a OV model(right) is plotted.

where n denotes number of roads with density 1, that is, fully occupied. The other is to use car agents obeying a optimal-velocity model, that is, position x of a car obeys an equation,

$$\frac{\mathrm{d}^2x}{\mathrm{d}t^2} = a[V(\Delta) - \frac{\mathrm{d}x}{\mathrm{d}t}], \quad V(\Delta) = \tanh(\Delta - 2) + \tanh 2, \tag{7.3}$$

where Δ denotes distance from a car in front and a is a constant. Each car randomly selects one of the N roads at everytime when they are approaching to the crossing.

MFD of a model which represent each road as a nonlinear register obeying a FD is in middle of Fig. 7.1), and another MFD of another model and simulation with agent cars obeying a OV model is in right of Fig. 7.1). The result of nonlinear register model, a continuum model of traffic, does not show unimodal but many branches depending of the number of roads, N. But an OV agent model shows unimodal MFD, and this agent model explains an origin of the observed MFD. Furthermore, a continuum flow model of traffic does not reproduce MFD of network traffic.

7.2.2.2 Evacuation planning

Evacuation planning is important to minimize damage from disasters and accidents. In the past year, we had studied evacuation simulation from Tsunami attack in coastal area of Kanazawa and Kamakura cities, assuming different scenarios and parameters up to four million. In this year 2017, we have challenged to select optimal evacuation plan from computer simulations and genetic optimization.

Finding an evacuation plan finishing in shortest time sounds to be the best but it tends to be complicated. Complicated plans will not be realized because most evacuees can not completely follow a lengthy order. There is a trade-off relation between complexity of plan(S) and evacuation time(T). So an optimal plan is one that no other plan has smaller S and T. Such plan will show a curve in S-T plane, and it is a Paleto optimal curve. Computer simulations are applied to find the curve for Nishiyodogawa ward in coastal low area of Osaka city using a evacuation model.

Nishiyodogawa ward has 73 areas and 86 safe evacuation places from Tsunami attack. Its road map has 2933 nodes and 8924 links. We assumed that there are 49276 evacuees distributed in the map. Evacuees in each of 73 areas are devided into two groups with population ratio x:$(1 - x)$, and each group is planned to go to one specified safe place via one of 533 check-points, which is big corner, landmark and others.

An evacuation plan consists of a list of population fraction $x_i (i = 1, 2, \cdots, 73)$ and $146 = 73 * 2$ check-points and 146 safe places Plan complexity S is measured with distribution entropy, $S = \sum_i x_i \log x_i$. This list is coded in a genetic sequence, and an evacuation simulation obeying one plan in a genetic sequence is executed and evacuation time is estimated. Starting from a random group of genetic sequences, their evacuation times, T are plotted versus their complexity, S(Fig. 7.4). Using a genetic optimization algorithm is applied to get a Paleto optimal evacuation plans. After hundreds generations, obtained Paleto plans converges to a curve(Fig. 7.5).

It is observed in the result in Fig. 7.5 that a evacuation time does not improve much for complex plan. From simplest plan, evacuation time reduces much adding a bit complexity to plan. Therefore we can conclude that one plan in left-bottom of the curve will be a good candidate for evacuation plan.

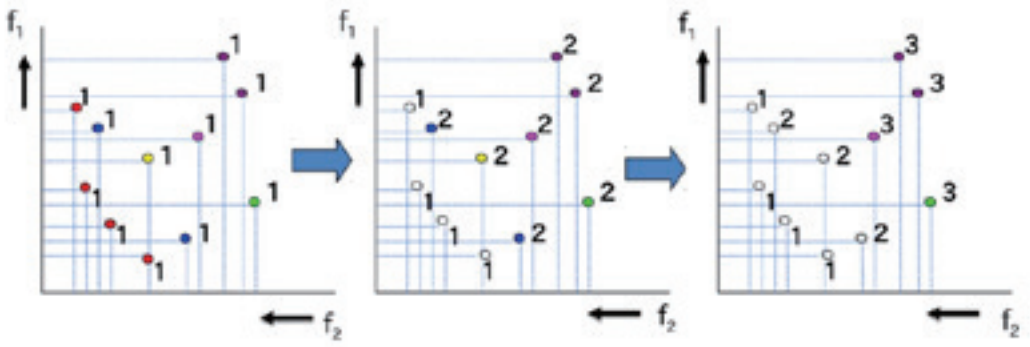

Figure 7.4: A group of genetic sequences of evacuation plans are simulated and their evacuation time is plotted versus their complexity. Sequences of Paleto optimal plan are selected for the next generation, and they are mutated and crossed over for the next generation of genetic pool. This procedure is repeated hundreds generations.

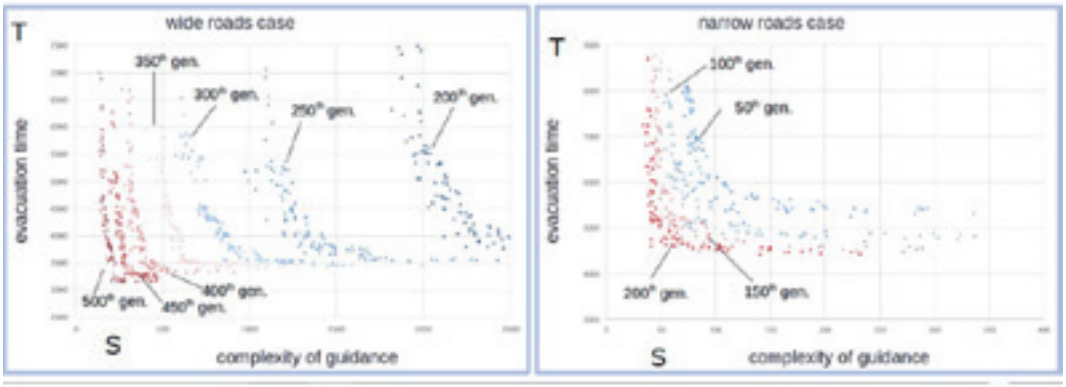

Figure 7.5: Paleto plans converges to a curve after hundreds generation. Left is for a case using only pedestrian area for evacuation, and right using all area of road.

This study was executed using the OACIS, and it will be an example that computer simulations help to make socio-political decision.

7.2.3 Other activities

In the year of 2017, following studies were published from this team:

[1] Model development of human relationship[5]

[2] Simulation study of pack-flock dynamics[6]

[3] Simulation study of particle incident on granular bed[7]

7.3 Schedule and Future Plan

From the research activities of DESRT so far, following problems are becoming clear:

[1] Simulation models, typically social ones, comprise with large input parameters and output numbers, and their behaviors are strongly nonlinear with various regimes.

[2] Social “big data” are often not big enough to picture details. It is clearly observed from our multivariate analysis of the traffic data. Thousands of samples are necessary to get minor traffic factors, but such

repetitions are not expected in the real traffic. Weather, economics, calendar, accidents and other factors varies every day.

[3] Development of multiscale social and economic models and simulations.

7.4 Publications

7.4.1 Articles

[1] Itsuki Noda, Nobuyasu Ito, Kiyoshi Izumi, Hideki Mizuta, Tomio Kamada and Hiromitsu Hattori, “Roadmap and research issues of multiagent social simulation using high-performance computing”, J. Comput. Soc. Sci. (2018) vol.1 p.155-166.
[2]Y. Murase, T. Uchitane and N. Ito, “An open-source job management framework for parameter-space exploration: OACIS”, J. Phys.: Conf. Ser. vol. 921 (2017) 012001.
[3]Shunki Takami, Kazuo Takayanagi, Shivashish Jaishy, Nobuhiro Ito, Kazunori Iwata, Yohsuke Murase, and Takeshi Uchitane “Proposed environment to support development and experiment in RoboCupRescue Simulation” to appear in RoboCup 2017: Robot World Cup XXI.
[4] 寺田健司、吉岡直樹、島田尚、伊藤伸泰、「単純な道路ネットワークにおける都市交通の巨視的基本図」、第 23 回交通流と自己駆動粒子系のシンポジウム論文集、5a-2 (2017).
[5]Janos Kertesz, Janos Torok, Yohsuke Murase, Hang-Hyun Jo, Kimmo Kaski ”Multiplex Modeling of the Society” to appear in the Springer volume on Multiplex Network, within H2020 Multiplex Project
[6]Makoto Masuko, Takayuki Hiraoka, Nobuyasu Ito, Takashi Shimada, “The effect of laziness in group chase and escape”, J. Phys. Soc. Jpn. vol.86 (2017) 085002.
[7]Takahiro Tanabe, Takashi Shimada, Nobuyasu Ito and Hiraku Nishimori, “Splash detail due to a single grain incident on a granular bed “, Physical Review E vol.95 (2017) 022906.

7.4.2 Invited Talks

[7]Nobuyasu Ito, “Social simulation on HPC” , IX Brazilian Meeting on Simulational Physics (BMSP) (Natal, Brazil, August 21-25, 2017).
[8]Nobuyasu Ito, “Car traffic modelings and simulations”, The 4th International Workshop on Physics of Social Complexity(May. 27, 2017, Sobaeksan Optical Astronomy Observatory, Danyang, Republic of Korea).
[9] 伊藤伸泰「自動車交通シミュレーションとその応用」(「計算社会科学の可能性」講演 (5)), 情報処理学会第 80 回全国大会（2018 年 3 月 13-15 日、早稲田大学西早稲田キャンパス）
[10] 伊藤伸泰「次世代スパコンと社会シミュレーション」, 経済・社会への分野横断的研究会（キヤノングローバル戦略研究所・東京、2017 年 9 月 25-26 日）
[11] 伊藤 伸泰「社会シミュレーションとスーパーコンピュータ」, 第 19 回 KEC テクノフォーラム（2018 年 1 月 23 日グランフロント大阪）
[12]Yohsuke Murase, Takashi Shimada, and Per Arne Rikvold”Effects of demographic stochasticity on biological community assembly on evolutionary time scales”, The 4th International Workshop on Physics of Social Complexity (PoSCo), Danyang, Republic of Korea, 26th - 28th May, 2017
[13] 村瀬洋介「網羅的シミュレーション実行フレームワーク」ポスト「京」萌芽的課題「基礎科学の挑戦」 サブ課題 B「相転移と流動」 公開シンポジウム

7.4.3 Oral Talks

[14]Nobuyasu Ito, “Car trffc simulation of Kobe city”, The Japan-Hungary bilateral workshop(March 22, 2018, Fukui, Japan).
[15]Nobuyasu Ito, “Order-disorder transition in repulsive self-propelled particle systems”, 8th Hungary-Japan Bilateral Workshop on Statistical Physics of Breakdown Phenomena(Nov. 23 2017, Debrecen, Hungary).
[16]Nobuyasu Ito, “Social simulation and HPC”, The 2nd Workshop on Self-Organization and Robustness of Evolving Many-Body Systems(September 8-9, 2017, Sapporo, Japan).
[17] 吉岡直樹・稲岡創・伊藤伸泰・Fengping Jin・Kristel Michielsen・Hans De Raedt「京による量子コンピュータのシミュレーション」(23aA19-8), 日本物理学会 2017 年秋季大会（岩手大学上田キャンパス、2017 年 9 月 21-24 日）
[18] 増子真・平岡喬之・伊藤伸泰・島田尚「集団追跡における怠けの効用」, 日本物理学会 2017 年秋季大会（岩手大学上田キャンパス、2017 年 9 月 21-24 日）

[19] 広谷渉・島田尚・伊藤伸泰「青空文庫における名詞バイグラムの解析」, 日本物理学会 2017 年秋季大会（岩手大学上田キャンパス、2017 年 9 月 21-24 日）
[20] 楳本大悟・土屋晴文・中澤知洋・湯浅孝之・榎戸輝揚・牧島一夫・古田禄大・玉川徹・伊藤伸泰「GROWTH 実験 2014 年度データを用いた雷雲ガンマ線のイベント探索法の改善」, 日本物理学会 2017 年秋季大会（宇都宮大学峰キャンパス、2017 年 9 月 12-15 日）
[21] 村瀬洋介「社会ネットワークにおけるサンプリングバイアス」, ネットワーク科学セミナー 2017
[22]Yohsuke Murase, Seung Ki Baek ” Finding Nash equilibria for the public-goods game using a supercomputer” The 2nd Workshop on Self-Organization and Robustness of Evolving Many-Body Systems
[23]Naoki Yoshioka, Hajime Inaoka, Nobuyasu Ito, Fengping Jin, Kristel Michielsen, Hans De Raedt, Simulations of quantum computers on supercomputers, 30th Annual Workshop on Recent Developments in Computer Simulation Studies in Condensed Matter Physics, (Georgia University, Athens, USA, Feb. 26-28, 2017).
[24] 島田尚、吉岡直樹、「粉体層中を準静的に動く球体間に働く相互作用」、日本物理学会第 72 回年次大会 (大阪大学、大阪、3 月 17-20 日, 2017).
[25] 吉岡直樹、稲岡創、伊藤伸泰、Fengping Jin、Kristel Michielsen、Hans De Raedt、「量子コンピュータの大規模並列シミュレーション」、日本物理学会第 72 回年次大会 (大阪大学、大阪、3 月 17-20 日, 2017).
[26]Naoki Yoshioka, Ferenc Kun, and Nobuyasu Ito, Kinetic Monte Carlo algorithm for thermally induced breakdown of fiber bundles, The 4th International Workshop on Physics of Social Complexity (PoSCo) (Sobaeksan, Korea, May 26-28, 2017).
[27]Naoki Yoshioka, Takashi Shimada, and Nobuyasu Ito, Stability and macroscopic fundamental diagram in simple model of urban traffic, The 2nd Workshop on Self-Organization and Robustness of Evolving Many-Body Systems (Hokkaido University, Sapporo, Japan, Sep. 8-9, 2017).
[28]Naoki Yoshioka, Ferenc Kun, and Nobuyasu Ito, Jump distance of epicenters in thermally induced cracking, 8th Hungary-Japan Bilateral Workshop on Statistical Physics of Breakdown Phenomena (Debrecen, Hungary, Nov. 22-23, 2017).
[29] 寺田健司、吉岡直樹、島田尚、伊藤伸泰、「単純な道路ネットワークにおける都市交通の巨視的基本図」、第 23 回交通流と自己駆動粒子系のシンポジウム (名古屋大学、名古屋、12 月 4-5 日, 2017).

7.4.4 Software

[30] OACIS and CARAVAN

Chapter 8

Computational Molecular Science Research Team

8.1 Members

Takahito Nakajima (Team Leader)

Noriyuki Minezawa (Research Scientist)

Takehiro Yonehara (Research Scientist)

Keisuke Sawada (Postdosctoral Researcher)

William Dawson (Postdosctoral Researcher)

Wataru Uemura (Postdosctoral Researcher)

Kizashi Yamaguchi (Visiting Researcher)

Takashi Kawakami (Visiting Researcher)

Muneaki Kamiya (Visiting Researcher)

8.2 Research Activities

8.2.1 Development of original molecular theory

An atomic- and molecular-level understanding of drug actions and the mechanisms of a variety of chemical reactions will provide insight for developing new drugs and materials. Although a number of diverse experimental methods have been developed, it still remains difficult to investigate the state of complex molecules and to follow chemical reactions in detail. Therefore, a theoretical molecular science that can predict the properties and functions of matter at the atomic and molecular levels by means of molecular theoretical calculations is keenly awaited as a replacement for experiment. Theoretical molecular science has recently made great strides due to progress in molecular theory and computer development. However, it is still unsatisfactory for practical applications. Consequently, our main goal is to realize an updated theoretical molecular science by developing a molecular theory and calculation methods to handle large complex molecules with high precision under a variety of conditions. To achieve our aim, we have so far developed several methods of calculation. Examples include a way for resolving a significant problem facing conventional methods of calculation, in which the calculation volume increases dramatically when dealing with larger molecules; a way for improving the precision of calculations in molecular simulations; and a way for high-precision calculation of the properties of molecules containing heavy atoms such as metal atoms.

8.2.2 New molecular science software NTChem

Quantum chemistry software comprises immensely useful tools in material and biological science research. Widely diverse programs have been developed in Western countries as Japan has lagged. In fact, only a few programs have been developed in Japan. The mission of our research team is to provide K computer users with a high-performance software for quantum molecular simulation. In the early stage of the K computer project, no quantum chemistry software was available for general purpose and massively parallel computation on the K computer because not every program was designed for use on it. Therefore, we have chosen to develop a new comprehensive ab initio quantum chemistry software locally: NTChem. NTChem is completely new software that implements not only standard quantum chemistry approaches, but also original and improved theoretical methods that we have developed in our research work. The main features of the current version, NTChem2013, are the following:

1). Electronic structure calculation of the ground state of atoms and molecules based on Hartree-Fock (HF) and density functional theory (DFT) methods.

2). Linear-scaling or low-scaling DFT: Gaussian and finite-element Coulomb (GFC) resolution-of-the-identity (RI) DFT, pseudospectral DFT/HF, and dual-level DFT.

3). Low-scaling SCF calculation using diagonalization-free approaches: purification density matrix, pseudo-diagonalization, and quadratic convergence SCF.

4). Excited-state DFT calculation: time-dependent DFT (TDDFT) and transition potential (DFT-TP).

5). Accurate electron correlation methods for ground and excited states: Møller-Plesset perturbation theory, coupled-cluster (CC) theory, and quantum Monte Carlo (QMC) method.

6). Massively parallel computing on the K computer and Intel-based architectures: HF, DFT, resolution-of-the-identity second-order Møller-Plesset (RI-MP2) method, and QMC method.

7). Two-component relativistic electronic structure calculation with spin-orbit (SO) interactions: Douglas-Kroll (DK) (DK1, DK2, and DK3), regular approximation (RA) (zeroth-order RA (ZORA) and infinite-order RA (IORA)), and Relativistic scheme for Eliminating Small Components (RESC).

8). Model calculations for large molecular systems: quantum mechanics/molecular mechanics (QM/MM) and Our own N-layered Integrated molecular Orbital and molecular Mechanics (ONIOM).

9). Calculation of solvation effects: COnductor-like Screening MOdel (COSMO) (interfaced with the HONDO program), averaged solvent electrostatic potential/molecular dynamics (ASEP/MD), and QM/MM-MD.

10). Efficient calculation for chemical reaction pathway.

11). Ab initio molecular dynamics calculation.

12). Calculation of magnetic properties: nuclear magnetic resonance (NMR) chemical shifts, magnetizabilities, and electron paramagnetic resonance (EPR) g tensors.

13). Population analysis: Mulliken and natural bond orbital (NBO) analysis (interfaced with NBO 6.0).

14). Orbital interaction analysis: maximally interacting orbital (MIO) and paired interacting orbital (PIO) methods.

8.3 Research Results and Achievements

8.3.1 Massively Parallel Linear Scaling Quantum Chemistry

The goal of this project is to develop techniques for efficiently performing quantum chemistry calculations on systems with thousands of atoms. There are two main operations required in quantum chemistry codes: computing the Fock matrix, and solving for the density matrix. Commonly used computational techniques have $O(N^3)$ or worse scaling behavior, which severely limits the size of systems that can be treated. Additionally, treating systems of this size requires parallel algorithms that reduce both the computational time and the memory footprint. In FY2016, we developed a parallel library for performing the sparse matrix operations which are at the heart of low order scaling methods. In this previous fiscal year, we built upon this library to enable calculations on large systems in the NTChem code.

In FY2017, we performed two studies to help understand different linear scaling solvers. Using the sparse matrix library we had developed, we implemented linear scaling methods based on density matrix purification

and minimization, and analyzed their performance on matrices from several different quantum chemistry codes. We also showed how the same techniques used in quantum chemistry can also be used for network science. As a part of the RIKEN-CEA collaboration, we helped benchmark and analyze the CheSS library which uses the Fermi Operator Expansion technique as a solver.

In Fig. 8.1, we compared the performance of the sparse matrix based solvers with the EigenExa eigensolver library. The sparse matrix based solver performs significantly better, enabling calculations using tens of thousands of basis functions.

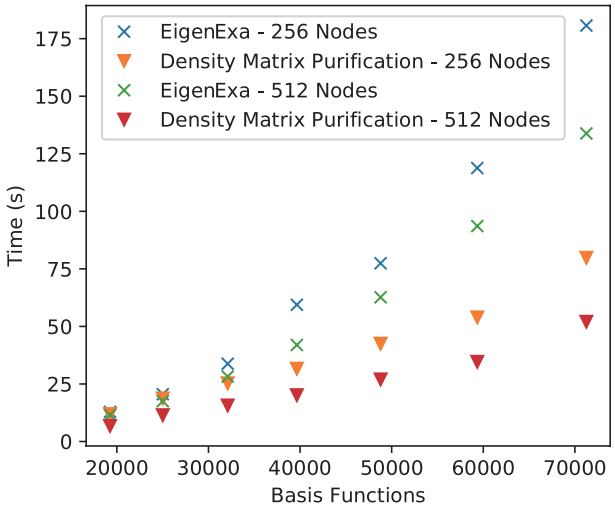

Figure 8.1: Performance of the density matrix solver.

8.3.1.1 Massively parallel sparse matrix function calculations with NTPoly[1]

We present NTPoly, a massively parallel library for computing the functions of sparse, symmetric matrices. The theory of matrix functions is a well developed framework with a wide range of applications including differential equations, graph theory, and electronic structure calculations. One particularly important application area is diagonalization free methods in quantum chemistry. When the input and output of the matrix function are sparse, methods based on polynomial expansions can be used to compute matrix functions in linear time. We present a library based on these methods that can compute a variety of matrix functions. Distributed memory parallelization is based on a communication avoiding sparse matrix multiplication algorithm. OpenMP task parallellization is utilized to implement hybrid parallelization. We describe NTPoly's interface and show how it can be integrated with programs written in many different programming languages. We demonstrate the merits of NTPoly by performing large scale calculations on the K computer.

8.3.1.2 Efficient Computation of Sparse Matrix Functions for Large-Scale Electronic Structure Calculations: The CheSS Library[2]

We present CheSS, the "Chebyshev Sparse Solvers" library, which has been designed to solve typical problems arising in large-scale electronic structure calculations using localized basis sets. The library is based on a flexible and efficient expansion in terms of Chebyshev polynomials and presently features the calculation of the density matrix, the calculation of matrix powers for arbitrary powers, and the extraction of eigenvalues in a selected interval. CheSS is able to exploit the sparsity of the matrices and scales linearly with respect to the number of nonzero entries, making it well-suited for large-scale calculations. The approach is particularly adapted for setups leading to small spectral widths of the involved matrices and outperforms alternative methods in this regime. By coupling CheSS to the DFT code BigDFT, we show that such a favorable setup is indeed possible in practice. In addition, the approach based on Chebyshev polynomials can be massively parallelized, and CheSS exhibits excellent scaling up to thousands of cores even for relatively small matrix sizes.

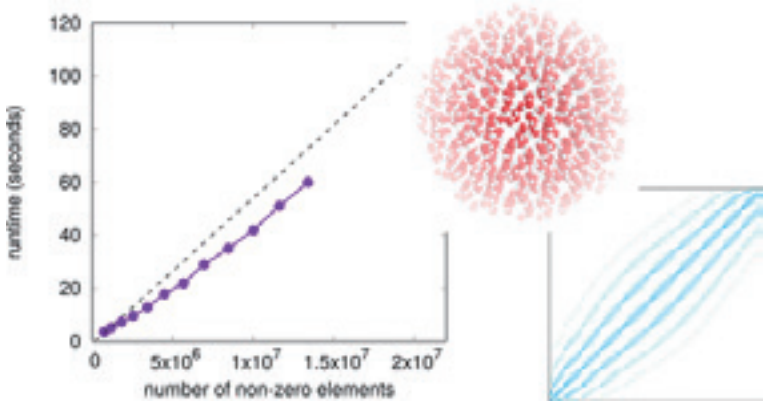

8.3.2 Relativistic Time-Dependent Density Functional Theory for Molecular Properties[3]

In this study, we introduce the two-component relativistic TDDFT with spin 窶登 rbit interactions to calculate linear response properties and excitation energies. The approach is implemented in the NTChem program. Our implementation is based on a noncollinear exchange 窶田 orrelation potential presented by Wang et al. In addition, various DFT functionals including the range-separated hybrid functionals have been derived and implemented with the aid of a newly developed computerized symbolic algebra system. The two-component relativistic TDDFT with spin 窶登 rbit interactions was successfully applied to the calculation of the frequency-dependent polarizabilities of SnH_4 and PbH_4 molecules containing heavy atoms and the excitation spectra of a HI molecule.

8.3.3 A coupled cluster theory with iterative inclusion of triple excitations and associated equation of motion formulation for excitation energy and ionization potential[4]

A single reference coupled cluster theory that is capable of including the effect of connected triple excitations has been developed and implemented. This is achieved by regrouping the terms appearing in perturbation theory and parametrizing through two different sets of exponential operators: while one of the exponentials, involving general substitution operators, annihilates the ground state but has a non-vanishing effect when it acts on the excited determinant, the other is the regular single and double excitation operator in the sense of conventional coupled cluster theory, which acts on the HF ground state. The two sets of operators are solved as coupled non-linear equations in an iterative manner without significant increase in computational cost than the conventional coupled cluster theory with singles and doubles excitations. A number of physically motivated and computationally advantageous sufficiency conditions are invoked to arrive at the working equations and have been applied to determine the ground state energies of a number of small prototypical systems having weak multi-reference character. With the knowledge of the correlated ground state, we have reconstructed the triple excitation operator and have performed equation of motion with coupled cluster singles, doubles, and triples to obtain the ionization potential and excitation energies of these molecules as well. Our results suggest that this is quite a reasonable scheme to capture the effect of connected triple excitations as long as the ground state remains weakly multi-reference.

8.3.4 Correlation effects beyond coupled cluster singles and doubles approximation through Fock matrix dressing[5]

We present an accurate single reference coupled cluster theory in which the conventional Fock operator matrix is suitably dressed to simulate the effect of triple and higher excitations within a singles and doubles framework. The dressing thus invoked originates from a second-order perturbative approximation of a similarity transformed Hamiltonian and induces higher rank excitations through *local renormalization* of individual occupied and unoccupied orbital lines. Such a dressing is able to recover a significant amount of correlation effects beyond singles and doubles approximation, but only with an economic n^5 additional cost. Due to the inclusion of higher rank excitations via the Fock matrix dressing, this method is a natural improvement over conventional

coupled cluster theory with singles and doubles approximation, and this method would be demonstrated via applications on some challenging systems. This highly promising scheme has a conceptually simple structure which is also easily generalizable to a multi-reference coupled cluster scheme for treating strong degeneracy. We shall demonstrate that this method is a natural lowest order perturbative approximation to the recently developed *iterative n-body excitation inclusive coupled cluster singles and doubles* scheme.

8.3.5 Solving the problem of many electronic system with the Antisymmetrized geminal powers

The problem of the many electronic system can be described by the diagonalization of the large matrix of the hamiltonian. When the size of the system is getting larger the dimension of the matrix grows exponentially so the true ground state becomes more and more difficult to obtain. To solve this problem there are proposed a variety of electronic wavefunctions including the matrix product states or the Jastrow Slater states. We propose more sophisticated way that is the superpostion of several antisymmetrized geminal states. We named this method as extended symmetric tensor decompositon (ESTD).

We obtained the method to obtain the second order reduced density matrix of the above mentioned state. This density matrix is a more extended version of the so called one electron density and containing more information. Since the electronic problem is a problem of two body interaction the density matrix could with no approximation describe the behavior of the electronic wavefunction.

By using the gradient based variational method for the parameters we obtained numerical results very close to the exact ground states(Fig. 8.2, Fig. 8.3). The calculation could be done with the time scaling of the fifth power of the system size so this method is likely to be extended to larger systems.

There are several way to develop this formalism on the quantum states. We could extend the variational method to the excited states by using the orthogonalization of each state. Also we could do the large scale calculation with the parralelization of the method. When using the tensor decomposition of the two electron matrix element further acceleration of the geminal states could be expected.

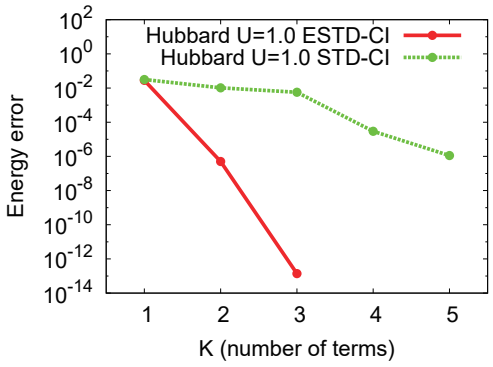

Figure 8.2: Energy error of 4 sites U=1.0 Hubbard model for ESTD (solid line with circle) and STD-CI (broken line with circle).

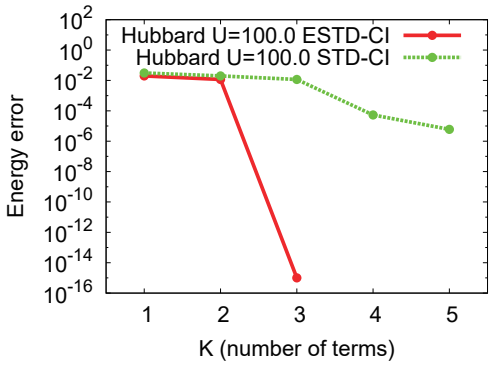

Figure 8.3: Energy error of 4 sites U=100.0 Hubbard model for ESTD (solid line with circle) and STD-CI (broken line with circle).

8.3.6 Development of a quantum dynamics method for excited electrons in molecular aggregate system using a group diabatic Fock matrix[6]

Our main research subject is to understand a photochemical quantum process in excited states associated with a light–energy conversion. Beyond a possible experimental mesurement for the ultrafast photochemistry, we advance a theoretical research on an excited electron dynamics in molecules coupled with light-matter, non-adiabatic, and SO interactions.

In FY2017, we developed a practical calculation scheme for a description of excited electron dynamics in molecular aggregates within a local group diabatic Fock representation. This scheme makes it easy to analyze the interacting time-dependent excitation of local sites in complex systems. We demonstrated the usability of the present method. NTChem was used for ab initio electronic structure calculation.

Fig. 8.4 shows the application of the present method to a 20-mer circle of ethylene molecules. For details, see its caption and article. The dynamics were characterized by the inherent gradient of electron affinities among the monomers under the employed conditions of initial excitations and external laser-electron couplings. Through local group analyses of the dynamical electrons, we can obtain an intuitive understanding of the electron transfers between the monomers. The present scheme is advantageous for the future ab initio modeling of excited electron migration dynamics in a complex molecular system.

With the use of the newly introduced method, we can investigate a size of electron Hilbert space involving electron migration in molecular aggregates, of which information has a critical importance for the understanding of the mechanism of light-energy convergion process intended for a modulation of it by varing constituent molecules and their enviromnents. This has a significance for an exploration of a creation of an efficient solar energy conversion system. For this purpose, in the next fiscal year, we will try to obtain a deeper insight about a dependence of properties of electron transfer network in excited states of aggregate systems on initial local excitations and external light fields associated with the characters of their electronic structures.

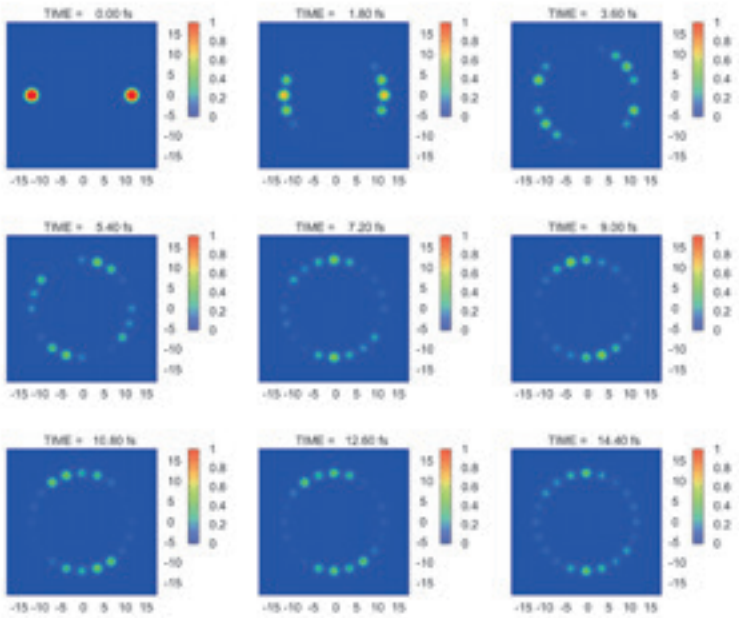

Figure 8.4: Schematics of the exciton dynamics in the circularly oriented 20mer ethylene aggregate system. A continuum light field is applied with the 700 nm wavelength and polarization vector of $\left(\frac{1}{\sqrt{3}}, \frac{1}{\sqrt{3}}, \frac{1}{\sqrt{3}}\right)$. The field strength is 0.02 a.u. The dynamics starts from local two excitations prepared as Frenkel exciton at 1-th and 11-th monomer. The coarse graining manner is employed with respect to each monomer in expressing an amount of exciton assigned to it.

8.3.7 Photochemistry of coumarin: Time-dependent density functional theory/-trajectory surface hopping simulation approach

In FY2017, we performed the research supported by MEXT as "Priority Issue on Post-K Computer" (Development of new fundamental technologies for high-efficiency energy creation, conversion/storage and use). The aim of the project is (1) to elucidate the working mechanisms of organic photovoltaic solar cells and (2) to establish the relationship between the microscopic molecular structures and the power conversion efficiency (PCE) by *ab initio* quantum mechanical methods. Since the efficient formation of a charge-separated state is crucial for realizing high-performance solar cells, it is necessary to simulate the exciton dynamics leading to the charge separation and to assess critical factor(s) controlling that process. Furthermore, due to the large size of a donor–acceptor system, the development of computationally efficient methods is of great importance to observe dynamical processes in the electronically excited states.

For that purpose, we developed the Tully's fewest switch surface hopping molecular dynamics (FSSH-MD) simulation combined with the linear-response TDDFT. The algorithm implemented is almost as fast as usual

Born–Oppenheimer MD. We interfaced the code with the electronic structure program package NTChem and performed a preliminary simulation. In the present study, we applied the program to the ring-opening reaction of unsubstituted coumarin on the excited state. The coumarin is usually a good fluorophore, and many coumarin molecules with functional groups have been synthesized industrially. Interestingly, coumarin with no functional group has a low quantum yield of fluorescence. Previous theoretical studies suggest that unsubstituted coumarin has nonradiative decay paths to the ground state via direct ($\pi\pi^*/S_0$) or indirect ($\pi\pi^* \rightarrow n\pi^* \rightarrow n\pi^*/S_0$) way. We examine the photochemical processes of this molecule after the excitation to the S_3 ($\pi\pi^*$) by TDDFT/FSSH-MD.

Fig. 8.5(a) shows the summary of the time-dependent population for each state (S_0–S_3) by averaging over 75 trajectories. The initial S_3 state halves its population in 100 fs, and the S_1 state increases at the same rate. The S_1 state is dominant through the maximum simulation time of 500 fs. The ground state begins to recover at the 300 fs, but 60 percent of trajectories still stay on the S_1 state. The fast relation to the S_1 state is consistent with Kasha's rule. Fig. 8.5(b) gives a typical trajectory that reaches the S_0/S_1 crossing. The molecular structure distorts significantly. The bond between the ether oxygen and the carbonyl carbon breaks and the six-membered ring loses the planarity. It is interesting that one could enhance nonradiative decay of other coumarin molecules with large fluorescence quantum yields by exciting the stretch motion selectively.

At present, the algorithm does not account for spin-forbidden processes. The thiophene molecule, which is one of the building blocks for solar cells, has an efficient intersystem crossing to the triplet state. Therefore, it is necessary to treat both the spin-allowed and spin-forbidden processes on an equal footing to understand the loss of PCE. The development of the TDDFT with SO-TDDFT is in progress, and the combination of SO-TDDFT and FSSH-MD is straightforward.

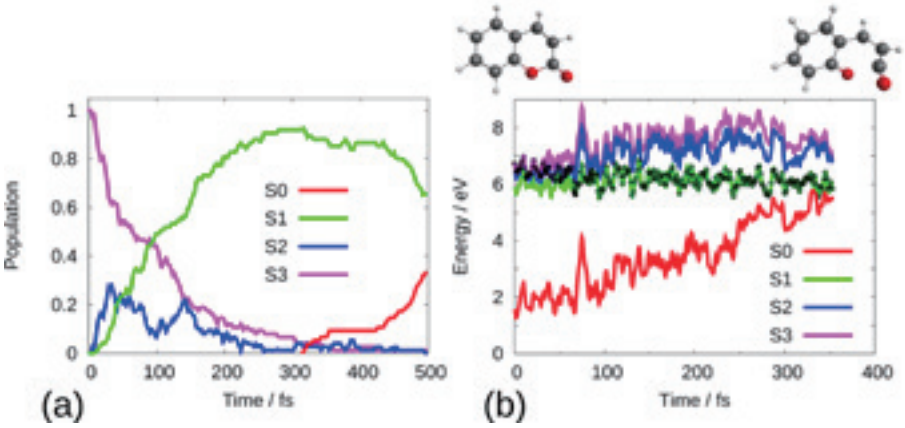

Figure 8.5: (a) Time-dependent population of state S_0–S_3. (b) Typical trajectory of coumarin leading to S_0/S_1 crossing.

8.3.8 Discovery of Pb-free Perovskite solar cells via high-throughput simulation on the K computer[7]

We performed a systematic high-throughput simulation with DFT for 11025 compositions of hybrid organic-inorganic halide compounds in ABX_3 and $A_2BB'X_6$ forms, where A is an organic or inorganic component, B/B' is a metal atom, and X is a halogen atom. The computational results were compiled as a materials database. We performed massive computational simulation by using the K computer, which is a massively parallel many-core supercomputer in Japan. By applying the screening procedure to all the compounds in the materials database, we discovered novel candidates for environmentally friendly lead-free perovskite solar cells and propose 51 low-toxic halide single and double perovskites, most of which are newly proposed in this study. The proposed low-toxic halide double perovskites are classified under six families: group-14-group-14, group-13-group-15, group-11-group-11, group-9-group-13, group-11-group-13, and group-11-group-15 double perovskites.

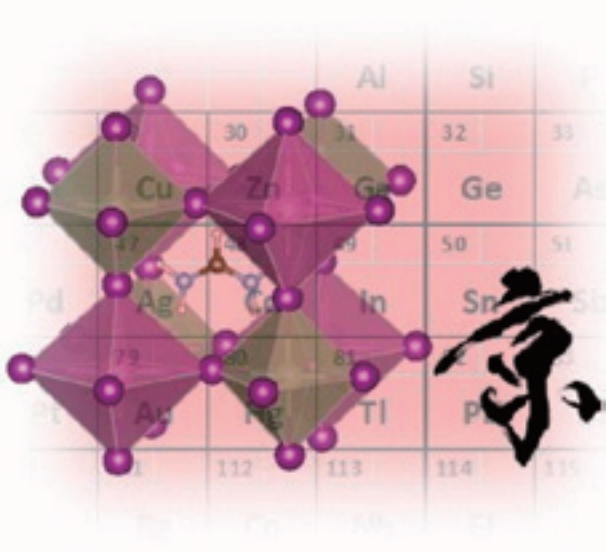

8.3.9 Can electron-rich oxygen (O^{2-}) withdraw electrons from metal centers? A DFT study on oxoanion-caged polyoxometalates[8]

The answer to the question "*Can electron-rich oxygen (O^{2-}) withdraw electrons from metal centers?*" is seemingly simple, but how the electron population on the M atom behaves when the O-M distance changes is a matter of controversy. A case study has been conducted for Keggin-type polyoxometalate (POM) complexes, and the first-principles electronic structure calculations were carried out not only for real POM species but also for "hypothetical" ones whose heteroatom was replaced with a point charge. From the results of natural population analysis, it was proven that even an electron-rich O^{2-}, owing to its larger electronegativity as a neutral atom, withdraws electrons when electron redistribution occurs by the change of the bond length. In the case where O^{2-} coexists with a cation having a large positive charge (e.g., $P^{5+}(O^{2-})_4 = [PO_4]^{3-}$), the gross electron population (GEP) on the M atom seemingly increases as the O atom comes closer, but this increment in GEP is not due to the role of the O atom but due to a Coulombic effect of the positive charge located on the cation. Furthermore, it was suggested that not GEP but net electron population (NEP) should be responsible for the redox properties.

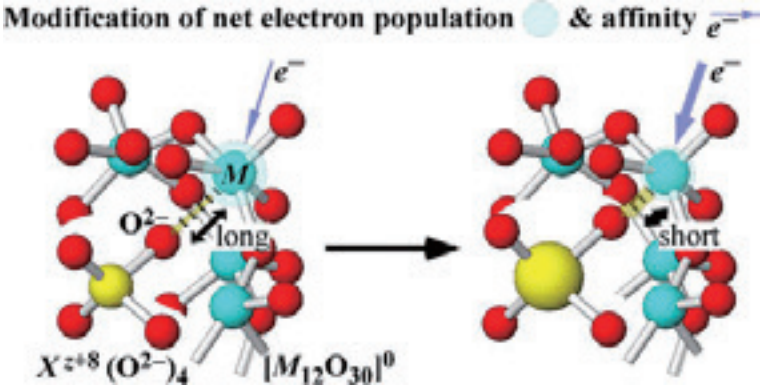

8.3.10 Quantum Chemical Study on the Multi-Electron Transfer of Keggin-Type Polyoxotungstate Anions: The Relation of Redox Potentials to the Bond Valence of μ_4-O-W[9]

By selectively investigating the effect of the bond valence using the hypothetical $[(PO_4)W_{12}O_{36}]^{3-}$ species having various bond valences, we could clearly reveal the origin of the linear dependence of the LUMO energy

(or the redox potential) on the bond valence. The LUMO of the Keggin-type polyoxotungstates mainly consists of W 5d. The energy of W 5d as well as of the LUMO goes down as the bond valence becomes large (i.e., as the net electron population on W decreases due to the electron-withdrawing effect of the μ_4-O atoms). This is the origin of the linear dependence of LUMO energy on the bond valence.

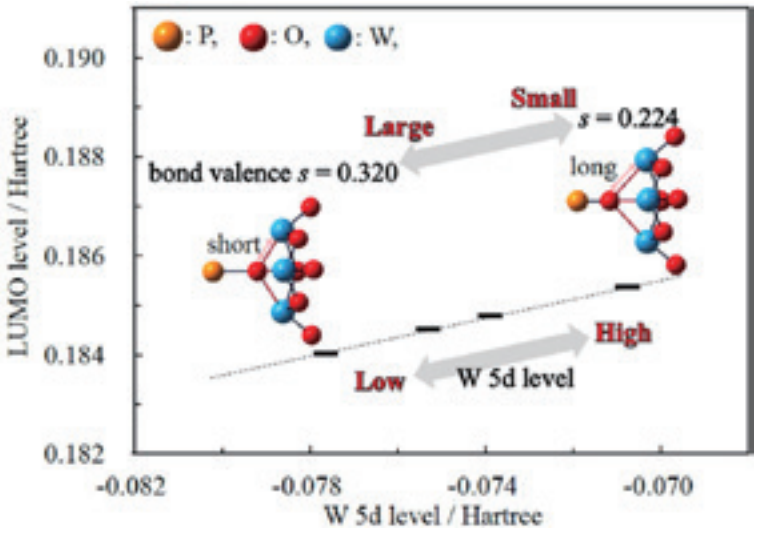

8.3.11 Full-valence density matrix renormalisation group calculations on meta-benzyne based on unrestricted natural orbitals. Revisit of seamless continuation from broken-symmetry to symmetry-adapted models for diradicals[10]

In this work, we show that the natural orbitals of unrestricted hybrid DFT (UHDFT) can be used as the active space orbitals to perform multireference (MR) calculations, for example, the density matrix renormalisation group (DMRG) and Mukherjee-type (Mk) MR coupled-cluster (CC) method. By including a sufficiently large number of these natural orbitals, full-valence (FV) active space can be identified without recourse of the expensive self-consistent procedures for DMRG-SCF. Several useful chemical indices are derived based on the occupation numbers of the natural orbitals for seamless continuation from broken-symmetry (BS) to symmetry-adapted (SA) methods. These procedures are used on 1,3-didehydrobenzene (meta-benzyne) to calculate its singlet (S)-triplet (T) gap. We compare our results to available experiments and computational results obtained by several other groups. We see our procedures as a seamless bridge between single-reference BS methods, such as UHDFT, and the SA MR methods, such as FV DMRG and MkMRCC.

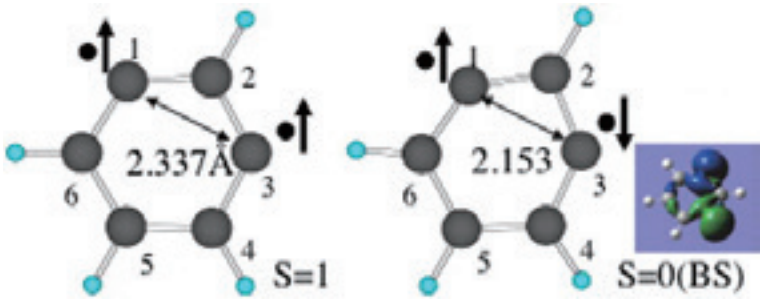

8.3.12 *Ab initio* computations of zero-field splitting parameters and effective exchange integrals for single-molecule magnets (Mn_{12}- and $Mn_{11}Cr$-acetate clusters)[11]

In this study, the zero-field splitting parameters (D, E) and effective exchange integrals (J) for a $Mn_{12}/Mn_{11}Cr$ mixed crystal were evaluated using *ab initio* molecular orbital (MO) computations based on the hybrid DFT methods for $Mn_{11}Cr^*$-acetate cluster (Mn_{12} and $Mn_{11}Cr$ mixing). In this study, Mn_{12}-acetate, $Mn_{11}Cr$-acetate, and $Mn_{12-n}Cr_n$-acetate clusters were focused on. The zero-field splitting (ZFS) parameters are obtained by UB3LYP methods, i.e. -0.339 cm^{-1} (Mn_{12}-acetate) and -0.351 cm^{-1} ($Mn_{11}Cr$-acetate). The energy barriers were estimated to be 53.7 K and 50.4 K, which showed good agreement with previously reported experimental values of 68.8 K and 56.8 K, respectively. The origin of such anisotropy is assumed to be the eight Mn^{III} ions with d^4-electrons in their outer ring subunits, where elongated conformation along the axial direction becomes very important and leads to negative D values. The spin networks in these clusters were discussed by using the effective exchange integral sets. The Js value, as estimated by the UB3LYP method revealed that the J_2, J_3, and J_3' interactions played important roles in describing the parallel spin ordering in cubane and ring subunits as well as the antiferromagnetic coupling between two subunits. The other interactions, i.e. J_1, J_1', J_4, and J_4' somewhat disturbed the spin ordering in the Mn_{12}-acetate cluster. The substitution of Mn^{IV} by Cr^{III} did not change the spin network. However, the total S value changed after the substitution.

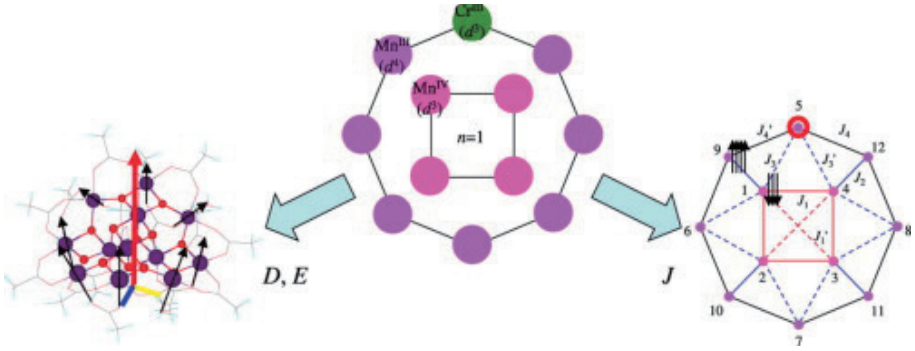

8.3.13 Theory of chemical bonds in metalloenzymes XXI. Possible mechanisms of water oxidation in oxygen evolving complex of photosystem II[12]

Possible mechanisms for water cleavage in oxygen evolving complex (OEC) of photosystem II (PSII) have been investigated based on broken-symmetry (BS) hybrid DFT (HDFT)/def2 TZVP calculations in combination with available XRD, XFEL, EXAFS, XES and EPR results. The BS HDFT and the experimental results have provided basic concepts for understanding of chemical bonds of the $CaMn_4O_5$ cluster in the catalytic site of OEC of PSII for elucidation of the mechanism of photosynthetic water cleavage. Scope and applicability of the hybrid DFT (HDFT) methods have been examined in relation to relative stabilities of possible nine intermediates such as Mn-hydroxide, Mn-oxo, Mn-peroxo, Mn-superoxo, etc., in order to understand the O-O (O-OH) bond formation in the S_3 and/or S_4 states of OEC of PSII. The relative stabilities among these intermediates are variable, depending on the weight of the HF exchange term of HDFT. The Mn-hydroxide, Mn-oxo and Mn-superoxo intermediates are found to be preferable in the weak, intermediate and strong electron correlation regimes, respectively. Recent different serial femtosecond X-ray (SFX) results in the S_3 state are investigated based on the proposed basic concepts under the assumption of different water-insertion steps for water cleavage in the Kok cycle. The observation of water insertion in the S_3 state is compatible with previous large-scale QM/MM results and previous theoretical proposal for the chemical equilibrium mechanism in the S_3 state. On the other hand, the no detection of water insertion in the S_3 state based on other SFX results is consistent with previous proposal of the O-OH (or O-O) bond formation in the S_4 state. Radical coupling and non-adiabatic one-electron transfer (NA-OET) mechanisms for the OO-bond formation are examined using the energy diagrams by QM calculations and by QM(UB3LYP)/MM calculations. Possible reaction pathways for the O-O and O-OH bond formations are also investigated based on two water-inlet pathways for oxygen evolution in OEC of PSII. Future perspectives are discussed in relation to post HDFT calculations of the energy diagrams for elucidation of the mechanism of water oxidation in OEC of PSII.

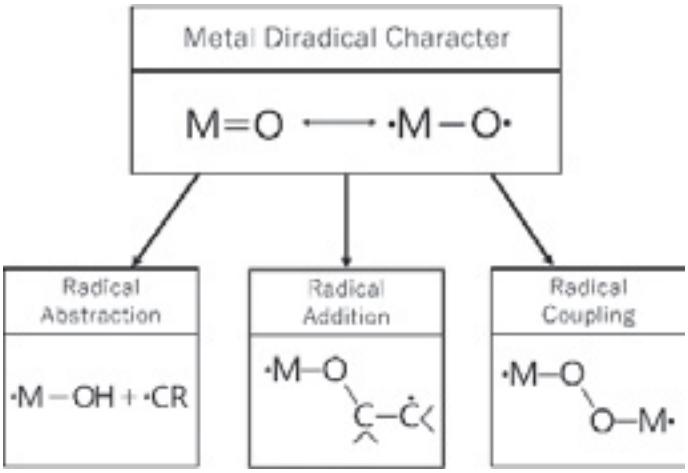

8.4 Schedule and Future Plan

In the next fiscal year, we will continue to develop new algorithms and improve the parallel efficiency of the NTChem suit of program. We will work to develop a new version of NTChem which can perform quantum chemistry calculations on systems with thousands of atoms. The NTPoly library will be utilized to develop a memory parallelization scheme, removing a significant cause of system size limitations from NTChem. We will replace the basic solver routines with linear scaling methods based on density matrix minimization and purification. We will also work to implement TDDFT with the same memory parallelization scheme. Moreover, we will continue to develop the SO-TDDFT, related methods for excited-state dynamics, and high-accuracy quantum chemical methods.

8.5 Publications

8.5.1 Articles

[1]W. Dawson and T. Nakajima, "Massively parallel sparse matrix function calculations with NTPoly", Comput. Phys. Commun. **225**, 154 (2018).
[2]S. Mohr, W. Dawson, M. Wagner, D. Caliste, T. Nakajima, and L. Genovese, "Efficient Computation of Sparse Matrix Functions for Large-Scale Electronic Structure Calculations: The CheSS Library", J. Chem. Theory Comput. **13**, 4684 (2017).
[3]M. Kamiya and T. Nakajima, "Relativistic Time-Dependent Density Functional Theory for Molecular Properties", Frontiers of Quantum Chemistry, 223 (2018).
[4]R. Maitra, Y. Akinaga, and T. Nakajima, "A coupled cluster theory with iterative inclusion of triple excitations and associated equation of motion formulation for excitation energy and ionization potential", J. Chem. Phys. **147**, 074103 (2017).
[5]R. Maitra and T. Nakajima, "Correlation effects beyond coupled cluster singles and doubles approximation through Fock matrix dressing", J. Chem. Phys. **147**, 204108 (2017).
[6]T. Yonehara and T. Nakajima, "A quantum dynamics method for excited electrons in molecular aggregate system using a group diabatic Fock matrix", J. Chem. Phys. **147**, 074110 (2017).
[7]T. Nakajima and K. Sawada, "Discovery of Pb-free Perovskite solar cells via high-throughput simulation on the K computer", J. Phys. Chem. Lett. **8**, 4826 (2017).
[8]A. Takazaki, K. Eda, T. Osakai, and T. Nakajima, "Can electron-rich oxygen (O^{2-}) withdraw electrons from metal centers? A DFT study on oxoanion-caged polyoxometalates", J. Phys. Chem. A **121**, 7684 (2017).
[9]A. Takazaki, K. Eda, T. Osakai, and T. Nakajima, "Quantum Chemical Study on the Multi-Electron Transfer of Keggin-Type Polyoxotungstate Anions: The Relation of Redox Potentials to the Bond Valence of μ_4-O-W", J. Comput. Chem. Jpn. **16**, 93 (2017).
[10]T. Kawakami, T. Saito, S. Sharma, S. Yamanaka, S. Yamada, T. Nakajima, M. Okumura, and K. Yamaguchi, "Full-valence density matrix renormalisation group calculations on meta-benzyne based on unrestricted natural orbitals. Revisit of seamless continuation from broken-symmetry to symmetry-adapted models for diradicals", Mol. Phys. **115**, 2267 (2017).

[11]S. Sano, T. Kawakami, S. Yoshimura, M. Shoji, S. Yamanaka, M. Okumura, T. Nakajima, and K. Yamaguchi, "*Ab initio* computations of zero-field splitting parameters and effective exchange integrals for single-molecule magnets (Mn_{12-} and Mn_{11}Cr-acetate clusters)", Polyhedron **136**, 159 (2017).
[12]K. Yamaguchi, M. Shoji, H. Isobe, S. Yamanaka, T. Kawakami, S. Yamada, M. Katouda, and T. Nakajima, "Theory of chemical bonds in metalloenzymes XXI. Possible mechanisms of water oxidation in oxygen evolving complex of photosystem II", Mol. Phys. **116**, 717 (2018).

Chapter 9

Computational Materials Science Research Team

9.1 Members

- Seiji Yunoki (Team Leader)
- Yuichi Otsuka (Research Scientist)
- Shigetoshi Sota (Research Scientist)
- Hiroshi Ueda (Research Scientist)
- Mohammad Khazaei (Research Scientist)
- Ahamad Ranjbar (Postdoctoral Researcher)
- Akiko Masaki-Kato (Special Postdoctoral Researcher, joint)
- Sandro Sorella (Senior Visiting Scientist)
- Takami Toyama (Senior Visiting Scientist)
- Yutaka Imamura (Visiting Scientist)
- Susumu Yamada (Visiting Scientist)
- Kazuhiro Seki (Visiting Scientist)
- Michele Casula (Visiting Scientist)
- Keiko Matsuoka (Assistant)

9.2 Research Activities

9.2.1 Large-scale QMC simulations for interacting fermions

We develop a quantum Monte Carlo (QMC) method, which is one of the most reliable and efficient techniques for Hubbard-type lattice models of interacting electrons. Typical target systems we aim are of the order of 10,000 electrons unless the notorious minus-sign problem occurs. One of the main focuses in our QMC project is to clarify quantum criticality of quantum phase transitions in strongly-correlated electrons with high accuracy, which would be impossible without the power of K computer.

We have implemented a highly efficient QMC code based on the auxiliary-field scheme for lattice fermion systems at zero temperature. Since numerical calculations involved in this formulation are mostly linear algebraic procedure such as matrix-matrix product and numerical orthogonalization, we can take advantage of the highly optimized numerical library on K computer to calculate physical observables with a high degree of accuracy on unprecedentedly large systems.

By using this improved code, we succeeded to clarify the nature of the Mott transition in interacting Dirac fermions in two spatial dimensions [Otsuka *et al.*, Phys. Rev. X. (2016)]. This quantum phase transition is known to belong to the chiral-$SU(2)$ class in terms of the celebrated Gross-Neveu model in the particle physics [Gross and Neveu, Phys. Rev. D. (1974)]. Soon after our report on the Mott transition, similar studies based on QMC calculations have followed focusing on another universality class, the chiral-Z_2 class [Hesselmann and Wessel, Phys. Rev. B. (2016)]. Since the universality classes are known to be categorized into three types in the framework of the Gross-Neveu theory, there is then one remaining universality class whose critical exponents are still unknown, at least by an unbiased numerically-exact method, which is the purpose of the research conducted since last year.

The remaining class is the chiral-$U(1)$ class, which describes a scenario that an order parameter for the $U(1)$ symmetry breaking generates a mass gap in the Dirac electrons. To study this type of quantum phase transition, we employ the attractive Hubbard model,

$$H = \sum_{<i,j>,\sigma} t_{ij} \left(c^{\dagger}_{i\sigma} c_{j\sigma} + \text{h.c.} \right) - U \sum_{i} n_{i\uparrow} n_{i\downarrow}, \tag{9.1}$$

where $c^{\dagger}_{i\sigma}$ create an electron with spin $\sigma(=\uparrow,\downarrow)$ at site i and $n_{i\sigma} = c^{\dagger}_{i\sigma} c_{i\sigma}$. The first term represents the kinetic energy coming from transfer integrals $t_{ij} = -|t|e^{\theta_{ij}}$. The attractive interaction measured by U/t drives the system to the s-wave superconducting phase. We study this model on the triangular lattice [Fig. 9.1(a)], to which alternating π-flux is added to construct the Dirac dispersion in the non-interacting limit [Fig. 9.1(b)]. Though being rather artificial, this model is suitable to study the quantum phase transition of the $U(1)$ symmetry breaking by the unbiased large-scale numerical simulations, because the attractive interaction can be studied by our highly improved QMC code without the notorious negative-sign problem even for the non-bipartite lattice.

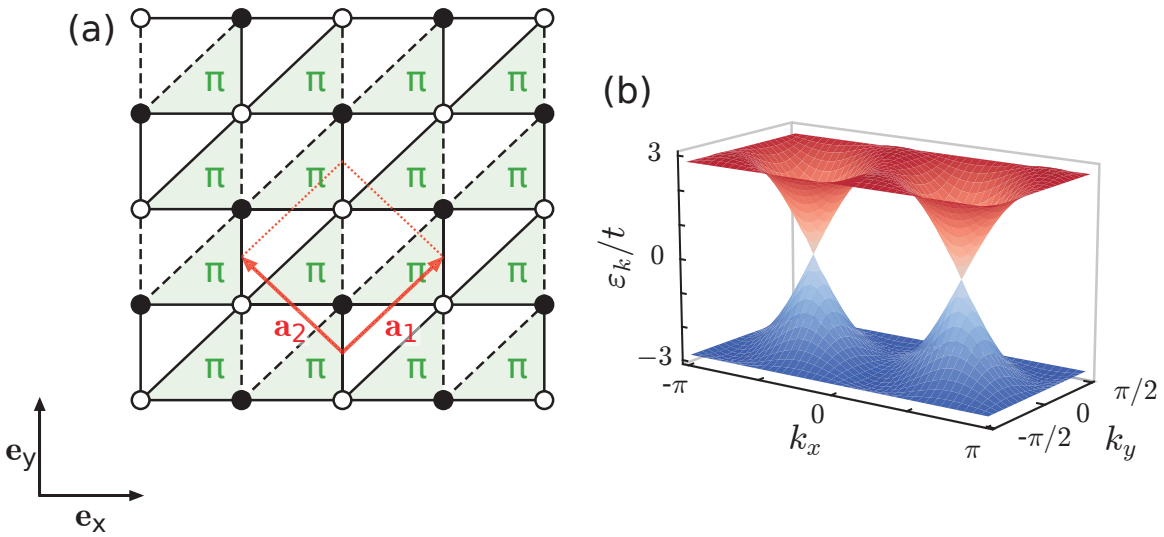

Figure 9.1: (a) Lattice structure of the triangular lattice with alternating π-flux. Each unit cell spanned by the primitive translational vectors (red arrows), $a_1 = (1, 1)$ and $a_2 = (-1, 1)$, contains two sites. Transfer integral between sites connected by solid (dashed) line is $t = -|t|$ ($t' = -|t|e^{i\pi}$), which phase factor results in a magnetic π flux penetrating through each shaded triangle. (b) Energy dispersion in the noninteracting limit ($U/t = 0$). The Fermi level is located at $\varepsilon_k/t = 0$ for half filling.

We calculate the correlation function for the s-wave superconductivity,

$$P_{\text{s}} = \langle \Delta^{\dagger} \Delta + \Delta \Delta^{\dagger} \rangle, \tag{9.2}$$

$$\Delta^{\dagger} = \frac{1}{\sqrt{N_{\text{s}}}} \sum_{l} c^{\dagger}_{l\uparrow} c^{\dagger}_{l\downarrow} \tag{9.3}$$

where N_{s} denotes the total number of the lattice sites. The QMC simulations are performed on finite size clusters of $(L\vec{e}_x, L\vec{e}_y)$ [Fig. 9.1(a)] with L being linear dimension of the cluster, i.e., $N_{\text{s}} = L^2$. Depending on whether each cluster has an allowed k point in the discretized reciprocal space, the clusters are divided into two

series, $L = 4n$ and $L = 4n+2$ (n: integer); the former has the k point just at the Dirac point and the latter does not. This difference is reflected in the asymptotic behavior of P_s toward to the thermodynamics limit (TDL) as a function of $1/L$ as shown in Fig. 9.2. However, it is confirmed that the extrapolated values are consistent for $L = 4n$ and $L = 4n + 2$ which corresponds to a square of the s-wave superconductivity order parameter, $\Delta_s^2 = \lim_{L\to\infty} P_s/N_s$. By plotting Δ_s as a function of U/t, we estimate the critical strength of the interaction, $U_c/t \simeq 7.0$ as well as the corresponding exponent $\beta \simeq 0.7 - 0.8$ assuming $\Delta_s \sim (U/U_c - 1)^{-\beta}$ [Fig. 9.3].

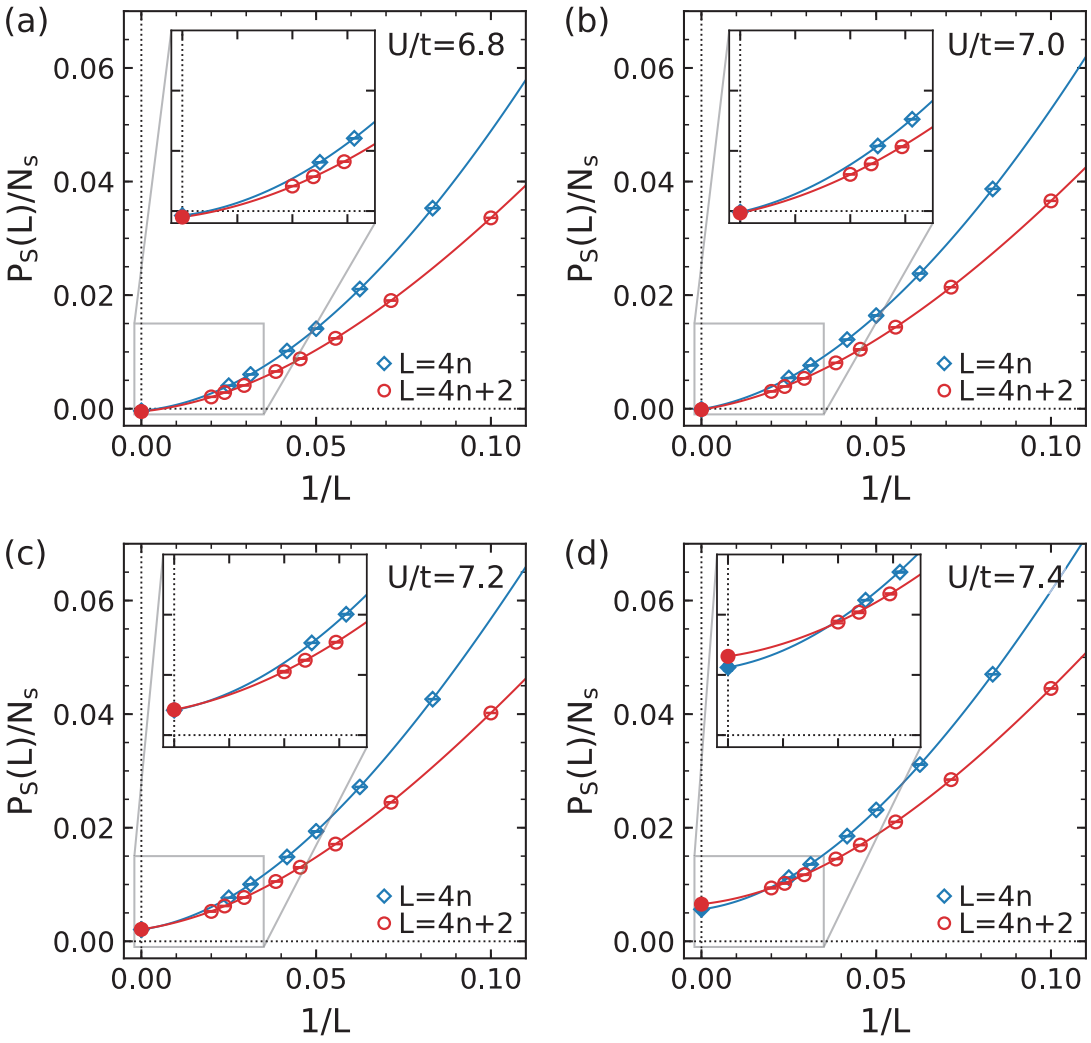

Figure 9.2: Extrapolation of P_s to the thermodynamics limit.

Since it was difficult to obtain β with high accuracy by the above-mentioned method, we then try to calculate β and also the other exponent ν, which is for the correlation length, by a more sophisticated manner, finite-size scaling analysis based on Bayesian inference, which has been shown to be reliable in our previous study on the Mott transition. We employ the form of the scaling ansatz,

$$\Delta_s(L, u) \equiv \sqrt{P_s/N_s} = L^{-\beta/\nu} f_\Delta(uL^{1/\nu}), \tag{9.4}$$

where $u = U/U_c - 1$, $f_\Delta(\cdot)$ represents a universal scaling function. As shown in Fig. 9.4 (left), by collapsing data for $L = 4n + 2$ we obtain U_s/t, β, and ν with sufficient accuracy.

We study the quantum criticality of this transition also in the region of the semi-metallic phase. Here, we focus attention on an element of the density matrix at the maximum distance on each finite-size cluster, $D(r_{\max}) = 1/N_s \sum_r \langle c^\dagger_{r+r_{\max}} c_r \rangle$. Recently, we have found that its ratio to those at $U/t = 0$, $Z_L = D(r_{\max})/D^0(r_{\max})$, can be used as a good estimator of the quasiparticle weight Z, by which we can study a collapse of metallic behavior.

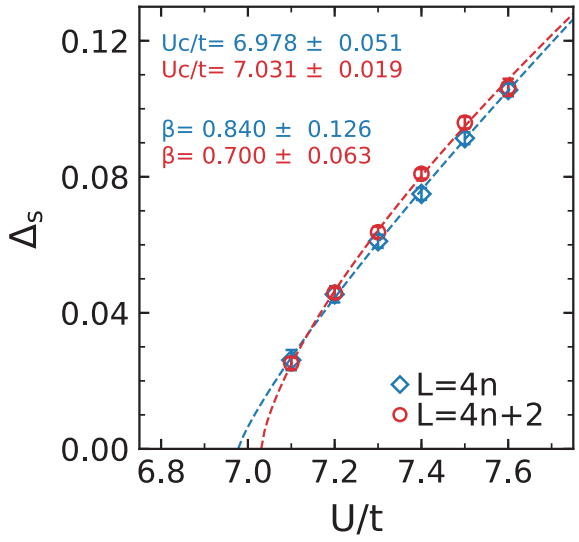

Figure 9.3: Order parameter as a function of U/t estimated from the extrapolations by polynomial fits.

The collapse fit of this quantity is shown in Fig.9.4 (right), where U_c/t and ν are in good agreement with those estimated from P_s, and the other exponent, i.e., fermion anomalous dimension η_ψ is obtained.

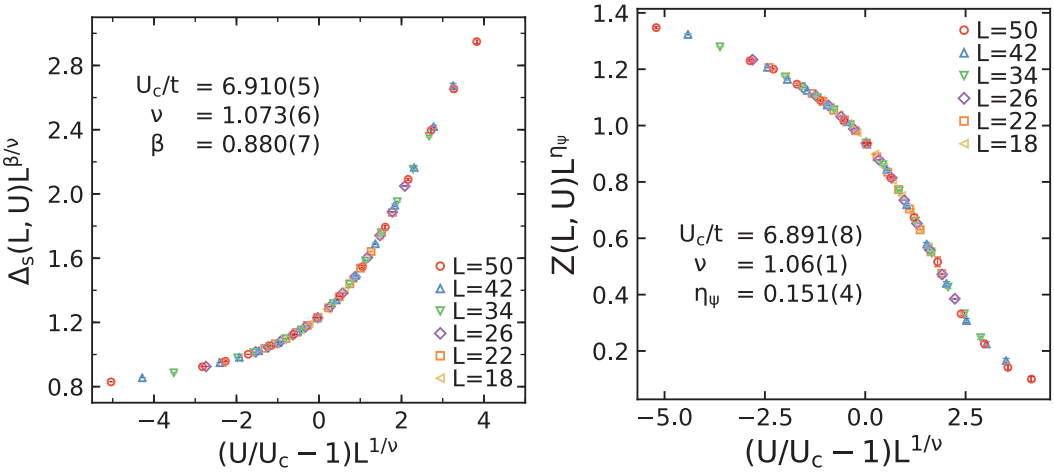

Figure 9.4: Collapse fits of $\Delta_s(L,U)$ (left) and $Z(L,U)$ (right).

Finally, in Table 9.1, we compare our results with those obtained by other numerical or analytical calculations for the same chiral-$U(1)$ universality class. Remarkably, our results, both for ν and β, agree well with the recent QMC results, which was obtained for the Kekulé VBS transition. Although the Kekulé VBS itself breaks Z_3 symmetry instead of $U(1)$, the field-theoretical arguments based on renormalization group predict that the $U(1)$ symmetry emerges at the quantum-critical point because of strong fluctuations in gapless fermion mode, implying that the quantum criticality of the Kekulé transition can be described in terms of the chiral-$U(1)$ universality class. The agreement of the critical exponents between the Kekulé and the SC transitions, the latter showing a genuine $U(1)$ symmetry breaking, strongly supports this scenario [Li *et al.*,, Nature (2017)].

Table 9.1: Critical exponents, ν, β, and η_ψ, for the chiral XY class. QMC results (upper three rows) are based on lattice models, while the following analytical results are obtained for the GN model.

Method	ν	β	η_ψ
QMC (present)	1.073(6)	0.880(7)	$\cdots$
QMC (present)	1.06(1)	$\cdots$	0.151(4)
QMC (Kekulé VBS)	1.06(5)	0.90(6)	$\cdots$
QMC (Kekulé VBS)	1.05(5)	0.92(5)	$\cdots$
Large-N, 1st order	1.25	0.75	0.083
Large-N, higher orders	1.11	1.05	0.0872
$4-\epsilon$, 1st order	0.726	0.619	0.071
$4-\epsilon$, 2nd order	0.837	0.705	0.063
$4-\epsilon$, 4th order	1.19	1.08	0.117
$4-\epsilon$, 4th order	1.19	1.06	0.108
functional RG	1.16	1.09	0.062

9.2.2 Development of massively parallel density matrix renormalization group (DMRG) algorithms

The DMRG method was originally proposed by S. White in 1992. Although the DMRG method is recognized as one of the best numerically exact methods for strongly correlated many-body quantum systems, the application is severely limited mostly to one-dimensional (1D) systems because of the exponential increase of degrees of freedom in higher spatial dimensions. However, owning to high performance computers that are recently availably, it has become realistic to apply the DMRG method even to 2D systems. We have been developing massively parallel DMRG algorithms to investigate strongly correlated quantum systems in two dimensions. We have already successfully developed our massively parallel DMRG code that employs many efficient parallelization techniques, and our massively parallel DMRG code "2D-DMRG" has been opened in public for general users of K computer. A typical performance of the present version of our massively parallel DMRG code is summarized in Fig. 9.5. For this example, we have calculated the optical conductivity for the 1D Hubbard model, using K computer with up to 82,488 nodes. We have performed the dynamical DMRG calculations with the DMRG truncation number m = 8, 064 (the number of bases kept during the calculation). The energy parallelization number is varied in such a way to correspond to the week scaling. As shown in Fig. 9.5, we have achieved the extremely high peak performance ratio of 73.6% when 82,488 nodes are used on K computer, which is about 7.8 PFLOPS. Figure 9.6(a) shows the m dependence of the theoretical peak performance ratio of the DGEMM part in our DMRG calculation. Since we fix the number of MPI parallelizations to be 768 for the matrix-matrix multiplication (with no energy an real space parallelizations), the matrix size for the DGEMM calculation increases linearly with m. As shown in Fig. 9.6(a), the performance of the DGEMM part increases with m, up to 91.5% (78.5% for the whole DMRG calculation) for $m = 8,064$, and remains almost the same for even larger m. In other words, in order to achieve a better performance, the matrix size for the DGEMM calculation has to be large enough. This is the main reason why the peak performance for the strong scaling shown in Fig. 9.5 is decreased down to 57% when 3,072 MPI parallelizations are employed, where the matrix size is as small as 2,016 and the DGEMM calculation is no longer a significant part of the whole calculation.

9.2.3 Massively parallel DMRG study of static and dynamic magnetic properties of the spin-$\frac{1}{2}$ inequilateral diamond-chain compounds $A_3Cu_3AlO_2(SO_4)_4$ (A = K, Rb, Cs)

Highly frustrated quantum magnets provide various exotic ground states, such as gapless spin-liquid and gapped singlet dimer phases. In a magnetic field, the magnets exhibit magnetization plateaus because of the competition of frustration and quantum fluctuations. The typical constituent of frustrated magnets is a triangular unit of spin with antiferromagnetic interaction for each bond. The spin-$\frac{1}{2}$ diamond chain where the triangular unit is connected linearly thus is regarded as a typical highly frustrated system in one dimension. Spin-$\frac{1}{2}$ compounds $A_3Cu_3AlO_2(SO_4)_4$ (A = K, Rb, and Cs) have one-dimensional (1D) inequilateral diamond chains. We analyze the temperature dependence of the magnetic susceptibility and determine the magnetic exchange

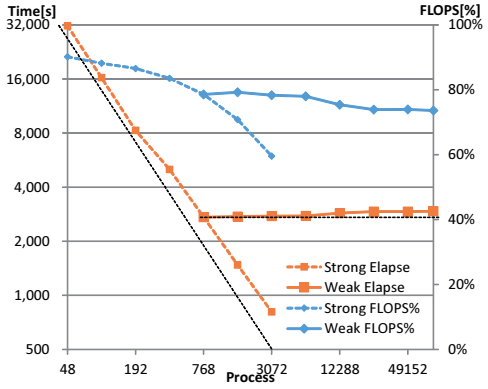

Figure 9.5: Performance of our massively parallel DMRG "2D-DMRG" code on K computer.

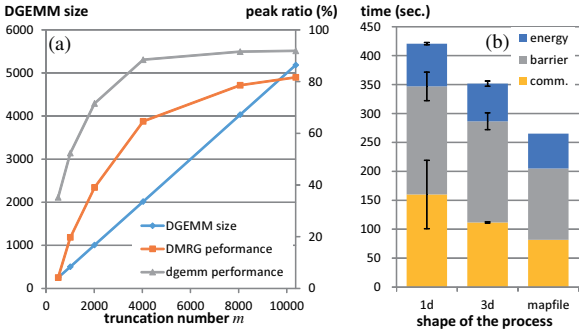

Figure 9.6: (a) The DMRG truncation number m dependence of the theoretical peak performance ratio of the DGEMM part (triangles, right axis). The peak performance ratio of the whole DMRG calculation (squares, right axis) and the matrix size (diamonds, left axis) are also plotted. Here we use 768 MPI parallelizations only for the matrix-matrix multiplications. (b) Elapsed time (except for the main calculation part) for three different shapes of MPI communicators.

interactions. In contrast to azurite, a dimer is formed on one of the sides of the diamond. From numerical analyses of the proposed model, we find that the dimer together with a nearly isolated 1D Heisenberg chain characterize magnetic properties including magnetization curve and magnetic excitations. This implies that a dimer-monomer composite chain without frustration is a good starting point for describing these compounds.

9.2.4 Massively parallel DMRG study of magnetization plateaus in the spin-$\frac{1}{2}$ antiferromagnetic Heisenberg model on a kagome-strip chain

The spin-$\frac{1}{2}$ Heisenberg model on a kagome lattice is a typical frustrated quantum spin system. The basic structure of a kagome lattice is also present in the kagome-strip lattice in one dimension, where a similar type of frustration is expected. We thus study the magnetization plateaus of the spin-$\frac{1}{2}$ Heisenberg model on a kagome-strip chain with three-independent antiferromagnetic exchange interactions using the density-matrix renormalization-group method. In a certain range of exchange parameters, we find twelve kinds of magnetization plateaus, nine of which have magnetic structures breaking translational and/or reflection symmetry spontaneously. The structures are classified by an array of five-site unit cells with specific bond-spin correlations. In a case with a nontrivial plateau, namely a 3/10 plateau, we find long-period magnetic structure with a period of four unit cells.

9.2.5 Dynamical DMRG Study of dispersive charge mode in hole-doped cuprates using resonant inelastic x-ray scattering at the oxygen K edge

We investigate electronic excitations in $La_{2-x}(Br,Sr)_xCuO_4$ obserbed by resonant inelastic x-ray scattering (RIXS) at the oxygen K edge by using our massively parallel dynamical DMRG method. RIXS spectra of the hole-doped cuprates show clear momentum dependence below 1 eV. The broad spectral weight exhibits

positive dispersion and shifts to higher energy with increasing hole concentration. Theoretical calculation of the dynamical charge structure factor on oxygen orbitals in a three-band Hubbard model is consistent with the experimental observation of the momentum and doping dependence, and therefore the momentum-dependent spectral weight is ascribed to intraband charge excitations which have been observed in electron-doped cuprates. Our results confirm that the momentum-dependent charge excitations exist on the order of the transfer energy (t), and the broad spectral line shape indicates damped and incoherent character of the charge excitations at the energy range in the doped Mott insulators.

9.2.6 Entanglement scaling analysis around the critical points and sophistication of exact diagonalization method near the magnetic suturation

We performed the corner transfer matrix renormalization group (CTMRG) method, which is a kind of tensor network methods, on the classical two-dimensional (2D) lattice model to reveal the relation between the criticality of the phase transition and the dependence of the cut-off dimension of CTMRG. Then we developed the entanglement scaling analysis not only at the critical point but also around the critical to capture the critical phenomena on 1D quantum / 2D classical many body systems. We applied the scaling analysis to investigate the critical behavior of the icosahedron model, where the interaction energy is defined as the inner product of neighboring vector spins of unit length pointing to the vertices of the icosahedron. We also extracted the central charge from the scaling analysis, which cannot be explained by the minimal series of conformal field theory.

We sophisticated the exact diagonalization method specialized in the analysis of spin-1/2 quantum spin systems near the magnetic saturation by taking into account both translational symmetry and point group symmetry of the lattice, and apply it to investigate the property of ground state near the magnetic saturation of XXZ model on the triangular lattice up to 1296 sites, which is 12 times larger than the reported size of lattice.

9.2.7 Two-dimensional materials for electronic and energy harvesting applications

The research activities aim at understanding the physical and chemical phenomena at the nanoscale so as to design and tailor advanced materials both for fundamental research and applications in electronic and energy devices. Owing to their reduced dimensionality, two-dimensional materials present opportunities for manifestation of concepts and phenomena that may not be prominent or have not been observed in bulk materials. It has been demonstrated in recent extensive studies that low-dimensional systems containing transition metals with open *d*-orbital shells may exhibit a multitude of interesting properties because of different oxidation and spin states, and relatively large spin-orbit coupling of the transitions metals. Hence, transition metal-based low-dimensional systems provide an excellent ground for exploring and exploiting the internal degrees of freedom of electrons − charge, orbital, and spin − and their interplay for fundamental research and device applications. There are many transition metal-based low dimensional systems in literature, e.g. dichalcogenides, which have been or may potentially be exfoliated in experiments. Among them, nowadays, MXenes are truly at the cutting edge of materials research and promise new scientific and technological horizons.

MXenes are a new class of two-dimensional (2D) transition metal carbides and nitrides with chemical formula of $M_{n+1}X_n$ (M= Sc, Ti, V, Cr, Zr, Nb, Mo, Hf, Ta; X= C, N; n=1–3) that have recently been synthesized through etching MAX phases [J. Mater. Chem. C 5, 2488 (2017)]. These 2D systems have been named as MXenes because they originate from the MAX phases by removing "A" elements and because they are structurally analogous to graphene. Very recently, significant progress in the growth of high quality crystalline MXenes has been achieved by the chemical vapor deposition technique. Moreover, the family of MXenes has been lately expanded to out of plane ordered double transition metals carbides $M'_2M''C_2$ and $M'_2M''_2C_3$ and in-plane ordered double transition metals carbides $(M'_{2/3}M''_{1/3})_2C_3$. Considering the large number of compositional variety of the MAX phase compounds, a large number of 2D MXenes with unprecedented properties is expected to be produced.

Previously, we have shown that some of the MXenes possess Dirac band dispersions crossing at the Fermi level. Therefore, they are highly suspected for being topological insulators (TIs). Indeed, we have found that among the members of functionalized M_2X MXenes, Mo_2CO_2 and W_2CO_2 are TIs [Phys. Rev. B 92, 075436 (2015)]. More recently, using first-principles electronic structure calculations, we demonstrated that in the newly discovered MXenes, oxide $M'_2M''C_2$ (M′ = Mo, W; M″ = Ti, Zr, Hf) are TIs with band gaps as large as 0.285 eV within the generalized gradient approximation and oxide $M'_2M''_2C_3$ are nontrivial topological semimetals [Phys. Rev. B 94, 125152 (2016)]. In addition to the above systems, we have discovered that a family of nitride-based MXenes, $M_3N_2F_2$ (M = Ti, Zr, Hf) are topological insulator/semimetals [Phys. Rev. B 96, 195414 (2017)]. The large band gap, resulting from the strong SOC in transition metals M′ and M″, is an attractive feature in these

newly proposed topological insulators since the experimental realization of these systems with large band gaps would pave the way for practical applications of topological insulators at room temperature. It is noteworthy that in addition to considering topological properties, we have also investigated the possibility of exfoliation of MAX phases to MXenes [Phys. Chem. Chem. Phys. 20, 8579 (2018)] , thermoelectric [Adv. Func. Mater 23, 2185 (2013); Phys. Chem. Chem. Phys. 16, 7841 (2014)] , as well as work function properties [Phys. Rev. B 92, 075411 (2015)] and nearly free states in MXenes [Phys. Rev. B 93, 205125 (2016)].

9.3 Schedule and Future Plan

9.3.1 Large-scale QMC simulations for interacting fermions

In the course of the study on the attractive Hubbard model, we have noticed that the quasiparticle weight can be estimated from the long-distance behavior of the equal-time Green's function. It is noted that the quasiparticle weight is one of the most fundamental quantities characterizing the interacting electrons, and also that the equal-time Green's function is calculated with very high accuracy without any extra computational cost in the auxiliary-field QMC simulations. Therefore, we plan to present benchmark results for this quantity on the basis of more realistic model, the Hubbard model on a honeycomb lattice, which is the canonical model for graphene. Since the many first-principles calculations have suggested that the electron-electron interaction in graphene is large, it would be important to study the fate of the quasiparticle vanishing into the insulating phase with increasing interaction. Specifically, we will investigate whether/how the Fermi-liquid description for the interacting electrons, which is one of the most celebrated theories in the condensed matter physics, is valid near the quantum critical point. We have already confirmed that the quasiparticle weight can be calculated on lattices with size up to 10,082 sites, which is the largest ever recored in the scheme of the auxiliary-field QMC.

9.3.2 Density matrix renormalization group (DMRG) method for quantum dynamics in two dimensions

The DMRG method is the most efficient numerical method for the ground state calculations of one-dimensional (1D) quantum systems. Also the DMRG method can be employed to study the ground state properties of two-dimensional (2D) quantum systems. Owning to high performance computers that are available recently, it has become possible to apply the DMRG method not only to the ground state calculations in 2D quantum systems but also to the excited state calculations, thermodynamics, as well as real time dynamics. However, these dynamical calculations are limited mostly to 1D systems. This is partially because of the exponential increase of degrees of freedom to be kept for 2D systems but mainly because of the lack of reliable algorithms for thermodynamics and real time dynamics in two dimensions. By combining the kernel polynomial method, we plan to develop a new scheme based on the DMRG method for thermodynamics and real time dynamics in two dimensions. This will provide the first reliable quantum dynamics calculation for 2D strongly correlated quantum systems.

9.3.3 Entanglement scaling analysis around the critical points and further improvement of exact diagonalization method

To clarify the mechanism of a non-trivial critical behavior in the icosahedron model is an important future issue. The next target is the dodecahedron model having twenty local degrees of freedom, which requires massive parallelized computations of CTMRG. In addition, it is an interesting problem to introduce the XY-like uniaxial anisotropy to the icosahedron and dodecahedron models; A crossover of universality between the icosahedron/dodecahedron model and the clock models can be expected.

To proceed sophistication of the technic of exact diagonalizations is always required for obtaining numerically exact results in frustrated models. In our current version of the program is not adapted for the lattice with sublattice structures. If we introduce the sublattice-symmetry-adapted exact diagonalization, the iterative method, e.g., Lanczos method and Jacobi-Davidson method, can be accelerate because we can use LEVEL3 BLAS for multiplication of the Hamiltonian and a vector to generate Krylov subspace.

9.3.4 Computational discovery of novel ternary borides and their 2D derivatives

Another group of compounds, which can potentially exhibit similar characteristics as MAX phases is transition metal borides. In analogue to MAX phases, the transition metal borides are called MAB phases with chemical

formula of MAB, M_2AB_2, $M_3A_2B_2$, M_3AB_4, and M_4AB_6, where M is a transition metal and A = Al. Experimentally, few ternary boride phases of Cr_2AlB_2, Cr_3AlB_4, Cr_4AlB_6, MoAlB, WAlB, Fe_2AlB_2, Mn_2AlB_2 have already been synthesized [Inorg. Chem. 54, 6122 (2015)]. However, the family of ternary borides can be expanded significantly. This is because many of the transition metal elements have both binary compounds of M-Al and M-B. This indicates that such transition metal elements might form ternary M-Al-B phases in particular experimental conditions. In order to expand the family of MAB phases, we will do the following steps to reach the above goal:

1) By a quick search in the available experimental databases such as "Springer Materials", "American Mineralogist Crystal Structure Database", and '"NIMS Materials Database", we will find the transition elements that possess both binary compounds of M-Al and M-B. 2) In order to determine the thermodynamic stability of the predicted layered MAlB phases with respect to their competing binary M-Al and M-B phases, we will investigate the diagram of their formation energies versus chemical potential. From such analyses, we will determine that in which chemical potential region for Al and B, the designed ternary compounds will be more stable than their competing binary compounds. If such chemical region exists, the considered MAB phase would be thermodynamically stable. 3) After finding the thermodynamically stable MAB phases, we will study the local stability of the predicted thermodynamically stable MAB phases by using a set of phonon calculations. 4) we will investigate the exfoliation possibility of the predicted MAlB phases into 2D transitional borides. 5) The electronic structures and applications of the predicated MAlB and their 2D derivative will be investigated.

9.4 Publications

9.4.1 Articles

[1] M. Y. Jeong, S. H. Chang, B. H. Kim, J.-H. Sim, A. Said, D. Casa, T. Gog, E. Janod, L. Cario, S. Yunoki, M. J. Han, and J. Kim, "Direct experimental observation of the molecular $J_{\rm eff} = 3/2$ ground state in the lacunar spinel GaTa4Se8", Nature Communications 8, 782/1-8 (2017).

[2] I. Santoso, W. Ku, T. Shirakawa, G. Neuber, X. Yin, M. Enoki, M. Fujita, R. Liang, T. Venkatesan, G. A. Sawatzky, A. Kotlov, S. Yunoki, M. Rübhausen, and A. Rusydi, "Unraveling local spin polarization of Zhang-Rice singlet in lightly hole-doped cuprates using high-energy optical conductivity", Phys. Rev. B 95, 165108/1-13 (2017).

[3] E. Kogan, K. Noda, and S. Yunoki, "Spin-anisotropic magnetic impurity in a Fermi gas: Integration of poor man's scaling equations", Phys. Rev. B 95, 165412/1-8 (2017).

[4] K. Morita, M. Fujihala, H. Koorikawa, T. Sugimoto, S. Sota, S. Mitsuda, and T. Tohyama, "Static and Dynamic Magnetic Properties of Spin-1/2 Inequilateral Diamond-Chain Compounds $A_3Cu_3AlO_2(SO_4)_4$ (A=K, Rb, and Cs)", Phys. Rev. B **95**, 184412/1-5 (2017).

[5] D. Yamamoto, H. Ueda, I. Danshita, G. Marmorini, T. Momoi, and T. Shimokawa, "Exact diagonalization and cluster mean-field study of triangular-lattice XXZ antiferromagnets near saturation", Phys. Rev. B **96**, 014431/1-12 (2017).

[6] T. Okubo, K. Shinjo, Y. Yamaji, N. Kawashima, S. Sota, T. Tohyama, and M. Imada, "Ground state properties of Na_2IrO_3 determined from ab-initio Hamiltonian and its extensions containing Kitaev and extended Heisenberg interactions", Phys. Rev. B **96**, 054434/1-13 (2017).

[7] H. Ueda, K. Okunishi, R. Krcmar, A. Gendiar, and S. Yunoki, and T. Nishino, "Critical behavior of the two-dimensional icosahedron model", Phys. Rev. E 96, 062112/1-5 (2017).

[8] K. Seki and S. Yunoki, "Topological interpretation of the Luttinger theorem", Phys. Rev. B 96, 085124/1-22 (2017).

[9] K. Ishii, T. Tohyama, S. Asano, K. Sato, M. Fujita, S. Wakimoto, K. Tustsui, S. Sota, J. Miyawaki, H. Niwa, Y. Harada, J. Pelliciari, Y. Huang, T. Schmitt, Y. Yamamoto, and J. Mizuki, "Observation of a dispersive charge mode in hole-doped cuprates using resonant inelastic x-ray scattering at the oxygen K edge", Phys. Rev. B **96**, 115148/1-8 (2017).

[10] Y. Liang, M. Khazaei, A. Ranjbar, M. Arai, S. Yunoki, Y. Kawazoe, H. Weng, Z. Fang, "Theoretical Prediction of Two- Dimensional Functionalized MXene Nitrides as Topological Insulators", Phys. Rev. B **96**, 195414 (2017).

[11] T. Shirakawa, T. Tohyama, J. Kokalj, S. Sota, and S. Yunoki, "Ground state phase diagram of the triangular lattice Hubbard model by density matrix renormalization group method", Phys. Rev. B **96**, 205130/1-11 (2017).

[12] K. Pradhan and S. Yunoki, "Nanoclustering phase competition induces the resistivity hump in colossal magnetoresistive manganites", Phys. Rev. B 96, 214416/1-6 (2017).

[13] K. Morita, T. Sugimoto, S. Sota, and T. Tohyama, 窶ｦovel magnetization plateaus in the spin-1/2 antiferromagnetic Heisenberg model on a kagome-strip chain", Phys. Rev. B **97**, 014412/1-6 (2018).

[14] H. Ueda, K. Okunishi, R. Krčmár, A. Gendiar, S. Yunoki, and T. Nishino, "Critical behavior of the two-dimensional icosahedron model", Phys. Rev. E **96**, 062112/1-5 (2017).

[15] M. Khazaei, A. Ranjbar, K. Esfarjani, D. Bogdanovski, R. Dronskowski, and S. Yunoki, "Insights into Exfoliation Possibility of MAX Phases to MXenes", Physical Chemistry Chemical Physics **20**, 8579 (2018).

[16] M. Khazaei, A. Ranjbar, M. Arai, T. Sasaki, S. Yunoki, "Electronic Structures and Applications of MXenes: a Theoretical Review", Journal of Material Chemistry C **5**, 2488 (2017).

[17] Q. Zhang, G. Chen, and S. Yunoki, "Surface ferromagnetism in HfO2 inducded by excess oxygen", Solid State Communications 252, 33-39 (2017).

[18] M. Babamoradi, S. Asgari, A. Ranjbar, R. V. Belosludov, and S. Yunoki, "Many-electron states of the N2 and N3 color centers in diamond: A first- principles and many-body study", Physica B 505, 17-21 (2017).

[19] Y. Otsuka and S. Yunoki, "Universal quantum criticality in two-dimensional interacting Dirac electrons", Solid State Physics **52**, 373-384 (2017) (in Japanese).

9.4.2 Invited Talks

[1] S. Yunoki, "Relativistic Mott insulator, superconductivity, and other exotic states in transition metal oxides with a large spin-orbit coupling", Moscow International Symposium on Magnetism (MISM 2017), July 1-5 (2017), Moscow (Russia).

[2] S. Yunoki, "Exotic ground states of a multi-orbital Hubbard model with a strong spin-orbit coupling", The International Conference on Strongly Correlated Electron Systems (SCES 2017), July 17-21 (2017), Prague (Czech Republic).

[3] S. Yunoki, "Emergence of massless Dirac dispersion in graphene on Ni(111) surface: A DFT+CPT study", 9th Asian Consortium Computational Materials Science (ACCMS-9), August 8-11 (2017), Kuala Lumpur (Malaysia).

[4] M. Khazaei, "Electronic structures of MAX phases and MXenes", The 9th conference of the Asian Consortium on Computational Materials Science (ACCMS-9), August 8-11 (2017), Kuala Lumpur, Malaysia.

[5] S. Yunoki, "Quantum criticality of the metal-insulator transition and possible spin liquid in 2D Hubbard models", 12th International Symposium on Crystalline Organic Metals, Superconductors, and Magnets (ISCOM), September 24-29 (2017), Miyagi (Japan).

[6] S. Yunoki, "Quantum criticality in the metal-insulator transition of two-dimensional interacting Dirac fermions", The Italian National Conference on the Physics of Matter (FisMat), October 1-5 (2017), Trieste (Italy).

[7] H. Ueda, "Classical analogue of finite entanglement scaling around the criticality", Novel Quantum States in Condensed Matter 2017, October 27 (2017), Kyoto (Japan). [Invited]

9.4.3 Oral Talks

[1] Y. Otsuka, K. Seki, S. Yunoki, and S. Sorella, "Semimetal to superconductor phase transition in Dirac fermions with attractive interactions II", Japan Physical Society 2017 Autumn Meeting, September 21-24 (2017), Iwate (Japan).

[2] K. Morita, T. Sugimoto, S. Sota, and T. Tohyama, "Magnetization plateau on Kagome strip chain", JPS 2017 autumn meeting, September 21-24 (2017), Morioka.

[3] K. Sasaki, T. Sugimoto, S. Sota, and T. Tohyama, "Magnetic excitation with finite magnetization in frustrated spin ladder", JPS 2017 autumn meeting, September 21-24 (2017), Morioka.

[4] S. Sota, "Dynamical and time-dependent DMRG method for higher dimensional systems", CBSM2 workshop, October 31 (2017), Kashiwa.

[5] K. Morita, T. Sugimoto, S. Sota, and T. Tohyama, "Novel magnetization plateaus in the spin-1/2 antiferromagnetic Heisenberg model on a kagome-strip chain", APS march meeting 2018, March 5-9 (2018), Los Angeles (US).

[6] S. Sota, T. Shirakawa, S. Yunoki, and T. Tohyama, "Development of time dependent DMRG method for higher dimensional systems and its application to quantum annealing", APS march meeting 2018, March 5-9 (2018), Los Angeles (US).

[7] T. Tohyama and S. Sota, "Magnetic Excitations and Charge Stripes in the t-t-J Model: Dynamical Density-Matrix Renormalization Group Study", JPS 73rd annual meeting, March 22-25 (2018), Noda.

[8] K. Sasaki, T. Sugimoto, S. Sota, and T. Tohyama, "Magnetic excitation in magnetization plateau of frustrated spin ladder", JPS 73rd annual meeting, March 22-25 (2018), Noda.

[9] H. Ueda, S. Onoda, Y. Yamaguchi, T. Kimura, D. Yoshizawa, T. Morioka, M. Hagiwara, M. Hagihala, M. Soda, T. Masuda, T. Sakakibara, K. Tomiyasu, S. O.-Kawamura, K. Nakajima, R. Kajimoto, M. Nakamura, Y. Inamura, M. Hase, and Y. Yasui, "Emergent spin-1 Haldane gap and ferroelectricity in a frustrated spin-1/2 ladder Rb2Cu2Mo3O12", APS March Meeting 2018, March 08 (2018), Los Angeles (USA).

[10] H. Ueda, "Tensor network algorithms and finite entanglement scaling around the criticality", International Workshop on Massively Parallel Programming for Quantum Chemistry and Physics, January 17 (2018), Wako (Japan).

[11] H. Ueda, S. Onoda, Y. Yamaguchi, T. Kimura, D. Yoshizawa, T. Morioka, M. Hagiwara, M. Hagihala, M. Soda, T. Masuda, T. Sakakibara, K. Tomiyasu, S. O.-Kawamura, K. Nakajima, R. Kajimoto, M. Nakamura, Y. Inamura, M. Hase, and Y. Yasui, "Emergent spin-1 Haldane gap and ferroelectricity in a frustrated spin-1/2 ladder Rb2Cu2Mo3O12", JPS 2018 Annual (73rd) Meeting, March 23 (2018), Noda (Japan).

[12] H. Ueda, "Phase transition in anisotropic polyhedron model", Workshop on CBSM^2 Sub-Challenge D: Fundamental Quantum Mechanics and Informatics, October 31 (2017, Kashiwa (Japan).

[13] H. Ueda, K. Okunishi, R. Krčmár, A. Gendiar, S. Yunoki, and T. Nishino, "Phase diagram and critical property of the icosahedral model on the square lattice", JPS 2017 Autum Meeting, September 24 (2017), Morioka (Japan).

[14] H. Ueda, "Phase diagram and critical property in two-dimensional regular polyhedral model", Workshop on tensor-network scheme and software of tensor calculations, August 04 (2017), Kobe (Japan).

[15] M. Khazaei, "Application of DFT calculations for predicting the structural and electronic properties of materials", The 8th AICS International Symposium on "Roadmap on computer science and computational science in the future AICS and HPC communities", February 7-8 (2018), RIKEN AICS, Kobe, Japan.

[16] M. Khazaei, "Insight into exfoliation possibility of MAX Phases to MXenes", Asian Consortium on Computational Materials Science–Virtual Organization, ACCMS-VO12, December 17-19 (2017), Sendai, Tohoku University.

[17] A. Ranjbar, “Magnetism in Cr-based MAX phases and their derived 2D MXenes”, 9th Asian Consortium Computational Materials Science (ACCMS-9), August 8-11 (2017), Kuala Lumpur (Malaysia).

[18] A. Ranjbar, “Magnetism in Cr-based MAX phases and their derivatives 2D MXenes”, Asian Consortium on Computational Materials Science–Virtual Organization, ACCMS-VO12, December 17-19 (2017), Sendai, Tohoku University.

9.4.4 Posters

[1] Y. Otsuka, K. Seki, S. Yunoki, and S. Sorella, “Large-scale quantum Monte Carlo study of semimetal-superconductor phase transition in Dirac fermions”, Italian National Conference on Condensed Matter Physics (FisMat2017), October 1-6 (2017), Trieste (Italy).

[2] Y. Otsuka, K. Seki, S. Yunoki, and S. Sorella, “Quantum criticality in two-dimensional interacting Dirac Fermions”, 12th International Symposium on Crystalline Organic Metals, Superconductors and Ferromagnets (ISCOM2017), September 24-29 (2017), Miyagi Zao (Japan).

[3] Y. Otsuka, K. Seki, S. Yunoki, and S. Sorella, “Quantum criticality of the semimetal-superconductor phase transition in the two-dimensional interacting Dirac fermions”, International Conference on Strongly Correlated Electron Systems (SCES2017), July 17-21 (2017), Prague(Czech).

[4] Y. Otsuka, S. Yunoki, and S. Sorella, “Universal quantum criticality in 2D interacting Dirac electrons”, International workshop on numerical methods and simulations for materials design and strongly correlated quantum matters, March 24-25, (2017), Kobe (Japan).

[5] S. Sota, T. Shirakawa, S. Yunoki, and T. Tohyama, “Time-dependent DMRG method for higher dimensional systems and its applications”, The 2nd CDMSI workshop, July 11-12 (2017), Tokyo.

[6] S. Sota, Y. Imamura, T. Nakajima, and S. Yunoki, ”Ab-initio DMRG method for infinite systems and its applications”, JPS 2017 autumn meeting, September 21-24 (2017), Morioka.

[7] S. Sota, T. Shirakawa, S. Yunoki, and T. Tohyama, ”Novel quantum phases induced by spin-orbit interaction and spin frustration in triangular spin models”, The Fourth Project Report Meeting, November 2 (2017), Tokyo.

[8] T. Tohyama, S. Sota, and S. Yunoki, ”Charge excitations of charge-transfer-type doped Mott insulators”, The Fourth Project Report Meeting, November 2 (2017), Tokyo.

[9] Y. Imamura, S. Sota, T. Nakajima, and S. Yunoki, ”Development and Application of Massively Parallel First-principles Density Matrix Renormalization Group”, The Fourth Project Report Meeting, November 2 (2017), Tokyo.

[10] S. Sota, T. Shirakawa, S. Yunoki, and T. Tohyama, ”Dynamical DMRG study of excitation dynamics on triangular lattice spin S=1/2 Heisenberg model”, JPS 73rd annual meeting, March 22-25 (2018), Noda.

9.4.5 Software

[1] S. Sota, T. Tohyama, and S. Yunoki, massively parallel DMRG program “2D-DMRG”, AICS software.

Chapter 10

Computational Biophysics Research Team

10.1 Members

Yuji Sugita (Team Leader)*

Osamu Miyashita (Senior Research Scientist)

Jaewoon Jung (Research Scientist (Concurrent))*

Chigusa Kobayashi (Research Scientist)

Yasuhiro Matsunaga (Research Scientist)

Motoshi Kamiya (Postdoctoral Researcher)

Koichi Tamura (Postdoctoral Researcher)

Hiromi Kano (Assistant)**

Hiraku Oshima (Postdoctoral Researcher)**

Suyong Re (Research Scientist)**

Ai Nittsu (Special Postdoctoral Research (Concurrent))*

Takaharu Mori (Research Scientist (Concurrent))*

Kiyoshi Yagi (Research Scientist (Concurrent))*

Michael Feig (Visiting Scientist)****

Naoyuki Miyashita (Visiting Scientist)*****

Mitsunori Ikeguchi (Visiting Scientist)******

Takao Yoda (Visiting Scientist)*******

* The main affiliation is Theoretical Molecular Science Laboratory, RIKEN CPR.
** The main affiliation of these people is Laboratory for Biomolecular Function Simulation, RIKEN BDR.
*** The main affiliation is Michigan State University.
**** The main affiliation is Kindai University.
***** The main affiliation is Yokohama City University.
****** The main affiliation is Nagahama Bio Institute.

10.2 Research Activities

We have developed GENESIS (Generalized Ensemble Simulation System), which is molecular dynamics and modeling software for biomolecular systems such as proteins, lipids, glycans, and their complexes. GENESIS is highly parallelized on K and other massively parallel supercomputers, and has a lot of enhanced conformational sampling methods. In March, 2014, we provided the first pre-released version of GENESIS as free software under the license of GPLv2.

In this fiscal year, we updated GENESIS with better performance and with advanced algorithms, which is released as GENESIS 1.2. For more accurate MD simulations under the isothermal-isobaric (NPT) conditions, we developed a more accurate pressure evaluation. Enahnced smapling algorithm was also developed. To enlarge the application of GENESIS for biological simulations, a data-driven modeling scheme that combines MD simulations with experimental measurements was proposed. GENEIS has been used for the research of conformational changes of Ca^{2+}-ATPase and computational modeling of a heme importer.

10.2.1 Release of GENESIS 1.2

In the last fiscal year, we released GENESIS 1.1 and 1.2 including new functions and advanced algorithms. After the release of GENESIS 1.1, we continued to release improvements as GENESIS 1.1.X. The main additions are (1) usage of Cartesian coordinates as collective variable in the string method, (2) enabling newer GPU drivers (version greater than 380).

In GENESIS 1.2.0, we implemented four-site models for water molecule. The four-site water modles enable us to perform MD simulations with more accurate physical properties of not only water molecules but also proteins, lipids, nucleic acids, and so on. Nowadays, a lot of active researches have been performed to find parameters to investigate dynamics and protein-protein interactions in more accurate ways. From the implmentation of the four-site water model, it is explected to enlarge the usage of GENESIS in biological simulations.

10.2.2 Accurate pressure evaluation in velocity Verlet integration

In molecular dynamics (MD) simulations, we perform simulations based on constant temperature or isothermal-isobaric conditions to generatre physically meaningful canonical ensemble. In these conditions, kinetic energy is essential to control pressure as well as temperature. Pressure is evaluated based on the virial theorem which connects the average kintic energy with the virial term. In MD, unfortunately, the virial theorem is not satisified using the finite time step if kinetic energy is caluclated at full time step ($(t, t + \Delta t, t + 2\Delta t, ...)$). To satisfiy the virial theorem, the kinetic energy should be calculated at the half-time steps ($(t - \Delta t/2)$ and $(t + \Delta t/2)$). The new kinetic energy at half time step should be also used to evaluate pressure, too. We tested the new kinetic energy for a 1,2-dispalmitoyl-sn-phophatidylcholine (DPPC) lipid bilayer and a box of water molecules in the isothermal-isobaric conditions, and confirmed that it has much more accurate results than existing ways. (Fig. 10.1) Based on the new definition of kinetic energy, we developed a multiple time step (MTS) integration scheme where time-consuming parts are evaluated less frequently. With the new MTS integration, we could improve the performance without any loss of accuracy. These developments are implemented in GENESIS MD software, and included in GENESIS 1.2.

10.2.3 Development of generalized replica exchange with solute tempering (gREST)

Replica exchange molecular dynamics (REMD) has been widely applied in many biological simulations to investigate macromolecular structure-dynamics-function relationships. REMD allows us to sample a wider conformational sample of macromolecules, like proteins or nucleic acids by performing a number of MD simulations in parallel (we call each simulation a replica) and exchanging temperatures between replicas at a certain frequency. The well-known drawback of REMD is that the number of replicas necessary increases rapidly if the system size becomes larger. Replica exchange with solute tempering (REST) was developed by Berne and his colleagues to overcome the problem. In REST, temperature of a predefined solute molecule is exchanged between replicas and thereby, we can reduce the number of replicas significantly. Our group extended the idea of REST and developed generalized REST (gREST), where the solute region is able to selected as a part of a molecule or a part of potential energy function terms. We applied gREST to protein folding simulations of a beta hairpin and Trp-cage in explicit water and observed the improved conformational sampling efficiency. gREST is able to be combined with replica-exchange umbrella sampling (REUS). The combined approach, which we call gREST/REUS, was applied to protein-ligand binding simulations, where a ligand and several

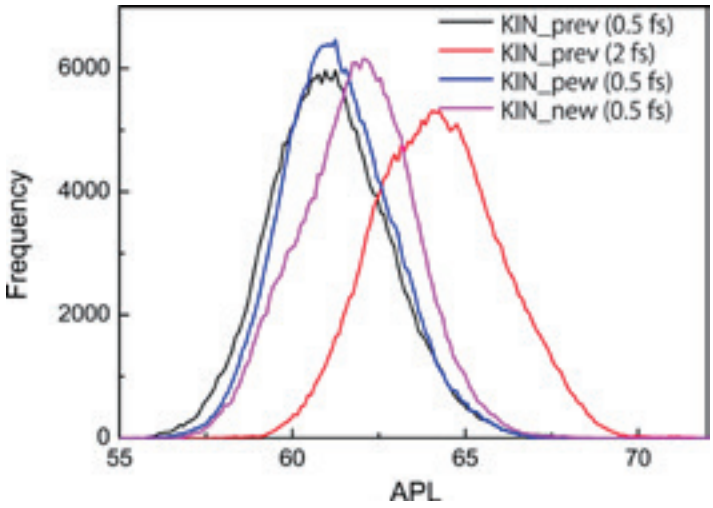

Figure 10.1: Area per lipid of DPPC system. KIN_prev and KIN_new are conventionally defined and our new kinetic energy evaluations

residues at the binding pocket are selected as the solute regions and the distance between a ligand and the binding pocket is used as a reaction coordinate in REUS. The gREST/REUS shows much better performance than the conventional REST/REUS and can sample not only the ligand-binding structure but also pre-bound form, which might be useful for understanding molecular mechanisms for protein-ligand binding in atomistic details. (Fig. 10.2)

10.2.4 Refining Markov State Models for conformational dynamics using ensemble-averaged data and time-series trajectories

A data-driven modeling scheme is proposed for conformational dynamics of biomolecules based on molecular dynamics (MD) simulations and experimental measurements. In this scheme, an initial Markov State Model (MSM) is constructed from MD simulation trajectories, and then, the MSM parameters are refined using experimental measurements through machine learning techniques. The second step can reduce the bias of MD simulation results due to inaccurate force-field parameters. Either time-series trajectories or ensemble-averaged data is available as a training data set in the scheme. Using a coarse-grained model of a dye-labeled polyproline-20, we compare the performance of machine learning estimations from the two types of training data sets. Machine learning from time-series data could provide the equilibrium populations of conformational states as well as their transition probabilities. It estimates hidden conformational states in more robust ways compared to that from ensemble-averaged data although there are limitations in estimating the transition probabilities between minor states. We discuss how to use the machine learning scheme for various experimental measurements including single-molecule time-series trajectories. (Fig. 10.3)

10.2.5 Conformational changes of Ca^{2+}-ATPase on dissociation of ADP and Ca^{2+}

Sarco(endo)plasmic reticulum Ca^{2+}-ATPase is a representative protein of P-type ATPases, which transports Ca^{2+} across membrane against a large concentration gradient (104 times) by utilizing ATP hydrolysis. Structural and biochemical studies have suggested functional roles of coupled motions between the cytoplasmic domains and the transmembrane helices in individual reaction steps. It is, however, difficult to investigate the coupled motion by simulating the reaction step due to its slow time-scale. To overcome this difficulty, we have introduced a rare event sampling method, string method, and installed it into a high-performance MD simulation package, GENESIS. We focused on release of Ca^{2+} due to dissociation of ADP in Ca^{2+}-ATPase. In the reaction step, three processes are shown; 1) Dissociation of ADP from interface of cytoplasmic domains, 2) Opening of lumen gate in Ca2+-binding site by conformational changes of transmembrane helices, 3) Release Ca^{2+} to lumen side. We performed the string method calculations using GENESIS and tried to understand the most probable reaction pathway on the reaction step. We find that large scale motion of the cytoplasmic

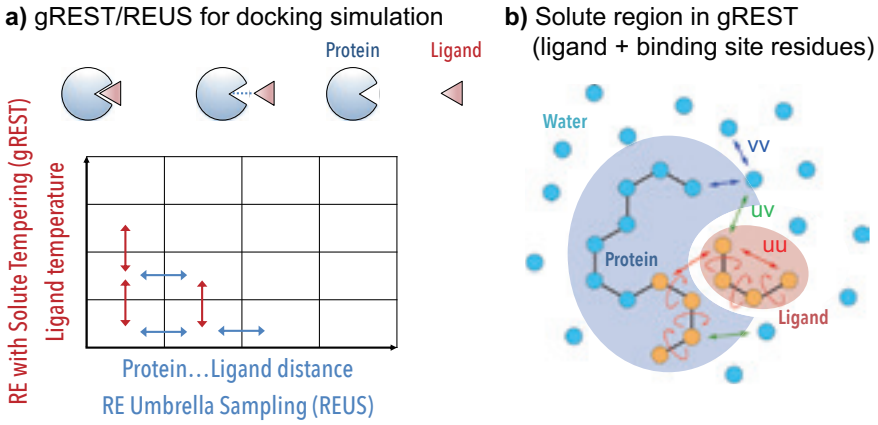

Figure 10.2: gREST/REUS for docking simulation and solute region in gREST.

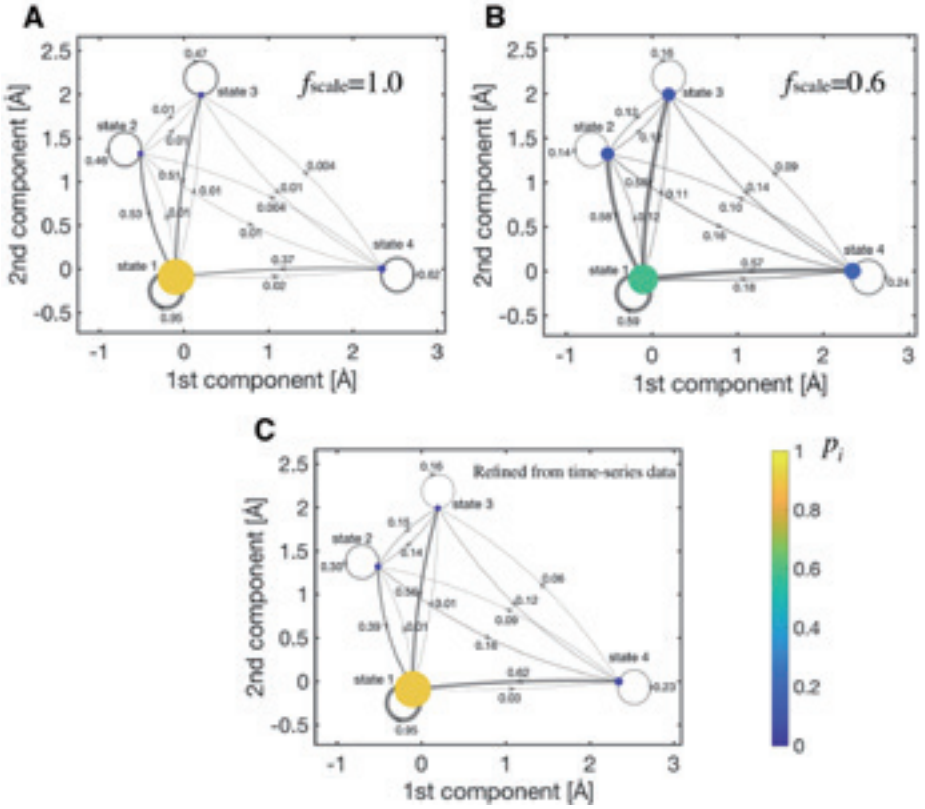

Figure 10.3: Results of data-driven refinement of a Markov state model. A. Accureate model used as a reference. B. Incorrect model to be refeind. C. Refined model by using machine learning from the time-series data generated by the accurate model

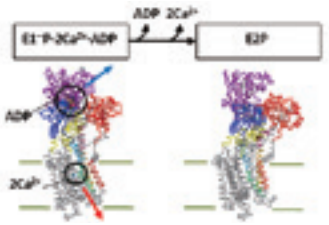

Figure 10.4: Conformational change of SERCA on dissocation of ligands.

domains causes rearrangements of transmembrane helices, and the rearrangements result in large opening of the lumen gate. We also propose atomistic structurers in intermediates, which have been proposed by biochemical studies. (Fig. 10.4)

10.2.6 Computational modeling of a heme importer in the unknown occluded form

Bacteria infecting in humans acquire iron from the heme in host cells. These bacteria have unique machine in its cell membrane and efficiently absorb heme iron. This molecular machine is called heme impoter. Heme importer belongs to the large family of type-II ATP-binding cassette (ABC) transporter. Transport of heme across the cell membrane involves large and global conformational changes of the protein during which two ATPs are consumed. Type-II ABC transporter to which heme importer belongs is believed to follow the alternating access mechanism where the transporter can alternate between an inward-facing (IF) form and an outward-facing (OF) one. The formation of the occluded (Occ) intermediate is a salient feature of transporters, which distinguish them from channels. Although the structure of the IF form of the heme importer has been known since 2016, those of the OF and the Occ forms are elusive. In this study, targeted molecular dynamics (tMD) simulation was adopted to predict the ATP-bound Occ form of the heme importer. In the tMD simulation, a part of the transporter in the IF form was pulled toward a reference structure. We adopted the recently predicted OF form as the reference structure to close the cytoplasmic gate of the IF form. The simulation successfully predicted the Occ form which was structurally stable during the equilibrium MD simulation. (Fig. 10.5)

10.3 Publications

10.3.1 Articles

[1] C. Kobayashi*, J. Jung*, Y. Matsunaga, T. Mori, T. Ando, K. Tamura, M. Kamiya, and Y. Sugita, “GENESIS 1.1: A hybrid-parallel molecular dynamics simulator with enhanced sampling algorithms on multiple computational platforms”, Journal of Computational Chemistry, vol. 38, 2193 – 2206 (2017) (* equally contributed).
[2] Y. Matsunaga, T. Yamane, T. Terada, K. Moritsugu, H. Fujisaki, S. Murakami, M. Ikeguchi, and A. Kidera, “Energetics and conformational pathways of functional rotation in the multidrug transporter AcrB”, eLife, vol. 7, e31715 (19 pages) (2018)
[3] J. Jung, C. Kobayashi, and Y. Sugita, “Kinetic energy definition in velocity Verlet integration for accurate pressure evaluation”, The Journal of Chemical Physics, vol. 148, 164109 (11 pages) (2018)

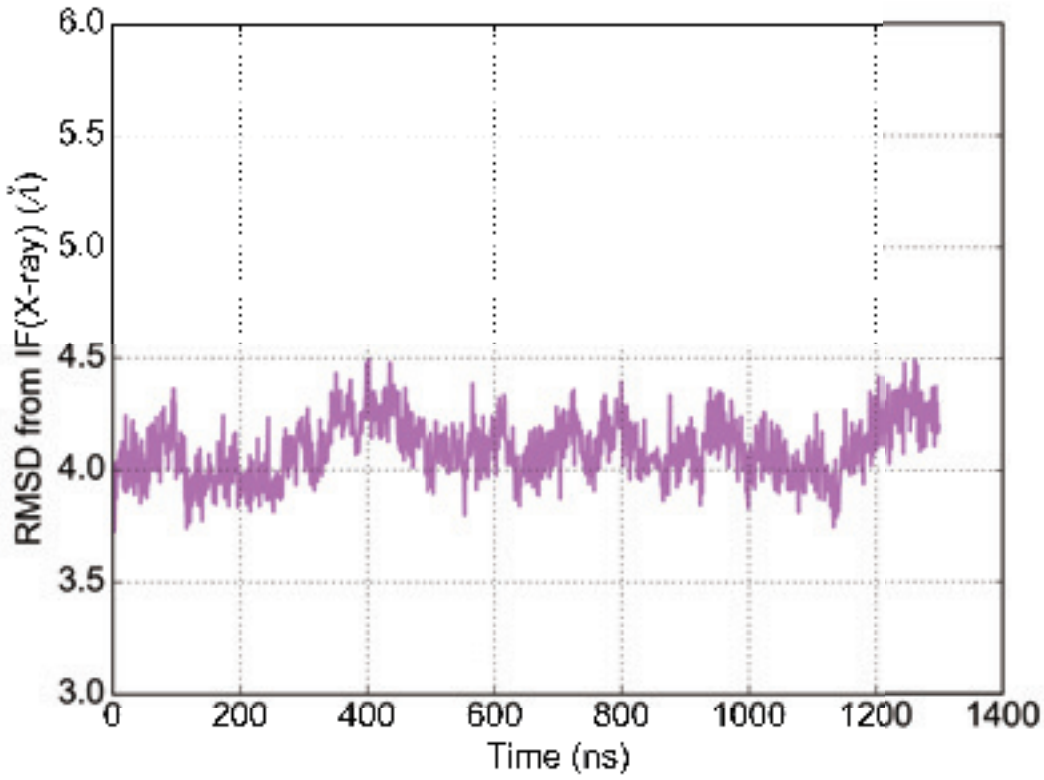

Figure 10.5: Time series of RMSD with respect to the IF form

[4] Y. Matsunaga, and Y. Sugita, "Refining Markov State Models for conformational dynamics using ensemble-averaged data and time-series trajectories", The Journal of Chemical Physics, vol. 148, 241731 (7 pages) (2018)
[5] Y. Matsunaga, and Y. Sugita, "Linking time-series of single-molecule experiments with molecular dynamics simulations by machine learning", eLife, vol. 7, e32668 (19 pages) (2018)
[6] M. Kamiya, and Y. Sugita, "Flexible selection of the solute region in replica exchange with solute tempering: Application to protein-folding simulations", The Journal of Chemical Physics, vol. 149, 072304 (11 pages) (2018)

10.3.2 Invited Talks

[7] Y. Matsunaga "Integrative modeling of protein folding dynamics from experiments and simulations" Telluride Workshop on "The Complexity of Dynamics and Kinetics from Single Molecules to Cells", Telluride, Colorado, USA, Jun. 20 – 24, 2017
[8] Y. Sugita "Molecular dynamics analysis of membrane protein structure and dynamics" Telluride Summer Conference on Macromolecular Crowding, Telluride, Colorado, USA, Jun. 25 – 30, 2017
[9] K. Tamura, and Y. Sugita, "Molecular dynamics simulations of membrane transport proteins", 7th JLESC Workshop, Illinois, USA, Jul. 19, 2017
[10] Y. Sugita, "Machine learning approach to link single-molecule FRET and molecular dynamics for understanding protein folding dynamics", Seminar at Department of Biochemistry in Michigan State University, Michigan, USA, Jul. 5, 2017
[11] Y. Sugita, "Protein diffusion, dynamics, stability in cellular environments", Seminar at NIH, Bethesda, USA, Jul. 7, 2017
[12] Y. Sugita "Machine learning approach for protein dynamics by combining smFRET and MD simulations" Telluride Summer Conference on Free Energy Calculations: Three decades of adventure in chemistry and biophysics, Telluride, Colorado, USA, Jul. 11 – 14, 2017
[13] Y. Sugita, "Molecular dynamics simulations of conformational changes in SR Ca^{2+}-ATPase", P-type ATPase Meeting, Shiga, Japan, Sep. 27, 2017

[14] Y. Sugita, "Rapid nitric oxide transport in the nitrite reductase: Nitric oxide reductase complex", The 1st Samsung Global Research Symposium on "Structure Dynamics, and Thermodynamics of Biomolecular Networks", Seoul, Korea, Nov. 3, 2017
[15] Y. Sugita, "Machine learning approach to connect time-series data of single-molecular experiments with molecular dynamics simulations of protein folding dynamics", Greater Boston Area Lecture Series, Boston, USA, Feb. 14, 2018
[16] K. Tamura, "Structural and functional analysis of biomembrane transport proteins with molecular simulations (Japanese)", Workshop of "Potential energy surface and dynamics of chemical reactions (Japanese)",Okinawa, Japan, Apr. 09, 2017
[17] Y. Sugita, "Molecular dynamics analysis of membrane protein structure and dynamics (Japanese)", The 17th Japanese Protein Science Society Annual Meeting (Japanese),Sendai, Japan, Jun. 20 – 22, 2017
[18] J. Jung, "Parallelization of Molecular Dynamics", Computational Science LectureA (2017) (Japanese), Osaka, Japan, Jul. 13, 2017
[19] C. Kobayashi, "Development of computer simulation method for conformational changes of proteins (Japanese)", Kobe biomedical innovation cluster seminar (Japanese), Tokyo, Japan, Aug. 4, 2017
[20] Y. Matsunaga "Integrative modeling of protein dynamics by using machine learning (Japanese)", KAKENHI on Innovative Areas 'Soft Molecular Systems' symposium for young scientists (Japanese), Tohoku University, Japan, Sep. 14, 2017
[21] Y. Sugita, "Experimental and computational analysis of protein-protein interaction in cellular environment", The 55th Annual Meeting of the Biophysical Society of Japan, Kumamoto, Japan, Sep. 19, 2017
[22] Y. Sugita, "Molecular dynamics simulations of conformational changes in SR Ca^{2+}-ATPase", P-type ATPase Meeting, Kumamoto, Japan, Sep. 27, 2017
[23] J. Jung, C. Kobayashi, and Y. Sugita, "Development of GENESIS for high performance computing of biolmolecular simulations", The 55th Annual Meeting of the Biophysical Society of Japan, Sympoisum of "Next-generation in-silico drug discovery using high-performance computing", Kumamoto, Japan, Sep. 19 – 21, 2017
[24] C. Kobayashi, Y. Matsunaga, J. Jung, and Y. Sugita, "Molecular dynamics simulations for conformational changes on E1/E2 transition of Ca^{2+}-ATPase", The 55th Annual Meeting of the Biophysical Society of Japan, Symposium, Kumamoto, Japan, Sep. 21, 2017
[25] Y. Matsunaga "Integrative modeling of protein dynamics by using machine learning (Japanese)" Kyoto University MACS program (Japanese), Kyoto, Japan, Nov. 29, 2017
[26] Y. Matsunaga "Energetics and Conformational Pathways of Functional Rotation in the multidrug transporter AcrB (Japanese)" Kindai University, Jan. 22, 2018
[27] Y. Matsunaga "Integrative modeling of protein dynamics by using machine learning (Japanese)", Advanced Industrial Science and Technology (AIST) Biomedical Research Institute, Feb. 27, 2018
[28] J. Jung, "Development of parallelization scheme in GENESIS molecular dynamics program", 2017 High performance workshop (Japanese), Japan, Mar. 23, 2018

10.3.3 Posters and presentations

[19] C. Kobayashi, Y. Matsunaga, J. Jung, and Y. Sugita, "Molecular Dynamics simulations for conformational changes on a reaction step of Ca^{2+}-ATPas", 62nd annual meeting of the biophysical society, San Francisco, USA, Feb. 19, 2018
[20] K. Tamura, Hiroshi Sugimoto, Yoshitsugu Shiro, and Yuji Sugita, "Computational modeling of the ATP-bound outward-facing form of a heme importer", The 55th Annual Meeting of the Biophysical Society of Japan, Kumamoto, Japan, Sep. 21, 2017
[21] J. Jung, C. Kobayashi, and Y. Sugita, "Kinetic energy definition in velocity Verlet integration for accurate pressure evaluation", The 31th Molecular Simulation Meeting (Japanese), Kanazawa, Japan, Nov. 29 – Dec. 1, 2017
[22] C. Kobayashi, Y. Matsunaga, J. Jung, and Y. Sugita, "Comutational simulation analysis of conformational changes on ligand dissociation in Ca^{2+}-ATPas (Japanese)", The 43th Annual Meeting of Japanese Bioenergetics Group (Japanese), Kyoto, Japan, Dec. 19, 2017

10.3.4 Software

[23] A molecular dynamics and modeling software GENESIS, https://www.r-ccs.riken.jp/labs/cbrt. Current release version is GENESIS 1.2.

Chapter 11

Particle Simulator Research Team

11.1 Members

(as of Apr 1, 2017)

Junichiro Makino (Team Leader)

Keigo Nitadori (Research Scientist)

Yutaka Maruyama (Research Scientist)

Masaki Iwasawa (Research Scientist)

Takayuki Muranushi (Postdoctoral Researcher)

Daisuke Namekata (Postdoctoral Researcher)

Long Wang (Postdoctoral Researcher)

Miyuki Tsubouchi (Technical Staff)

11.2 Research Activities

We are developing particle-based simulation software that can be used to solve problems of vastly different scales.

Simulation schemes for hydrodynamics and structural analysis can be divided into grid-based and particle-based methods. In grid-based methods, the computational region is mapped to regular or irregular grids. Continuous distributions of physical values are represented by discrete values at grid points, and the governing partial differential equation is approximated to a set of finite difference equations.

In the case of the particle-based methods, physical values are assigned to particles, while the partial differential equation is approximated by the interactions between particles.

Both methods are widely used, and they have their advantages and disadvantages. The computational cost of grid-based schemes is generally lower than that of particle-based methods with similar number of freedoms. Thus, if an near-uniform grid structure is appropriate for the problem to be solved, grid-based methods perform better.

The advantage of the particle-based methods comes from the fact that they use "Lagrangian" schemes, in which the particles move following the motion of the fluid in the case of the CFD calculation. In the case of grid-based methods, we generally use "Eulerian" schemes, in which the grid points do not move.

There are three points in which the Lagrangian schemes are better than Eulerian schemes. One is that the Lagrangian schemes are, to some extent, adaptive to the requirement of the accuracy, since when a low-density region is compressed to become high density, Second one is that the timestep criteria are quite different. In the case of the Lagrangian schemes, the timestep is determined basically by local sound velocity, while in the Eulerian scheme by global velocity. Thus, if a relatively cold fluid is moving very fast, the timestep for the Eulerian schemes can be many orders of magnitude shorter than that for Lagrangian schemes. Finally, in the case of fast-moving low-temperature fluid, the required accuracy would be very high for Eulerian scheme, since

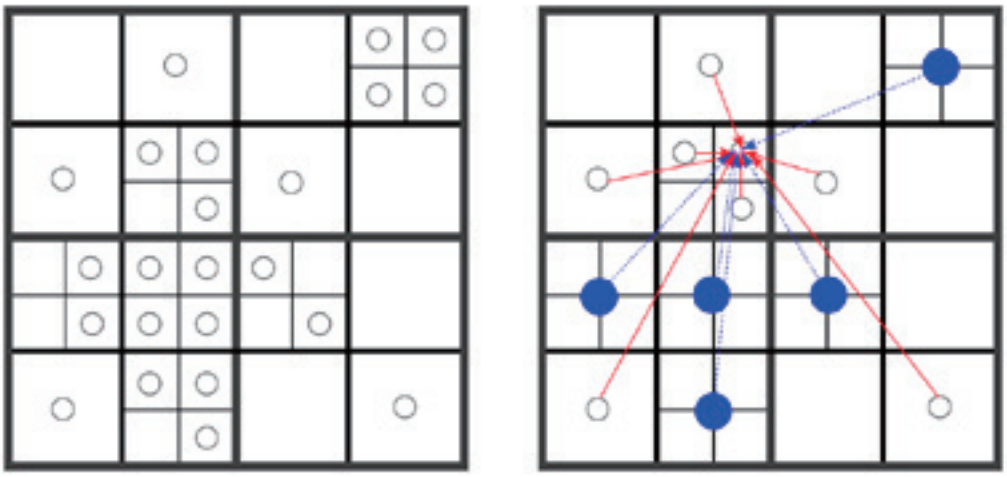

Figure 11.1: Basic idea of tree algorithm

the error comes from the high velocity, while that error would be transferred to internal energy of the fluid element which is much smaller than that of the kinetic motion.

Of course, there are disadvantages of Lagrangian schemes. The primary one is the difficulty of construction of such schemes in two or higher dimensions. In the case of one-dimensional calculation, it is easy to move grid points following the motion of the fluid, but in two or higher dimensions, the grid structure would severely deform if we let the grid points follow the flow. Thus, we have to reconstruct the grid structure every so often. This requirement causes the program to become complex. Moreover, reconstruction of the grid structure (so called remeshing) means we lose numerical accuracy.

Particle-based methods "solve" this difficulty by not requiring any mesh. In particle-based methods, particles interact with its neighboring particles, not through some connection through grid, but through distance-dependent kernel functions. Thus, there is no need of remeshing. As a result, particle-based schemes are simple to implement, and can give reasonable results even when the deformation is very large. Another important advantage is that it is relatively easy to achieve high efficiency with large-scale particle-based simulation.

In the case of grid-based schemes, in order achieve some adaptivity to the solution, we have to use either irregular grid or regular grid with adaptive mesh refinment. In both cases, adaptivity breaks the regularity of the mesh structure, resulting in non-contiguous access to the main memory. In the case of the particle-based schemes, it does require some irregular memory access, but it is relatively straightforward to make good use of spacial locality, and thereby achieving high efficiency. Similarly, very high parallel performance can be achieved.

However, it has its own problems. In the case of the SPH method, it has been known that the standard scheme cannot handle the contact discontinuity well. It also require rather strong artificial viscosity, which results in very low effective Reynolds number.

Thus, in many fields of computational sciences, many groups are working on implementation of high-performance particle-based simulation codes for their specific problem.

One serious problem here is that, high-performance, highly-parallel simulation codes for particle-based simulations are becoming more and more complex, in order to make full use of modern supercomputers. We need to distribute particles to many computing nodes in an appropriate way, so that the communication between nodes is minimized and at the same time near-optimal load balance is achieved. Within each nodes, we need to write an efficient code to find neighbor particles, rearrange data structure so that we can make good use of the locality, make good use of multiple cores and SIMD units within each core.

Even for the case of very simple particle-particle interaction such as the Lenard-Jones potential or Coulomb potential, the calculation code tends to be very large, and since the large fraction of the code is written to achieve a high efficiency on a specific architecture, it becomes very hard to port a code which is highly optimized to one architecture to another architecture.

Our goal is to develop a "universal" software that can be applied to a variety of problems whose scales are vastly different. In designing such universal software, it is important to ensure that it runs efficiently on highly parallel computers such as the K computer. Achieving a good load balance with particle-based simulation is a difficult task, since using a regular spatial decomposition method causes severe load imbalance, though this

works well for grid-based software. Consequently, we have developed an adaptive decomposition method that is designed to work in a way that the calculation time on each node is almost the same, resulting in near-optimal load balance.

The strategy to develop such a universal software is as follows.

We first construct an highly parallel and very efficient implementation of the TreePM algorithm for gravitational N-body problem. This is actually not a completely new implementation, but the GreeM code developed by researchers of the Strategic Program for Innovative Research (SPIRE) Field 5 " The origin of matter and the universe. In collaboration with the Field 5 researchers, we improve the efficiency of the code and study the issues of the data structure, domain decomposition, load balance strategy etc.

In the second stage, we will develop a prototype of the parallel particle simulation platform. We will design the platform so that it can be used for multiple physical systems. In practice, we consider the following three applications as the initial targets.

[1] Gravitational N-body simulation

[2] Smoothed Particle Hydrodynamics

[3] Molecular Dynamics

In the meantime, we will also investigate the way to improve the performance and accuracy of the current particle-based algorithms for hydrodynamics.

11.3 Research Results and Achievements

As we stated in section 1, we are working on the three major subtopics, in order to develop the universal platform for particle simulations.

In the following, we briefly describe the status of our research in each subtopic.

11.3.1 High-performance gravitational N-body solver.

We use the TreePM algorithm as the basic method for the evaluation of gravitational interaction between particles. TreePM is a combination of the tree method and the P^3M (particle-particle particle-mesh) scheme. Figure 1 shows the basic idea of the tree algorithm. The space is divided into a hierarchical octree structure (quadtree in the figure). Division is stopped when a cell contains one or no particle. When we calculate the force on a particle, we evaluate the force from a group of particles, with size larger for more distant particles. In this way, we can reduce the calculation cost from O(N2) to O(N log N).

The tree algorithm is widely used, but when the periodic boundary condition is applied, we can actually use a more efficient efficient scheme, since we can calculate the long-range, periodic term using FFT. The P^3M scheme has been used for such problem, but it has the serious problem that when the density contrast becomes high, the calculation cost increases very quickly. The TreePM scheme solves this difficulty by using the tree algorithm to evaluate the forces from nearby particles. Even when there are very large number of neighbor particles, the calculation cost does not increase much, since the calculation cost of the neighbor force is proportional to the logarithm of the number of neighbors.

In order to map the problem to the distributed-memory parallel computer such as the K computer, we adopted the approach to divide the space into domains and assign particles in one domain to one calculation node. We used the orthogonal recursive multisection method developed by the team leader some years ago. It is the generalization of the orthogonal recursive bisection (ORB), which has been widely used in many parallel implementations of the tree algorithm.

With ORB, we recursively divide space into two halves, each with the same number of particles. An obvious disadvantage of the ORB approach is that it can utilize the computing nodes of integral powers of two. Thus, in the worst case we can use only half of the available nodes.

The difference between the multisection method and the ORB is that with the multisection method we allow the divisions to arbitrary number of domains, instead of bisection. This would allow too many possible divisions. In our current implementation, we limit the number of levels to three, and make the numbers of divisions at all levels as close as possible. Thus, our domain decomposition is topologically a simple three-dimension grid. This fact makes the multisection method well suited to the machines with the 3D torus network like the K computer.

We have developed a "reference code" for gravitational N-body simulation on the K computer. This code is fairly well optimized for the K computer, and shows quite good scalability for even for relatively small-size problems. The asymptotic speed per timestep for large number of nodes is around 7ms. This speed is comparable to that of highly optimized molecular dynamics codes on K, even though our code is designed to handle highly inhomogenous systems.

We used this code as the reference implementation for more generalized particle simulation platform which will be described in the next subsection.

11.3.2 Particle Simulation Platform.

In FY 2014, We have completed and released Version 1.0 of the particle simulation platform, which we call FDPS (Framework for Developing Particle Simulator). In FY 2015, we have applied a number of improvements to FDPS.

The basic idea of FDPS is that the application developer (or the user) specified the way the particles interact with each other, and the rest is taken care by FDPS. Here, "the rest" includes domain decomposition and re-distribution of particles, evaluation of interactions between particles, including those in different domains (different MPI processes, for example).

In practice, there are many additional details the user should give. Consider a relatively simple case of particles interacting with softened 1/r potential. There are a number of small but important points one has to decide on. For example, what algorithm should be used for the interaction calculation? Even if we limit the possibilities to reasonably adaptive schemes for open boundary problems, we have the choice between Barnes-Hut tree and FMM. For both algorithms, there are many different ways to parallelize them on distributed-memory parallel computers. Also, there are infinitely many variations for the time integration schemes.

The base layer of FDPS offers the domain decomposition based on the recursive multisection algorithm, with arbitrary weighting function for the load balancing. It also offers the parallel implementation of interaction calculation between particles.

The domain decomposition part takes the array of particles on each node as the main argument. It then generates an appropriate domain for each node, redistribute particles according to their locations, and returns.

The interaction calculation part takes the array of particles, the domain decomposition structure, and the specification of the interaction between particles as main arguments. The actual implementation of this part need to take into account a number of details. For example, the interaction can be of long-range nature, such as gravity, Coulomb force, and interaction between computational elements in the boundary element method (BEM). In this case, the user should also provide the way to construct approximations such as the multipole expansion and the way to estimate error. The interaction might be of short-range nature, with either particle-dependent or independent cutoff length. In these cases, the interaction calculation part should be reasonably efficient in finding neighbor particles.

We have successfully implemented all of these functionalities in FDPS version 1.0.
(https://github.com/FDPS/FDPS). Using FDPS, a gravitational N-body simulation code can be written in 120 lines, and that code is actually fully scalable even to full-node runs on K computer. For SPH calculations, we have also achieved similar scaling.

FDPS is implemented as a class template library in C++ language. It receives the class definition of particles and a function (or multiple functions in the case of complex interactions) to evaluate the interaction between particles. When a user program is compiled with the FDPS library, the class template is instantiated with the user-specified definition of the particle class. Thus, even though the FDPS library functions are generic ones not specialized to a particular definition of particles, it behaves as if it is a specialized one.

The measured performance of applications developed using FDPS is quite good. Both for gravity-only calculation and SPH calculation, weak-scaling performance is practically perfect, up to the full-node configuration of K computer. Moreover, the measured efficiency, in terms of the fraction of the peak floating-point performance, is also very high. It is around 50% for gravity-only calculation. For SPH calculations, at the time of writing the performance is around 10%.

In FY 2015, we have extended FDPS in several important directions. The first one is the improvement of the strong scaling. The algorithm used for the domain decomposition contains one serial bottleneck. The "sampling" algorithm used in FDPS 1.0 works well only when the average number of particles per MPI process is significantly larger than the total number of MPI processes. We developed a new parallel algorithm, in which $O(p^{1/3}$ MPI processes are used to decompose the computational domain. Here p is the total number of MPI processes. Thus now the requirement for the number of particle is relaxed from larger than p to larger than $p^{2/3}$.

Now we can achieve pretty good performance for around 1 billion particles, on the full nodes of K computer. Previously we need near 100 billion particle to achieve good efficiency.

The second one is the addition of new interface method to interaction calculation function, which allows efficient use of accelerator hardware such as GPGPU or Intel MIC. In order to achieve high performance on accelerators, it is important to pass a large chunk of work at one time. In order to achieve this goal, in the current version of FDPS the CPU creates the list of multiple interaction lists, and send all of them at once so that the overhead of the initialization of the accelerator would not become a bottleneck. This interface has been tested on NVIDIA GPGPUs as well as the PEZY-SC processor.

In FY 2016, we have released FDPS 3.0. The most important new feature of this release is the interface to application programs written in Fortran. FDPS itself is implemented using C++. The reason why we adopted C++ is to use its "template" functions. Using templates, we can write library functions which accept user-defined data types as template arguments. This means we can effectively generate "specialized" libraries for user-specified particle data types, without knowing the data types beforehand.

In FY 2017, we have released several new versions of FDPS, up to 4.0a. There are a number of improvements, mostly for improved performance, For example, we have implemented the reuse of the interaction list. In the case of the calculation of short-range interactions, the neighbor-list method or so-called bookkeeping method has been used in many applications. On the other hand, to our knowledge, such a method has not been applied to Barnes-Hut treecode or FMM. There is no fundamental difficulty in combining the two methods, and the reason why such a combination has not tried before is probably it was not really necessary. The calculation cost of constructing the tree structure and traversing the tree to construct the interaction lists is, int the case of Barnes-Hut algorithm, a small fraction of the total calculation cost. Thus, it is usually unnecessary to try to reduce the cost of the tree construction and tree traversal.

However, some of recent high-performance computers have rather extreme ratios in various aspects, and thus require the performance improvements which were not necessary. One example is the Sunway SW26010. It's architecture is rather extreme in two aspects. First, its "core group" consists of one MPE (management processing element) and 64 CPEs (computing processing elements). MPE has data cache and runs the primary thread, and CPEs do not have cache. Thus, it is difficult and very time-consuming to develop the program which runs on CPEs, in particular for complex operations like tree construction. On the other hand, MPE is very slow compared to CPE, and thus we need to minimize the computational work of MPE.

Another aspect is the rather low memory bandwidth. The B/F number of SW26010 is around 0.03, which is around 1/15 of that of K computer. Thus, in order to achieve reasonable performance on SW26010, we need to minimized the main memory access per timestep.

The reuse of the interaction list turned out to be very effective on SW26010 and other machines with relatively low memory bandwidth, such as NVIDIA P100/V100 and PEZY-SC2.

11.3.3 Improvements on Particle-based CFD

SPH (Smoothed Particle Hydrodynamics) has been used in many field, including astrophysics, mechanical engineering and civil engineering. Recently, however, it was pointed out that the standard formulation of SPH has numerical difficulty at the contact discontinuity. The reason is that the formulation of the standard SPH requires that the density is differentiable, which is by definition no the case at the contact discontinuity.

We have been working on the possible solution on this problem. One approach is to reformulate SPH so that it does not use the density in the right-hand side of the equation of motion. We one way to achieve the density independence. We constructed an SPH scheme which uses artificial density-like quantity as the base of the volume estimator. It evolves through usual continuity equation, but with additional diffusion term. Thus, we can guarantee the continuity and differentiability of this quantity, except at the initial condition or at the moment when two fluid elements contact with each other. This scheme seems to work extremely well, and we are currently working on the way to extend this scheme so that it can handle free surface accurately.

We are also working on a completely different approach, in which we replace the SPH formulation to evaluate the gradient to other schemes. SPH has a known problem that its kernel estimate contains O(1) error, since the summation of contributions from neighbor particles is not guaranteed to be unity. The reason why SPH uses this mathematically inconsistent formulation is to achieve symmetry and conservation. In SPH discretization, interaction between two particles is symmetric, which guarantees the conservation of linear and angular momenta. However, the use of SPH approximation resulted in rather low accuracy, which limits the reliability of the results obtained using SPH. We have developed a completely different scheme, which can achieve much higher accuracy, while losing some of the nice features of SPH such as the symmetry of interaction.

Our new approach, which we call CPHSF (Consistent Particle Hydrodynamics in Strong Form), is based on high-order MLS (moving least square fit). In SPH, particles have mass and energy (or entropy). Particle mass is automatically conserved, and SPH differentiation is constructed so that the total energy is conserved. Thus, SPH is quite robust, since conserved quantities are always conserved. However, this formulation makes it practically impossible to construct high-order schemes, express boundary condition explicitly or handle contact discontinuity. Therefore, in CPHSF, we gave up the exact conservation of mass and energy, but instead achieved the conservation by the scheme which is of higher order in both space and time.

One unique feature of CPHSF is that with CPHSF we can obtain high-order space derivatives with very small additional cost, since we do construct high-order MLS fitting. Thus, instead of using usual Runge-Kutta method to achieve high-order accuracy in time, we can use high-order space derivatives to construct high-order time integration scheme. We adopted 4th-order Hermite scheme, which has been widely used in the field of stellar dynamics. The Hermite scheme is the generalization of Adams-Bashforth-Moulton (ABM) linear-multistep method. In the ABM method, previous values of first time derivatives (the rhs values of the ordinary differential equations) are used to construct high-order polynomial fitting through Lagrange interpolation. In Hermite method, not only the rhs value itself but also its time derivatives are used to construct high order fitting polynomial through Hermite interpolation. The 4th-order Hermite scheme is the simplest Hermite scheme, in which the second time derivatives are calculated directly from the original differential equation and two-point interpolation is used to construct third-order fitting polynomial. The clear advantage of the Hermite scheme is that it requires only one evaluation of the derivatives per one timestep, if used in the PEC form. Runge-Kutta schemes with 4th-order accuracy require four evaluations per timestep and thus four times more expensive.

11.4 Schedule and Future Plan

We plan to improve the performance of FDPS further in FY 2018. In particular, we investigate the way to make FDPS more efficient on machines with heterogeneous architecture and limited memory and network bandwidth.

11.5 Publications

11.5.1 Journal Articles

[1] Y. Maruyama and A. Mitsutake, “Stability of Unfolded and Folded Protein Structures Using a 3D-RISM with the RMDFT”, J. Phys. Chem. B 121, 9881-9885 (2017).

[2] T. Sumi, Y. Maruyama, A. Mitsutake, K. Mochizuki, and K. Koga, “Application of reference-modified density functional theory: Temperature and pressure dependences of solvation free energy” J. Comp. Chem. 39, 202-217 (2018).

[3] A. Sills, S. Rieder, J. Scora, J. McCloskey, S. Jaffa, “Dynamical evolution of stars and gas of young embedded stellar sub-clusters”, Monthly Notices of the Royal Astronomical Society, 2018

[4] M. Iwasawa, S. Oshino, M. S. Fujii, Y. Hori, “PENTACLE: Parallelized particle–particle particle-tree code for planet formation”, Publications of Astronomical Society Japan, 69, 5, 2017

[5] M. S. Fujii, A. Tanikawa, J. Makino, “The detection rates of merging binary black holes originating from star clusters and their mass function”, Publications of Astronomical Society Japan, 69, 94, 2017

[6] S. Yamamoto, J. Makino, “A formulation of consistent particle hydrodynamics in strong form”, Publications of Astronomical Society Japan, 69, 2, 2017

[7] N. Hosono, M. Iwasawa, A. Tanikawa, K. Nitadori, T. Muranushi, J. Makino, “Unconvergence of very-large-scale giant impact simulations”, Publications of Astronomical Society Japan, 69, 26, 2017

[8] J. Makino, “Introduction of FDPS (1)”, Newsletter of the Molecular Simulation Society of Japan “Ensemble”, 19, 2, 2017. (in Japanese)

[9] M. Iwasawa, “Introduction of FDPS (2)”, Newsletter of the Molecular Simulation Society of Japan “Ensemble”, 19, 3, 2017. (in Japanese)

[10] K. Nomura, ”Introduction of FDPS (3)”, Newsletter of the Molecular Simulation Society of Japan “Ensemble”, 19, 4, 261, 2017. (in Japanese)

[11] K. Nomura, ”Introduction of FDPS (4)”, Newsletter of the Molecular Simulation Society of Japan “Ensemble”, 20, 1, 46, 2018. (in Japanese)

11.5.2 Invited Talks

[1] K. Nomura, ”Development of molecular dynamics simulation code using FDPS”, Post-K Exploratory Challenge “Challenge of Basic Science Sub-Challenge B: Phase Transition and Flows Symposium, Sendai, Nov. 24, 2017.

11.5.3 Oral Presentations

[1] Y. Maruyama and A. Mitsutake, ”Stability of protein structure using new solvation free energy functional”, 40th Symposium on Solution Chemistry of Japan, Himeji, Japan Oct. 18-20, 2017
[2] S. Rieder, ”Simulations of young star clusters: the MYSTIX case”, MODEST 17, Praque, Czech Republic, Sep 18-22, 2017
[3] M. Iwasawa, “Accelerator interface of FDPS”, 2017 Autumn meeting of the Astronomicay Society of Japan, Sapporo Japan, Sep 11-13, 2017 (in Japanese)
[4] D. Namekata, M. Iwasawa, K. Nitadori, A. Tanikawa, T. Muranushi, L. Wang, N. Hosono, J. Makino, ”Development of a fortran interface to FDPS (Framework for Developing Particle Simulators)”, 2017 Autumn Meeting of Astronomical Society of Japan, Sapporo, 11-13 Sept., 2017. (in Japanese)
[5] K. Nitadori, “High-order Hermite integrator based on high-order derivatives of Newtonian gravity”, Annual meeting of JSIAM, Tokyo, Japan, Sep 6-8, 2017 (in Japanese)
[6] K. Nomura, “Development of Molecular Dynamics code using FDPS”, Symposium of Sub-Challenge B: Phase Transitions and Flows, Post-K Exploratory Challenge rontiers of Basic Science: Challenging the Limits, Sendai, Japan, Nov 24, 2017
[7] J. Makino, “Optimization of FDPS for planetary formation and planetary rings”, 2017 Autumn Meeting of Astronomical Society of Japan, Sapporo, 11-13 Sept., 2017. (in Japanese)
[8] J. Makino “FDPS: Framework for Developing Particle Simulator”, Numerial Integration Methods in Planetary Science, Toronto, Canada, Aug. 13-16, 2017
[9] Hosono, N., Karato, S., Makino, J., Saitoh, R.T., ”Terrestrial magma ocean origin of the Moon: A numerical study of a giant impact incorporating the difference of the equations of state for liquids and solids”, JpGU-AGU joint meeting, Chiba, Japan, 20-25 May 2017
[10] Hosono, N., Iwasawa, M., Tanikawa, A., et al., ”Development of an SPH code which works on the PEZY-SC devices and application to the giant impact”, JpGU-AGU joint meeting, Chiba, Japan, 20-25 May 2017

11.5.4 Software

[1] FDPS, http://fdps.jmlab.jp/ Versions 3.0a, 4.0 and 4.0a.

Chapter 12

Computational Climate Research Team

12.1 Members

Hirofumi Tomita (Team Leader)

Yoshiyuki Kajikawa (Senior Scientist)

Seiya Nishizawa (Research Scientist)

Hisashi Yashiro (Research Scientist)

Sachiho A. Adachi (Research Scientist)

Tsuyoshi Yamaura (Research Scientist)

Ryuji Yoshida (Postdosctoral Researcher)

Kenta Sueki (Postdosctoral Researcher)

Toshiki Matsushima (Postdosctoral Researcher)

Kazuto Ando (Technical Staff I)

Yuta Kawai (Jonior Research Associate)

Hiroaki Miura (Guest Researcher)

Hiroshi Taniguchi (Guest Researcher)

Yoshiaki Miyamoto (Guest Researcher)

Yousuke Sato (Guest Researcher)

Shinichiro Shima (Guest Researcher)

Kazuyoshi Kikuchi (Guest Researcher)

Mizuo Kajino (Guest Researcher)

Tomoko Ohtani (Research Assistant)

Keiko Muraki (Research Assistant)

Shoko Kojima (Research Assistant)

12.2 Research Activities

Our research team conducts the pioneering research work to lead the future climate simulation. In order to enhance the reliability of climate model, we have aimed to construct a new climate model based on the further theoretically physical principles. Conducting such a new model needs tremendously large computer resources. Therefore, it is necessary to design the model to pull out the capability of computers as much as possible. Recent development of supercomputers has a remarkable progress. Hence another numerical technique should be needed under the collaboration of hardware research and software engineering for the effective use on the future HPC, including the K computer and Post K computer.

For the above research purpose and background, our team is cooperating with the computational scientists in other fields and computer scientists. We enhance the research and development for the future climate simulations including effective techniques; we build a next-generation climate model. The establishment of the above basic and infrastructure research on the K Computer is strongly required, because this research leads to the post K computer or subsequent ones in the future.

We have proposed the subject Estimation of different results by many numerical techniques and their combination as a synergetic research to MEXT from 2011. We develop a new library for numerical simulation. In this fiscal year, we improved computational performance of SCALE library and validation of its physical performance, aiming at the reliability of SCALE. In addition, for the user expansion and promotion, we vigorously maintained the users manual and model document. New developments are highlighted as follows.

12.2.1 Redesign of Structure and API of SCALE

SCALE contains a library providing fundamental components (SCALE-lib) and an atmospheric regional model using the library (SCALE-RM). So far, SCALE-lib has been developed to be used by SCALE-RM. The design of SCALE is not suitable for use in programs for pre- and post-processes. We redesign the structure and application programming interfaces (APIs) of SCALE-lib for the general purposes. The followings are the key points of the redesigning.

- reduction of dependency between individual components
- minimization of initialization of the components for individual use of each component
- dynamical grid size handling for multiple problem sizes in a program
- trace information in the error messages for improving traceability
- standardization of name of files and modules for easier understanding of the structure

In this year, we redesigned the whole structure APIs and implemented the modules for the physical processes. We also prepared sample programs for analysis using a part of physical process calculations to provide use case and template for users.

12.3 Research Results and Achievements

12.3.1 Research for Estimating Complex Disaster Risk in Hyogo-Kobe COE Establishment Project

The Hyogo-Kobe COE establishment project newly accepted the six research subjects in this fiscal year. Our team participates one of six subjects “Computational Research on Estimation to Complex Disaster Risk for Better Urban Planning.” In this project, our team is responsible for future regional climate projection by a model with high spatial resolution and sophistication of the model for it.

Recently, climate changes associated with global warming are observed in the world: increase of air temperature and changes in precipitation. Studies projecting future climate change by the numerical simulations have been actively carried out to provide information of the future climate. To consider adaptation plans to future climate change, it is important not only to estimate range of projections but also to understand mechanisms controlling regional climate. Previous studies often used a downscaling method (pseudo global warming (PGW) method) that considers only changes in ”mean state” of large-scale climate as influential factor to regional climate. However, this method cannot precisely evaluate future regional climate change because the method

does not consider changes in "perturbation" of large-scale climate, i.e., changes in weather disturbances such as typhoon and midlatitude cyclones.

We extended the PGW downscaling method considering only the changes in mean state and proposed a new downscaling method considering the changes in perturbation. The proposed method uses four downscaling experiments: two direct dynamical downscaling (DDS) experiments for the present and future climates and two experiments with boundary conditions exchanging either climatology or perturbation components between the two climates. The DDS experiments are conventional downscaling simulations, for which boundary conditions are given directly from global circulation model (GCM) outputs. From these four experiments, we can estimate both influences of changes in mean state and changes in perturbation of large-scale climate on regional climate change. In addition, the method allows the influence due to the nonlinear effect between the two components to be extracted. That is, from four experiment, we can separate the regional climate change Δ into contributions of three factors: (1) changes in mean state ΔC, (2) changes in perturbation ΔP, and (3) the nonlinear effect Δcp.

To demonstrate the usefulness of the method, we applied the method to the future precipitation change in western Japan. The results indicate that the changes in perturbation account for a large part of the decrease in mean precipitation (Fig. 12.1 a). It means that consideration of only the mean state change is insufficient for projection of the future precipitation change. The result of extreme precipitation shows little change between the present and future climates (Fig.12.1 b), The small change between the present and future climates is simply a consequence of cancelling the contributions from mean state and perturbation changes, i.e., ΔC and ΔP. On the perspective of an adaptation strategy, both the changes in the cumulative precipitation amount and those in the frequency and intensity of precipitation are important. The former information is related to securing water resources, while the latter information is helpful to reduce the risk of disaster. An analysis shows that the changes in mean state have a large impact on the intensity of precipitation. On the other hand, the changes in perturbation strongly affect on the cumulative precipitation amount. These results are published as Adachi et al. (2017).

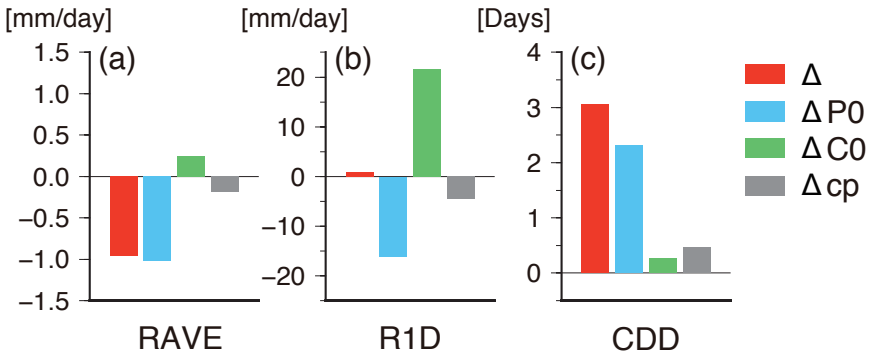

Figure 12.1: Differences from the present climate in 25-year means of the **a** daily mean precipitation (RAVE), **b** maximum one-day precipitation (R1D), and **c** maximum number of consecutive dry days (CDD), respectively. Δ is the total change estimated by the DDSs (Future-DDS−Present-DDS). ΔP_0 and ΔC_0 indicate the contributions of the perturbation and climatology, respectively. Δcp is the contribution of the nonlinear effect.

12.3.2 Development of Super Droplet Method (SDM)

In this year, we confirmed the validity of the SDM coupled with SCALE (SCALE-SDM) through the comparison between the results of SCALE-SDM and those of SCALE coupled with two-moment bulk microphysical scheme (Seiki and Nakajima 20014; SCALE-bulk). The validity of SCALE-bulk has been confirmed by previous studies (e.g., Sato et al. 2014, Sato et al. 2015, Adachi et al 2017), and the comparison between SCALE-SDM and SCLAE-bulk enables us to confirm the validity of SCALE-SDM.

For the comparison, we conducted the numerical simulations targeting on the shallow cumulus using the SCALE-SDM and SCALE-bulk. The experimental setup was based on one of the common experimental setups called the Barbados Oceanographic and Meteorological Experiment (BOMEX: Siebesma et al. 2003). In Siebesma et al. (2003), the horizontal (vertical) grid resolution of 100 (40) m was used, but we conducted

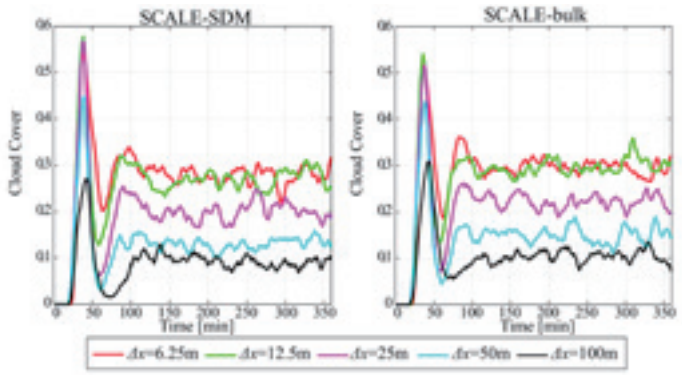

Figure 12.2: The temporal evolution of cloud cover simulated by (left) SCALE-SDM and (right) SCALE-bulk. Cited and from Sato et al. (2018).

the same simulation with changing the horizontal (vertical) grid resolution from 100 (80) m to 6.25 (5) m. We conducted the experiment using both SCALE-SDM and SCALE-bulk, and compared the results of SCALE-SDM and SCALE-bulk.

The results indicate that the cloud cover increased with higher the grid resolution, and the cloud cover with the grid resolution of 6.25 m and 12.5 m were similar. The numerical convergence was achieved with the horizontal (vertical) grid resolution of 12.5 (10) m. This indicates that the grid resolution used in Siebesma et al. (2003) was insufficient to accurately simulate the cloud cover, and the grid resolution of 12.5 m or finer is required. The resuls also indicate that the dependency of the cloud cover on the grid resolution was commonly seen in the results of SCALE-SDM and SCALE-bulk (Fig. 12.2). Since the validity of which has already confirmed through the several previous studies, the validity of the SCALE-SDM was confirmed.
We also investigated the reason of the numerical convergence of the cloud cover with the grid resolution of 12.5 m or finer. Our analyses elucidated that the numerical convergence of the cloud cover was originated from the numerical convergence of the turbulence structure below cloud (sub-cloud layer). The roll convection (LeMone 1973) was clearly seen in the sub-cloud layer simulated with the numerically converged grid resolution (dx = 12.5 m or finer). On the other hand, the roll convection was unclear with the coarse grid resolution.

We indicate that the number of layers near the surface was critical for the accurate simulation of the cloud cover. Based on the discussion in Skamarock (2004), numerical models can hardly simulate the phenomena whose spatial scale is smaller than six to seven times the grid length. With the coarse grid resolution, only a few layers existed near the surface, and the number of layers near the surface was insufficient to reproduce the turbulence structure in sub-cloud layer. In this case, the roll convection was unclear. With the fine grid resolution, in contrast, the number of layers near the surface was sufficient to accurately simulated the turbulence structure, and therefore, the roll convection and the cloud cover was accurately simulated.

These results were submitted as two papers, one was published as Sato et al. (2017), the other was accepted as Sato et al. (2018).

12.3.3 Understanding of Back Building Meso-scale Convective Systems

Quasi-stationary meso-scale convective systems (MCSs) cause heavy rainfall and lead to natural disasters such as floods and landslides. Back-Building MCSs (BBMs), in particular, cause heavy rains during the Baiu season in western Japan (Kato and Goda, 2001, Seko et al., 1999, Yoshizaki et al., 2000). It is essential to understand the maintenance process of BBMs for disaster prevention and mitigation. Moteki et al. (2004) proposed a conceptual environmental condition of the BBMs in the Baiu season. BBMs are observed around the confluence zone of a synoptic scale Baiu front and a water vapor front. However, this conceptual environmental condition

Table 12.1: Numerical simulation model settings

Items	Settings
Micro physics	Six-category one-moment bulk scheme (Tomita 2008)
Radiation	k-distribution scheme (Sekiguchi and Nakajima 2008)
Planetary boundary layer	MYNN level 2.5 scheme (Nakanishi and Niino 2009)
Time integration period	2010/07/10 09 JST ? 2010/07/12 09 JST
Initial and boundary condtions input data	GSM-GPV data (1 x 1 degree with 30 levels, 3 hourly)

is proposed on the ground of a case study. Therefore, confirmations are necessary to consolidate the conceptual environmental condition.

In this study, a heavy rainfall event during June 11?-12, 2010, in western Japan was numerically simulated using SCALE-RM (Nishizawa et al., 2015, Sato et al., 2015). Three computational domains are set by using 1-way online nesting system of CONeP (Yoshida et al. 2017). The outermost domain is 7.5 km grid spacing with 48 layers, the intermediate domain is 2.5 km grid spacing with 60 layers, and the innermost domain is 0.5 km grid spacing with 80 layers. Other model settings are shown in Tab. 12.1.

Fig. 12.3 shows simulated BBM in 2.5 km grid spacing. A linear precipitation area (rainband) is simulated. The rainband consists of multiple smaller precipitation area, and each area is simulated BBMs. These are simulated with a similar linear shape at similar location to these of the observed BBM. Vertical cross sections of a BBM which locates at the western edge of the rainband are shown in Fig. 12.4. Concentrated areas of hydrometeor correspond to convective cells, and the BBM consists of multiple convective cells. The new convective cells are formed at the western side of the BBM, and move eastward in the BBM. This is a typical back-building structure of MCSs.

Fig. 12.5 shows environmental conditions of specific humidity and temperature at 750 m height. The initiation point of the new convective cells in the BBM (indicated by yellow circle) is located over the meso-scale confluence zone of the synoptic-scale cold fronts and the meso-scale moist area at low-level. In the confluence zone, the synoptic-scale cold front can continuously trigger an updraft, and the meso-scale moist area supplies water vapor to the updraft. This suggests that new cells are continuously formed in the meso-scale confluence zone over the synoptic-scale cold front. This environmental condition is similar to the conceptual environmental conditions for BBMs proposed by Moteki et al. (2004). Therefore, this simulated BBM and its environmental condition support the conceptual environmental condition. On the other hand, the meso-scale moist area is a significant characteristic in this case, which is not reported in Moteki et al. (2004). Although Moteki et al. (2004) emphasized a local minimum of temperature in a cold front, such a characteristic is not observed in this case.

12.3.4 Improvement of Numerical Stability with Steep Mountains

In SCALE-RM, a terrain-following coordinate scheme is employed to introduce the effect of topography. So far, simulations in which maximum slope of the topography exceeds the grid aspect ratio of the bottom layer often result in an error due to a numerical instability. We improved numerical stability of the terrain-following coordinate scheme to enable simulations with more realistically steep mountains. The improvements contain the following three points:

- higher accuracy in calculation of the horizontal pressure gradient
- introducing a limiter to reduce numerical instability
- removing high-frequency components in the topography data

With these improvements, we can execute a simulation with 5 times steeper topography than before (Fig. 12.6. The details of the improvements follows. The horizontal pressure gradient is calculated from anomaly pressure from a reference. The reference was calculated with the linear interpolation. We change to use the spline interpolation to calculate the reference. This reduces error in the horizontal pressure gradient and consequent spurious acceleration of the horizontal wind (Fig. 12.7). In the terrain-following coordinate scheme, calculation of metrics due to coordinate transform. In SCALE, momentum is defined at staggered grid point depending on its direction. The metric terms in the momentum equation for each direction are calculated at the individual grid point. This may cause inconsistency between the different directions. We introduce a limiter to the calculation of the metric terms in the vertical momentum equation to reduce the inconsistency from those in

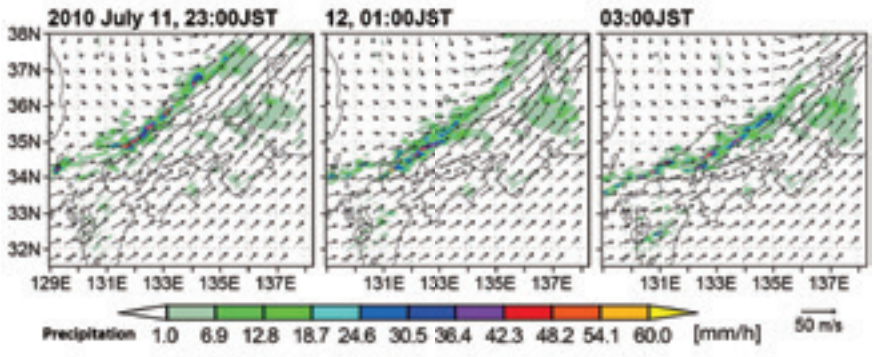

Figure 12.3: Horizontal distribution of the simulated precipitation in Domain 2 (2.5 km grid spacing). Vectors shows horizontal wind at 750 m height.

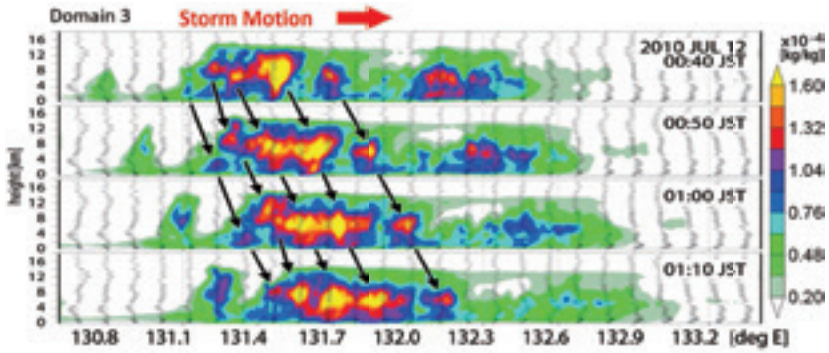

Figure 12.4: Vertical-longitudinal cross section for total mixing ratio of hydrometeors. Hydrometeors are defined as the sum of the mixing ratios of cloud water, rain droplets, cloud ice, snow, and graupel at each level. Each variable is averaged in the latitudinal direction from 33.8 ° N to 34.9 ° N, which is the rainband width. Black arrows trace the movement of each cell.

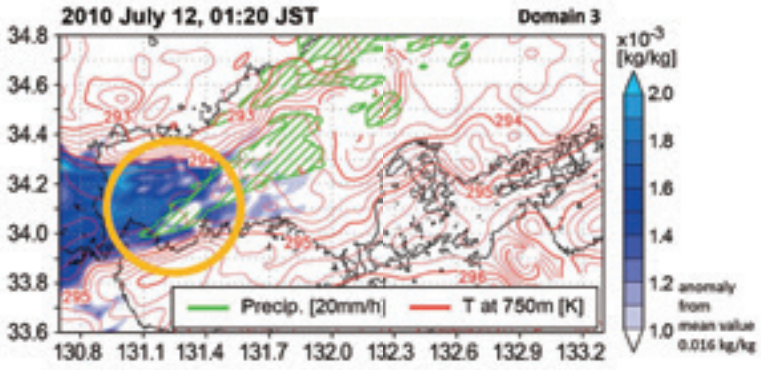

Figure 12.5: Positional relationship between cold fronts and moist air. Areas within green contours have a precipitation rate of 20 mm/h and the red contours represent the temperature at 750 m height. The color scale shows the residual specific humidity (Qv) relative to the average specific humidity of the area (0.016 kg/kg). Shaded areas have higher moisture content than the average specific humidity of the area.

the horizontal momentum equations. This enhances the numerical stability. The topography data is generated from a DEM dataset with the Laplacian filter not to exceed the given slope. Even if the maximum slop of obtained topography does not exceed the given slope, high-frequency components may still remain. The high-frequency components act as an external noise forcing and cause artificial atmospheric variability. Therefore, we use a high-order filter aiming removing high-frequency components together with the Laplacian filter. It results in reducing high-frequency noise in the atmospheric variability.

12.4 Schedule and Future Plan

We continue to sophisticate the basic library SCALE. At the present, the main processes, both of dynamics and physics, have already been developed comprehensively. We will pursue higher usability for the outside users. We keep elaborating the advanced climate model based on schemes in principle and indicate a direction to future climate model. At the same time, not only to make computational and physical performance of simulation code higher but also to provide useful analysis methods of simulation results is a main issue in the next phase. This is of great importance for acceleration of scientific output and social outcome.

The research for contribution of prevention from future heavy rainfall event and thermal environment in urban is also continuous in the second term COE project, which starts from the FY2017. There are still many uncertainties for the future prediction due to model bias. One of main causes is bias in regional model itself. Since SCALE has already implemented many components and schemes, construction of different models is easy. This advantage would be able to evaluate biases caused from regional models. This is done by the way of multi-model ensembles with data assimilation science.

12.5 Publications

12.5.1 Articles

[1] Sato, Y., D. Goto, T. Michibata, K. Suzuki, T. Takemura, H. Tomita, and T. Nakajima (2018): Aerosol effects on cloud water amounts were successfully simulated by a global cloud-system resolving model, *Nature Communications*, 9, 985, Doi: 10.1038/s41467-018-03379-6

[2] Nishizawa, S., S. A. Adachi, Y. Kajikawa, T. Yamaura, K. Ando, R. Yoshida, H. Yashiro, and H. Tomita (2018): Decomposition of the large-scale atmospheric state driving downscaling: a perspective on dynamical downscaling for regional climate study, *Progress in Earth and Planetary Science*, 5, 2, Doi: 10.1186/s40645-017-0159-0 [2017]

[3] Adachi, S. A., S. Nishizawa, R. Yoshida, T. Yamaura, K. Ando, H. Yashiro, Y. Kajikawa, and H. Tomita

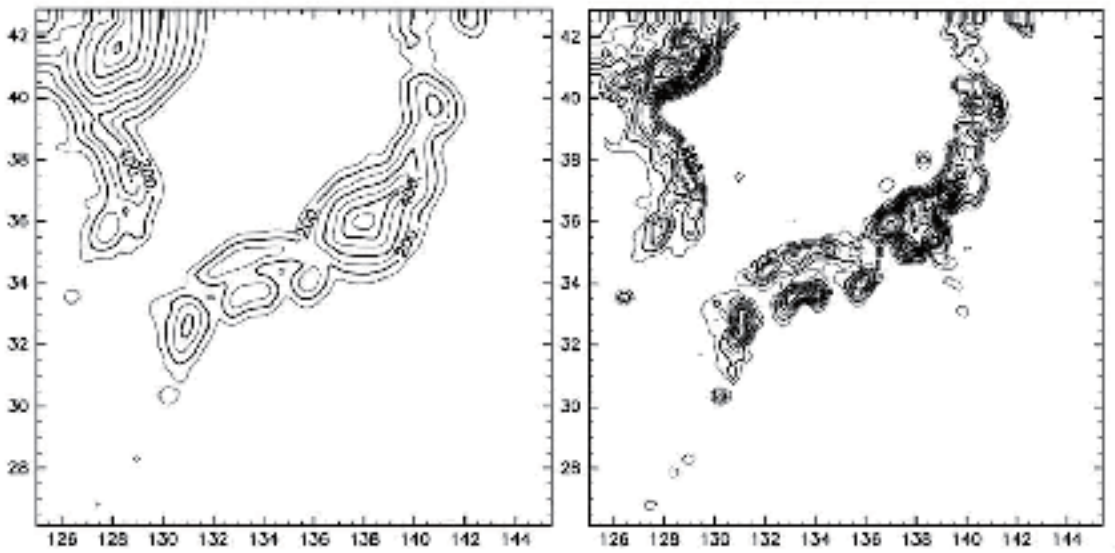

Figure 12.6: The topography in 20-km resolution simulation (left) before and (right) after the improvoment. The contour intervals are 100 m.

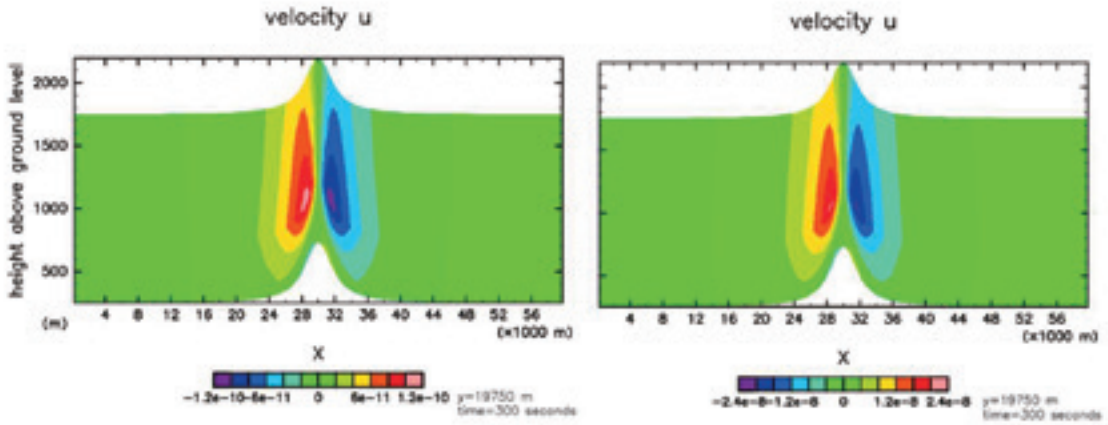

Figure 12.7: The horizontal and vertical corros section of thehorizontal wind field at t=300 s acceralated by the suprious horiaontal pressure gradient force from the steady state in the hydrostatic balance. The result of simulations with the reference generated using (left) the spline interpolation and (right) linera interpolation. Only a part of the calculation domain is drawn in vertically. The tone interval is (left) 2.0×1^{-11} and (right) 4.0×10^{-9} m/s.

(2017): Contributions of changes in climatology and perturbation and the resulting nonlinearity to regional climate change, *Nature Communications*, 8, 2224, Doi: 10.1038/s41467-017-02360-z

[4] Miyakawa, T., H. Yashiro, T. Suzuki, H. Tatebe, and M. Satoh (2017): A Madden-Julian Oscillation event remotely accelerates ocean upwelling to abruptly terminate the 1997/1998 super El Nio, *Geophysical Research Letters*, 44, 18, 94899495, Doi: 10.1002/2017GL074683

[5] Satoh, M., H. Tomita, H. Yashiro, Y. Kajikawa, Y. Miyamoto, T. Yamaura, T. Miyakawa, M. Nakano, C. Kodama, A. T. Noda, T. Nasuno, Y. Yamada, and Y. Fukutomi (2017): Outcomes and challenges of global high-resolution non-hydrostatic atmospheric simulations using the K computer, *Progress in Earth and Planetary Science*, 4, 13, Doi: 10.1186/s40645-017-0127-8

[6] Goto, D., Y. Sato, H. Yashiro, K. Suzuki, and T. Nakajima (2017): Validation of high-resolution aerosol optical thickness simulated by a global non-hydrostatic model against remote sensing measurements, *AIP Conference Proceedings*, 1810, 1, Doi: 10.1063/1.4975557

[7] Trieu, T. T. N., D. Goto, H. Yashiro, R. Murata, K. Sudo, H. Tomita, M. Satoh, and T. Nakajima (2017): Evaluation of summertime surface ozone in Kanto area of Japan using a semi-regional model and observation, *Atmospheric Environment*, 153, 163-181, Doi: 10.1016/j.atmosenv.2017.01.030

[8] Sato, Y., S. Shima, and H. Tomita (2017): A grid refinement study of trade wind cumuli simulated by a Lagrangian cloud microphysical model: the super-droplet method, *Atmospheric Science Letters*, 18, 9, 359-365, Doi: 10.1002/asl.764

[9] Tokutake, H., H. Hiraguri, and S. Nishizawa (2017): Exploration of Wind Structure on Mars using an Airplane and Flight Feasibility Study, *Transactions of the Japan socienty for aeronautical and space sciences*, 60, 4, 212-220, Doi: 10.2322/tjsass.60.212

[10] Yoshida, R., S. Nishizawa, H. Yashiro, S. A. Adachi, Y. Sato, T. Yamaura, and H. Tomita (2017): CONeP: A cost-effective online nesting procedure for regional atmospheric models, *Parallel Computing*, 65, 21-31, Doi: 10.1016/j.parco.2017.04.004

[11] Takane, Y., Y. Kikegawa, M. Hara, T. Ihara, Y. Ohashi, S. A. Adachi, H. Kondo, K. Yamaguchi, and N. Kaneyasu (2017): A climatological validation of urban air temperature and electricity demand simulated by a regional climate model coupled with an urban canopy model and a building energy model in an Asian megacity, *International Journal of Climatology*, 37, S1, 10351052, Doi: 10.1002/joc.5056

[12] Adachi, S. A. (2017): Sophisticated model infrastructure for urban climate study. *Annual issue of Heat island institute international*, 12, 23-27 (in Japanese).

12.5.2 Presentations and Posters

[13] Sato, Y., D. Goto, T. Michibata, K. Suzuki, T. Takemura, H. Tomita, and T. Nakajima: Estimation of the second indirect effect by using a “Global Cloud System Resolving Model, *Aerosols, Clouds, Precipitation and Climate(ACPC) 639. WE-Heraeus-Seminar*, Bad Honnef, Germany, Apr. 3-4, 2017. (Invited)

[14] Sato, Y., H. Miura, H. Yashiro, D. Goto, T. Takemura, T. Michibata, K. Suzuki, and T. Nakajima: Suggestions from a global cloud system resolving simulation to global climate model -Transportation of black carbon aerosol to the Arctic-, *JpGU-AGU Joint Meeting 2017*, Chiba, Japan, May 22, 2017. (Invited)

[15] Yamaura, T., and H. Tomita: Optimum numerical calculation with mixed precision floating point number for a regional shallow-water model, *JpGU-AGU Joint Meeting 2017*, Chiba, Japan, May 20, 2017.

[16] Yoshida, R.: CONeP: A Cost-Effective Online Nesting Procedure for Regional Climate Model, *7th JLESC Workshop*, Urbana, USA, Jul. 17, 2017.

[17] Yamaura, T., and H. Tomita: Optimum Numerical Calculation with Mixed Precision Floating Point Number for a Regional Shallow-Water Model, *7th JLESC Workshop*, Urbana, USA, Jul. 17, 2017.

[18] Sueki, K., and H. Niino: Entrainment rate of typhoon-associated supercells estimated by a large eddy simulation, *9th European Conference on Severe Storms*, Pula, Croatia, Sep. 19, 2017.

[19] Sueki, K., T. Yamaura, H. Yashiro, and H. Tomita: Numerical Convergence for Statistical Characteristics of Deep Moist Convection, *Comparison of tornadic supercells and their environmental condition in Japan and Italy*, Lecce, Italy, Sep. 27, 2017.

[20] Adachi, S. A., S. Nishizawa, R. Yoshida, T. Yamaura, K. Ando, H. Yashiro, Y. Kajikawa, and H. Tomita: Downscaling Procedure for Evaluating Future Regional Climate Change, *International Workshop on Climate Downscaling Studies*, Tsukuba, Japan, Oct. 2, 2017.

[21] Kajikawa, Y., and T. Yamaura: Decadal change in the boreal summer intraseasonal oscillation, *Sixth International Workshop on Monsoons*, Singapore, Nov. 14, 2017.

[22] Kajikawa, Y., T. Yamaura, H. Tomita, and M. Satoh: Impact of Tropical Disturbance on the Indian Summer Monsoon Onset simulated by a Global Cloud-System-Resolving Model., *Sixth International Workshop on Monsoons*, Singapore, Nov. 16, 2017.
[23] Kajikawa, Y., and T. Yamaura: Decadal change in the boreal summer intraseasonal oscillation, *2017 AGU Fall Meeting*, New Orleans, USA, Dec. 12, 2017.
[24] Tomita, H., S. A. Adachi, S. Nishizawa, R. Yoshida, T. Yamaura, K. Ando, H. Yashiro, and Y. Kajikawa: How does the regional climate assessment make more advance?, *The 8th AICS INTERNATIONAL SYMPOSIUM*, Kobe, Japan, Feb. 8, 2018.

12.5.3 Software

[28] SCALE version 5.1.0–5.2.5, URL:https://scale.aics.riken.jp/

Chapter 13

Complex Phenomena Unified Simulation Research Team

13.1 Members

Makoto Tsubokura (Team Leader)

Keiji Onishi (Postdoctoral Researcher)

Rahul Bale (Postdoctoral Researcher)

Koji Nishiguchi (Postdoctoral Researcher)

Wei-Hsiang Wang (Postdoctoral Researcher)

Chung-Gang Li (Visiting Researcher)

Ryoichi Kurose (Visiting Researcher)

Tetsuro Tamura (Visiting Researcher)

Duong Viet Dung (Visiting Researcher)

Huilai Zhang (Visiting Researcher)

Leif Niclas Jansson (Visiting Researcher)

13.2 Research Activities

The objective of our research team is to propose a unified simulation method of solving multiple partial differential equations by developing common fundamental techniques such as the effective algorithms of multi-scale phenomena or the simulation modeling for effective utilization of the massively parallel computer architecture. The target of the unified simulation is supposed to be complex and combined phenomena observed in manufacturing processes in industrial cycles and our final goal is to contribute to enhance Japanese technological capabilities and industrial process innovation through the high-performance computing simulation.

Most of the complex flow phenomena observed in manufacturing processes are relating to or coupled with other physical or chemical phenomenon such as turbulence diffusion, structure deformation, heat transfer, electromagnetic field or chemical reaction. While computer simulations are rapidly spreading in industry as useful engineering tools, their limitations to such coupled phenomena have come to realize recently. This is because of the fact that each simulation method has been optimized to a specific phenomenon and once two or more solvers of different phenomena are coupled for such a complicated target, its computational performance is seriously degraded. This is especially true when we utilize a high-performance computer such as K-computer. In such a situation, in addition to the fundamental difficulty of treating different time or spatial scales, interpolation of physical quantities like pressure or velocity at the interface of two different phenomena requires additional computer costs and communications among processor cores. Different mesh topology and hence data structures

among each simulation and treatment of different time or spatial scales also deteriorate single processor performance. We understand that one of the keys to solve these problems is to adopt unified structured mesh and data structure among multiple simulations for coupled phenomena. As a candidate of unified data structure for complicated and coupled phenomena, we focused on the building-cube method (BCM) proposed by Nakahashi [1].

[1]Nakahashi, K., "Building-cube Method for Flow Problems with Broadband Characteristic Length," In: Armfield S., Morgan R., and Srinivas K., editors. Computational Fluid Dynamics. (Springer, 2002, 2003), pp.77-81.

13.2.1 Implementation of fluid-structure unified coupled simulation framework into design system and basic validation of vehicle aerodynamics

13.2.1.1 Improvement of accuracy by upgrading Immersed Boundary Method (IBM) model and validation analysis by full vehicle geometry

For the transition to the automobile test method by WLTP (Worldwide harmonized light vehicles Test Procedure)[1] which is anticipated from the Ministry of Land, Infrastructure and Transport in the field of automotive aerodynamics from 2018, the evaluation test of aerodynamic drag using Computational Fluid Dynamics (CFD) has been conducted as an effort to obtain the certification of the method. In WLTP, it is necessary for automobile manufacturers themselves to acquire the certification, but as a research institute, it is expected that the provided software will prove to satisfy the accuracy / calculation load requirement sufficiently. Therefore, aerodynamic analysis was performed repeatedly on the actual vehicle full model CAD data group of two aerodynamic configuration models provided by Suzuki Motor Corporation, Mazda Corporation, and Nissan Motor Co., Ltd. The program "CUBE" have developed that sees WLTP system requirements by fine adjustment of IBM methodology, called as topology independent IBM[2], and correction of calculation code. It was necessary to repeatedly execute a product run by full vehicle model to check over several times (about ten and several times) before the accuracy to withstand practical use was achieved. But as a result, improvement in accuracy could be realized. In the "practical use" development, such adjustment work by trial and error is inevitable, and it is significant that what we could do using "sophisticated use" K-computer resource. For WLTP, CFD will be adopted for fuel consumption measurement for the first time, but it is expected that only the numerical value of the configuration difference is used instead of the absolute value of the aerodynamic drag. It is expected that many configurations can be evaluated efficiently and quickly. Then in this study, the aerodynamic drag difference due to the difference in configurations was mainly evaluated.

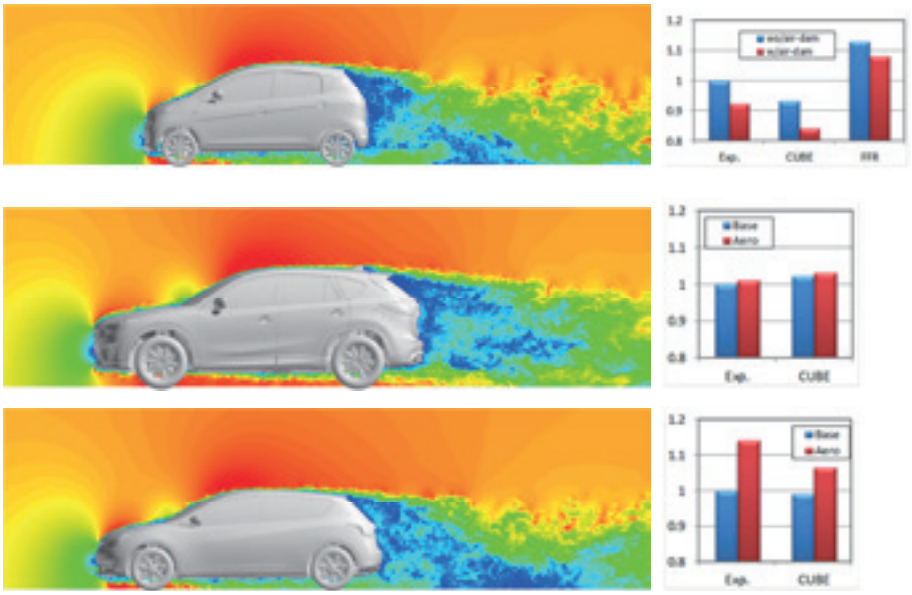

Figure 13.1: Comparison of 3 different vehicle cases with Base model and Aero model.(Left: Velocity magnitude of center section of Base case, Right: Cd values)

The model used in study was small cars, SUV and hatchback type vehicles. The difference from the Aero specification with aerodynamic parts such as spoiler or undercover added to the Base vehicle is evaluated. The vehicle model is an open-grill condition, a heat exchanger including a radiator condenser, and an intercooler is modeled. A unified solution framework CUBE is used for analysis and incompressible fluid scheme by IBM is applied. The grid resolution is about 6 mm, and generation of about 120 million cells is completed in about 10 minutes. It finally used 771 nodes from 558 nodes per each case, and about 15 to 22 computational hours in the analysis of about 3.0 seconds physical time. This is fundamentally quick when considering that the conventional method requires about several days to two weeks for grid generation and several days to one week for calculation. The final goal of this research theme is to speed up the calculation time to about half of this. The results of the typical flow velocity distribution and the drag coefficient (Cd) value obtained are shown in Fig.13.1. Differences in as compared with wind tunnel measurement test. This shows that better results are obtained than the conventional commercial softwares, and since the accuracy sufficiently meeting the requirements of WLTP is obtained in a short time, it can be said that this is a remarkable achievement. However, there is still room for improvement in detail comparison with the flow field and absolute value prediction. It is planning to spend efforts so that it will come closer to the true value as much as possible.

13.2.1.2 Development of a rotating boundary method by IBM and automobile aerodynamic analysis under tire rotation conditions

It is recommended in WLTP that measurement condition should be a condition involving tire / wheel rotation close to the real-world running condition. The CFD method also requires using method with moving boundary. Generally, it is not easy to do for an actual vehicle model involving tire rotation with a commercial software that is used in aerodynamic design now, because it has problems in calculation time required for preparation and unsteady flow calculation. The CUBE developed in this study is also good at handling moving boundary problems. So the methodology to apply it into wheel rotating vehicle aerodynamics problems is developed in this study. For the non-slip condition of the wall using IBM, an extension to give boundary velocity and to advect shape geometry information according to rotation are devised. Based on the topology independent IBM used in previous section, boundary velocity is added to the definition of external force term as shown in Eq.(13.1).

$$f_i^{n+1/2} = \frac{(V_i^{n+1} - u_i^n)}{\Delta t} - RHS^{n+1/2}, \tag{13.1}$$

where $V_i^(n+1)$ is a boundary velocity of next discrete time $n+1$ in i direction, RHS is a sum of advection, diffusion, pressure gradient term in discrete time n. As for the advection of shape geometry information, the geometry position is re-calculated in every time step, then the shape information of topology independent method is advected. The axis-projection information is also updaed by refreshing the information of intersection point and distance. Then initialization of shape information was performed once per every several steps to prevent the degradation of accuracy of the original shape due to advection. At this time, the computation time to initialize the shape becomes very large. So the algorithm is revised so that the initialization routine can be fully parallelized. It is written by MPI+OpenMP hybrid parallel rule. As a result, the initialization time required for about 1 minute when calculating the full vehicle geometry of about 910,000 facets and 91 million cells can be accelerated to about 5 to 10 seconds [3] (However, FLOPS rate are not considered because shape pre-processing is almost an integer operation). Figure 13.2 shows an example of the result of application to the flow around the two-dimensional rotating cylinder as the basic verification problem of this method. The Re number is 200, the angular velocity is $\omega = 2V^n = 1$. This is in good agreement with the analysis result of the previous report using boundary fitting grid of Saiki et al. [4], indicating that this method has a reasonable accuracy to the rotating body problem. Next, calculations involving tire rotation were performed on full vehicle models including the engine room. The grid resolution is about 6 mm and about 91 million cells are used. The calculation was carried out using 588 nodes of K-Computer. The inlet flow velocity is 27.778 m/s, and the rotational angular velocity of the tire is 103.26 rad/s matching with the main flow velocity at the upper end of the tire. Figure 13.3 shows the results of the velocity field obtained for times 0.317 s and 0.321 s. As the tire rotates, the position of the front wheels / rear wheels changes, and accordingly the flow blown out from the gap of the wheel to the outside of the car body is observed, and a qualitatively appropriate flow is obtained. In next step, the detail validation using the measured values of the wind tunnel with the moving belt will be performed comparing with the aerodynamic drag with the tire rotation.

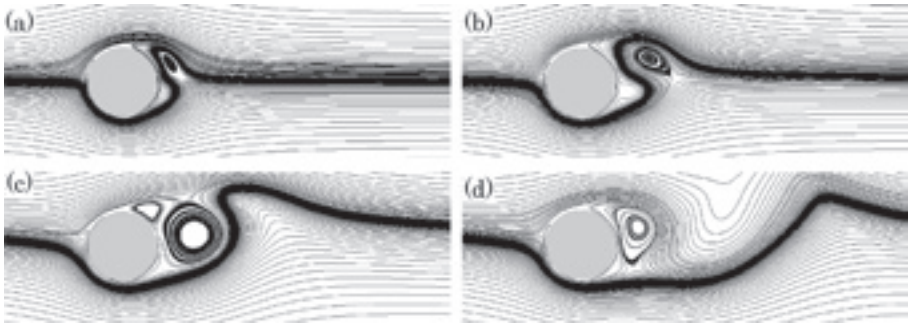

Figure 13.2: Streamlines around rotating cylinder at Re=200. (a) t=1.0, (b) t=2.0, (c) t=4.0, (d) t=6.0.

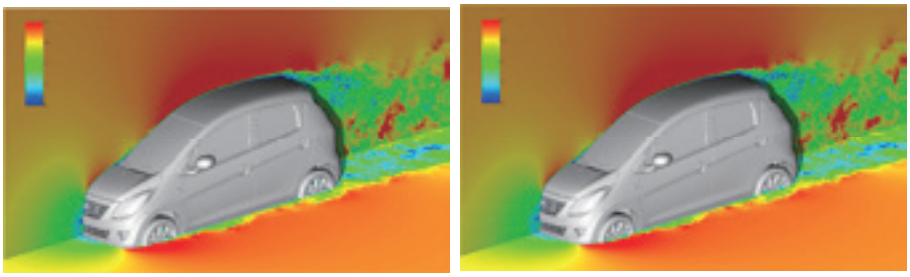

Figure 13.3: Flow velocity magnitude in the center section of the vehicle body and the tire height section. (Left: t=0.317 s, Right: t=0.321 s).

13.2.1.3 Real vehicle demonstration analysis for acquiring WLTP certification through collaboration with Honda

For the WLTP, the evaluation test of aerodynamic drag using CFD has been conducted as an effort to obtain the certification of the method. The aerodynamic analysis was performed on the practical vehicle full model CAD dataset including 6 configurations provided by Honda R&D Co.,Ltd. In this study, the aerodynamic drag difference ΔCdA due to the difference in configurations was mainly evaluated. Figure 13.4 shows the difference according to the total 6 configurations, which is a sedan type vehicle, with a different wheel, a spoiler / deflector and other aerodynamic parts. The vehicle model is an open grill condition. The heat exchangers including a radiator, condenser, intercooler are modeled. The unified solution framework CUBE is used for analysis and incompressible fluid scheme by topology independent IBM is applied. The computational grid resolution is about 6 mm, and is generated for about 120 million cells completed in about 10 minutes. The calculation finally uses the K computer 617 node for each case. The analysis result of 2.0 seconds of physical time is obtained in about 14 to 15 hours. The typical flow velocity distribution obtained are shown in Fig.13.5 and the result of Cd value are shown in Fig.13.6. The difference in Cd due to the difference in configurations is well captured as compared with the actual value measured by the wind tunnel test. In the analysis by the commercial general purpose software using the conventional method, it was difficult to obtain the accuracy of same level for the results varying on the configurations. And the ΔCdA sufficiently satisfies the required accuracy of $\pm 0.015m2$ for WLTP as shown in Fig.13.7. In addition, the lift (front lift, rear lift) which was conventionally considered difficult to predict, have also evaluated, and good results have been obtained, too.

The above results are appealed to automobile manufacturers through the “Consortium for Next Generation Automotive CAE using HPC” organized by RIKEN. And active inquiries have already benn received form several manufacturers. However, it is recommended in WLTP that measurement condition should be a condition involving tire / wheel rotation. So it is planning to apply CUBE for the conditions accompanying tire rotation in next step. We will keep demonstrating the superiority of the CUBE compared with the conventional method to the automotive companies through the Consortium activity.

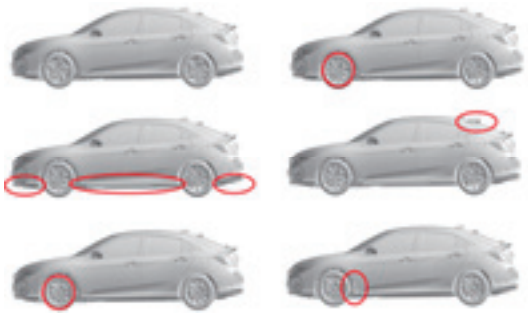

Figure 13.4: Configurations of full vehicle model.

Figure 13.5: Instantaneous velocity magnitude distribution of center section.

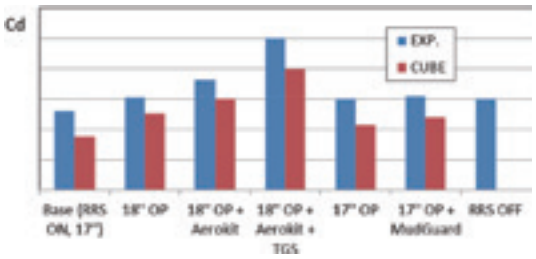

Figure 13.6: Comparison of drag coefficient.

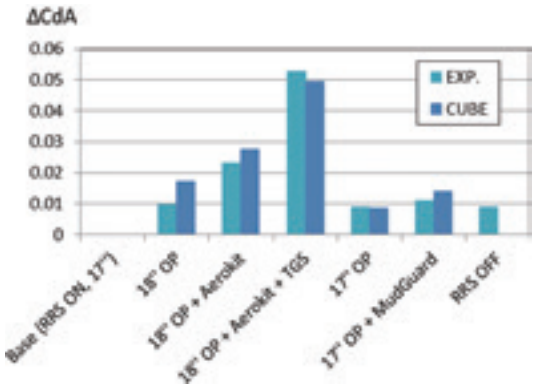

Figure 13.7: ΔCdA of different configurations.

13.2.1.4 6 DOF moving boundary analysis by collaboration with Mazda

Continuing from the previous fiscal year, using the fluid-structure unified solution based on the coupling of the Lagrangian particle method and the Eulerian method, "Research for Next-generation Automotive Aerodynamics Evaluation Technology Simulated with Vehicle Dynamic Motion by Super-large-scale Transient Fluid Calculation" has been conducted by collaboration with Mazda Motor Corporation. The actual running condition of sedan type real vehicle full model is succeessfully reproduced, and the evaluation by comparison with the actual running test result is tried. Unfortunately, in this study it has many problems on the driving test side too. So it was difficult to realize reliable quantitative evaluation. But, it was possible to provide certain numerical data explaining the mechanism of vehicle behavior from the simulation results. In the future, we plan to contribute to development of unsteady aerodynamic technology by setting appropriate target problems which are more easily evaluated (ex. influence of vehicle behavior under the inflow gusty wind condition).

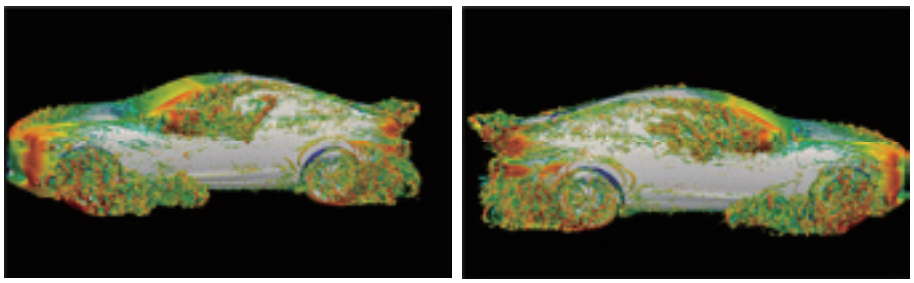

Figure 13.8: Vortex structures around wheel houses as it undergoes the lane change maneuver.

13.2.1.5 Direct numerical ssimulation of narrowband noise around a engine hood by collaboration with Suzuki

Narrowband noise generated in automobile manufacturing is a matter of quality as a problem on the design requiring a great deal of effort to solve. But it is extremely difficult to predict in the early design stage before creating a prototype vehicle model. Numerous analysis methods including commercial softwares have been proposed, but prediction accuracy is still considered insufficient. In this study, in order to reduce vehicle development cost and shorten the development period, for the purpose of examining the mechanism for preventing the occurrence of narrowband noise using CFD, the simulation by the unified compressibility algorithm by the CUBE is proceded. The method developed in this study is also applicable to other products having complicated geometric shapes to predict narrow band noise. For direct simulation of narrowband noise and flow field, it is necessary to use high precision numerical scheme to capture pressure fluctuations. In this fiscal year, the new time integration argorithm based on LUSGS and solution limited time stepping scheme proposed by Lian et al [5] has been implemented. As shown in the Fig.13.9, verification was carried out using the narrowband noise problem for the cavity shape. The results show that with adequate resolution, the peak of the frequency can be well captured even CFL number lager than 10.

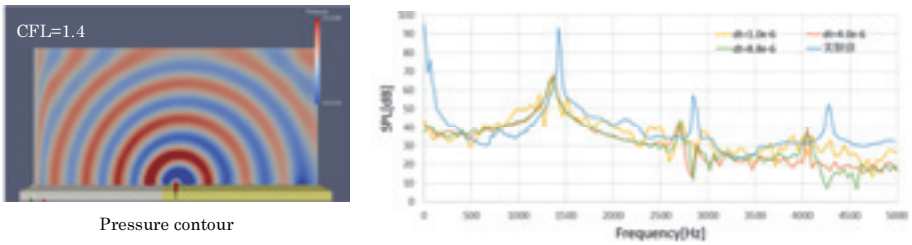

Figure 13.9: Cavity narrowband noise.

It is indicated that the current method can tremendously save the CPU time and obtain accurate result. The preliminary result of the vehicle in Fig.13.10 shows that the propagation of the pressure fluctuation from the noise source around the hood area can be captured with this method. The core technology was developed in this fiscal year's efforts, but due to the limitation of allocated computational resources, it has not yet been completed to calculate the full vehicle model case. Moreover, it is important to improve the calculation grid resolution further in order to improve the calculation accuracy. It is in a situation to wait for allocation of computational resources for further high resolution / large scale calculation. In the future we will continue to work on acquiring computational resources and plan to improve prediction accuracy.

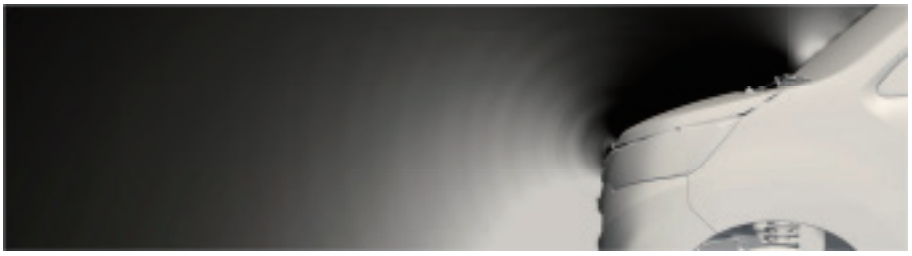

Figure 13.10: The propagation of the pressure fluctuation.

13.2.1.6 Construction of automobile aerodynamics multiobjective optimization framework by collaboration with Mazda

For the purpose of efficient optimization of aerodynamic performance at the early design stage, a preparation for constructing a multiobjective optimization framework using fluid-structure unified solution framework. In this fiscal year, the conditions required for software used for constructing the framework were examined, and its performance was confirmed. As the feasibility study, the vehicle shape and objective function to be analyzed are examined. In this framework, the fluid solver CUBE developed in this study, the multiobjective evolutionary

optimization software CHEETAH developed under the sub-theme of the "post-K priority issue 8" taken by Japan Aerospace Exploration Agency, and the shape morphing software MeshWorks[6] developed by Detroit Engineered Products in US are selected. It is considering that each software will link by exchanging information via a text-based result or parameter files. Since CUBE is based on the hierarchical Cartesian grid it can be used with a single calculation grid for a multiple vehicle shape changes, the problem on mesh regeneration and morphing in the conventional method can be avoided. Since CHEETAH can solve the multiobjective optimization problem quickly, it is suitable for automobile development that has multiple specification conditions to be satiefied. Since MeshWorks can operate the shape morphing on batch mode through text input, it is suitable for shape optimization. In addition, the morphing software is required to be able to change shape according to individual shape parameters obtained by CHEETAH, and it is also required to generate new shape data which can be directly read into CUBE. In this fiscal year, the performance of shape change of morphing software and linking method between softwares are examined by checking the applicability for coordination of a system. In addition, as one of the tasks of this feasibility study, discussion with collaborative company and agencies has been done, and the following task has been assigned: The target will be a sedan type automobile model of simplified shape, the objective function will be drag and lift when the vehicle is traveling straight ahead and when the approaching flow has yaw angle, the scale of the optimization will be about 30 generations for the 30 individuals by considering the practical usage demonstration of CHEETAH. In the last, a verification analysis using the basic vehicle model has been conducted, and confirmed that reasonable solution for both aerodynamic force and flow field has been obtained that is suitable for optimization calculation.

Figure 13.11: Flow field visualization of basic vehicle model.

13.2.1.7 References

[1] About partial revision of notice etc. that defines the details of safety standards of road transport vehicles: Press Release of Ministry of Land, Infrastructure, Transport and Tourism and Minister of Economy, Trade and Industry, October 31, 2016.
[2] Onishi, K., Obayashi, S., Nakahashi, K., and Tsubokura M., "Use of the Immersed Boundary Method within the Building Cube Method and its Application to Real Vehicle CAD Data," AIAA paper 2013-2713, 2013.
[3] Keiji Onishi, Niclas Jansson, Rahul Bale, Wei-Hsiang Wang Chung-Gang Li, Makoto Tsubokura, "A Deployment of HPC Algorithm into Pre/Post-Processing for Industrial CFD on K-computer," SC17 poster, 2017.
[4] Saiki, E. M., Biringen, S., "Numerical Simulation of a Cylinder in Uniform Flow: Application of a Virtual Boundary Method," J. Comp. Phys., Vol. 123, pp.450465, 1996.
[5] Chenzhou Lian, Guoping Xia, Charles L. Merkle, "Solution-limited time stepping to enhance reliability in CFD applications," Journal of Computational Physics, Volume 228, Issue 13, 2009, pp. 4836-4857.
[6] https://www.depusa.com/meshworks/, [cited 1 May 2018].

13.2.2 Acceleration of solver kernel toward Exa-scale computing

13.2.2.1 Single node performance tuning in K-computer for unified compressibile solver

The single node performance improvement on compressible solver is conducted in K-computer. The target problem is a simple cavity flow, and a scheme assuming acoustic analysis was used. The MUSCL and Roe scheme are used for evaluation of the flux at the cell interface, and the third order Runge-Kutta method is used for time integration and the second order central difference is used for the viscous term. The number of Cube is 64, and 262,114 cells divided into 16 in each direction are arranged in a single node. The thread parallelism within the node is done using OpenMP. For the performance measurement, the calculation time for the 500 timestep was evaluated. When the performance of the original code was measured, the execution time

of the whole program was 79.89 seconds, the peak performance ratio was 13.74%, and the cost for calculation of MUSCL and Roe scheme, evaluation of viscous flux, and Runge-Kutta method was found to be consuming operation cost mostly. As a result of promoting SIMD usage by removing IF branches and increasing loop size by changing thread level on these kernel codes, the execution time became 50.81 seconds and the peak performance ratio was 23.67%, which is about 1.57 times faster than original. However, from the performance measurement results, scheduling problems such as waiting for floating point operation remain, and it is confirmed that there is room for speedup. Therefore, as a next step, further improvement trial by loop splitting algorithm are undergoing. Parallel performance measurements are also conducted. For this purpose, the original code before applying the above single node tuning was used. Weak scaling test measurement is done using K-computer by fixing the number of Cube per node to 64 up to 32,768 nodes. As a result, the effective parallelization ratio is 99.99954%, the parallelization efficiency is 89.142268%, and the parallelization efficiency estimated when using full nodes of K-computer is 75.324899%.

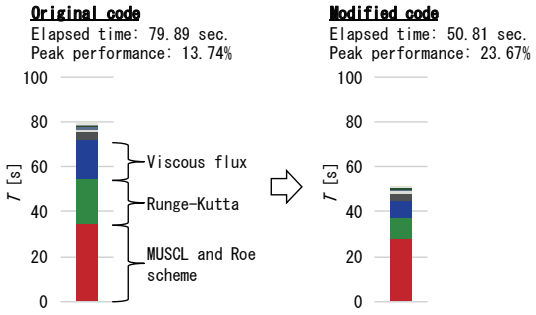

Figure 13.12: Results of performance evaluation and tuning of compressible solver.

13.2.2.2 Implementation of in-situ visualization

There do not need to discuss about the importance of visualization technology in science and technology simulations. Acceleration of the pre / post process of scientific computing in the HPC environment is a hidden task to be solved by using a HPC technology toward the Exa scale. Concerning the pre-processing, it is expected to get a solution by the activity of real-time simulation technology development of this research. On the other hand, the data size obtained by analysis increases year by year, and visualization becomes difficult as computation becomes larger scale, so the speeding up of post-processing is also an issue. "In-Situ visualization" is a generic term for technologies that directly access simulation data on memory in the HPC environment and visualize it. In order to realize it, the selection of related libraries, implementation of interface to CUBE, and porting to K-computer is conducted. In this study, "Libsim" is selected which is a library of open source scientific visualization software VisIt being developed at Lawrence Livermore National Laboratory. To operate Libsim, it requires a rendering pipeline (using GPU hardware or using a library to emulate it) with OpenGL (2D and 3D graphics API). But, K-computer doesn't have a GPU. So, an appropriate library have to be built adjusting o the environment. The visualization library Mesa3D developed by VMware, Inc. is the de facto standard in this field, and there is an emulation library "OSMesa (Off-Screen Mesa)" as its function. In this study, the standard swrast driver on OSMesa is used. In addition, Libsim requires a VTK (Visualization Tool Kit) library developed by Kitware, Inc. and additional libraries such as Python and HDF5. These are ported to K-computer. All of these libraries are available as open source. Data access is operated through a metadata access pipeline that provides direct access (or copy access) to data on memory. This is necessary for the user to create according to each physical solver, and here we implemented it directly in CUBE. This closely combines Libsim and the physical solver. Metadata is parallelized based on Cube based BCM grid domain which is partitioned using Z-ordering or Parmetis libraries. For compiling, the Fujitsu cross compiler environment is used with MPI, OpenMP and suto parallelization options for K-computer. Figure 13.13 shows a schematic diagram of the entire processing system.

As an example, in-situ visualization results are shown in actual vehicle aerodynamic analysis using 558 nodes of K-computer. Analysis was completed in about 21 hours for 290,000 steps (physical time 2.9 seconds), and it took about 7 hours to generate 2,900 image frames out of them. This indicates that each frame can be visualized in about 7.5 seconds [1], which is sufficiently fast. An example of the visualized image obtained is shown below.

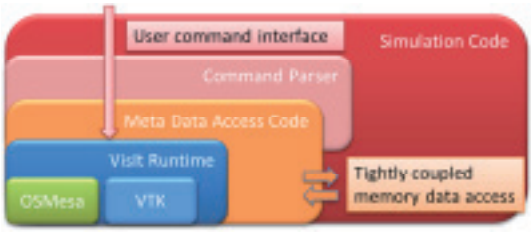

Figure 13.13: Schematic view of libsim, including user command interface and meta-data access code.

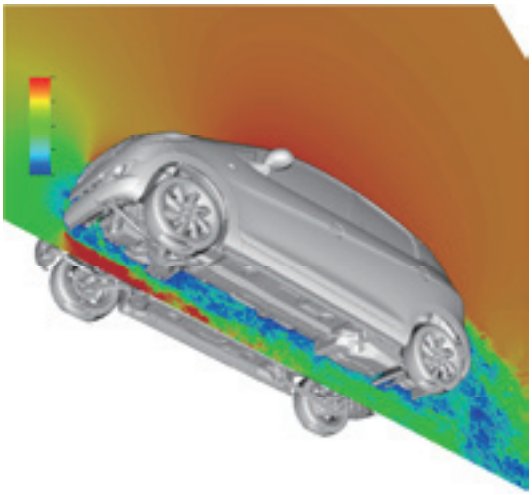

Figure 13.14: Parallel rendering result of a CFD simulation data on the K computer.

13.2.2.3 Feasibility study of AMR (Adaptive Mesh Refinement)

Adaptive Mesh Refinement is a method for concentrating computational grid only in the necessary region when solving a resolution-sensitive physical phenomenon, typified like turbulent flow. It is a calculation method designed to dynamically change the grid resolution distribution to save calculation memory and computation time. Many countries are engaged in research and development as core technologies towards the Exa scale, because they can perform calculations efficiently in the HPC environment. For example, in the United States, it was announced that Lawrence Berkeley National Laboratory will lead the AMR co-design work towards the Exa scale in the country. In European countries, many research and development activities of AMR are observed towards the Exa scale. On the other hand, since this technology dynamically changes the data structure, programming becomes complicated. In particular, advanced knowledge is required for parallel calculation, so it is often difficult to install it. In this study, feasibility study is conducted aiming to implement this method on CUBE. In AMR, the data structure that specifies division becomes important. In this study, the octree-based data structure proposed by Burstedde et al. [2] are adopted as an efficient algorithm already proven in the HPC field, from the results of the literature survey. It has tree information on an integer operation and has an algorithm for manipulating trees with binary operations. In this study, algorithm that refines / combines the block (Cube unit) is adopted with high affinity for CUBE data structure. In addition, because it is pointed out that calculation efficiency in binary operation in K-computer is deteriorated, it is not adopted in this fiscal year. First, a basic refining / combining function are implemented and applied to a simple flow case around a sphere. About the criterion of refinement, vorticity is used in this study for the sake of simplicity.

In BCM, there is a unique feature that size change rate in local resolution variance must be the fixed factor of 2. The adjustment for this requirement is a future task. In the next step, we are planning to iimplemet parallelization by MPI, dynamic load balancing, calculation speed improvement by local time increment, practical error / estimator, and so on.

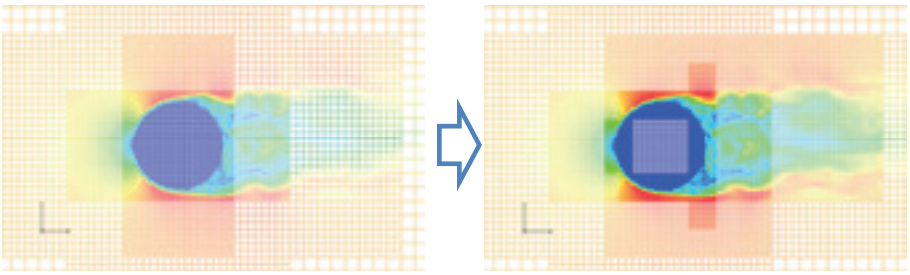

Figure 13.15: Example of AMR, refining from 1184 cubes to 4607 cubes.

13.2.2.4 Sophisticated research of legacy software accompanying establishment of "RIKEN software center"

From this fiscal year, the establishment of a "RIKEN software center" is discussed to promote the transfer of HPC technology to the STEM industry and strengthen its support capacity. In addition, it was decided that RIKEN will maintain the Frontflow/red-HPC, which is a general purpose thermal-fluid simulation software based on the finite volume method with an unstructured grid, it is an conventional legacy code. Development of Frontflow/red-HPC was started at the IT program sponsored by the Ministry of Education, Culture, Sports, Science and Technology (MEXT) "Frontier Simulation Software for Industrial Science" (IIS, University of Tokyo, 2002-2005). Furthermore, it has been developed through the following projects: "Revolutionary Simulation Software (RSS21)" as a part of the next-generation IT program sponsored by MEXT (IIS, University of Tokyo, 2005-2008), "Industrial Technology Research Grant Program" from the New Energy and Industrial Technology Development Organization (NEDO) Hokkaido University, 2007-2011), "Strategic Programs for Innovative Research" Field No. 4: Industrial Innovations from the MEXT (IIS, University of Tokyo, Hokkaido University, 2011-2016). It has been adopted since 2017 by "Social and scientific priority issues to be tackled by using post-K computer, Priority Issue 6 Accelerated Development of Innovative Clean Energy Systems". It has a history of about 15 years. The Navier-Stokes equations with a spatial filter of LES (Large Eddy Simulation) are used as governing equations. It has various eddy viscosity model or RANS turbulence model, compressive / low-Mach approximation fluid model, combustion model, sliding mesh, ALE (Arbitrary Lagrangian Eulerian) moving boundary model, grid refining function, etc. are included. For spatial discretization, a polyhedral volume at the node center is used, which is constructed from a general unstructured grid such as a tetrahedron, a pentahedron, or a hexahedron as input. It is a typical industrial application software that solves a large scale sparse matrix as a pressure solver. Frontflow/red-HPC has already been tuned for K-computer, and has a track record in large-scale aerodynamic analysis. In this fiscal year, in order to cope with the accelerated calculation methos with the accelerator type environment which is expected as a mainstream in the future computer environment, the tuning for the GPGPU of NVIDIA Corporation is tried. As a matrix solver for large scale sparse matrices, ICCG (Incomplete Cholesky Conjugate Gradient) method is adopted. The OpenACC is used for tuning, and the ability how fast it can be done in a short work period is examined. First, OpenACC directive tuning on existing K-computer code has been tried. Single node test with the NVIDIA Tesla P100 1 GPU (on the Reedbush-H system of University of Tokyo, Information technology Center) gave only about 18% improvement in calculation time comparing with the single core run on the Intel Broadwell generation CPU. This is considered to be due to the fact that the efficiency of data transfer between the CPU and the GPU has not yet been sufficiently investigated, so the effect of the calculation speed up is canceled by the overhead of data movement. It turned out that it is difficult to speed up just by inserting the directive. Next, with the support of the Nakajima laboratory of the University of Tokyo Information Technology Center that has expertise in this field, the ICCG matrix solver that was tuned with OpenACC has been tried. As a result, a computation time improvement of about 12 times on 1 GPU run compared with single core run on CPU has been achieved. At the same time, an improvement of about 8 times on 18 core CPU run has been got. In response to this result, the above code is installed in the latest version of Frontflow/red-HPC, and it is maintained so that it can be used in industrial applications. However, there is still room for speeding up with OpenACC, and we will continue to improve the performance by collaborating with Nakajima laboratory.

13.2.2.5 References

[1] Keiji Onishi, Niclas Jansson, Rahul Bale, Wei-Hsiang Wang Chung-Gang Li, Makoto Tsubokura, "A Deployment of HPC Algorithm into Pre/Post-Processing for Industrial CFD on K-computer," SC17 poster, 2017.
[2] Carsten Burstedde, Lucas C. Wilcox, and Omar Ghattas, "p4est: Scalable Algorithms for Parallel Adaptive Mesh Refinement on Forests of Octrees," SIAM J. Sci. Comput. Vol.33, No.3, pp. 1103-1133.

13.2.3 Implementation of Euler structural analysis method into design system and basic validation of vibration structure analysis

13.2.3.1 Implementation PIC (Particle in Cell) method in Eulerian structural analysis method

In the conventional Eulerian structure analysis method, since the dissipative interface capturing method such as the VOF method and the Level-set method was used, there was a problem that the numerical diffusion of the interface became larger as the calculation advanced. Therefore, it was difficult to simulate the thin plate structure and the structure having a sharp interface. So in this fiscal year, a fluid-structure unified solution based on PIC (Particle in Cell) method [1] which is one kind of particle method is we developed. In the PIC method, solid regions are represented by Lagrangian particles, and Lagrangian particles have solid internal variables (stress and deformation tensor). On the other hand, the spatial derivative and the equation of motion are calculated on the fixed Eulerian mesh. By introducing the PIC method, it is possible to avoid numerical diffusion of interfaces and solid internal variables, which was a problem of the conventional Eulerian structure analysis method, while taking advantage of the fixed Euler mesh method. In the benchmark problem of Fig.13.16, it is confirmed that the same precision is obtained with 1/8 of the spatial resolution of the conventional Eulerian structure analysis method, and the analysis accuracy has been greatly improved.

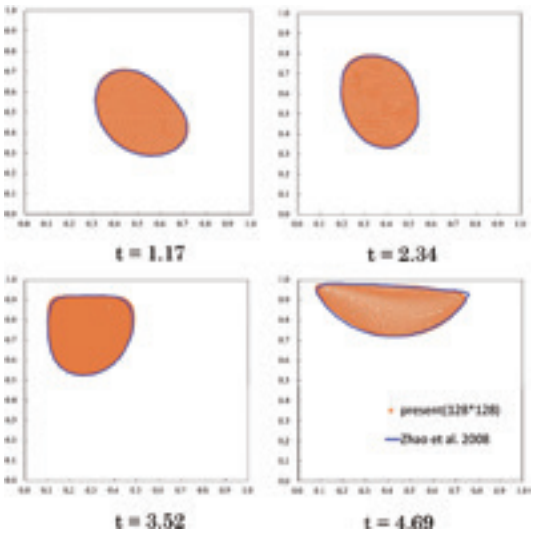

Figure 13.16: Result of FSI benchmark.

13.2.3.2 Implementation of implicit time integration method

When treating a hard solid like a steel plate, practical calculation is difficult in the explicit time integration method because it has strict time increment restriction by the stress wave. Therefore, in order to ease the time increment constraint due to the solid stress wave, an implicit time integration of fluid-structure unified solution has been implemented based on the above PIC method. In the formulation of the implicit method, a method for linearizing the solid stress proposed by Ii et al. [2] has been introduced. At this time, the equation of motion is expressed by the following equation.

$$\rho_{mix}^{n}\left\{\frac{\boldsymbol{v}^{*}-\boldsymbol{v}^{n}}{\Delta t}-\frac{3}{2}(\boldsymbol{v}^{n}\cdot\nabla)\boldsymbol{v}^{n}+\frac{1}{2}(\boldsymbol{v}^{n-1}\cdot\nabla)\boldsymbol{v}^{n-1}\right\}=\frac{1}{2}\nabla\cdot(\boldsymbol{\sigma}_{mix}^{*}+\boldsymbol{\sigma}_{mix}^{n})+\rho_{mix}^{n}\boldsymbol{b}^{n}$$

In the above equation, the unknown solid stress is linearized by the following equation (13.2).

$$\boldsymbol{\sigma}_s^* = \boldsymbol{\sigma}_s^n + \frac{\partial \boldsymbol{\sigma}_s}{\partial \boldsymbol{B}} : \Delta \boldsymbol{B}^n, \Delta \boldsymbol{B}^n = \frac{\Delta t}{2} \left\{ (\nabla \boldsymbol{v}^* + \nabla \boldsymbol{v}^n) \cdot \boldsymbol{B}^n + \boldsymbol{B}^n \cdot (\nabla \boldsymbol{v}^{*T} + \nabla \boldsymbol{v}^{nT}) \right\}$$

As a result, it became possible to acquire a large time increment, and reduce calculation time fundamentary.

13.2.3.3 Feasibility study on the rigidity analysis of white body by collaboration with Suzuki

A feasibility study on the stiffness analysis of the white body has been conducted using the fluid-structure unified analysis method based on the PIC method described above. In this example, the structure has the Young's modulus and mass density of steel, the fluid region is set by the viscosity and mass density of water at 20°C. The total number of cells is about 139 million. The 1024 nodes of K-computer is used for calculation, and it was confirmed that it runs successfuly without stress oscillation and so on. An example of successful rigid analysis using an Eulerian structure analysis method based on Cartesian grid in a three-dimensional model based on automobile thin plate steel is probably the world's first. From collaboratetive companies, including companies through the activities of the "Consortium for Next Generation Automotive CAE using HPC" organized by RIKEN, voices of surprises and expectation for software development have been received. We are planning to continue development for practical application in near future.

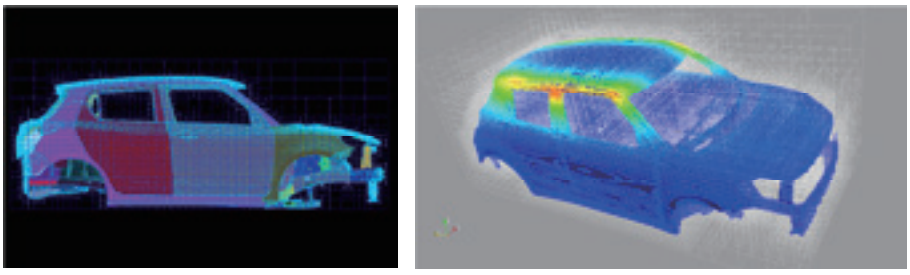

a) CUBE division b) Mises stress distribution

Figure 13.17: Trial simulation of white body of Suzuki.

13.2.3.4 References

[1] Sugiyama, K., Nagano, N., Takeuchi, S., II, S., Takagi, S., and Matsumoto, Y., "Particle-in-cell method for fluid-structure interaction simulations of neo-Hookean tube flows," Theoretical and Applied Mechanics Japan, 59, pp.245-256, 2011.
[2] Ii, S., Sugiyama, K., Takeuchi, S., Takagi, S., and Matsumoto, Y. , "An implicit full Eulerian method for the fluidstructure interaction problem," International Journal for Numerical Methods in Fluids, 65(1 窶?), pp.150-165, 2011.

13.2.4 Deployment of unified simulation framework to practical problems

13.2.4.1 Construction of ski-jump aerodynamic simulation framework

The purpose of this research is to realize a simulation framework for predicting unsteady aerodynamic characteristics in ski-jumping competitions. Because the competition is intense in this field, training using scientific methods is extensively studied in each country, and there are many cases where CFD is applied. However, at this time, transient characteristics from take-off are expected to greatly influence the flight distance, but in the conventional method CFD, it is difficult to apply to the moving boundary problem with large complicated shape change. So, an example evaluating the transient response has not been reported yet. Therefore, in this research, in order to apply the developed framework to actual competition, the posture change is reconstructed from the sagittal plane (the plane perpendicular to the left and right with respect to the human body) obtained from the image (2D model) , aerodynamics simulation has been carried out. However, in this study, it is focused on take-off motion only on the period of the initial flight phase. Moreover, in order to verify the validity of the result, it is compared with the simulation result (3D model) obtained from the 3 dimensional motion measured by motion capture facility. Figure 13.18 shows the computational domain, the boundary condition, and the

distribution of the calculation grid (Cube) around the jumper. Each Cube shown in the figure contains 4,096 calculation cells (16 in each direction).

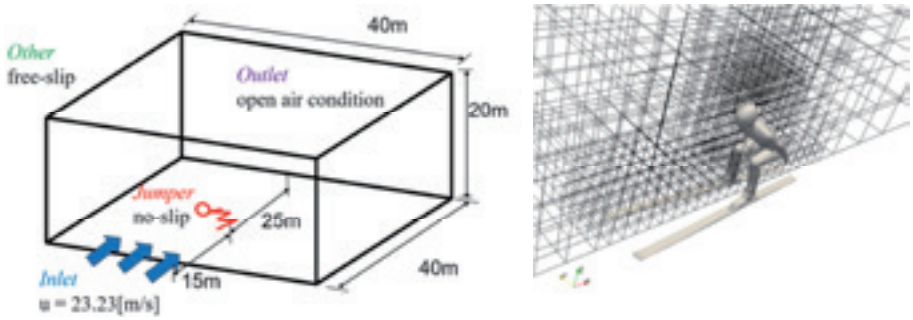

Figure 13.18: Dimension of numerical domain, boundary conditions (left) and distribution of numerical elements around the jumper (right).

Figure 13.19 show the pressure distribution in the sagittal plane of the jumper for each instantaneous time. The left shows the result of 3D model and the right shows the resut of 2D model.

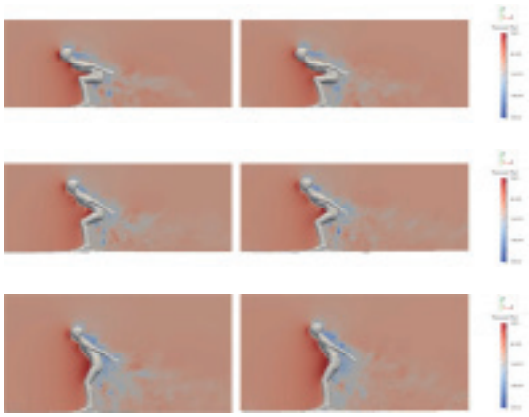

Figure 13.19: Pressure distribution in the sagittal plane of the jumper. (Top: at 0.1 sec., Middle: at 0.4 sec., Bottom: at 0.5 sec.).

Comparing the results of the 2D model with the results of the 3D model, there is a small difference between the pattern of the negative pressure and the absolute value, but the main flow structures such as the vortex structure and the separation point behind the jumper are very similar. It can be said that they both capture the same flow field fundamentally. Next, L/D (aerodynamic lift divided by aerodynamic drag) of both models are compared. Figure 13.20 shows the time history of L/D. It decreases in the vicinity of about 0.48 seconds. This is because as the angle of attack of the upper body increases, the lift force decreases due to the expansion of the wake area. This trend was observed in both models as well.

From the results of this study, it was confirmed that the 2D model which can reproduce the ski-jumper attitude in a short time when used in the actual competition can be sufficiently used for aerodynamic simulation of ski-jump take-off motion.

13.2.4.2 Underwater Dolphin kick simulation in swimming competition

In three competitive swimming styles, a dolphin kick (underwater undulatory swimming, UUS) mode is used by swimmers to maximize the swimming performance and minimize the time to finish. In recent years, professional swimmers are allowed to spend extended periods of time underwater performing UUS at the start and after turns in competitive swimming. Therefore, an understanding of the hydrodynamic mechanisms of thrust generation and drag inducement would be beneficial in guiding professional swimmers how their UUS strokes can be optimized. Most works on computational analysis of swimming hydrodynamics focus on underwater gliding

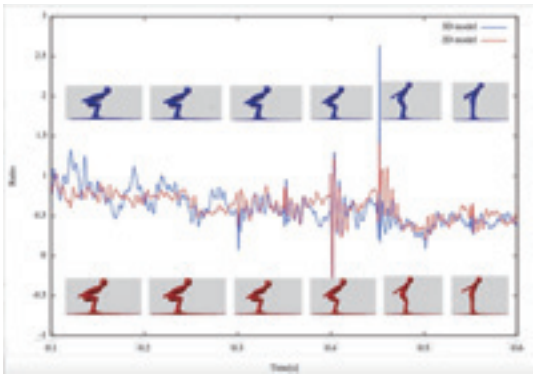

Figure 13.20: Time history of lift-drag ratio.

motion of the swimmer. The literature on the hydrodynamics of unsteady swimming motion is limited. To this end, we present an unsteady computational fluid dynamics analysis of forward and backward UUS modes using constraint based immersed boundary method [1]. The numerical method is validated with experimental data of Vennel [2] by performing simulations of swimmers in glide motion. The input data for the numerical simulations were obtained by experimental measurements using high speed video with 60 fps. The measurement of professional swimmers performing UUS were carried out to obtain the undulatory motion data, and 3D scanners in Chukyo University were used to generate 3D morphological data of each of the swimmers.

Figure 13.21: Forward and backward UUS motion postue taken by video.

Figure 13.22: 3D scanned geometry model of a swimmer.

The motion of the swimmer is reproduced using a simple algorithm which interpolated points were determined with the closest posint to the 3D geometry file. And with the displacement matrices and the hypothesis of neglecting the body elasticity, it was considered that the displacement of a point of 3D geometry from a frame to another was the same than its closest interpolated point. The other methods was also considered, for example, making polynomial interpolation for adding new time step of the position of the "body joints". At first, we feared that the computational time would be too large but the fact that it takes only a few seconds on a laptop and that it was going to be added in CUBE and thus done by the K computer comforted us in our will to use this method. We obtained good results as the motion of the swimmer seemed almost perfectly natural. Hence, we tried a test simulation to check if the motion was working properly. So, we implemented this function in CUBE and tried running the easiest simulation possible for us: recreating the motion of the swimmer in the videos (only a few undulations). Natual motion could not be obtained due to an error by fixing the core of the body direction to determine a posture from a two-dimensional video image, or an error resulting from a small number of interpolation points. A simple linear interpolation algorithm by sequentially reading the 3D shape created for a time series reproduced a reasonabe motion of swimmer, without the large computational time overhead for reading multiple file like as it feared. The simulation has conducerd for few undulations, and

it gave satisfying results since the motion of the swimmer was exactly following the video. The reversed Von Karman sheet in the wake of the swimmer has been observed. There was, as said in some articles the big vortex when the feet are whipping toward the up direction and a smaller one when they're whipping in the opposite direction (Fig.13.23). The time history of the drag force is also showing the strength of these two vortices. Even though the simulation seems to converge only at the end (it was just to verify if the new function on CUBE was working properly), the value of the drag force was credible (Fig.13.24). The inflow velocity of the simulation was 2 m/s while the swimmer was actually doing UUS at a speed of 1.76m/s. This explains why, at the end of the curve, the mean of the drag force was not equal to 0 N, but was close enough to 0 that the simulation results were reasonable.

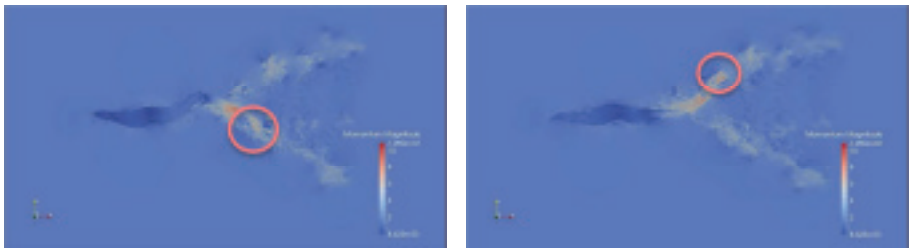

Figure 13.23: Release of the small vortex after the downward stroke and upward stroke.

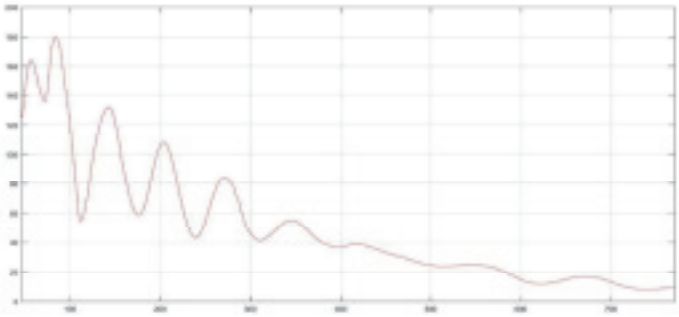

Figure 13.24: Drag forces on swimmer in UUS.

13.2.4.3 References

[1] A. P. S. Bhalla, R. Bale, B. E. Griffith, and N. A. Patankar, "A unified mathematical framework and an adaptive numerical method for fluid-structure interaction with rigid, deforming, and elastic bodies," J. Comput. Phys., Vol. 250 , pp.446-476, 2013.
[2] R. Vennell, D. Pease, and B. Wilson, "Wave drag on human swimmers," Journal of Biomechanics, Vol. 39(4), 664671, 2006.

13.2.5 An accelerated strategy toward practical use of automobile whole engine simulation and building test bed

The objective of this research project is to realize large scale simulation in combustion simulation of automobile engine by dramatically increasing the resolution of computational grid to be independent of empirical physical model on the analysis. Historically, low-resolution grids have been widely used to simulate engines relatively easily or due to lack of computational resources. This is due to the fact that the engine combustion is a complicated problem that is not suitable for parallel computation including the moving boundary and spraying, that the calculation load is extremely high and it is difficult to increase the efficiency. In the conventional software used for the engine analysis, it is common to use coarse grid solution model, and run it with roughly hundreds of thousands to several million elements. It is executed in parallel calculation scale of at most dozens of processes or in single process. However, many researchers have reported that spraying and combustion models

strongly depend on grid resolution, but in the field of automobile design, it had to accept uncertainty such as selection of models which relied on experiences and estimation of error factors. In order to accurately express the proper physics of spraying and combustion, it is desired to be realized a higher grid resolution simulation under the progress of parallel computation technology of CFD and large-scale computational environments. The simulation framework CUBE has multiphysics models such as thermal / fluid / chemical reaction / spraying which can be solved on the same computational grid. Large scale calculations of thousands to tens of thousands of parallels are possible on the scale of several hundreds of millions to several billion cells. There are no restrictions on piston / valve shape, valve moving direction, and valve openning / closing timing can be arbitrarily set. In addition to being able to expect reduction of calculation time by large scale calculation, though care should be taken for the handling of the wall boundary modeling by adopting the Cartesian grid, there is no deterioration of calculation stability accompanying the calculation grid distortion. Figure 13.25 shows the framework of compressible flow and chemical reaction solver of CUBE for combustion problems. In order to improve the calculation accuracy, it is important to improve the resolution of the computational grid. But in the case of the combustion calculation, it is already recognized that as the speed of sound increases with the temperature rise, the computation time step becomes smaller and the calculation load increases. Therefore, in this research, we will accelerate the development of high precision spray / combustion model which can be applied to real automobile engine analysis, receiving strategic allocation of computational resources in order to execute further high resolution / large scale calculation.

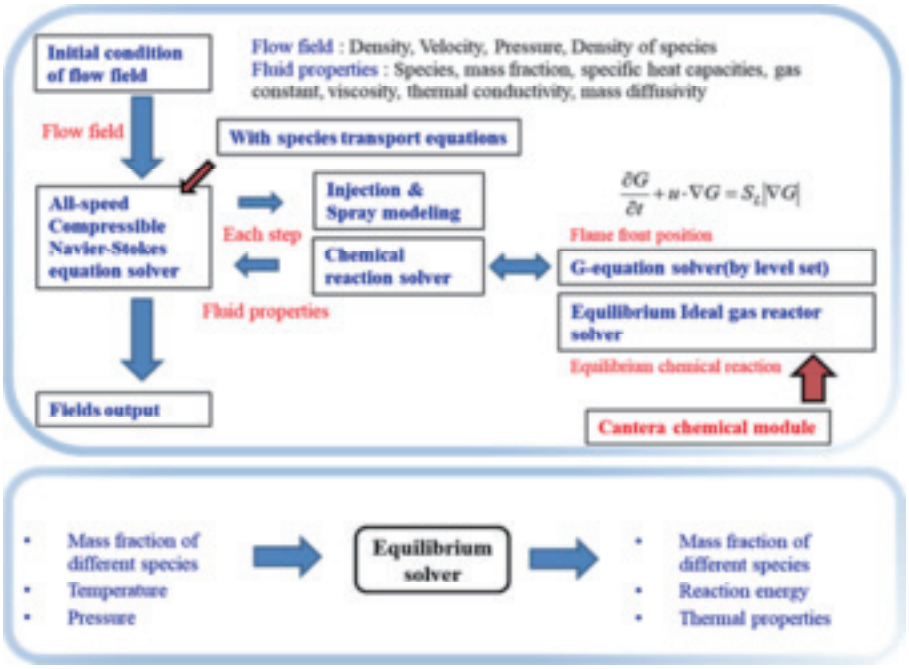

Figure 13.25: Combustion framework of CUBE.

13.2.5.1 Basic validation of species transport equations

The validation of species transport equations in CUBE is conducted by a point source problem. In the computation domain, there are three species of fluids including H2, H and Ar. Each species has different mass fraction and diffusion coefficient. At the source point, mass fraction of 0.01,0.01 and 0.98 of H2, H and Ar are set, while other region only Ar is existed. The results are compared with analytical solution of transport equation as follows.

$$C(x,y,z,t) = \left(\frac{M}{(4\pi t)^{3/2}\sqrt{D_x D_y D_z}} \right) e^{-\frac{1}{4t}\left(\frac{x^2}{D_x}+\frac{y^2}{D_y}+\frac{z^2}{D_z}\right)}$$

Figure 13.26 shows the results of diffusion of each species. The x-axis is time and y-axis is density of species. The dot point is the results calculated by CUBE and blue line is the analytical solution. P1, P2, P3 indicate

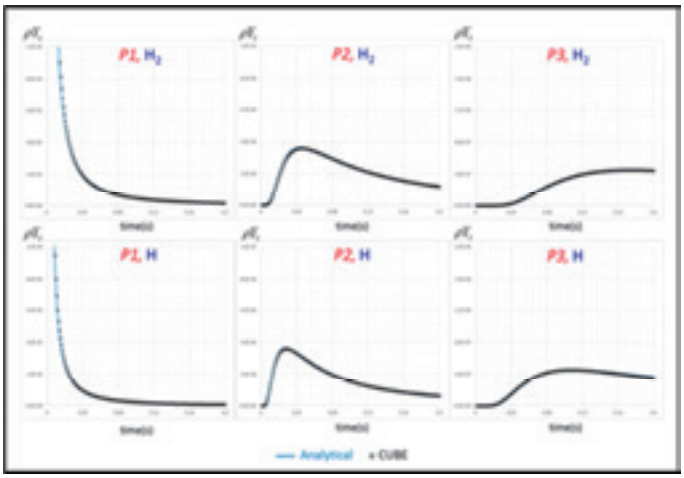

Figure 13.26: Validation of species transport diffusion in CUBE.

different position away from the source point. The CFD results by CUBE are well consistent with the analytical results with high accuracy.

13.2.5.2 Basic validation of spray modeling

In a typical fuel spray the atomization leads to droplets as small as few micrometer and as large as few millimeter. Numerical simulations that fully resolves the droplets at all the scales are not feasible by today's and also near future HPC facilities as the mesh resolution necessary to resolve the smallest drops is prohibitively small. In this scenario, reduced order models for modeling spray atomization are invaluable. As the fuel spray droplets are modeled as discrete set of Lagrangian particles, incorporation of spray model into CUBE was straight forward through the building cube Lagrangian data structure. A fresh validation of spray model implementation in CUBE was carried out using experimental data of Sato et al for Methyl Ethyl Ketone (MEK). The results of the simulation are compared with the experimental and simulation data of Sato et al. In Fig.13.27 the ratio of evaporated vapor mass to the injected spray mass, evaporation ratio, is compared with experimental data. In the same figure the spray tip penetration is also compared with the experimental data. In Fig.13.28, the equivalence ratio of the simulation results is compared with that of the experiment and simulation results of Sato et al. It showed a good agreement.

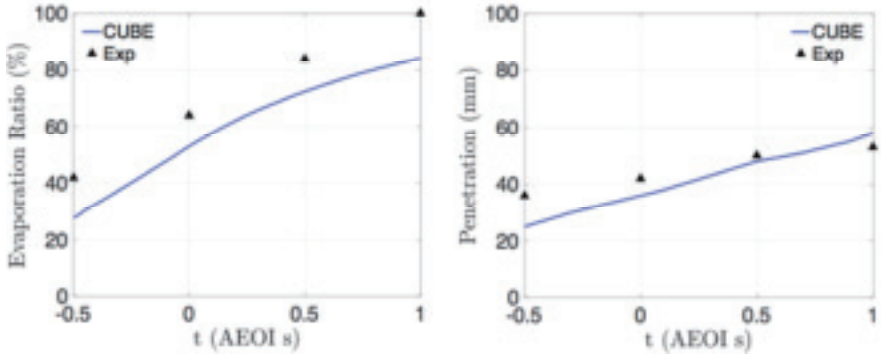

Figure 13.27: Validation of evaporation ratio (left) and penetration of MEK spray.

In order to evaluate the performance implementation of the spray model in CUBE, strong scaling and spray cost analysis was carried out. For the strong scaling analysis, a computational mesh with 33,554,432 cells was chosen which resulted in a mesh resolution of 0.6mm. The number of spray parcels were fixed at 106,000. The results of the strong scaling analysis is presented in Fig.13.29. Figure 13.29 shows the speed up rate of CUBE compared to the ideal speed up. A parallel efficiency of 80% was achieved. To evaluate the efficiency of the

spray model implementation in CUBE, a spray cost analysis is carried out by changing the number of spray parcels from 45,000 to 350,000. The runtime normalized by the runtime of the base case (no spray calculation) showed that for smallest case (45,000 spray parcels), the increase in runtime is marginal, and for the largest case (350,000 spray parcels), the increase in runtime is less than 50%. This is remarkably good efficiency showing the applicability for large scale spray simulation in future supercomputer.

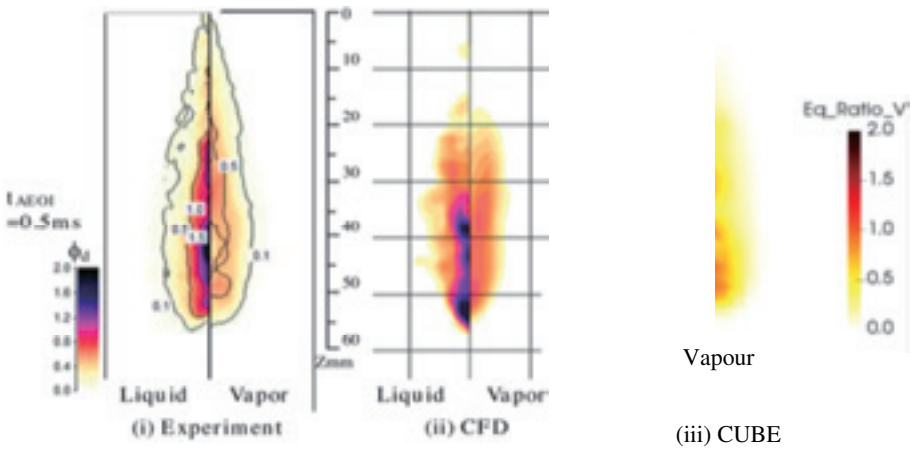

Figure 13.28: Validation of equivalence ratio of vapor phase.

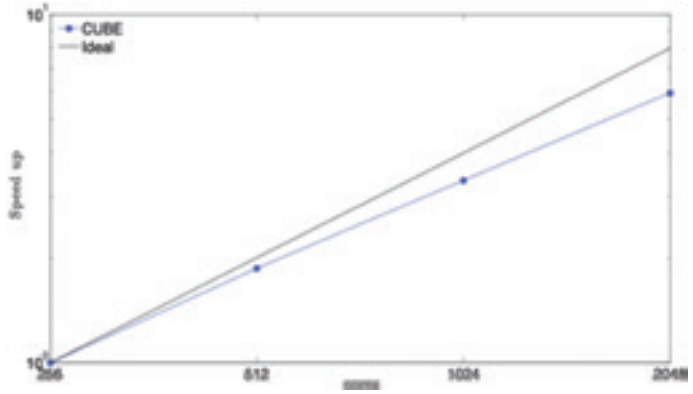

Figure 13.29: Strong scaling evaluation of spray model in CUBE.

13.2.5.3 The Rapid Compression Expansion Machine (RCEM) test

The Rapid Compression Expansion Machine (RCEM) is an experimental device that reproduces the compression expansion stroke in the engine once, in order to observe the combustion / spray behavior in the engine cylinder in detail. The RCEM test has been conducted by the Japanese automobile company. The simulation is done by CUBE and investigated the phenomena. The physical model of this study is indicated in Fig.13.30(a). Figure 13.30(b) shows the detail spark plug and chamber geometry. Figure 13.31 shows the grid distribution, and the whole computation domain is divided by several cubes, and each cube contains 16x16x16 cells.

In this work, we discussed two conditions of RCEM as listed in Table 13.1. Case A has an initial pressure of 200 kPa and with stationary piston at TDC, where case B is at 101.3 kPa of pressure and piston moves from BDC to TDC. Both cases are premix iso-octane/air and the equivalence ratio is equal to 1.0.

In case A, the computation domain contains only the region of upper chamber above TDC, where in case B the whole domain is calculated. The total grid number of case A is around 5M and for case B is around 24M, both with a minimum cell size equals to 0.4mm near wall. In case B, the piston is moving from BDC to TDC, and then the ignition and combustion are started. In this situation, for the computation before combustion, the species transport equations and G equation are not necessary, and can be removed from the governing equations

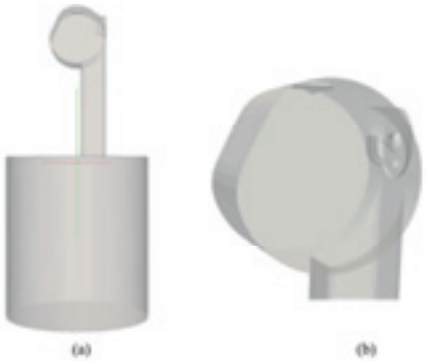

Figure 13.30: RCEM geometry.

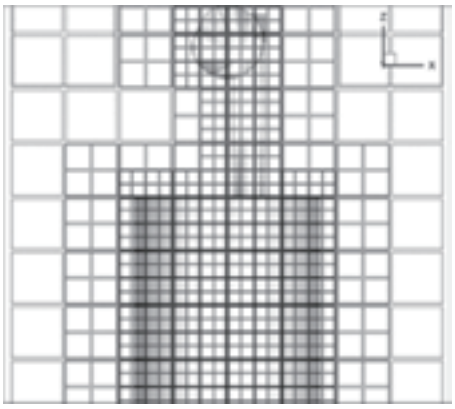

Figure 13.31: Cube distribution.

Table 13.1: RCEM conditions

	Fuel	Initial temperature(K)	Initial pressure(kPa)	Equivalence ratio	Ignition time	Compression ratio
Case A	Iso-octane	300	200	1.0	0ms	-
Case B	Iso-octane	300	101.3	1.0	80ms	13

to reduce the computation cost. The total physical time for case A is 0.03s and for case B is 0.1s. The total time steps for case A is 240000 steps and for case B is 320000(without combustion) plus 160000(with combustion) steps.

i) Case A: Premixed combustion without piston motion

The premixed combustion without piston motion is investigated. The fluids near the spark plug are heated and burned. Figure 13.32 shows the comparison of CFD results and experimental snapshots. The flame shape and flame speed of CFD are well consistent with the snapshots of experiments at almost every time step even for those wrinkles at the tip of flames. However, since the ignition condition is difficult to represent perfectly at the initial stage, there is a small difference between CFD and experimental results when ignition occurred.

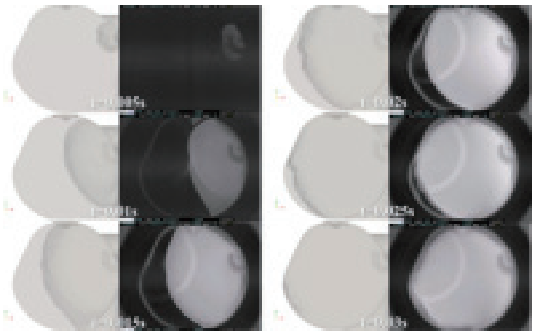

Figure 13.32: The comparison of flamefront of CFD (left) and experiments (right) with time of case A.

ii) Case B: Premixed combustion with piston motion

The premixed combustion with piston motion is investigated. From $t = 0$ to $t = 80ms$, the piston moves from BDC to TDC. The density is increased due to the compression process. In Fig.13.33, as the piston moving, the momentum magnitude inside the chamber is increased and even higher than the piston speed due to the geometry of the neck of the chamber. It makes the flow condition much more different and complicated than case A. The pressure result showed that is increased as the piston going to the TDC, and dramatically raised after 80ms due to the ignition. Before 40ms, the CFD results are well consistent with the experimental results, but has discrepancy after that. It is considered due to the insufficient mesh resolution inside the chamber. In Fig.13.34,

the flamefront visualization results of CFD are compared with experimental snapshots. Due to the shape of the combustion chamber, the flame-front appears near the spark plug at beginning, and then counterclockwise moves through upper part and finally propagates to the whole chamber. The flame propagation speed and trends of CFD are similar to the experimental results though the full consistency is difficult to show because there are overlap flames inside the chamber.

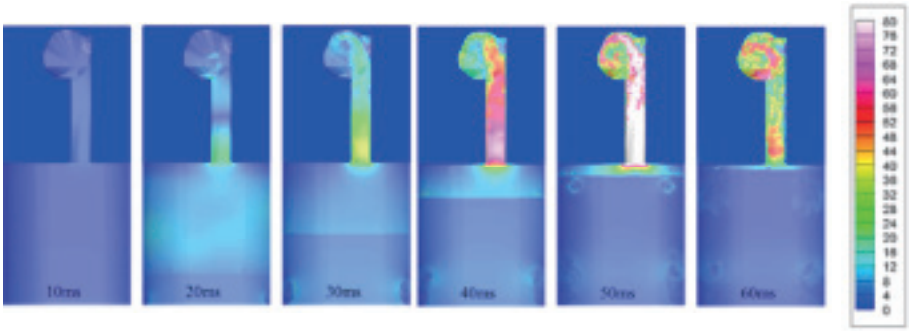

Figure 13.33: Momentum magnitude contours of slice at of case B.

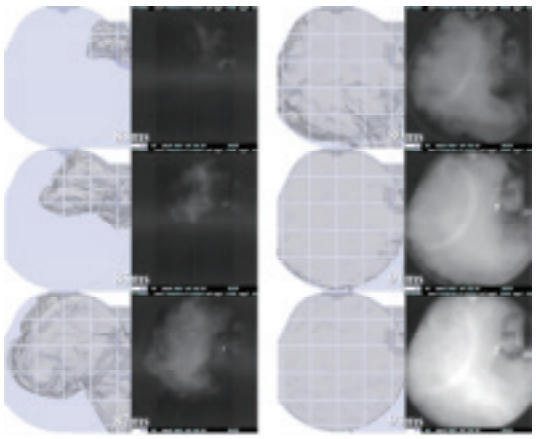

Figure 13.34: The comparison of flamefront of CFD (left) and experiments (right) with time of case B.

iii) Evaluation of the heat flux from the engine cylinder wall

In a reciprocating piston engine, estimating the engine cooling, that is, the heat loss from the combustion chamber wall corresponds to considering the heat transfer from the gas in the cylinder to the coolant. It has a particularly important meaning in engine engineering. Reducing the heat loss from the combustion gas to the wall of the combustion chamber is considered to be the most important issue, for achieving low fuel consumption. When finding heat transfer with CFD, it is necessary to predict the turbulence near the wall surface with high accuracy, and it depends largely on grid resolution or wall model. In this study, in order to accurately estimate wall heat transfer from RCEM equipment, an evaluation method that can be predicted efficiently considering practicality has been developed. First, the large time step advancement method has been developed. The time step of the conventional way to deal with the time advancement for compressible flows is limited by CFL condition. In order to satisfy the CFL condition to maintain the numerical stability, the time step will be extremely small because the sound speed dominates the convective speed for the CFL number. To overcome this problem, LUSGS with SLTM has been implemented in this project. With this method, the physical time step can be drastically increased to reduce the calculation time. Next, the wall modeling to evaluate heat flux is developed. The basic definition of heat flux is constructed with the temperature difference of wall and gas, divided by grid resolution. To accurately evaluate the heat flux neat the wall, fine grid resolution around wall is required to capture thin thermal boundary layer. It is possible in CFD to capture the boundary layer accurately conducting DNS (Direct Numerical Simulation) or wall resolved LES (Large Eddy Simulation), but it is not a practical way for daily basis usage because of the large calculation resource it requires. As

the alternative method, corrected equations obtained from experiments are widely used like as correlated heat transfer coefficient of Woschni, Nusselt, Annand, etc. These models are depending on the steady-state solution, they are not able to use prediction of local behavior or the effect of turbulence varying with the motion. So in this study, the evaluation method based on the wall model is developed to enable the CUBE to evaluate transient and 3 dimensional field of heat convection phenomena. The definition of heat flux is shown in Eq.(13.2),

$$\begin{aligned} q_w &= \frac{\rho C_p u_\tau T_g}{\alpha \ln y^+ + \beta} \ln(\frac{T_g}{T_w}), \\ u_\tau &= C_\mu \sqrt{k}, \\ y^+ &= \frac{y u_\tau}{\nu} \end{aligned} \tag{13.2}$$

where α, β, C_μ is constants to define turbulence thermal boundary layer, and C_p is a heat capacity of air. The friction velocity τ is calculated iteratively form the compressible flow solution of velocity and density. The validation of method is conducted under the conditions of RCEM experiment. With the SLTM, the time step can be increased to 4e-5, which CFL equals to 20 based on sound speed. For the usual method, the CFL number couldn't be larger than 1. Hence, SLTM can tremendously save computational cost. Figure 13.35 shows the temperature contour and heat flux on the observation point compared with the experimental result.

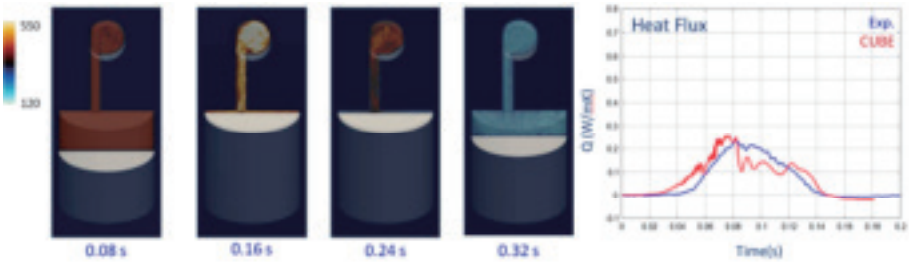

Figure 13.35: Temperature contour and heat flux estimation.

From the temperature contours, the temperature increment and decrement due to the compression and decompression processes can be cleanly observed. This is evidence that the present software CUBE follows the conservative property so it can be used on engine simulations. Based on the distribution of the heat flux, the result is acceptable agreement with the experimental result, which demonstrates the accuracy of the present method.

13.2.5.4 Practical engine simulation

The practical real-designed engine cycle simulation has been conducted to validate the accuracy of the method, and realize the large scale simulation with motion. The 3 dimensional geometry CAD data is received from Japanese automobile company. The result of cold flow analysis which the company tried to validate the accuracy using commercial software has been compared with the result of this study. In order to make it close to the practical situation, the inlet and outlet conditions are assigned by fixed temperature and pressure. Figure 13.36 shows the distributions of temperature, density and pressure compared with the result of the commercial software based on unstructured grids. The present results show qualitatively good agreement with the commercial software result. It means that the numerical method developed in this study is able to deal with the practical engine simulation. So far, the 1.5 billion grid number based on 0.1mm grid size has been conducted. The preliminary result and estimated CPU time are shown in Fig.13.37, since it could not be completed because of the limitation of received calculation resources. However, the capability of performing large scale simulation has been shown, therefore the high accuracy and efficiency can be expected for engineering applications if we can get an additional computational resources in near future.

13.3 Schedule and Future Plan

In the research and development of unified simulation framework 'CUBE' from 2012, the following goals has been achieved:

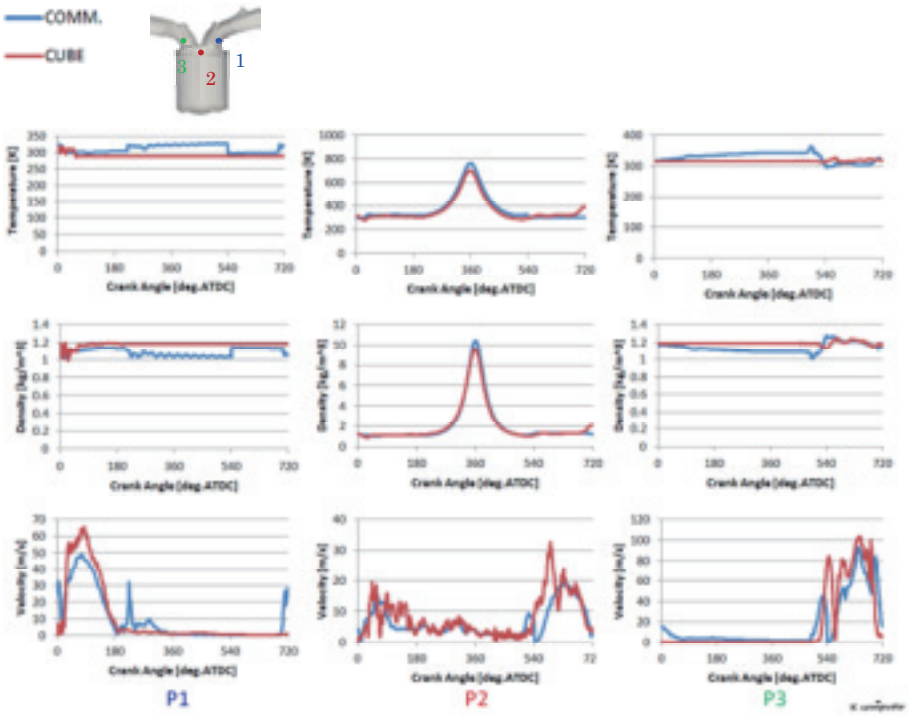

Figure 13.36: Practical engine simulation result.

[1] Construction and development of the simulation technology for bringing out the performance of K-computer

[2] Validation and practical usage of industrial applications such as vehicle aerodynamics, aeroacoustics, unsteady motion aerodynamics, engine combustion, city area wind environment analysys, sport CFD, and structure analysis

[3] Preparation of the simulation technologies of HPC toward EXA-scale

In the long-term objectives, the following target is considered:

[1] Establishment of the research and development center for industrial simulation technology

[2] Contribution to computer science by expanding the developed simulation technology to different fields

In terms of using Cartesian grids, the problems that the analysis accuracy in the vicinity of the wall surface decreases due to the limitation of immersed boundary method is becoming clear. In the future, through the deployment of CUBE to the industrial applications, the introduction of higher order schemes, wall modeling and advance sophisticated research of immersed boundary method are planning.

In terms of using Hierarchical grid system, the problems that the interface communication in each halo of cubes will spoil the performance on future supercomputers is becoming clear. In the future, the enhancement to the current communication / calculation overwrapping technique, or tuning for the interface communication, introduction of adaptive refinement scheme are planning.

From collaboratetive companies, including companies through the activities of the “Consortium for Next Generation Automotive CAE using HPC” and “Consortium for Next Generation Combustion CAE using HPC” organized by RIKEN, voices of surprises and expectation for software development have been received. We are planning to continue development for practical application in near future.

Method	RoeAMTP	RoeAMTP	RoeAMTP
Time scheme	SLTS	SLTS	SLTS
Time step(s)	$2x10^{-5}$	$1x10^{-5}$	$4x10^{-6}$
CFL	17 / 0.5	17 / 0.5	17 / 0.5
Grid size (mm)	0.5	0.25	0.1
Cube num.	8,052	35,177	362,091
Cell num.	32,980,992	144,084,992	1,483,124,736
Node num.	504	2,199	22,630
CPU time	10,080	87,960	1,810,400
Comp. hrs	20	40	80

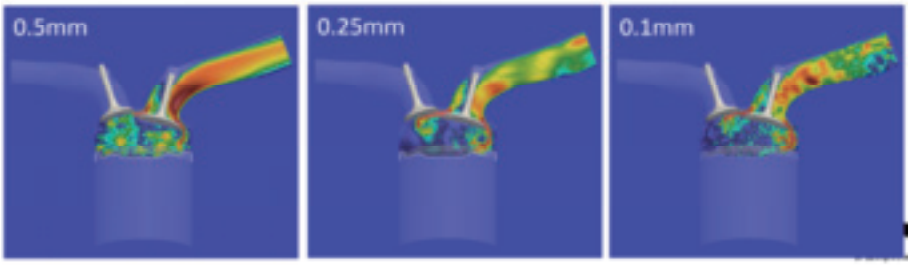

Figure 13.37: Large scale simulation and CPU time estimation.

13.4 Publications

13.4.1 Articles

[1] ChungGang Li, Makoto Tsubokura, "An implicit turbulence model for low-Mach Roe scheme using truncated Navier-Stokes equations," Journal of Computational Physics, Volume 345, 15, 2017, pp.462-474.
[2] Keiji Onishi, Yasunori Ando, Kosuke Nakasato, Makoto Tsubokura , "Evaluation of an Open-grill Vehicle Aerodynamics Simulation Method Considering Dirty CAD Geometries," SAE Technical Paper 2018-01-0733, 2018.
[3] Koji Nishiguchi, Shigenobu Okazawa, Makoto Tsubokura, "Multi-material Eulerian finite element formulation for pressure-sensitive adhesives," International Journal for Numerical Methods in Engineering, Volume 114, Issue 13, 2018, pp.1368-1388.
[4] Koji NISHIGUCHI, Rahul BALE, Shigenobu OKAZAWA, Makoto TSUBOKURA, "Fully Eulerian solid-fluid interaction analysis using hierarchical Cartesian mesh method for large-scale parallel computing," Journal of Japan Society of Civil Engineers, Ser. A2 (Applied Mechanics (AM)), 73(2), p. I_153-I_163, 2017.
[5] Nakasato, K., Tsubokura, M., Ikeda, J., Onishi, K. et al., "Coupled 6DoF Motion and Aerodynamic Cross-wind Simulation Incorporating Driver Model," SAE Int. J. Passeng. Cars - Mech. Syst. 10(2):662-670, 2017.

13.4.2 Conference Paper (reviewed)

[6] Keiji Onishi, Makoto Tsubokura, "IMMERSED BOUNDARY METHOD FOR PRACTICAL VEHICLE AERODYNAMIC ANALYSIS USING HIERARICHICAL CARTESIAN GRID," the Ninth JSME-KSME Thermal and Fluids Engineering Conference, Okinawa(Japan), 2017.10.
[7] Rahul Bale, Niclas Jansson, Keiji Onishi, Makoto Tsubokura, Neelesh Patankar, "A STENCIL PENALTY APPROACH FOR IMPROVING ACCURACY OF CONSTRAINT IMMERSED BOUNDARY METHOD," the Ninth JSME-KSME Thermal and Fluids Engineering Conference, Okinawa(Japan), 2017.10.
[8] Jorji Nonaka, Motohiko Matsuda, Takashi Shimizu, Naohisa Sakamoto, Masahiro Fujita, Keiji Onishi, Eduardo Camilo Inacio, Shun Ito, Fumiyoshi Shoji, Kenji Ono, "A Study on Open Source Software for Large-Scale Data Visualization on SPARC64fx based HPC Systems," HPC Asia 2018, 2018.1.

13.4.3 Posters (reviewed)

[9] Keiji Onishi, Niclas Jansson, Rahul Bale, Wei-Hsiang Wang, Chung-Gang Li, Makoto Tsubokura, "A Deployment of HPC Algorithm into Pre/Post-Processing for Industrial CFD on K-computer," SC17 - International

Conference for High Performance Computing, Networking, Storage and Analysis, Denver(CO), 2017.11.

13.4.4 Invited Talks

[10] Keiji Onishi, "Encouragement of Accelerating Pre/Post processing towards Exascale CFD," ISC17 - High Performance conference 2017, Workshop, Frankfurt(Germany), 2017.6.

13.4.5 Oral Talks

[11] ChungGang Li, Makoto Tsubokura, Rahul Bale, WeiHsiang Wang, Keiji Onishi, "An immersed boundary method for compressible flows at low Mach numbers on engineering applications using massive parallelization systems," IACM 19th International Conference on Finite Elements in Flow Problems - FEF 2017, Rome(Italy), 2017.04.
[12] Keiji Onishi and Makoto Tsubokura. "The development of a simulation method for the practical full vehicle aerodynamics analysis," In: Proceedings of the Conference on Computational Engineering and Science, F-09-1, 2017.6.
[13] Keiji Onishi, Makoto Tsubokura, "An immersed boundary method for modeling a dirty geometry data," 70th Annual Meeting of the APS Division of Fluid Dynamics, 2017.11, Denver, CO.
[14] K. Onishi, R. Bale and M. Tsubokura. "Numerical study of open-shell immersed boundary method applied to flow around rotating body," In: Proceedings of the symposium on computational fluid dynamics, F01-3, 2017.12.
[15] Koji Nishiguchi, Rahul Bale, Keiji Onishi, Shigenobu Okazawa, Makoto Tsubokura, "Eulerian dynamic analysis of structures based on Building-Cube Method for large scale parallel simulations," In: Proceedings of the Conference on Computational Engineering and Science, F-08-1, 2017.6.
[16] Koji NISHIGUCHI, Rahul BALE, Shigenobu OKAZAWA and Makoto TSUBOKURA, "Fully Eulerian solid-fluid interaction analysis using hierarchical Cartesian mesh method for large-scale parallel computing," In: Proceedings of 20th Applied Mechanics symposium. No.C000014, 2017.5.
[17] Koji Nishiguchi, Rahul Bale, Shigenobu Okazawa, Makoto Tsubokura, "A fixed Cartesian mesh approach for large-scale parallel simulations of fluid-structure interaction problems," Proceedings of ECCOMAS MSF 2017 THEMATIC CONFERENCE, 4 pages, Ljubljana(Slovenia), 2017.9.
[18] Koji Nishiguchi, Rahul Bale, Shigenobu Okazawa, Makoto Tsubokura, "A fixed Cartesian mesh method for large-scale parallel simulation of complex vehicular structures," Proceedings of the 14th U.S. National Congress on Computational Mechanics (USNCCM14), Montréal(Canada), 2017.7.
[19] Rahul Bale, Niclas Jansson, Keiji Onishi, Makoto Tsubokura, and Neelesh Patankar, "A stencil penalty approach for improving accuracy of constraint immersed boundary method," Proceedings of Computational Engineering Conference JSCES, Vol. 22, 2017.6.
[20] Rahul Bale, Amneet Pal Singh Bhalla, Niclas Jansson, Keiji Onishi, Tsubokura Makoto, "Interface approach for constraint IB," In: Proceedings of the symposium on computational fluid dynamics, F01-2, 2017.12.
[21] Wei-Hsiang Wang, Chung-Gang Li, Wu-Shung Fu and Makoto Tsubokura, "Investigation of open boundary problem in pure thermal plume by hybrid boundary condition with multi-GPU implementation," The 3rd Thermal and Fluids Engineering Conference, Fort Lauderdale, FL, USA, March 4-7, 2018.
[22] Wei-Hsiang Wang, Chung-Gang Li, Rahul Bale, Keiji Onishi and Makoto Tsubokura, "The four-stroke IC engine simulation using hierarchical Cartesian mesh framework by CUBE," The 31st Computational Fluid Dynamics Symposium, Kyoto, Japan, December 12-14, 2017.12.
[23] Wei-Hsiang Wang, Chung-Gang Li, Keiji Onishi and Makoto Tsubokura, "Fully compressible aerodynamics and aeroacoustics simulation of a full-scale road vehicle," The 14th International Conference on Flow Dynamics, Sendai, Japan, November 1-3, 2017.
[24] Wei-Hsiang Wang and Makoto Tsubokura, "Fully compressible aerodynamics simulation of a full-scale road vehicle and its application to aeroacoustics analysis," The 22nd Computational Engineering Conference, Saitama, Japan, May 31-June 2, 2017.
[25] Duong Viet Dung, Cao Yong, Tetsuro Tamura, Hidenori Kawai, Bale Rahul, Keiji Onishi, Makoto Tsubokura, "BCM-LES of Separated Shear Layer Instability Around 2D Square Cylinder," In: Proceedings of Annual Meeting, Japan Society of Fluid Mechanics, pp. 184, 2017.8.
[26] Tetsuro Tamura, Hidenori Kawai, Viet Dung Duong, Rahul Bale, Keiji Onishi, Makoto Tsubokura, "BCM-LES analysis of turbulent flows over and within actual urban canopy," 9th Asia-Pacific Conference on Wind Engineering, APCWE-IX, Dec. 2017.

[27] Duong Viet Dung, Cao Yong, Tetsuro Tamura, Hidenori Kawai, Bale Rahul, Keiji Onishi, MakotoTsubokura, "IBM-based Treatments in Building Cube Method for Complex Flows," In: Proceedings of the symposium on computational fluid dynamics, B10-2, 2017.12.
[28] Hidenori KAWAI, Tetsuro TAMURA, Rahul BALE, Keiji ONISHI, Makoto TSUBOKURA, "Characteristics of coherent structure in actual city consisting of scattered high-rise buildings," In: Proceedings of the symposium on computational fluid dynamics, B06-4, 2017.12.
[29] Yong Cao, Hidenori Kawai, Tetsuro Tamura, Rahul Bale, Keiji Onishi, Makoto Tsubokura, "Mean flow topology and mean surface pressure on a surface-mounted square cylinder," In: Proceedings of the symposium on computational fluid dynamics, B10-1, 2017.12.
[30] Keiji Onishi, Niclas Jansson, Rahul Bale, Makoto Tsubokura, "A parallel algorithm of pre- and post- processing for industrial CFD applications," 18th SIAM Conference on Parallel Processing for Scientific Computing, 2018.3.
[31] Rahul Bale, Niclas Jansson, Keiji Onishi, Makoto Tsubokura, Neelesh Patankar, "A Stencil Penalty Approach For Improving Accuracy of Constraint Immersed Boundary Method," 18th SIAM Conference on Parallel Processing for Scientific Computing, 2018.3.

Chapter 14

HPC Programming Framework Research Team

14.1 Members

Naoya Maruyama (Team Leader)

Motohiko Matsuda (Research Scientist)

Shinichiro Takizawa (Research Scientist)

Mohamed Wahib (Postdoctoral Researcher)

Satoshi Matsuoka (Senior Visiting Scientist)

Tomoko Nakashima (Assistant)

14.2 Research Activities

We have developed high performance, highly productive software stacks that aim to simplify development of highly optimized, fault-tolerant computational science applications on current and future supercomputers, notably K computer. In this report, we present an overview of one of our high productivity frameworks.

14.3 Research Results and Achievements

14.3.1 A Programming Framework for Hierarchical N-Body Algorithms

Hierarchical tree-based algorithms are often used in simulations such as molecular-dynamics and particle simulations, and especially, algorithms such as Barnes-Hut and Fast Multipole Method (FMM) are the most popular ones in N-body simulations. To assist experiments of such algorithms, a prototype framework called *Tapas* is being developed for distributed memory CPU/GPU computers. Direct interaction calculations, which compute pairwise forces among nearby subsets of the bodies, are still important even in sophisticated tree-based algorithms. Direct interaction calculations are algorithmically simple *all-pairs* operations, but they contribute to a non-negligible part of the total execution time in practice. In some modest-scale experiments, roughly a half of the execution time is consumed in all-pairs operations. It is compute-intensive, and thus, requires state-of-the-art adaptations to particular architectures of varying platforms of CPUs and GPUs.

An all-pairs operation mainly consists of nested loops working on two vectors. There is numerous work on all-pairs implementations on manycore CPUs and GPUs. But, existing implementations have flaws in its interface design, possibly because it is too simple and not seriously designed. Using an example of the force calculation in an N-body simulation, decomposition of an all-pairs operation reveals three loops: one for a pair-wise force calculation, one for a summation of forces to each body, and one for updating vectors of positions and velocities. These are carried out in sequence by a mapping-of-mappings for a force calculation, by a mapping-of-reductions for a summation of forces, and a mapping for updating. Existing implementations ignore the updating part,

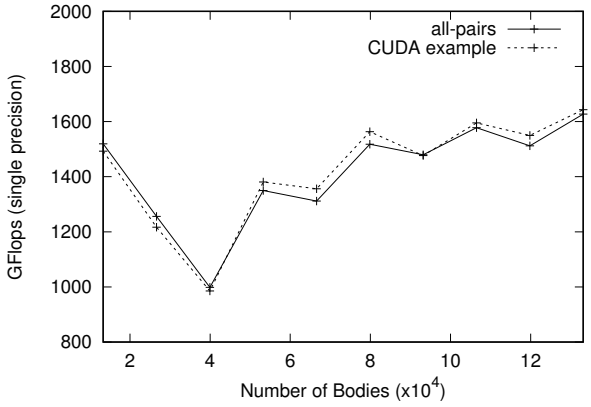

Figure 14.1: Comparison of N-body simulations between the all-pairs code and the CUDA example code on a GPU (K80).

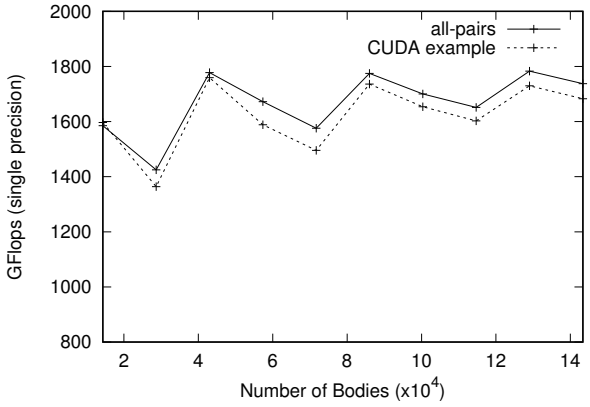

Figure 14.2: Comparison of N-body simulations between the all-pairs code and the CUDA example code on a GPU (K20Xm).

and it is implicitly performed in the summation. The updating part is a non-nested single loop, and it was thought to be performed simply. It is not that simple. It is known that the loops for a mapping-of-mappings and a mapping-of-reductions can be fused. However, it is known that the loops for a mapping for updating and a mapping-of-reductions cannot be fused. Thus, the design of the all-pairs operation should consider the updating part explicitly. Adding an explicit mapping for updating increases flexibility in adopting the all-pairs operation in the application code. It makes, for example, the code simple in absorbing the mismatch of the representation of vectors of positions and velocities, such as array-of-structures (AoS) or array-of-structures (SoA), which are specific to the applications.

It is important to keep the performance critical code to be abstract and compact. Although an all-pairs could be performed by a composition of mappings and reductions, the CUDA language for GPUs does not well admit such nested compositions of mappings and reductions due to its host-device distinction and difficulty in using the fast scratchpad memory. Thus, the all-pairs operation should be defined as a single fused-form, which is important for performance. Making a properly designed interface also facilitates direct comparison with existing fast reference implementations such as given in the CUDA examples.

In the evaluation, the performance of a direct N-body simulation are compared between the reference code in the CUDA examples and the code using the all-pairs. In addition, the performance of an FMM N-body simulation are compared between the hand-written code and the code using the all-pairs. These performance indications support the suitability of the all-pairs interface. The evaluation is done with using two GPU platforms K80 and K20Xm, both with the Kepler micro-architecture. K80 has 13 SMs (streaming multiprocessors) with micro-architecture revision 3.7, and K20Xm has 14 SMs with micro-architecture revision 3.5. K80 runs at 823 MHz and its memory at 2505 MHz, while K20Xm runs at 732 MHz and its memory at 2600 MHz. K80's memory is a bit slower. The host for K80 is Intel Xeon E5-2698 2.3 GHz, and the host for K20Xm is Intel Xeon E5-2670 2.6 GHz. The compilers are CUDA 8.0 and Intel ICC 16.0.4 both for K80 and K20Xm.

The first evaluation uses the direct N-body simulation code in the CUDA examples. The purpose of this evaluation is to check the overhead of abstraction is small enough, because the all-pairs implementation has a very similar structure to the code in the CUDA examples. Figure 14.1 shows the performance on K80, and Figure 14.2 shows the performance on K20Xm, which compare the performance of Tapas's all-pairs and the code in the CUDA examples. The measurements were run using a single GPU. The floating-point numbers are single-precision in this benchmark. GFlops is calculated as 20 operations per interaction in the same way as the CUDA examples. Note that the different steps for the number of bodies (X-axis) are used to make them multiples of the number of SM's. The step is 13×1024 for K80, and 14×1024 for K20Xm. The appearances of the code are very different, because the main parts of the calculations are extracted as function objects in the all-pairs case but they are laid out in the code in the CUDA examples. However, the both code has very similar structures in the GPU kernels, and the difference in performance is very small. K80 is generally slower than K20Xm in our runs, but we did not investigate the reasons.

The second evaluation compares an FMM N-body simulation between Tapas's original hand-written code and the code using the all-pairs. Figure 14.3 and Figure 14.4 show the GPU performance, and Figure 14.5 shows the CPU performance. Two GPUs on a single host are used in this benchmark, because Tapas runs

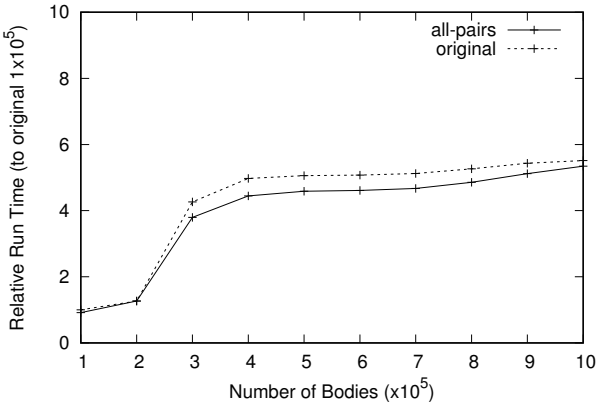

Figure 14.3: Comparison of Tapas runs between the all-pairs code and the hand-written code (original) on GPUs (using two K80).

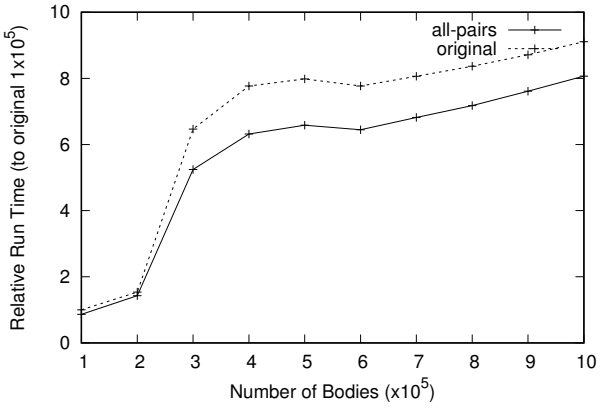

Figure 14.4: Comparison of Tapas runs between the all-pairs code and the hand-written code (original) on GPUs (using two K20Xm).

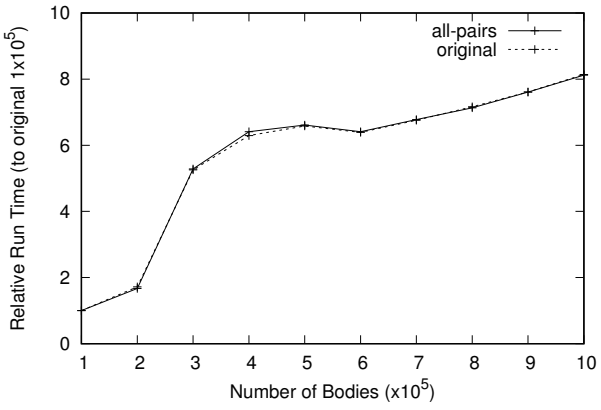

Figure 14.5: Comparison of Tapas runs between the all-pairs code and the hand-written code (original) on CPUs (Xeon E5-2670).

with at least two processes. The measurements in the benchmarks are on the first round of interactions, where the bodies are uniformly distributed initially. Both of the all-pairs code and the hand-written code (labeled as original) show similar performance, obviously because the all-pairs is the redesign of the interface and the difference in the code fragments is very small. However, unexpectedly, there is some observable speed-up in performance. It is unintended, but there are actually some differences in the register usage. The report of *ptxas info* (the assembler of GPU) from the CUDA compiler tells "Used 46 registers, 436 bytes cmem[0], 44 bytes cmem[2]" for the all-pairs code, while "Used 40 registers, 400 bytes cmem[0], 44 bytes cmem[2]" for the original code. The reports are the same for the both architectures of K80 and K20Xm.

We introduced a fused-form of the all-pairs operation which takes an explicit update function. The restricted execution model of CUDA prevents expressing nested calls as a composition of a mapping of mappings or a mapping of reductions. Thus, an all-pairs operation needs to be defined as a single operation. The explicit update function is suggested by considerations of algorithmic skeletons, where it in general cannot be fused the compositions of a function application to the result of a reduction. Recent programming in C++ is approaching to functional programming, where the important aspect is composability. However, building libraries with composable functions is still difficult. In introducing the all-pairs operation, we make it generalized to compensate the loss of composability of mappings and reductions in CUDA. Systematic development with the help of algorithmic skeletons has been successful in this regard. It provides a way to an appropriate design of data-parallel libraries in C++.

14.4 Schedule and Future Plan

Over the last five years, our team has developed tools and frameworks for simplifying developing high performance applications on large-scale computing systems. While our team is now closed, we hope that our software as well as the research results presented as peer-reviewed papers will continue to contribute to productive high performance computing.

14.5 Publications

14.5.1 Conference Papers

[1] Motohiko Matsuda, Keisuke Fukuda, Naoya Maruyama. "A Portability Layer of an All-pairs Operation for Hierarchical N-Body Algorithm Framework Tapas", In Proceedings of the International Conference on High Performance Computing in Asia-Pacific Region, HPC Asia 2018 (2018).

[2] Shinichiro Takizawa, Motohiko Matsuda, Naoya Maruyama, Yoshifumi Nakamura. "A Scalable Multi-Granular Data Model for Data Parallel Workflows", In Proceedings of the International Conference on High Performance Computing in Asia-Pacific Region, HPC Asia 2018 (2018).

14.5.2 Software

[3] KMR version 1.8.1 (April 2016). URL: http://mt.r-ccs.riken.jp/kmr.

Chapter 15

Advanced Visualization Research Team

15.1 Members

Kenji Ono (Team Leader)

Jorji Nonaka (Researcher)

Tomohiro Kawanabe (Technical Staff)

Kazunori Mikami (Technical Staff)

Masahiro Fujita (Visiting Technician)

Naohisa Sakamoto (Visiting Researcher)

Mario Antonio Ribeiro Dantas (Visiting Researcher)

Takashi Shimizu (Student Trainee)

Steve Petruzza (Student Trainee)

Eduardo Camilo Inacio (Intern)

Aya Motohashi (Assistant)

15.2 Research Activities

The research and development activities of this team, in these six years of continuous activities, have covered a broad range of the end-to-end simulation pipeline, focusing on the study, design, and development of effective tools and mechanisms for enabling high performance visualization functionalities on the K computer operational environment. The resulting libraries, tools, and applications have been publicly released as open-source software codes via GitHub, and they are listed in the deliverables subsection. In this final year of the continuous activities, we focused on enhancing the functionalities of the HIVE (Heterogeneously Integrated Visual analytics Environment) visualization application, including the input (xDMlib: Data Management Library), output (ChOWDER: Cooperative Tiled Display System), and rendering (PBVR: Particle Based Volume Rendering) capabilities. In addition, we have also worked on a workflow management system (WHEEL), and on a performance measurement and visualization tool (PMlib).

15.2.1 Heterogeneously Integrated Visual-analytics Environment (HIVE)

HIVE has been one of the main developments of this team, and was designed to run in the heterogeneous environments of traditional HPC infrastructures, which obviously includes the K computer environment that is composed of the supercomputer itself, the post-processing servers, and a research-oriented visualization cluster. As shown in Fig. 15.1, the HIVE is composed of several modules, most of them were internally developed and some are third-party developed modules, each possessing different functionalities. The HIVE adopted the Client/Server approach, and currently the HIVE Server is able to run on SPARC64fx and x86 hardware systems

running Linux, MacOSX and Windows (via Windows Subsystem for Linux). On the other hand, the HIVE Client only requires a Web browser and an appropriate network connection to the HIVE Server. The aforementioned HIVE modules are loosely-coupled via Lua scripting language, and the communication between the HIVE Server and Client is executed via Websocket connection. The Web-based user interface can serve as a user friendly GUI for selecting the visualization parameters for preparing the "Visualization Scenes" to be used in the large-scale parallel rendering job submissions via Command Line Interface (CLI). The right side of the Figure. 15.1 shows an visualization example of this CLI-based visualization of a large-scale particle-based simulation result rendered by using the data loading mechanism of PDMlib (Particle Data Management Library), and the ray-tracing rendering functionality of SURFACE (Scalable and Ubiquitous Rendering Framework for Advanced Computing Environments). In this rendering, the buildings are treated as particle data and the particle data representing tsunami was converted to polygonal data, via own developed OpenVDB-based polygonal data converter, and rendered as a semi-transparent object.

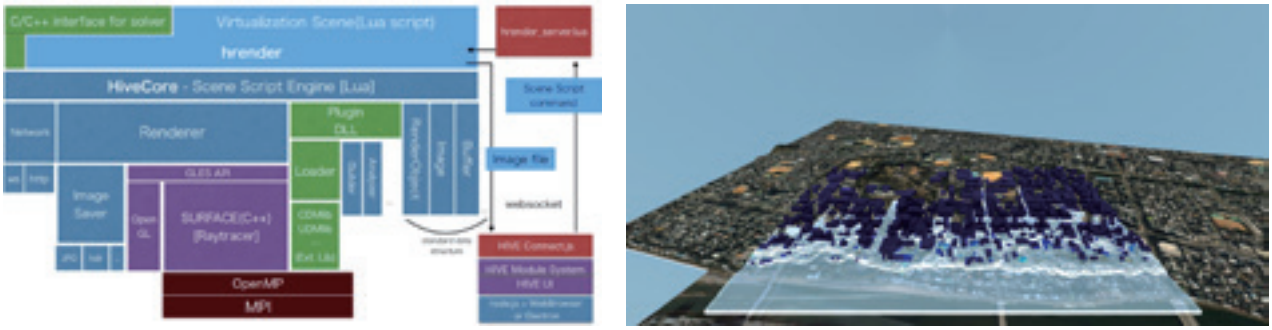

Figure 15.1: An overview of the HIVE software stacks showing the main modules, and a visualization example of a particle-based tsunami simulation rendered by the HIVE (using PDMlib and SURFACE functionalities).

As described in the previous paragraph, two of the most important characteristics of the HIVE are the Server/Client architecture and the loosely-coupled module integration via Lua scripting language. By taking advantage of these two characteristics, in this fiscal year, we focused on enhancing the HIVE functionality by including the Particle-Based Volume Rendering (PBVR), and mechanisms for visual causal exploration. For this purpose, we utilized the functionalities provided by the KVS (Kyoto Visualization System) initially developed at the Kyoto University, and currently maintained by the Kobe University. For the PBVR framework, we utilized the particle generation functionality of KVS, and stored the generated particle data as PDMlib (Particle Data Management library) data. For the visual causal exploration framework, we utilized the causality volume data generation functionality of KVS, and stored as CDMlib (Cartesian Data Management library) data. We also developed some shader codes for rendering these data sets via SURFACE ray-tracing functionalities, and these examples are shown in Fig. 15.2.

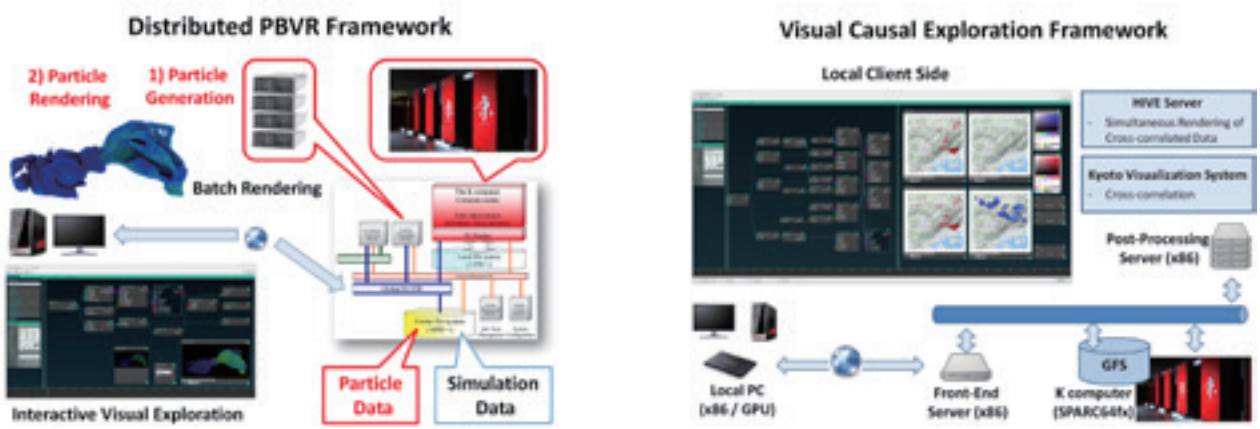

Figure 15.2: HIVE Functionality Enhancements: Distributed Particle-Based Volume Rendering (PBVR) Framework and a Visual Causal Exploration Framework.

15.2.2 Data Management Library (xDMlib)

The xDMlib data management library has been designed to support the I/O during simulations, such as the restart with different resolution size or number of computational nodes, and also to make a bridge between the I/O of simulation and visualization applications. The "x" in the xDMlib represents the type of data format: "C" for the Cartesian Data (CDMlib) such as voxel data; "P" for the Particle Data (PDMlib); "U" for the Unstructured Data (UDMlib) such as defined by the CGNS (CFD General Notation System) library; and "H" for the Hierarchical Data (HDMlib) such as the hierarchical block-structured data. One of the main characteristics of this library is the data aggregation and repartition mechanism for providing a flexible data I/O functionality, which can absorb the difference between the number of files (M) and the number of nodes (N) for reading or writing as shown in the Fig. 15.3.

Considering that the number of nodes available in hardware systems for post processing is usually much smaller than the number of generated files during the large job runs, the $M \times 1$ and $M \times N$ loading mechanism becomes the most important features from the visualization point of view. As shown in Fig. 15.3, the $M \times N$ data loading can be *aligned* or *unaligned* based on the selected partitioning parameters, and it is worth noting that unaligned data partitioning can impact the I/O performance. Another important mechanism of xDMlib is the use of lightweight meta-information for the distributed data management in order to maintain the original simulation data intact while extracting only the necessary data for the analysis and visualization processes. For this purpose, xDMlib utilizes two meta-information for managing the distributed files: information related to the contents of the data (index.dfi); and the information related to the data distribution among the processes (proc.dfi).

Among the several simulation codes running on the K computer, the SCALE (Scalable Computing for Advanced Library and Environment) is one of the representative large-scale simulation codes. This is a computational climate simulation code, and has been generating a vast amount of time-varying, multivariate simulation results. Therefore, a flexible data loading mechanism for the visualization and analysis of the already stored data sets as well as the upcoming simulation results becomes highly valuable. However, the file I/O is based on the NetCDF (Network Common Data From) file format, and can use the HDF5 for storing the compressed data as NetCDF4/HDF5 data. As a result, we extended the CDMlib library by including the necessary functionalities provided by the NetCDF (Version 4.2) and HDF5 (Version 1.8.10 patch 1) libraries. Figure 15.3 shows an overview of the implemented "metadata" generator (netcdf2dfi), and the extended CDMlib API for enabling the flexible data I/O of NetCDF4/HDF5-based computational climate simulation results.

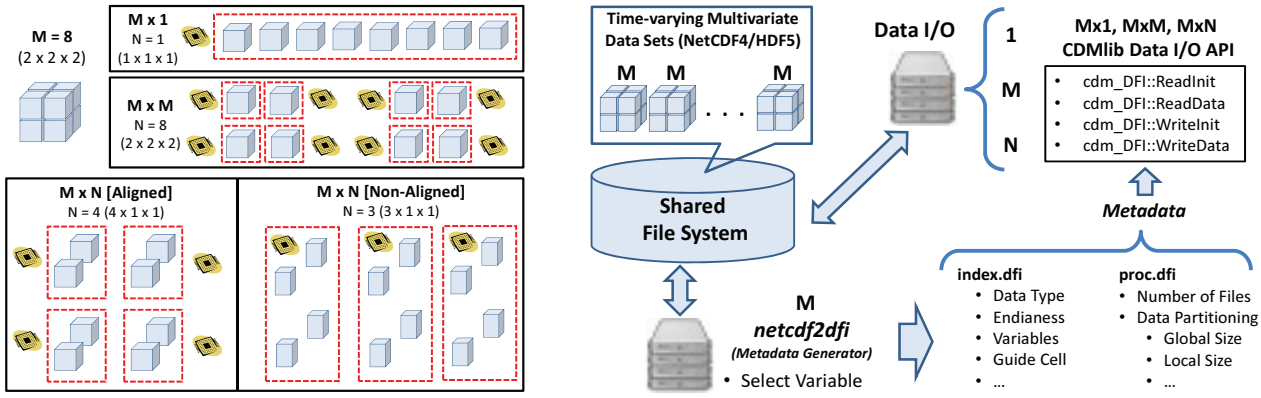

Figure 15.3: An overview of the data loading mechanism and the metadata generation process.

15.2.3 Cooperative Tiled Display System (ChOWDER)

ChOWDER (Cooperative Workspace Driver) is a web-based Tiled Display Wall (TDW) system that can be used to enhance collaborative works among multiple sites over the internet. By using the concept of "Virtual Display Area (VDA)", it can dynamically change the size of display area and the magnification ratio of the contents without the constraints on the limitations of the resolution on the physical display side reffig:VDA. When sharing a VDA among multiple sites, even they having TDW with different resolutions or aspect ratios, the ChOWDER can appropriately adjust the display magnification ratio of the VDA for each of the sites.

Besides, the ChOWDER was designed to allow dynamic change of participants, that is, any remote participant can dynamically add or remove their physical displays to the VDA even during the run-time.

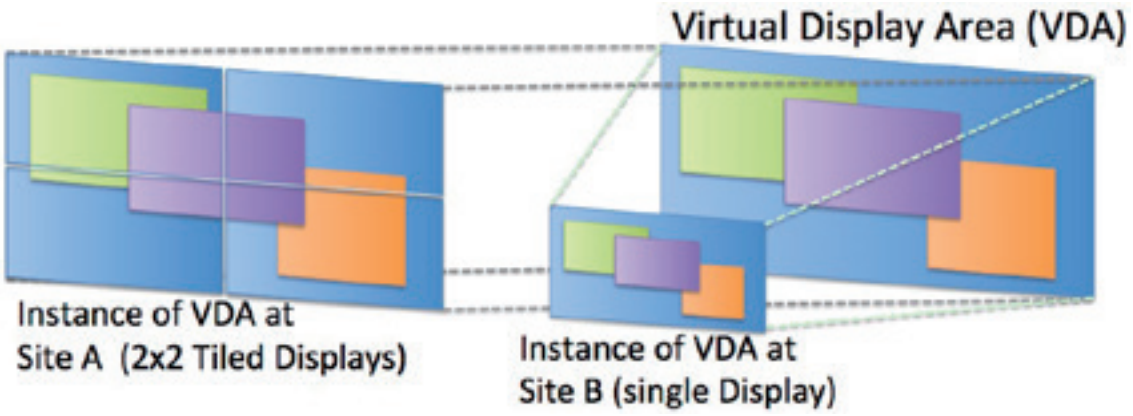

Figure 15.4: The concept of Virtual Display Area (VDA).

In this fiscal year, we developed some additional functionalities to the ChOWDER for enabling contents sharing of Movies, Screens, and Webcams. These functionalities are built using the P2P data transmission protocol called WebRTC, and the contents data is sent directly from the sender device to the display devices where the contents will be displayed. As a real-world usage scenario, we evaluated the effectiveness of these new functionalities by setting up an collaborative work scene using the TDWs placed at the Team's Laboratory, here in Kobe, and at the RIIT (Research Institute of Information Technology) at Kyushu University, in Fukuoka, as shown in Fig 15.5.

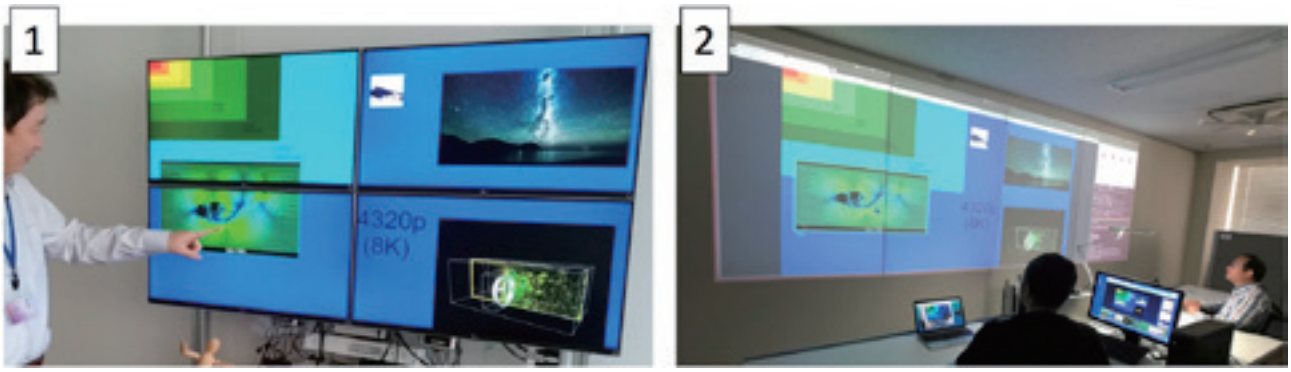

Figure 15.5: Distributed collaboration between Kyushu University (1) and RIKEN R-CCS (2) using ChOWDER.

15.2.4 Workflow Management System (WHEEL)

Typical end-to-end processing workflow on the HPC systems is just a repetition of a routine involving pre-processing and post-processing. The repetitive execution of this kind of workflow may waste the time of researchers and engineers and reducing the time for analysis and understanding of the simulated phenomenon, and interfering in the knowledge acquisition process. In order to solve this problem, this team has worked on a workflow management system named WHEEL (Workflow in Hierarchical distributEd parallEL), and is supported by the Ministry of Education, Culture, Sports, Science and Technology (MEXT) as one of the "Priority Issue on Post-K computer".

The WHEEL is based on another workflow management system named SWF, jointly developed by our team and the Kyushu University in last fiscal year. The developments have been focused on the refinement of the web-based user interface, and the addition of new functionalities. The WHELL can be defined as a multi-platform automated job preparation environment, including pre- and post-processing, for the efficient job

execution on the HPC systems. Since it uses web-based GUI, and run on web browser, thus it does not depend on the executing hardware platform. The main processing is handled by the *Node.js*, which is a cross-platform runtime environment, and enables its use on the Linux, Mac, and Windows hardware platforms. Users can define the "tasks" for each of the processing units via this web-based GUI, and can define the execution order by connecting these tasks under the GUI workspace, as shown in Figure 15.6.

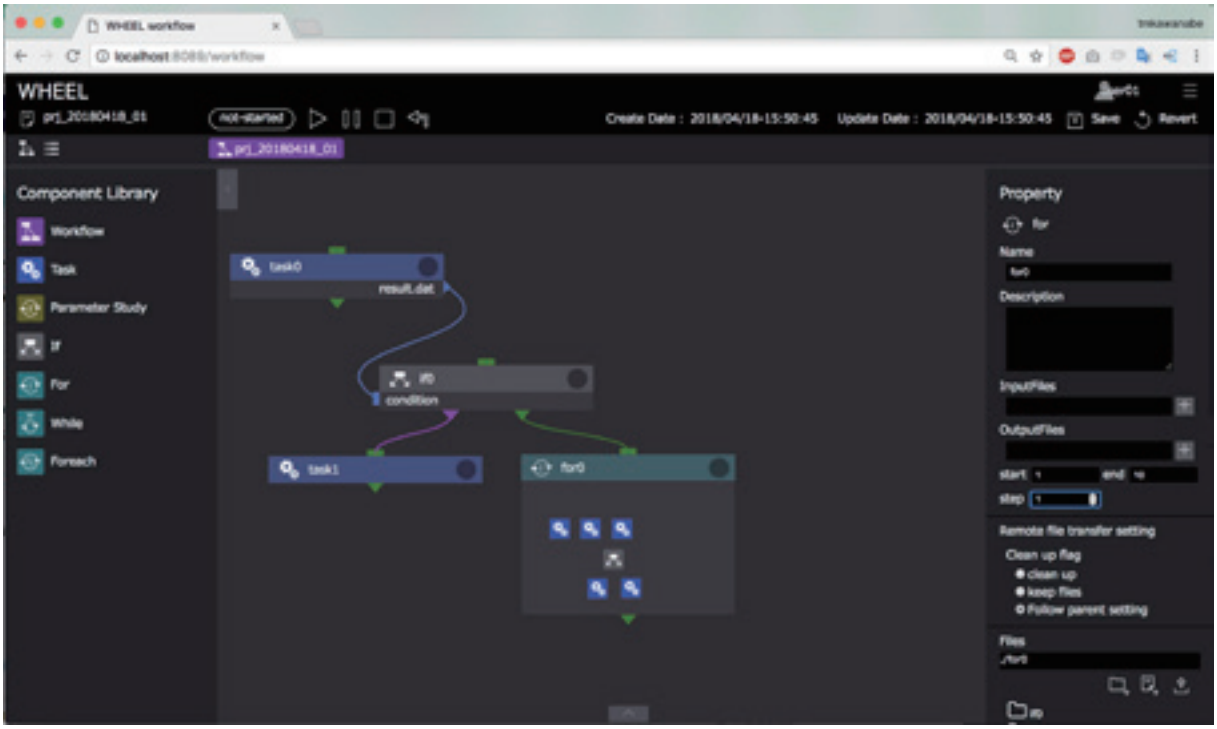

Figure 15.6: An overview of the WHEEL and its web-based GUI.

One of the distinctive features of the WHEEL is its parameter study execution component. By editing the parameter file of the simulation software inside the text editor incorporated in the WHEEL, and designating the sweep range of arbitrary parameter value, the simulation jobs for the specified parameter combinations are automatically executed. After the job execution, the users will receive the result data files that the users specified in advance for receiving after the execution. Compared to the SWF, some components have been added: Iterative processing; Conditional branching; and Sub-workflow. By using these components, in a combined manner, users can also build multi-objective design exploration workflow by using evolutionary calculation module based on genetic algorithm. In this fiscal year, we built and evaluated the operation of this workflow, using the evolutionary calculation module named "cheetah", which is provided by the JAXA.

15.2.5 Performance Monitoring Library (PMlib)

PMlib is designed to monitor the computational performance of scientific applications and to visualize their characteristics. The computational performance information such as flops and/or bandwidth can be obtained from the actually executed system workload which is automatically read through the hardware performance counters embedded in the modern CPUs. The alternative performance information can be obtained based on the theoretical requirement by the source program. The PMlib accepts the explicitly provided user arguments for such purposes.

The development effort during this fiscal year was focused on expanding the support of new CPU products such as the Intel Skylake and SPARC64 XIfx (Fujitsu PRIMEHPC FX100) which have new hardware instructions and corresponding event sets. By covering those event sets, the PMlib provides useful information regarding the effective computational performance for the specific micro architecture such as wide SIMD computation. As an example, the net computational performance of the loop body of the following basic kernels will be shown.

```
do i=1,n ; c(i)=a(i)+b(i) ; end do
do i=1,n ; c(i)=a(i)+b(i)*d ; end do
do i=1,n ; c(i)=b(i)/a(i) ; end do
do i=1,n ; c(i)=sqrt(a(i)) ; end do
```

All of the computations are performed with a unit stride with the innermost loop length of $n = 1, 2, 3, .., 50$. The SIMD instructions are generated by the compilers for such non-recurrent loops. Figure 15.7 shows the performance results on FX100 with the variables defined as double precision. The curves show non-monotonic increase, which are often observed on SIMD implemented CPU architectures. The performance jumps according to the SIMD width (SIMD bit width / data bit width), and on the FX100, these jumps occurred at loop length of $256/64 = 4$'s multiple. This fig 15.7 indicates that a careful programming practice will lead to the significant performance difference in short loops. Figure 15.8 shows the results of the same kernel with variables defined as single precision. A major impact was observed for the loop lengths which coincides with multiple of $256/32 = 8$.

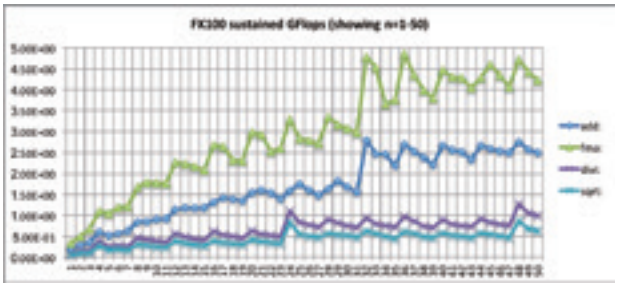

Figure 15.7: PMlib-fx100-R8

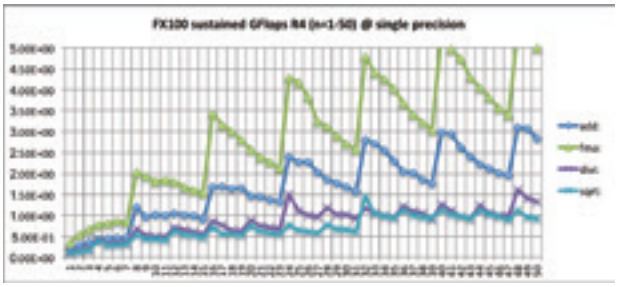

Figure 15.8: PMlib-fx100-R4

We also made some enhancements to the Web-based visualization package, named TRAiL, and designed for the PMlib. In addition to the default PMlib report, users can now produce the time dependent performance trace files in the open trace format, which can be visualized using the TRAiL. Figure reffig:TRAiL-512MPI shows a partial TRAiL view of a 512 process PMlib job.

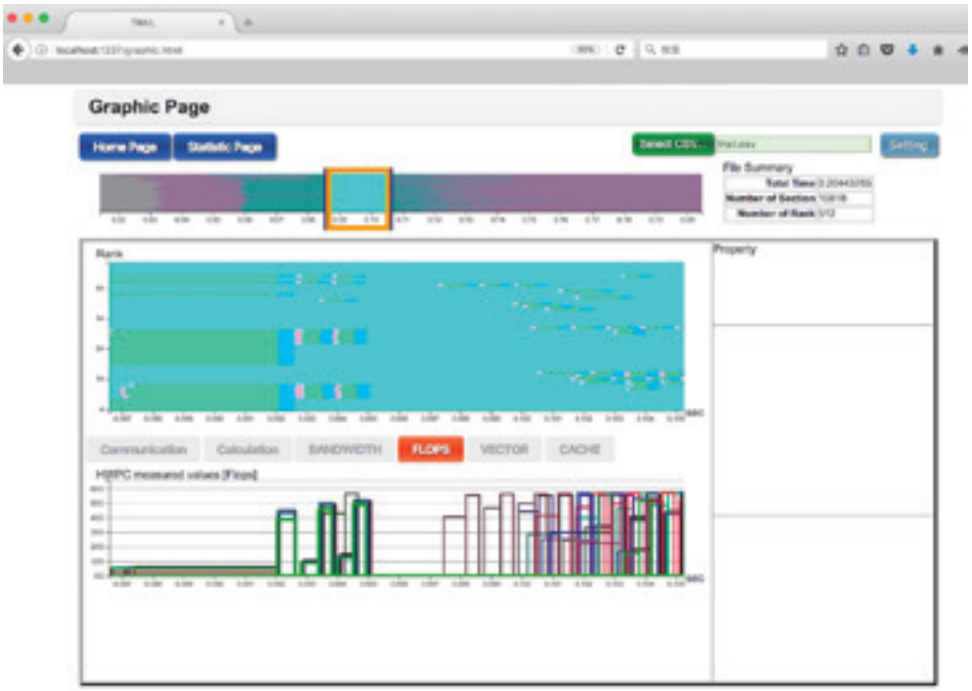

Figure 15.9: PMlib-TRAiL visualization

15.2.6 Summary

The Advanced Visualization Research Team has actively conducted the research and development of visualization related techniques from 2012 to 2018. The team has aimed to derive and promote scientific discovery and explore the essence of the simulated phenomenon inside the large-scale data sets generated from huge computational resources such as the K computer, and hence, to assist the knowledge creation and improvement of industrial design. Visualization and data processing are interdisciplinary research area among the information science, computational science, and computer science. Our team has been intensively focused and researched the methodologies to efficiently handle, analyze, and visualize data from various application fields. Therefore, our research area covered a wide range of topics, e.g., visualization of large-scale dataset, data compression with sparse modeling, parallel data management, execution environment for large-scale parallel computation, performance monitoring during the application run-time, performance visualization, and the parallel time integration technique. The Advanced Visualization Research Team can be characterized not only by the conducted research activities, but also for being conscious of the importance to feedback the research results to the society, and has conducted a wide range of activities, and our main contribution can be summarized as follows:

[1] We developed some core technologies and an integrated system which is capable of efficiently assist the visualization and data analysis on large-scale HPC environment such as the K computer environment, and potentially on the coming Post-K computer.

[2] The developed visualization system has been applied to the post-processing of the simulation results generated from various applications, and contributed to the outreach of the K computer.

[3] The developed visualization system has been continuously enhanced and maintained, and the users has also benefited from the visualization support and assistance.

[4] The team has contributed to the human resource development, and our team fostered over eight researchers, two technical staffs, and five student trainees, including some from overseas.

In addition to the R-CCS internal budget, our team successfully obtained more than five competitive external funds from MEXT and JSPS. Some collaborative research projects have been conducted with academia and private companies, including the University of Utah, in the USA, and the Federal University of Santa Catarina, in Brazil.

15.3 Publications

15.3.1 Journal Articles

[1] Jorji Nonaka, Kenji Ono, and Masahiro Fujita. “234Compositor: A Flexible Parallel Image Compositing Framework for Massively Parallel Visualization Environments”. In: *Elsevier Future Generation Computer Systems*, Vol. 82, pp. 647-655, May 2018.
[2] Jorji Nonaka, Eduardo Camilo Inacio, Kenji Ono, Mario Antonio Ribeiro Dantas, Yasuhiro Kawashima, Tomohiro Kawanabe, Fumiyoshi Shoji. “Data I/O Management Approach for the Post-hoc Visualization of Big Simulation Data Results”. International Journal of Modeling, Simulation, and Scientific Computing, https://doi.org/10.1142/S1793962318400068 (Onlilne Ready).
[3] Kazunori Mikami, Kenji Ono. “Performance Measurement and Performance Visualization Method using PMlib (in Japanese)”. IPSJ-SIG on HPC, 2018-HPC-163, 2017.

15.3.2 Conference Papers

[4] Jorji Nonaka, Naohisa Sakamoto, Takashi Shimizu, Masahiro Fujita, Kenji Ono, and Koji Koyamada. “Distributed Particle-based Rendering Framework for Large Data Visualization on HPC Environments” In: *The 2017 International Conference on High Performance Computing & Simulation (HPCS 2017)*, Genoa, Italy, 2017.
[5] Jorji Nonaka, Naohisa Sakamoto, Yasumitsu Maejima, Kenji Ono, Koji Koyamada. “A Visual Causal Exploration Framework / Case Study: A Torrential Rain and a Flash Flood in Kobe City”. In: *ACM SIGGRAPH Asia 2017 Symposium on Visualization*, Bangkok, Thailand, 2017.

[6] Kengo Hayashi, Takashi Shimizu, Naohisa Sakamoto, Jorji Nonaka."Parallel Particle-based Volume Rendering using Adaptive Particle Size Adjustment Technique". In: *ACM SIGGRAPH Asia 2017 Symposium on Visualization*, Bangkok, Thailand, 2017.
[7] Jorji Nonaka, Motohiko Matsuda, Takashi Shimizu, Naohisa Sakamoto, Masahiro Fujita, Keiji Onishi, Eduardo Camilo Inacio, Shun Ito, Fumiyoshi Shoji, Kenji Ono. "A Study on Open Source Software for Large-Scale Data Visualization on SPARC64fx based HPC Systems". In: *International Conference on High Performance Computing in Asia-Pacific Region (HPC Asia 2018)*, Tokyo, Japan, 2017.
[8] Eduardo Camilo Inacio, Jorji Nonaka, Kenji Ono, Mario Antonio Ribeiro Dantas. "Analyzing the I/O Performance of Post-Hoc Visualization of Huge Simulation Datasets on the K Computer". In: *XVIII Brazilian Symposium on High Performance Computational Systems*, Sao Paulo, Brazil, 2017.
[9] Kazunori Mikami, Kenji Ono. "Performance Measurement and Performance Visualization Method using PMlib (in Japanese)". IPSJ-SIG on HPC, Ehime, Japan, 2017.

15.3.3 Oral Talks and Posters

[10] Jorji Nonaka, Kenji Ono, Tomohiro Kawanabe. "TDW-based Visualization using HIVE-ChOWDER (Oral Talk)". *NIFS (National Institute for Fusion Science) Research Meetings for Advanced Visualization Technique*, Toki, Japan, 2017.
[11] Kengo Hayashi, Yoshiaki Yamaoka, Naohisa Sakamoto, Jorji Nonaka. "Parallel Particle-based Volume Rendering with 234Compositor for Large-Scale Unstructured Volume Data Visualization (Poster)". *The 8th AICS International Symposium 2018*, Kobe, Japan, 2018.
[12] Kazuki Koiso, Naohisa Sakamoto, Jorji Nonaka, Fumiyoshi Shoji. "Development of a Visual System for Failure Analysis using HPC Log Data (Poster)". *The 1st Visualization Workshop*, Yokohama, Japan, 2018.
[13] Yoshiaki Yamaoka, Kengo Hayashi, Naohisa Sakamoto, Jorji Nonaka. "Parallel Particle Based Volume Rendering using 234Compositor (Poster)". *The 1st Visualization Workshop*, Yokohama, Japan, 2018.
[14] Yusuke Imoto, Daisuke Tagami, Mitsuteru Asai, Yoshitaka Watanabe, Kenji Ono, Naoto Mitsume, Daisuke Nishiura, Jorji Nonaka. "Accuracy Improvement of the Particle-based Method and its Application to Large Scale Fluid Simulator (Poster)". *The 9th JHPCN Symposium, Joint Usage/Research Center for Interdisciplinary Large-Scale Information Infrastructures.* Tokyo, Japan, 2017.

15.3.4 Deliverables

[15] *HIVE (Heterogeneously Integrated Visual-analytics Environment).* http:// avr-aics-riken.github.io/HIVE
[16] *ChOWDER (Cooperative Work Driver).* https://github.com/SIPupstream Design/ChOWDER
[17] *PMlib (Performance Monitoring Library).* http://avr-aics-riken.github.io/PMlib
[18] *CDMlib (Cartesian Data Management Library).* http://avr-aics-riken.github.io/CDMlib
[19] *Cutlib (Cut Information Library).* https://github.com/avr-aics-riken/Cutlib
[20] *PDMlib (Particle Data Management Library).* http://avr-aics-riken.github.io/PDMlib
[21] *HDMlib (Hierarchical Data Management Library).* https://github.com/avr-aics-riken/HDMlib
[22] *UDMlib (Unstructured Data Management Library).* http://avr-aics-riken.github.io/UDMlib
[23] *Polylib (Polygon Management Library).* http://avr-aics-riken.github.io/Polylib
[24] *TPLib (Text Parser Library).* http://avr-aics-riken.github.io/TextParser
[25] *V-Isio (VCAD Visualizer).* http://avr-aics-riken.github.io/V-Isio
[26] *FFVC (FrontFlow Violet Cartesian).* http://avr-aics-riken.github.io/ffvc_package
[27] *LPTlib (Lagrangian Particle Tracking Library).* http://avr-aics-riken.github.io/LPTlib
[28] *JHPCN-DF (Jointed Hierarchical Precision Compression Number - Data Format).*
http://avr-aics-riken.github.io/JHPCN-DF

Chapter 16

Data Assimilation Research Team

16.1 Members

Takemasa Miyoshi (Team Leader)

Koji Terasaki (Research Scientist)

Shigenori Otsuka (Research Scientist)

Shunji Kotsuki (Research Scientist)

Keiichi Kondo (Postdoctoral Researcher)

Guo-Yuan Lien (Postdoctoral Researcher)

Takumi Honda (Postdoctoral Researcher)

Atsushi Okazaki (Postdoctoral Researcher)

Toshiki Teramura (Postdoctoral Researcher)

Kohei Tatakama (Postdoctoral Researcher)

James Taylor (Postdoctoral Researcher)

Yasumitsu Maejima (Research Associate)

Hazuki Arakida (Technical Staff)

Taeka Awazu (Technical Staff)

Hideyuki Sakamoto (Technical Staff)

Marimo Ohhigashi (Technical Staff)

Shinichiro Shima (Visiting Scientist)

Juan J. Ruiz (Visiting Scientist)

Shu-Chih Yang (Visiting Scientist)

Stephen G. Penny (Visiting Scientist)

Kozo Okamoto (Visiting Scientist)

Michiko Otsuka (Visiting Scientist)

Yohei Sawada (Visiting Scientist)

Shohei Takino (Visiting Scientist)

Kenta Kurosawa (Research Assistant)

Cheng Da (Intern)

Krishnamoorthy Chandramouli (Intern)

Paula Maldonado (Intern)

Sam Hatfield (Intern)

Taiga Shibata (Intern)

Takuya Ganeko (Intern)

Takuya Kurihana (Intern)

Stefan Geiss (Student Trainee)

Yukie Komori (Assistant)

Rie Deguchi (Assistant)

Kuki Kuniya (Assistant)

Ayumi Kikawa (Assistant)

Hitomi Mori (Assistant)

16.2 Research Activities

Data Assimilation Research Team (DA Team) was launched in October 2012 and is composed of 23 research and technical staff including 8 visiting members as of March 2018. Data assimilation is a cross-disciplinary science to synergize computer simulations and real-world data, using statistical methods and applied mathematics. As computers become more powerful and enable more precise simulations, it will become more important to compare the simulations with actual observations. DA Team performs cutting-edge research and development on advanced data assimilation methods and their wide applications, aiming to integrate computer simulations and real-world data in the wisest way. Particularly, DA Team tackles challenging problems of developing efficient and accurate data assimilation systems for "big simulations" with real-world "big data" from various sources including advanced sensors. The specific foci include 1) theoretical and algorithmic developments for efficient and accurate data assimilation, 2) data assimilation methods and applications by taking advantage of the world-leading K computer and "big data" from new advanced sensors, and 3) exploratory new applications of data assimilation in wider simulation fields. These advanced data assimilation studies will enhance simulation capabilities and lead to a better use of the K computer.

In FY2017, we continued on the ongoing data assimilation research in the following aspects: 1) theoretical research on challenging problems, 2) leading research on meteorological applications, 3) optimization of computational algorithms, and 4) exploratory research on wider applications. We also explored close collaborations with several research teams within the AICS Research Division. We have made substantial progress on the following research items:

Theoretical research

- Non-Gaussian PDF in DA was investigated using the Lorenz-63 3 variable model.
- The observation error correlation was investigated with the Lorenz96 model. Reconditioning of observation error covariance matrix was introduced.
- A particle filter was applied to the cellular automaton of 3 state sheep model.
- Impact of assimilation order of the serial EnSRF was investigated (1 paper published).

Leading research on meteorological applications

- The development work of the SCALE-LETKF data assimilation system, which consists of SCALE (Scalable Computing for Advanced Library and Environment) and LETKF (Local Ensemble Transform Kalman Filter), was continued. New functions including the random additive noises, online-nested domain LETKF, and improved observation departure diagnostics were implemented. The computational speed was also continued to be improved.
- The study on the assimilation of Phased Array Weather Radar (PAWR) data with the SCALE-LETKF was continued. A new convective rainfall case on July 16, 2017 was conducted, with which the impacts of assimilation intervals, random additive noises, and a deterministic analysis member on the forecast skill were studied.
- A system to assimilate observations by two PAWRs simultaneously has been investigated.
- Weather radar observations from an Argentinian operational radar were assimilated by using the SCALE-LETKF system.
- Himawari-8 satellite all-sky infrared radiance observations were assimilated with SCALE-LETKF. Case studies on Typhoon Soudelor (2015) and the Kanto-Tohoku rainfall event were conducted (2 papers published).
- Himawari-8 satellite all-sky infrared radiances were assimilated in a typhoon-induced heavy precipitation event in Japan.
- A series of experiments on the Kanto-Tohoku heavy rain event in September 2015 was conducted with the SCALE-LETKF. Various observations including Himawari-8 infrared images and dense surface observations provided by NTT DoCoMo were assimilated. River discharge simulations using the SCALE-LETKF precipitation forecasts were conducted.
- Experiments with NHM-LETKF were conducted to investigate an impact of assimilating Himawari-8 observations on detecting a local severe storm at an early stage of its development.
- An ocean mixed layer model was implemented into SCALE-LETKF to investigate the role of flow-dependent sea surface temperature perturbations in the atmospheric DA system.
- The 3D precipitation nowcasting system with PAWR was operated in real time. Forecasts were disseminated via a smartphone application in collaboration with MTI Ltd. (press release on 4 July 2017).
- The 30-second-update 100-m-mesh DA experiments on a sudden local rainfall event on September 11, 2014 were performed with NHM-LETKF (1 paper published).
- A DA system for Advanced Microwave Sounding Unit (AMSU)-A radiance data was developed with Nonhydrostatic Icosahedral Atmospheric Model (NICAM)-LETKF (1 paper published).
- A new adaptive covariance inflation method was developed and applied to the NICAM-LETKF system (1 paper published).
- An ensemble-based model parameter estimation was investigated with NICAM-LETKF.
- A high resolution NICAM-LETKF was developed to assimilate dual frequency precipitation radar (DPR) of global precipitation measurement (GPM) core satellite.
- The heavy ice precipitation flag of the GPM/DPR was compared with the 3.5-km-resolution NICAM simulations.
- Including the observation error correlation in DA was investigated with the NICAM-LETKF system. We found that reconditioning the observation error covariance matrix stabilizes the data assimilation and improves the analyses.
- The NICAM-LETKF system was upgraded to assimilate microwave humidity sounder data.
- An impact of each observation in the NICAM-LETKF was investigated with the Ensemble Forecast Sensitivity to Observation (EFSO) method.
- Global precipitation nowcasting with the LETKF has been operated in real time using JAXA's Global Satellite Mapping of Precipitation (GSMaP) (GSMaP RIKEN Nowcast (RNC)). Forecast data in the past two years were analyzed.
- A precipitation forecasting system which merges forecasts by NWP and nowcast has been developed.
- A DA method for dense precipitation radar data was investigated with SCALE-LETKF.
- Non-Gaussian statistics in global atmospheric dynamics were investigated with a 10240-member ensemble Kalman filter using an intermediate AGCM.
- An object-based verification method of precipitation pattern was investigated using pattern recognition techniques.
- An LETKF system to assimilate pattern features of precipitation areas was implemented with an intermediate AGCM.

- An atmosphere-river coupled DA system was developed with NHM-LETKF and a river discharge model. An OSSE assimilating river discharge observation showed a positive impact on the atmospheric variables (1 paper published).
- A prototype of dam operation optimization system was developed with the machine learning in collaboration with Tokyo Electric Power Company Holdings, Incorporated.
- A land-atmosphere-coupled DA system was developed.
- A new methodology to accelerate development of a new observation system was proposed using the ensemble forecast sensitivity to observations (EFSO) with a global numerical weather prediction system (1 paper published).

Computational optimization

- The computational performance of the "Big Data Assimilation" problem with the SCALE-LETKF was improved.
- We started incorporating the Data Transfer Framework (DTF) developed by System Software Research Team into the SCALE-LETKF system to enable the real-time "Big Data Assimilation" experiments.
- A tree-based geographical search algorithm in LETKF was implemented in collaboration with Prof. Hideyuki Kawashima's group in the University of Tsukuba. The algorithm was implemented with the SCALE-LETKF and SPEEDY-LETKF.

Wider applications

- A particle filter was applied to a dynamical vegetation model known as the SEIB-DGVM (Spatially-Explicit, Individual-Based Dynamic Global Vegetation Model). Uncertainties in the state variables and the parameters were greatly reduced by assimilating satellite-based Leaf Area Index (1 paper published).
- The SEIB-DGVM DA system was applied to a wider region in the northeastern Eurasia to estimate spatially-varying vegetation parameters.
- The SEIB-DGVM DA system was applied to a deciduous broad-leaved forest in Japan to optimize leaf area index and the related variables.
- Feasibility of applying the SEIB-DGVM DA system to vegetation management was investigated toward the sustainable development goals (SDGs).
- A DA method for time-averaged data was investigated with SPEEDY-LETKF for paleoclimate reconstruction.
- A feasibility of predicting coastal ocean environments was investigated using a regional ocean model (ROMS).

Several achievements are selected and highlighted in the next section.

16.3 Research Results and Achievements

16.3.1 Himawari-8 satellite "Big Data Assimilation" for typhoon and heavy-rainfall prediction

Weather prediction models attempt to predict future weather by running simulations based on current conditions taken from various sources of data. However, the inherently complex nature of the systems, coupled with the lack of precision and timeliness of the data, makes it difficult to conduct accurate predictions, especially with weather systems such as sudden precipitation. As a means to improve models, we are using powerful supercomputers to run simulations based on more frequently updated and accurate data. We decided to work with data from Himawari-8, a geostationary satellite that began operating in 2015. Its instruments can scan the entire area it covers every ten minutes in both visible and infrared light, at a resolution of up to 500 meters, and the data is provided to meteorological agencies. Infrared measurements are useful for indirectly gauging rainfall, as they make it possible to see where clouds are located and at what altitude.

For one study, we looked at the behavior of Typhoon Soudelor (known in the Philippines as Hanna), a category 5 storm that wreaked damage in the Pacific region in late July and early August 2015. In a second study, we investigated the use of the improved data on predictions of heavy rainfall that occurred in the Kanto region of Japan in September 2015. These articles were published in Monthly Weather Review and Journal of Geophysical Research: Atmospheres. For the study on Typhoon Soudelor, we adopted a recently

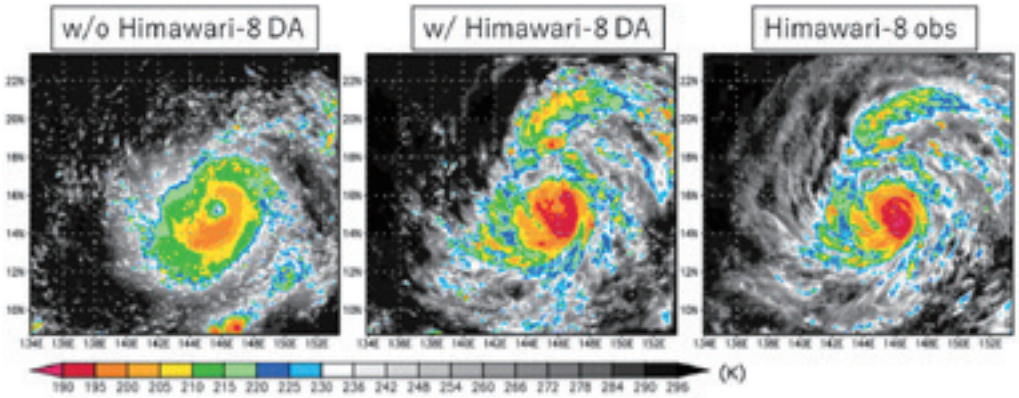

Figure 16.1: Himawari-8 band 13 (10.4 μm) brightness temperature analyses (K) for DA experiments (left) without and (middle) with Himawari-8, and (right) corresponding Himawari-8 observation.

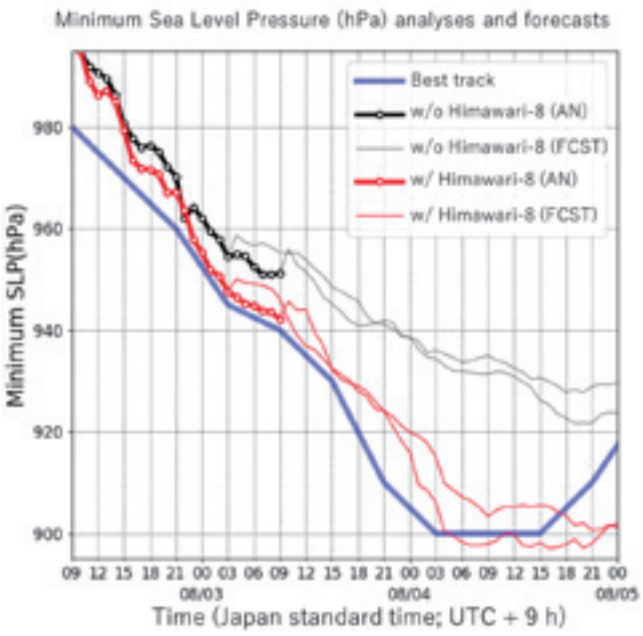

Figure 16.2: Analyses (thick) and forecasts (thin) of minimum sea level pressure of Typhoon Soudelor. Red and black curves correspond to the experiments with and without Himawari-8 DA, respectively. Blue curve shows the JMA best track analysis.

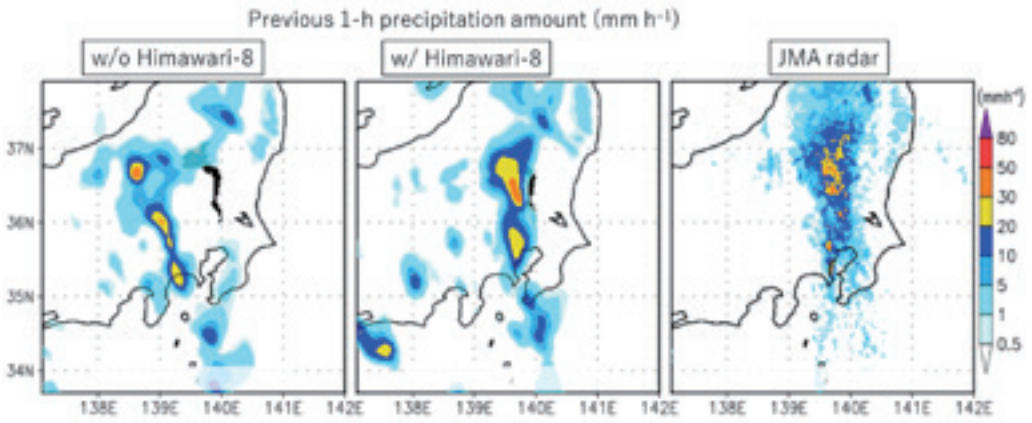

Figure 16.3: Horizontal maps of 12-hour forecast precipitation (mm h^1, previous 1-hour accumulation) for the experiments (left) without and (middle) with Himawari-8 DA, and (c) corresponding JMA radar estimate.

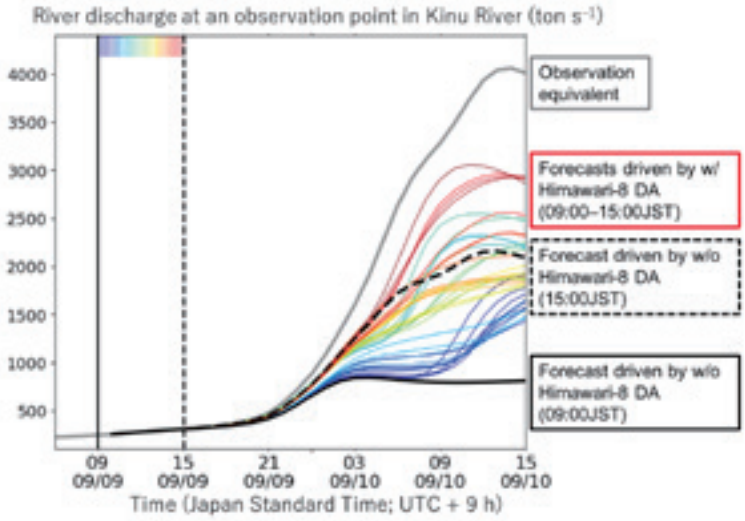

Figure 16.4: River discharge forecasts driven by the rainfall inputs from the experiments with and without Himawari-8 DA. Black curves show the forecasts without Himawari-8 DA, initiated at 0900 JST (solid) and 1500 JST (dashed). Colored curves show the forecasts with Himawari-8 DA, where warmer colors indicate a later initial time corresponding the colors shown at the top between 0900 JST and 1500 JST. Gray curve corresponds to the observed river discharge.

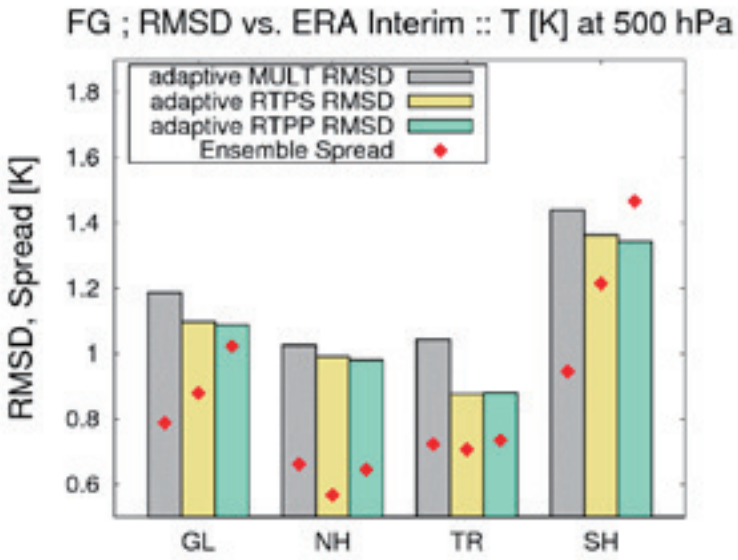

Figure 16.5: Time-mean background root mean square differences (RMSDs) and ensemble spreads of temperature (K) at 500 hPa relative to the ERA Interim reanalysis for the global (GL), Northern Hemisphere (NH), tropics (TR), and Southern Hemisphere (SH) domains, averaged over a month in August 2014. Grey, yellow, and green bars show the RMSDs of adaptive-MULT, adaptive-RTPS, and adaptive-RTPP, respectively. Red dots indicate the ensemble spreads. Adopted from Kotsuki et al. (2017, QJRMS).

developed weather model called SCALE-LETKF—running an ensemble of 50 simulations—and incorporated infrared measurements from the satellite every ten minutes, comparing the performance of the model against the actual data from the 2015 tropical storm. We found that compared to models not using the assimilated data, the new simulation more accurately forecast the rapid development of the storm (Figs. 16.1 and 16.2). We tried assimilating data at a slower speed, updating the model every 30 minutes rather than ten minutes, and the model did not perform as well, indicating that the frequency of the assimilation is an important element of the improvement.

To perform the research on disastrous precipitation, we examined data from heavy rainfall that occurred in the Kanto region in 2015. Compared to models without data assimilation from the Himawari-8 satellite, the simulations more accurately predicted the heavy, concentrated rain that took place, and came closer to predicting the situation where an overflowing river led to severe flooding (Fig. 16.3). With every-10-minute Himawari-8 DA, we can refresh precipitation and river discharge forecasts every 10 minutes, i.e., 36 times in 6 hours (Fig. 16.4). The every-10-minute refresh can provide warning information at an earlier time; having a longer lead time by even 10 minutes may save lives. We plan to apply this new method to other weather events to make sure that the results are truly robust. This research result was highlighted by RINEK Press Release on 18 January 2018 (`http://www.riken.jp/en/pr/press/2018/20180118_1/`).

16.3.2 Improving the error covariance inflation approach in NICAM-LETKF

Covariance relaxation is a widely-used inflation technique, which plays an essential role in the ensemble Kalman filter because the ensemble-based error variance is usually underestimated mainly due to limited ensemble size and model imperfections. To avoid computationally-expensive manual tuning of the relaxation parameter, this study pioneers to propose adaptive covariance relaxation (ACR) approaches based on Desroziers' innovation statistics (2005, QJRMS). Two ACR methods are implemented: relaxation to prior spread based on Ying and Zhang (2015, QJRMS), and relaxation to prior perturbations. We conduct a series of experiments in the real-world global atmosphere with both conventional observations and satellite radiances for the first time.

The results demonstrate that the proposed ACR approaches provide nearly optimal relaxation parameter values and improve the analyses and forecasts compared to a baseline control experiment with an adaptive multiplicative inflation method (Fig. 16.5). The adaptive relaxation methods are turned out to be robust to changes in the observing networks and observation error settings. We mathematically show that the innovation statistics for the analysis error covariance (a-minus-b o-minus-a statistics are more robust than those for the

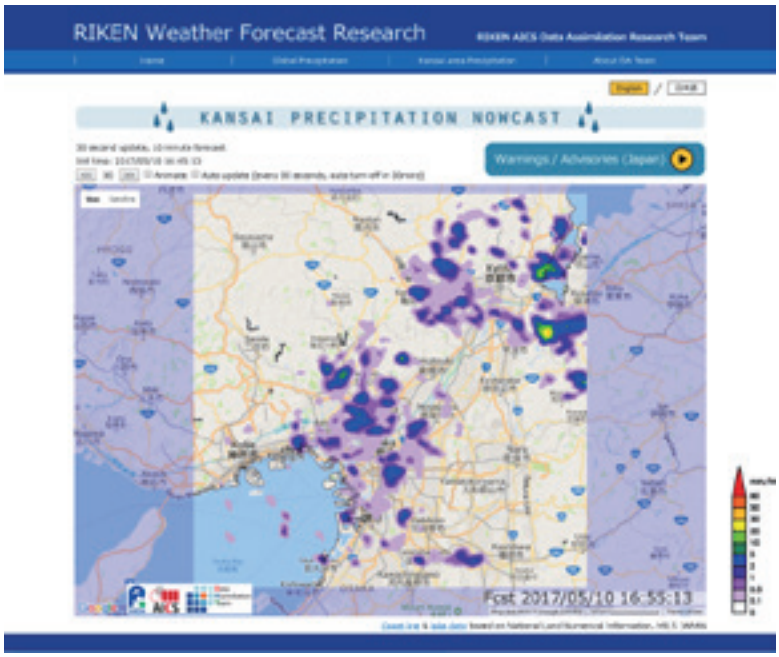

Figure 16.6: A screenshot of the weather prediction website.

background error covariance (o-minus-b o-minus-b or a-minus-b o-minus-a statistics) if the observation and background error variances are imperfect.

16.3.3 Phased-Array Weather Radar 3D Nowcast

Today, nowcasting—a term that refers to short-term weather forecasts made in real-time—is generally done using parabolic radar antennas, which take five to ten minutes to scan about 15 layers of the entire sky. Typically, it is done by looking at a single layer of the sky, detecting the rain there, and then extrapolating from weather conditions where the rain will be falling at a later time. However, though nowcasting requires much less computing power than weather simulations, it is not able to accurately predict rainfall from rapidly developing thunderclouds, where there are rapid vertical movements in the rain patterns. Recently, however, a novel type of system, called a phased-array radar, was installed on the Suita Campus of Osaka University. The radar can be targeted very quickly—it can scan the entire sky in ten to thirty seconds, looking at approximately 100 angles with a range of 60 kilometers. The radar can be precisely targeted by manipulating the beams emitted by a number of devices, allowing a flat radar to scan the whole sky very rapidly.

In an effort to improve the forecasting capability of the radar, we developed an algorithm that takes the enormous amount of observational data from the radar, updated every 30 seconds, and makes rapid forecasts based on the 3D rain data. This allows the extremely frequent and accurate forecasts to be made. The forecasts, which cover the Kansai (Osaka, Kyoto and Kobe) area of Japan, are available online at: `https://weather.riken.jp/` (Figs. 16.6 and 16.7). As part of the effort to make the system practical, we are collaborating with an app designer that offers weather forecasting apps to smartphone users (see `http://www.aics.riken.jp/en/topics/170324.html`). We also look forward to collaborating with other phased-array radar facilities to provide forecasts for a more widespread area. This research result was highlighted by RINEK Press Release on 4 July 2017 (`http://www.riken.jp/en/pr/press/2017/20170704_1/`).

16.4 Schedule and Future Plan

In FY2017, DA team had three additional full-time research staff. We have been working on various aspects of DA including theoretical problems, meteorological applications, and wider applications. We continued working on the prototype system of “Big Data Assimilation” (BDA). In FY2017, we obtained promising results for the Himawari-8 satellite radiance assimilation. In addition, the computational speed of the phased-array weather radar assimilation was also improved. Although it is still not sufficient to run the BDA system in real time on

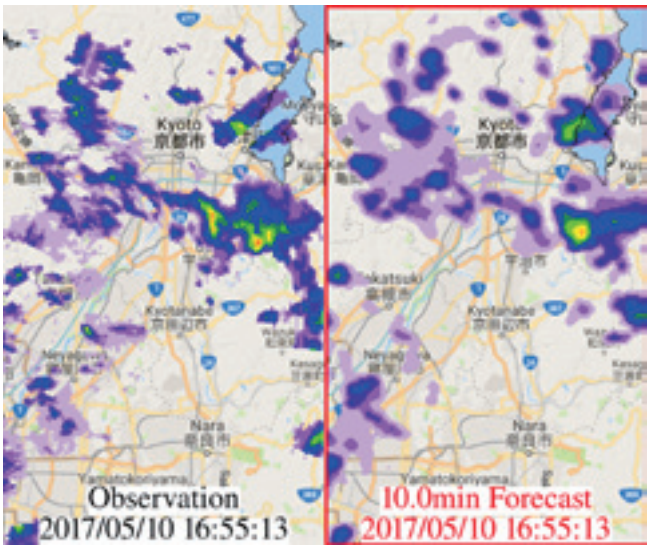

Figure 16.7: Prediction made ten minutes earlier (right) versus the actual rainfall (left).

the K computer, we will continue the effort to make it fast enough for the real-time computation in FY2018. We will also continue improving the physical performance of the 30-minute prediction.

Beyond the direct future of the BDA effort, we can extend the idea of BDA to a broader perspective: integration of "Big Data" and "Big Simulation." New sensors provide orders of magnitude more data, and simulations become more precise. Collaborative work with computer scientists will be essential to utilize the complex high-performance computer system effectively. In addition, dense sensor data tend to have correlated errors, and the proper treatment is necessary to fully utilize the "Big Data." The current DA methods commonly assume no correlation in the observation errors. Based on our previous theoretical research on the observation-error correlations, we are developing methods to consider the observation error correlations in realistic NWP applications. This is also relevant to satellite data assimilation. The current NWP systems use only a small fraction of available data partly because of the observation error correlations.

Treating the model errors and non-Gaussian probability distribution has been grand challenges in DA. Big Ensemble Data Assimilation with the largest-ever 10,240 samples was a milestone providing fundamental data to investigate the non-Gaussian probability distribution. We have developed expertise and exclusive dataset to tackle these challenges.

For further enhancing our research activities, collaborations with other AICS (R-CCS) teams, RIKEN-wide partners (iTHEMS, RIKEN Engineering Network), MOU partners (University of Maryland, University of Reading), domestic and international research partners (NICT, Tokyo Metropolitan University, JMA, Meteorological Satellite Center, Meteorological Research Institute, Kyoto University, Argentinean National Meteorological Service, University of Buenos Aires, Barcelona Supercomputing Center, LMU Munich , University of Tokyo, Taiwan National Central University, Pennsylvania State University, JAXA, JAMSTEC, Tokyo Institute of Technology, University of Tsukuba, Ritsumeikan University, Institut Mines-Télécom-Atlantique), and industry partners (Tokyo Electric Power Company Holdings, Incorporated, Meisei Electric Co., Ltd., MTI Ltd.) will be the key to success. We will continue expanding our collaborative activities further.

In FY2017, we continued the "DA innovation hub" project to expand our activity to wider fields and to attract more people in experimental, computational, and theoretical sciences. We organized the RIKEN DA Workshop, RIKEN DA Camp, RIKEN International School on Data Assimilation (RISDA2018), and the RIKEN Uncertainty Quantification Workshop. In addition, we awarded the DA fund to five RIKEN researchers in various fields (biology, medical science, brain science, and engineering) to seek for new DA applications. In FY2018, we will continue seeking for new collaborations and seeds of new DA applications.

16.5 Publications

16.5.1 Awards

[1] The Most Cited Paper Award 2017 by Japan Geoscience Union. Satoh, M., H. Tomita, H. Yashiro, H. Miura, C. Kodama, T. Seiki, A. Noda, Y. Yamada, D. Goto, M. Sawada, T. Miyoshi, Y. Niwa, M. Hara, T. Ohno, S. Iga, T. Arakawa, T. Inoue, and H. Kubokawa, 2014: The non-hydrostatic icosahedral atmospheric model: description and development. Progress in Earth and Planetary Science, 1:18. doi:10.1186/s40645-014-0018-1, 18 April 2017.

[2] The 9th RIKEN Research Incentive Award, Takumi Honda, Improvement of Typhoon and heavy rainfall predictions by assimilating radiance observations from a new generation satellite "Himawari-8," 15 March 2018.

[3] RIKEN R&D performance incentives, Takemasa Miyoshi, Research to connect Data Assimilation and Simulation, 30 March 2018.

16.5.2 Articles

[1] Okazaki, A. and K. Yoshimura, 2017: Development and evaluation of a system of proxy data assimilation for paleoclimate reconstruction. *Clim. Past*, **13**, 379–393, doi:10.5194/cp-13-379-2017.

[2] Okamoto, K., 2017: Evaluation of IR radiance simulation for all-sky assimilation of Himawari-8/AHI in a mesoscale NWP system. *Quart. J. Roy. Meteorol. Soc.*, **143**, 1517–1527, doi:10.1002/qj.3022.

[3] Kotsuki S., Y. Ota, and T. Miyoshi, 2017: Adaptive covariance relaxation methods for ensemble data assimilation: Experiments in the real atmosphere. *Quart. J. Roy. Meteorol. Soc.*, **143**, 2001–2015, doi: 10.1002/qj.3060.

[4] Getirana, A., A. Boone, C. Peugeot, and ALMIP2 Working Group (Full List in Appendix), 2017: Streamflows over a West African basin from the ALMIP-2 model ensemble. *J. Hydrometeorol.*, **18**, 1831–1845, doi:10.1175/JHM-D-16-0233.1.

[5] Grippa, M., L. Kergoat, A. Boone, C. Peugeot, J. Demarty, B. Cappelaere, L. Gal, P. Hiernaux, E. Mougin, A. Ducharne, E. Dutra, M. Anderson, C. Hain, and ALMIP2 Working Group (Full List in Appendix), 2017: Modelling surface runoff and water fluxes over contrasted soils in pastoral Sahel: evaluation of the ALMIP2 land surface models over the Gourma region in Mali. *J. Hydrometeorol.*, **18**, 1847–1866, doi:10.1175/JHM-D-16-0170.1.

[6] Sawada, Y., H. Tsutsui, and T. Koike, 2017: Ground Truth of Passive Microwave Radiative Transfer on Vegetated Land Surfaces. *Remote Sens.*, **9**, 655, doi:10.3390/rs9070655.

[7] Otsuka, S., N. J. Trilaksono, and S. Yoden, 2017: Comparing simulated size distributions of precipitation systems at different model resolution. *SOLA*, **13**, 130–134, doi:10.2151/sola.2017-024.

[8] Sawada, Y., T. Koike, K. Aida, K. Toride, and J. P. Walker, 2017: Fusing microwave and optical satellite observations to simultaneously retrieve surface soil moisture, vegetation water content, and surface soil roughness. *IEEE Trans. Geosci. Remote Sens.*, **55**, 6195–6206, doi: 10.1109/TGRS.2017.2722468.

[9] Hotta, D., T.-C. Chen, E. Kalnay, Y. Ota and T. Miyoshi, 2017: Proactive QC: a fully flow-dependent quality control scheme based on EFSO. *Mon. Wea. Rev.*, **145**, 3331–3354, doi:10.1175/MWR-D-16-0290.1.

[10] Yang, S.-C., S.-H. Chen, K. Kondo, T. Miyoshi, Y.-C. Liou, Y.-L. Teng, and H.-L. Chang, 2017: Multilocalization data assimilation for predicting heavy precipitation associated with a multiscale weather system. *J. Adv. Model. Earth Syst.*, **9**, 1684–1702, doi:10.1002/2017MS001009.

[11] Arakida, H., T. Miyoshi, T. Ise, S.-I. Shima, and S. Kotsuki, 2017: Non-Gaussian data assimilation of satellite-based leaf area index observations with an individual-based dynamic global vegetation model. *Nonlin. Processes Geophys.*, **24**, 553–567, doi:10.5194/npg-24-553-2017.

[12] Maejima, Y, M. Kunii, and T. Miyoshi, 2017: 30-second-Update 100-m-Mesh Data Assimilation Experiments: A Sudden Local Rain Case in Kobe on 11 September 2014, *SOLA*, **13**, 174–180, doi:10.2151/sola.2017-032.

[13] Terasaki, K. and T. Miyoshi, 2017: Assimilating AMSU-A Radiances with the NICAM-LETKF. *J. Meteorol. Soc. Japan*, **95**, 433–446, doi:10.2151/jms.j2017-028.

[14] Hotta, D., E. Kalnay, Y. Ota, and T. Miyoshi, 2017: EFSR: Ensemble Forecast Sensitivity to Observation Error Covariance. *Mon. Wea. Rev.*, **145**, 5015–5031, doi:10.1175/MWR-D-17-0122.1.

[15] Kotsuki S., S. Greybush, T. and Miyoshi, 2017: Can we optimize the assimilation order in the serial ensemble Kalman filter? A study with the Lorenz-96 model. *Mon. Wea. Rev.*, **145**, 4977–4995, doi:10.1175/MWR-D-17-0094.1.

[16] Honda, T., T. Miyoshi, G.-Y. Lien, S. Nishizawa, R. Yoshida, S. A. Adachi, K. Terasaki, K. Okamoto, H. Tomita, and K. Bessho, 2017: Assimilating All-Sky Himawari-8 Satellite Infrared Radiances: A Case of Typhoon Soudelor (2015). *Mon. Wea. Rev.*, **146**, 213–229, doi:10.1175/MWR-D-16-0357.1.

[17] Honda, T., S. Kotsuki, G.-Y. Lien, Y. Maejima, K. Okamoto, and T. Miyoshi, 2018: Assimilation of Himawari-8 all-sky radiances every 10 minutes: Impact on precipitation and flood risk prediction. *J. Geophys. Res. Atmos.*, **123**, 965–976, doi:10.1002/2017JD027096.

[18] Sawada, Y., T. Nakaegawa, and T. Miyoshi, 2018: Hydrometeorology as an inversion problem: Can river discharge observations improve the atmosphere by ensemble data assimilation? *J. Geophys. Res. Atmos.*, **123**, 848–860, doi:10.1002/2017JD027531.

[19] Lien, G.-Y., D. Hotta, E. Kalnay, T. Miyoshi, and T.-C. Chen, 2018: Accelerating assimilation development for new observing systems using EFSO. *Nonlin. Processes Geophys.*, **25**, 129–143, doi:10.5194/npg-25-129-2018.

16.5.3 Invited Talks

[1] Miyoshi, T., Data Assimilation Research at RIKEN: Toward extreme-scale computation, An examination of data assimilation algorithms, observations, and applications in the context of next-generation computing, National Science Foundation, Arlington, VA, USA., 4/7/2017.

[2] Lien, G.-Y., T. Miyoshi, and J. Ruiz, 30-second-cycle LETKF assimilation of phased array weather radar data, JpGU-AGU Joint Meeting 2017, Chiba, 5/20/2017.

[3] Terasaki, K. and T. Miyoshi, Reconditioning the observation error covariance matrix in a local ensemble transform Kalman filter: experiments with Lorenz-96 model, JpGU-AGU Joint Meeting 2017, Chiba, 5/22/2017.

[4] Okazaki, A., K. Yoshimura, and T. Miyoshi, Development and evaluation of isotopic proxy data assimilation system, First workshop of the PAGES working group on Paleoclimate Reanalyses, Data Assimilation and Proxy System modelling (DAPS), Louvain-la-Neuve, Belgium, 5/30/2017.

[5] Lien, G.-Y. and T. Miyoshi, 30-second-cycle LETKF assimilation of phased array weather radar data, South China Sea Science Conference 2017, Kaohsiung, Taiwan, 6/4/2017.

[6] Miyoshi, T., “Big Data Assimilation” for 30-second-update 100-m-mesh Numerical Weather Prediction, Data Science & Environment, Brest, France, 7/6/2017.

[7] 三好建正, “Big Data Assimilation” Revolutionizing Weather Prediction, 金曜日セミナー, 東京大学地震研究所, 東京, 7/14/2017.

[8] 小槻峻司，三好建正: 全球大気アンサンブルデータ同化システム NICAM-LETKF による衛星降水観測データ同化. 地震研特定共同研究 (B)「データ同化」勉強会, 東京大学, 東京, 7/14/2017.

[9] 三好建正, データ同化:シミュレーションと観測をつなぐ, 気象衛星シンポジウム, 東京, 7/22/2017.

[10] Miyoshi, T., Data Assimilation: Integrating model and measurements, South-East Asian School on Tropical Atmospheric Science (SEASTAS), Singapore, 7/24/2017.

[11] Miyoshi, T., “Big data assimilation” for 30-second-update 100-m-mesh numerical weather prediction, The 3rd International Workshop on Extreme Weather in Changing Climate in the Maritime Continent, Singapore, 7/25/2017.

[12] 近藤圭一, 三好建正, ビッグデータ同化研究における研究例、社会実装例、及び事務的支援, 第 7 回関西地域大学研究支援スタッフミーティング, 京都, 8/6/2017.

[13] Miyoshi, T., G.-Y. Lien, M. Kunii, J. Ruiz, Y. Maejima, S. Otsuka, K. Kondo, T. Teramura, H. Seko, S. Satoh, T. Ushio, K. Bessho, K. Kamide, H. Tomita, S. Nishizawa, T. Yamaura, and Y. Ishikawa, "Big Data Assimilation" for 30-second-update 100-m-mesh Numerical Weather Prediction, Asia Oceania Geosciences Society (AOGS) 14th Annual Meeting, Singapore, 8/8/2017.

[14] Miyoshi, T., S. Kotsuki, K. Terasaki, K. Kondo, G.-Y. Lien, M. Satoh, H. Tomita, and E. Kalnay, Enhancing Data Assimilation of GPM Observations, Asia Oceania Geosciences Society (AOGS) 14th Annual Meeting, Singapore, 8/8/2017.

[15] 三好建正, "Data Assimilation Research at RIKEN: Numerical Weather Prediction and Beyond", Atmosphere-ocean Joint Seminar, 東京大学, 東京, 9/11/2017.

[16] Miyoshi, T., "Big Data Assimilation" revolutionizing weather prediction, CREST Big Data Application Symposium, AKIBA Hall, Tokyo, Japan, 9/16/2017.

[17] Lien, G.-Y., Toward an operational high-resolution regional LETKF data assimilation system for a small area: challenges and promises, Taiwan Typhoon and Flood Research Institute, Taipei, Taiwan, 9/22/2017.

[18] Miyoshi, T., "Big Data Assimilation" for 30-second-update 100-m-mesh Numerical Weather Prediction, International Symposium on Earth-Science Challenges 2017, Kyoto, Japan, 10/4/2017.

[19] Keynote: Miyoshi, T., G.-Y. Lien, T. Honda, M. Kunii, J. Ruiz, Y. Maejima, S. Otsuka, K. Kondo, S. Kotsuki, K. Terasaki, T. Teramura, H. Seko, S. Satoh, T. Ushio, K. Bessho, K. Kamide, H. Tomita, S. Nishizawa, T. Yamaura, and Y. Ishikawa, "Big Data Assimilation" Revolutionizing Weather Prediction, ICMCS-XII, Taipei, Taiwan, 10/18/2017.

[20] 三好建正, 天気予報シミュレーションと衛星降水観測を結ぶデータ同化研究の最先端, 平成 29 年度全球降水観測計画（GPM）シンポジウム「宇宙から見る雨〜これまでの 20 年、これからの 20 年〜」, 東京, 11/29/2017.

[21] Lien, G.-Y., T. Miyoshi, and T. Honda, Roles and issues of a high-resolution regional ensemble data assimilation system for a small area, Central Weather Bureau, Taipei, Taiwan, 12/19/2017.

[22] 三好 建正, 「ビッグデータ同化」による天気予報革命, JST・NSF 国際連携シンポジウム, 東京, 12/20/2017.

[23] Miyoshi, T., H. Tomita, S. Satoh, T. Ushio, and Y. Ishikawa, Project Progress Report, CREST International Symposium on Big Data Application, Tokyo, Japan, 1/17/2018.

[24] 小槻峻司, 黒澤賢太, 三好建正: EFSO の現状と惑星気象研究への発展の可能性. 第 19 回惑星圏研究, 東北大学青葉サイエンスホール, 仙台, 2/28/2018.

[25] Miyoshi, T., Advancing Data Assimilation as a Science Hub, Departmental Seminar, AOSC, University of Maryland, MD, USA, 3/15/2018.

[26] Miyoshi, T., Data Assimilation Research at RIKEN, ESSIC Seminar, University of Maryland, MD, USA, 3/15/2018.

[27] Miyoshi, T., Advancing Data Assimilation as a Science Hub, ADAPT seminar, The Pennsylvania State University ADAPT Center, University Park, PA, USA, 3/20/2018.

16.5.4 Oral Presentations

[1] 三好建正, Enhancing Data Assimilation of GPM Observations, NICAM-LETKF and Satellite DA Mtg, 神戸, 4/13/2017.

[2] 寺崎康児, 観測誤差相関を考慮したデータ同化手法の開発, ポスト「京」重点課題 4 サブ課題 A 第 1 回研究連絡会, 東京, 4/17/2017.

[3] Miyoshi, T., G.-Y. Lien, M. Kunii, J. Ruiz, Y. Maejima, S. Otsuka, K. Kondo, H. Seko, S. Satoh, T. Ushio, K. Bessho, K. Kamide, H. Tomita, S. Nishizawa, T. Yamaura, and Y. Ishikawa, "Big Data Assimilation" for 30-second-update 100-m-mesh Numerical Weather Prediction, EGU2017, Vienna, Austria, 4/25/2017.

[4] Kotsuki, S., K. Terasaki, H. Yashiro, H. Tomita, M. Satoh, and T. Miyoshi: Model Parameter Estimation Using Ensemble Data Assimilation: A Case with the Nonhydrostatic Icosahedral Atmospheric Model NICAM and the Global Satellite Mapping of Precipitation Data, EGU 2017, Vienna, Austria, 4/27/2017.

[5] Honda, T., G.-Y. Lien, S. Kotsuki, Y. Maejima, K. Okamoto, and T. Miyoshi, Assimilating All-Sky Himawari-8 Satellite Infrared Radiances: A Case of Heavy Rainfalls and Floods, JpGU-AGU Joint Meeting 2017, Chiba, Japan, 5/20/2017.

[6] Kondo, K., K. Terasaki, and T. Miyoshi, Assimilating satellite radiances without vertical localization using the Local Ensemble Transform Kalman Filter with up to 1280 ensemble members, JpGU-AGU Joint Meeting 2017, Chiba, Japan, 5/20/2017.

[7] Kotsuki, S., K. Terasaki, H. Yashiro, H. Tomita, M. Satoh, and T. Miyoshi: Model Parameter Estimation Using Ensemble Data Assimilation: A Case with the Nonhydrostatic Icosahedral Atmospheric Model NICAM and the Global Satellite Mapping of Precipitation Data, JpGU-AGU Joint Meeting 2017, Chiba, Japan, 5/21/2017.

[8] Okazaki, A., K. Yoshimura, and T. Miyoshi, Application of data assimilation to paleoclimate, JpGU-AGU Joint Meeting 2017, Chiba, Japan, 5/22/2017.

[9] Sawada, Y., T. Nakaegawa, and T. Miyoshi, Potential of assimilating river discharge observations into the atmosphere by strongly coupled data assimilation: Hydrometeorology as an inversion problem, JpGU-AGU Joint Meeting 2017, Chiba, Japan, 5/22/2017.

[10] 荒木田葉月, 小槻峻司, 大塚成徳, 澤田洋平, 三好建正：シベリアの複数地点における動的植生モデル SEIB-DGVM への MODIS LAI のデータ同化. JPGU-AGU Joint Meeting 2017, 千葉, 5/25/2017.

[11] 近藤圭一, 三好建正, アンサンブルデータ同化における鉛直誤差相関の調査, 日本気象学会春季大会, 東京, 5/25/2017.

[12] 大塚成徳, 三好建正, 大東真利茂, 佐藤晋介, 石川裕: フェーズドアレイ気象レーダを用いた三次元降水補外予測のリアルタイム運用実験. 日本気象学会春季大会, 東京, 5/25/2017.

[13] 寺崎康児, 三好建正, 非対角な観測誤差共分散行列の Reconditioning によるデータ同化の安定性について, 日本気象学会春季大会, 東京, 5/25/2017.

[14] 前島康光, G.-Y. Lien, 三好建正, 2015 年 9 月の関東・東北豪雨事例における高密度地上観測のデータ同化実 験, 日本気象学会春季大会, 東京, 5/25/2017.

[15] 小槻峻司, 寺崎康児, 八代尚, 富田浩文, 佐藤正樹, 三好建正, アンサンブルデータ同化を用いた NICAM のモデルパラメータ推定, 日本気象学会春季大会, 東京, 5/25/2017.

[16] 粟津妙華, 大塚成徳, 三好建正, 降水領域の形状特徴による降水予測の検証手法, 日本気象学会春季大会, 東京, 5/25/2017.

[17] 澤田洋平, 岡本幸三, 国井勝, 三好建正, ひまわり 8 号輝度温度データの同化による局地的大雨の再現性向上の試み, 日本気象学会春季大会, 東京, 5/28/2017.

[18] 本田匠, G.-Y. Lien, 小槻峻司, 前島康光, 岡本幸三, 三好建正, ひまわり 8 号輝度温度観測のデータ同化研究: 平成 27 年 9 月関東・東北豪雨事例 (第 2 報), 日本気象学会春季大会, 東京, 5/28/2017.

[19] 大塚成徳, ゲリラ豪雨リアルタイム予測に向けて, CREST 若手研究者合宿研究会, 神戸, 6/3/2017.

[20] Lien, G.-Y., D. Hotta, E. Kalnay, T. Miyoshi, T.-C. Chen, Accelerating assimilation development for new observing systems using Ensemble Forecast Sensitivity to Observation (EFSO), The 2nd Taiwan West Pacific Global Forecast System Development Workshop, Taipei, 6/7/2017.

[21] 小槻峻司，寺崎康児，八代尚，富田浩文, 佐藤正樹, 三好建正: アンサンブルデータ同化を用いた NICAM のモデルパラメータ推定. ポスト「京」重点課題 4 サブ課題 A 第 2 回研究連絡会, 7/10/2017.

[22] Kotsuki, S. and T. Miyoshi: Leading Research on Data Assimilation in Numerical Weather Prediction. AICS CAFE, 7/19/2017.

[23] 寺村俊紀, 三好建正, 乱流ダイナミクスと非線形データ同化手法, RIMS 研究集会 「非一様乱流の数理」, 京都大学数理解析研究所, 7/28/2017.

[24] 小槻峻司, 寺崎康児, 三好建正: NICAM-LETKF を用いた GPM/DPR データ同化実験． モデル衛星連携研 究会, 東京大学, 東京, 8/1/2017.

[25] 三好 建正, Enhancing Data Assimilation of GPM Observations, NICAM-LETKF and Satellite DA Mtg, 神戸, 8/17/2017.

[26] 荒木田葉月： 「1．シミュレーション知識開発セッション」, EN-Sustainable Development Goals の 包括的解決へ向けて？ 第 1 回フィールド巡検ワークショップ, 和光, 8/24/2017.

[27] 三好 建正, シミュレーションと実測データを融合するデータサイエンス, スーパーコンピュータ 京×データサイエンスシンポジウム, 東京, 8/25/2017.

[28] 本田匠, 気象における最新のメソスケールデータ同化, シンポジウム「HPC と IoT ?観測・計測系 IoT と HPC を繋ぐ?」, 福岡, 8/25/2017.

[29] 荒木田葉月, 寺村俊紀, 三好建正：シミュレーションの実際と社会実装への展望 - 和光でのシミュレーションの構想. EN-Sustainable Development Goals の包括的解決へ向けて？ 第 2 回フィールド巡検ワークショップ, 和光, 9/8/2017.

[30] Kondo, K. and T. Miyoshi, Exploring localization for multiscale dynamics and satellite radiances: experiments with real observations using the global nonhydrostatic atmospheric model NICAM, 7th International WMO Symposium on Data Assimilation, Florianópolis, Brazil, 9/11/2017.

[31] Kotsuki S., K. Terasaki, and T. Miyoshi: Ensemble-Based Data Assimilation of GPM/DPR Reflectivity into the Nonhydrostatic Icosahedral Atmospheric Model NICAM. 7th International WMO Symposium on Data Assimilation, Florianópolis, Brazil, 9/12/2017.

[32] Lien, G.-Y., J. Ruiz, and T. Miyoshi, 30-second-cycle LETKF assimilation of phased array weather radar data, 7th International WMO Symposium on Data Assimilation, Florianópolis, Brazil, 9/12/2017.

[33] 寺村俊紀, 三好建正, データ同化における正規分布近似の力学系的評価, 日本物理学会 2017 年秋季大会, 岩手 大学, 9/23/2017.

[34] 荒木田葉月： 「シベリアの複数地点における動的植生モデル SEIB-DGVM への MODIS LAI のデータ同化」, 第 2 回理研データ同化ワークショップ, 神戸, 9/26/2017.

[35] Okazaki, A, K. Yoshimura, and T. Miyoshi, Evaluation of an isotopic proxy data assimilation system, Third Annual LMR Workshop: Climate Dynamics with the Last Millennium Reanalysis, NCAR, Boulder, CO, US, 10/3/2017.

[36] 寺崎康児, 三好建正：NICAM-LETKF の開発と観測誤差相関を考慮したデータ同化について. 理研気象庁ワークショップ, 気象庁, 10/11/2017.

[37] Honda, T., T. Miyoshi, G.-Y. Lien, S. Nishizawa, R. Yoshida, S. A. Adachi, K. Terasaki, K. Okamoto, H. Tomita, and K. Bessho, Assimilating All-Sky Himawari-8 Satellite Infrared Radiances: A Case of Typhoon Soudelor (2015), International Conference on Mesoscale Convective Systems and high impact weather in East Asia (ICMCS) XII, Taipei, Taiwan, 10/18/2017.

[38] 寺崎康児, 三好建正：NICAM-LETKF の開発状況. NICAM 開発者会議, 淡路島, 10/25/2017.

[39] 小槻峻司，寺崎康児，三好建正: NICAM-LETKF を用いた GPM/DPR データ同化実験. 理研シンポジウム 超高解像度大気モデル開発 WS, 淡路, 10/26/2017.

[40] 前島康光, G.-Y. Lien, 三好建正, 高密度地上観測のデータ同化による降水予測改善のプロセス, 日本気象学会 2017 年度秋季大会, 北海道大学, 10/31/2017.

[41] 澤田洋平, 岡本幸三, 国井勝, 三好建正, Running-In-Place 法を用いたひまわり 8 号全天輝度温度データ同化による局地的大雨の予測精度向上の試み, 日本気象学会秋季大会, 札幌, 10/31/2017.

[42] 澤田洋平, 仲江川敏之, 三好建正, 逆問題としての水文気象学：河川-大気強結合アンサンブルデータ同化の試み. 日本気象学会秋季大会, 札幌, 11/1/2017.

[43] 前島康光, G.-Y. Lien, 三好建正, 高密度地上観測のデータ同化による豪雨予測研究の報告, 第 3 回ポスト「京」重点課題 4 研究連絡会, JAMSTEC 横浜研究所, 11/13/2017.

[44] 寺崎康児、K. Chandramouli, 三好建正：MHS の同化と観測誤差相関を考慮したデータ同化研究の進捗. ポスト京重点課題 4 サブ課題 A 研究連絡会, JAMSTEC, 11/13/2017.

[45] 三好 建正, データ同化: シミュレーションと実測データをつなぐデータサイエンス, 理研シンポジウム：第 1 回ものづくりワークショップ：データ駆動型ものづくりの実現に向けて, 和光, 11/20/2017.

[46] 三好 建正, データ同化: シミュレーションと実測データを融合するデータサイエンス, 理研-水産機構 包括連携キックオフワークショップ, 横浜, 11/27/2017.

[47] 三好 建正, NICAM-LETKF による衛星降水観測データ同化, PMM 国内会合, 東京, 11/30/2017.

[48] 三好 建正, Enhancing Data Assimilation of GPM Observations, NICAM-LETKF and Satellite DA Mtg, 神戸, 12/13/2017.

[49] Honda, T., S. Kotsuki, G.-Y. Lien, Y. Maejima, K. Okamoto, and T. Miyoshi, Every-10-minute Refresh of Precipitation and Flood Risk Predictions by Assimilating Himawari-8 All-sky Satellite Radiances, American Geophysics Union Fall meeting, 11-15 Dec. 2017, New Orleans, LA, USA, 12/14/2017.

[50] 小槻峻司，三好建正: 適応型共分散膨張法と EFSO から見るアンサンブル予報初期値への課題. 第 4 回アンサンブルデータ同化摂動に関する研究会, 広島, 12/16/2017.

[51] Lien, G.-Y., T. Miyoshi, and T. Honda, Roles and issues of a high-resolution regional ensemble data assimilation system for a small area, Research Center for Environmental Changes, Academia Sinica, Taipei, Taiwan, 12/18/2017.

[52] 三好 建正, 「ビッグデータ同化」の技術革新の創出によるゲリラ豪雨予測の実証, AIP ネットワークラボ主催　NSF 連携ビッグデータ合同領域会議, 東京, 12/19/2017 (英).

[53] 本田匠, G.-Y. Lien, 小槻峻司, 前島康光, 寺崎康児, 三好建正, 岡本幸三, 別所康太郎, 西澤誠也, 吉田龍二, 足立幸穂, 富田浩文, ひまわり 8 号輝度温度観測のデータ同化研究:豪雨と台風事例 , ポスト「京」重点課題 4 第 2 回成果報告会, 東京, 12/21/2017.

[54] 小槻峻司，寺崎康児，三好建正:全球大気アンサンブルデータ同化システム NICAM-LETKF による衛星降水観測データ同化, ポスト「京」重点課題 4 第 2 回成果報告会, 東京, 12/21/2017.

[55] 三好 建正, データ同化：ゲリラ豪雨予測から異分野連携へ, 第 2 回 MACS コロキウム「数理から生物多様性まで?同時にはめったに聞けないおもろい話?」, 京都, 12/26/2017.

[56] Okazaki, A., T. Miyoshi, K. Yoshimura, and F. Zhang, Exploring online data assimilation for paleoclimate reconstruction using an idealized OSSE framework, Third Symposium on Multi-scale Predictability: Data-model Integration and Uncertainty Quantification for Climate and Earth System Monitoring and Prediction (the 98th Annual Meeting), Austin, TX, US, 1/8/2018.

[57] Miyoshi, T., S. Kotsuki, K. Terasaki, K. Kondo, G.-Y. Lien, K. Kurosawa, M. Satoh, H. Tomita, and E. Kalnay, Enhancing Data Assimilation of GPM Observations, 98th American Meteorological Society Annual Meeting, Austin, Texas, USA, 1/8/2018.

[58] Honda, T., S. Kotsuki, G.-Y. Lien, Y. Maejima, K. Okamoto, and T. Miyoshi, Every-10-minute Refresh of Precipitation and Flood Risk Predictions by Assimilating Himawari-8 All-sky Satellite Radiances, American Meteorological Society Annual Meeting, Austin, Texas, 1/11/2018.

[59] 小槻峻司, 黒澤賢太，三好建正: 全球大気データ同化システム NICAM-LETKF を使った EFSO 観測インパクト推定． 第 8 回データ同化ワークショップ, 明治大学, 中野区, 東京, 1/19/2018.

[60] 前島康光, G.-Y. Lien, 三好建正、平成 27 年関東東北豪雨事例における稠密地上観測データ同化のインパクト, 第 8 回データ同化ワークショップ, 明治大学中野キャンパス, 1/19/2018.

[61] Miyoshi, T., S. Kotsuki, K. Terasaki, K. Kondo, G.-Y. Lien, K. Kurosawa, M. Satoh, H. Tomita, and E. Kalnay, Enhancing Data Assimilation of GPM Observations, 平成 29 年度 地球環境観測ミッション合同 PI 報告会 (PMM)?個別報告?, 東京, 2/5/2018.

[62] 小槻峻司, 黒澤賢太，三好建正: 全球大気データ同化システム NICAM-LETKF を使った EFSO 観測インパクト推定. 第 8 回 理研・京大合同データ同化研究会, 神戸，2018/2/21.

[63] 本田匠, ひまわり 8 号と「京」が拓く 新しい天気予報, ポスト「京」重点課題 4 第 3 回シンポジウム, 東京, 3/1/2018.

[64] Honda, T., S. Kotsuki, G.-Y. Lien, Y. Maejima, K. Okamoto, and T. Miyoshi, Assimilation of Himawari-8 All-Sky Radiances Every 10 Minutes: A Case of the September 2015 Kanto-Tohoku rainfall, 6th International Symposium on Data Assimilation, Ludwig-Maximilians-Universitat, Munich, Germany, 3/5/2018.

[65] Kotsuki, S., K. Terasaki, and T. Miyoshi: Ensemble-Based Data Assimilation of GPM/DPR Reflectivity into the Nonhydrostatic Icosahedral Atmospheric Model NICAM. 6th International Symposium on Data Assimilation, Ludwig-Maximilians-Universitat, Munich, Germany, 3/5/2018.

[66] Miyoshi, T., J. Ruiz, G.-Y. Lien, T. Teramura, Y. Maejima, K. Kondo, and H. Sakamoto, Is 30-second update fast enough for convection-resolving data assimilation?, 6th International Symposium on Data Assimilation, Ludwig-Maximilians-Universitat, Munich, Germany, 3/7/2018.

[67] 本田匠, ひまわり 8 号観測を用いたデータ同化研究, 対流圏・中層大気流体力学研究集会, 福岡, 3/17/2018.

[68] 板橋隆久, 佐藤朗, 高久圭二, 友野大, 川島祥孝, 坂本英之, 合流法によるミューオニック原子の脱励起の観測とその応用, 日本物理学会第 73 回年次大会, 東京理科大学, 3/22/2018.

16.5.5 Poster Presentations

[1] Kondo, K., K. Terasaki, and T. Miyoshi, Assimilating satellite radiances without vertical localization using the Local Ensemble Transform Kalman Filter with up to 1280 ensemble members, 19th EGU General Assembly, EGU2017, 23-28 April, 2017 in Vienna, Austria, 4/27/2017.

[2] Miyoshi, T., J. Ruiz, G.-Y. Lien, T. Teramura, K. Kondo, Y. Maejima, T. Honda, and S. Otsuka, Is 30-second update fast enough for convection-resolving data assimilation?, EGU2017, Vienna, Austria, 4/27/2017.

[3] Okazaki, A., T. Honda, S. Kotsuki, and T. Miyoshi, Data assimilation of dense precipitation radar, JpGU-AGU Joint Meeting 2017, Chiba, Japan, 5/20/2017.

[4] Otsuka, S., S. Kotsuki, and T. Miyoshi: GSMaP RIKEN Nowcast (GSMaP_RNC): an overview, JpGU-AGU Joint Meeting 2017, Chiba, Japan, 5/20/2017.

[5] Terasaki, K., S. Kotsuki, and T. Miyoshi, Two-year analysis experiments with NICAM-LETKF, JpGU-AGU Joint Meeting 2017, Chiba, Japan, 5/20/2017.

[6] Maejima, Y. and T. Miyoshi, Impacts of dense surface observations on predicting torrential rainfalls on September 9, 2015 around Tochigi and Ibaraki prefectures, JpGU-AGU Joint Meeting 2017, Chiba, Japan, 5/20/2017.

[7] Kondo, K. and T. Miyoshi, Multi-scale localization with NICAM-LETKF using real observations, JpGU-AGU Joint Meeting 2017, Chiba, Japan, 5/22/2017.

[8] Lien, G.-Y. and T. Miyoshi, Implicit thinning and localization of dense observation data in the LETKF: A case of phased array weather radar, JpGU-AGU Joint Meeting 2017, Chiba, Japan, 5/22/2017.

[9] 岡淳史, 本田匠, 小槻峻司, 三好建正, 高密度降水レーダ反射強度の観測システムシミュレーション実験, 日本気象学会 2017 年度春季大会, 東京, 5/25/2017.

[10] 近藤圭一, 三好建正, NICAM-LETKF を用いたマルチスケールデータ同化, 日本気象学会 2017 年度春季大会, 東京, 5/26/2017.

[11] Okazaki, A., T. Honda, S. Kotsuki, M. Yamaji, T. Kubota, R. Oki, T. Iguchi, and T. Miyoshi, Simulating a precipitation radar onboard a geostationary satellite, AMS 38th Conference on Radar Meteorology, Chicago, IL, USA, 8/28/2017.

[12] Kotsuki, S., Y. Ota, and T. Miyoshi: Adaptive covariance relaxation methods for ensemble data assimilation based on innovation statistics. 7th International WMO Symposium on Data Assimilation, 9/11/2017.

[13] Kondo, K. and T. Miyoshi, Non-Gaussianity in the atmospheric dynamics revealed with a 10240-member ensemble Kalman filter, WMO DAS2017, Florianópolis, Brazil, 9/11/2017.

[14] 小槻峻司，寺崎康児，八代尚，富田浩文, 佐藤正樹, 三好建正: アンサンブルデータ同化を用いた全球大気モデル NICAM のモデルパラメータ推定. 第 2 回理研データ同化ワークショップ, 9/25/2017.

[15] 本田匠, 小槻峻司, G-Y. Lien, 前島康光, 岡本幸三, 三好建正, ひまわり 8 号全天輝度温度観測の高頻度同化: 降水および洪水リスク予測へのインパクト, 第 2 回理研データ同化ワークショップ, 神戸, 9/25/2017.

[16] 粟津妙華, 大塚成徳, 三好建正: 降水領域の形状特徴量を用いたデータ同化. 第 2 回理研データ同化ワークショップ, 9/25/2017.

[17] 大塚成徳, 小槻峻司, 近藤圭一, 大東真利茂, 石川裕, 三好建正, 佐藤晋介, 牛尾知雄, データ同化を適用したリアルタイム降水ナウキャストシステム, 第 2 回理研データ同化ワークショップ, 9/25/2017.

[18] 寺崎康児, 三好建正 : NICAM-LETKF システムを用いた衛星データ同化. 第 2 回理研データ同化ワークショップ, 9/25/2017.

[19] Takatama, K., T. Miyoshi, J. Kikuchi, and K. Ito: 東京湾の短期赤潮予報に向けて、第 2 回理研データ同化ワークショップ, 9/25/2017.

[20] Otsuka, S., N. J. Trilaksono, and S. Yoden, Comparing observed and simulated size distributions of tropical convective systems, Joint SPARC Dynamics & Observations Workshop, Kyoto, 10/10/2017.

[21] 粟津妙華, 大塚成徳, 三好建正: 降水領域の形状特徴量を用いたデータ同化実験． 日本気象学会 2017 年度秋季大会, 札幌, 10/30/2017.

[22] 三好建正, ゲリラ豪雨予測を目指した「ビッグデータ同化」の研究, 第 4 回「京」を中核とする HPCI システム利用研究課題　成果報告会, 東京, 11/2/2017,

[23] 粟津妙華, 大塚成徳, 三好建正: 気象シミュレーションにおける 衛星画像データ同化への機械学習の応用. 第 20 回情報論的学習理論ワークショップ, 東京、11/8/2017.

[24] Arakida, H., S. Kotsuki, S. Otsuka, Y. Sawada, and T. Miyoshi, Data assimilation experiments with MODIS LAI observations and the dynamic global vegetation model SEIB-DGVM over Siberia, Commemorative workshop for Professor Graham Farquhar, 2017 Kyoto Prize laureate: Modelling Plant Responses to Environmental Factors, Tokyo, 11/17/2017.

[25] Amamiya, K., K. Koizumi, B.-G. Kwon, S.-Y. Chung, K. Takatama, B. S. Brezel, K. Saido, and T. Hiaki, Monitoring on Styrene Oligomer Surround Japan and Diffusion to North West Pacific Ocean, 環境ホルモン学会第 20 回研究発表会, 神戸, 12/11/2017.

[26] 大塚成徳, フェーズドアレイ気象レーダを用いた 3 次元降水ナウキャスト, AIP 若手研究交流会, 東京, 12/19/2017.

[27] 前島康光, G.-Y. Lien, 三好建正, 平成 27 年関東東北豪雨における稠密地上観測データ同化のインパクト, 第 2 回ポスト「京」重点課題 4 成果報告会, 気象庁講堂 12/21/2017.

[28] 三好建正、大塚成徳、寺崎康児、G.-Y. Lien、小槻峻司、本田匠、前島康光、岡崎淳史、坂本英之 : 観測ビッグデータ同化実現に向けた取り組み. ポスト「京」重点課題 4 第 2 回成果報告会、気象庁、12/21/2017.

[29] Awazu, T., S. Otsuka, and T. Miyoshi, Data assimilation using shape features of rainfall areas, The 8th AICS International symposium, RIKEN AICS, Kobe, 2/7/2018.

[30] Maejima, Y., G.-Y. Lien, and T. Miyoshi: Impacts of dense surface observations on predicting a torrential rainfall event on September 9 and 10, 2015 in the east Japan area. The 8th AICS International symposium, RIKEN AICS, Kobe, 2/7/2018.

[31] Lien, G.-Y., D. Hotta, E. Kalnay, T. Miyoshi, and T.-C. Chen, Accelerating assimilation development for new observing systems using EFSO, The 8th AICS International Symposium, Kobe, Japan, 2/7/2018.

[32] Otsuka, S., S. Kotsuki, M. Ohhigashi, Y. Ishikawa, T. Miyoshi, S. Satoh, and T. Ushio, RIKEN precipitation nowcasting systems, The 8th AICS International Symposium, RIKEN AICS, Kobe, Japan, 2/7/2018.

[33] Terasaki, K. and T. Miyoshi, Accounting for the observation error correlation in data assimilation. The 8th AICS International Symposium, RIKEN AICS, Kobe, Japan, 2/7/2018.

[34] Okazaki, A., T. Honda, S. Kotsuki, and T. Miyoshi, Assimilating dense precipitation radar data: a simulation study, The 8th AICS International Symposium, RIKEN AICS, Kobe, Japan, 2/7/2018.

[35] Takatama, K., T. Miyoshi, J. Kikuchi, and K. Ito: Towards a coastal ocean prediction. The 8th AICS International Symposium, RIKEN AICS, Kobe, Japan, 2/7/2018.

[36] Kotsuki, S., K. Kurosawa, and T. Miyoshi: Ensemble Forecast Sensitivity to Observations Verified with Multiple References. The 8th AICS International Symposium, RIKEN AICS, Kobe, Japan, 2/8/2018.

[37] Kotsuki, S., K. Kurosawa, and T. Miyoshi: Ensemble Forecast Sensitivity to Observations Verified with Multiple References. RIKEN International Workshop on Uncertainty Quantification (UQWS), RIKEN AICS, Kobe, Japan, 2/19/2018.

[38] Ohhigashi, M., S. Kotsuki, T. Miyoshi, and S. Takino: Dam Operation Optimization by Machine Learning, RIKEN International Workshop on Uncertainty Quantification (UQWS), RIKEN AICS, Kobe, Japan, 2/19/2018.

[39] Arakida, H., S. Kotsuki, S. Otsuka, Y. Sawada, and T. Miyoshi, Data assimilation experiments with MODIS LAI observations and the dynamic global vegetation model SEIB-DGVM over Siberia, RIKEN International Workshop on Uncertainty Quantification (UQWS), RIKEN AICS, Kobe, Japan, 2/19/2018.

[40] Awazu, T., S. Otsuka, and T. Miyoshi, Data assimilation using shape features of rainfall areas, RIKEN International Workshop on Uncertainty Quantification (UQWS), RIKEN AICS, Kobe, Japan, 2/19/2018.

[41] Takatama, K., T. Miyoshi, J. Kikuchi, and K. Ito: Towards a coastal ocean prediction, RIKEN International Workshop on Uncertainty Quantification (UQWS), RIKEN AICS, Kobe, Japan, 2/19/2018.

[42] Sakamoto, H., T. Teramura, and T. Miyoshi, Non-Gaussian Measure in Gaussian Filtering Problem, RIKEN International Workshop on Uncertainty Quantification (UQWS), RIKEN AICS, Kobe, Japan, 2/19/2018.

[43] Lien, G.-Y. and T. Miyoshi, Issues regarding maintaining ensemble spreads, balance, and high-resolution information in rapid-update-cycle radar data assimilation with the LETKF, 6th International Symposium on Data Assimilation, Munich, Germany, 3/5/2018.

[44] Lien, G.-Y., D. Hotta, E. Kalnay, T. Miyoshi, and T.-C. Chen, Accelerating assimilation development for new observing systems using EFSO, 6th International Symposium on Data Assimilation, Munich, Germany, 3/5/2018.

[45] Kotsuki, S., S. J. Greybush, and T. Miyoshi: On the assimilation order of the serial ensemble Kalman filter: A study with the Lorenz-96 model. 6th International Symposium on Data Assimilation, Ludwig-Maximilians-Universitat, Munich, Germany, 3/5/2018.

[46] Kotsuki, S., K. Kurosawa, and T. Miyoshi: Ensemble Forecast Sensitivity to Observations Verified with Multiple References. 6th International Symposium on Data Assimilation, Ludwig-Maximilians-Universitat, Munich, Germany, 3/5/2018.

[47] Arakida, H., S. Kotsuki, S. Otsuka, Y. Sawada, and T. Miyoshi, Data assimilation experiments with MODIS LAI observations and the dynamic global vegetation model SEIB-DGVM over Siberia, The 65th Annual Meetings of Ecological Society of Japan (ESJ65), Sapporo, 3/17/2018.

Chapter 17

Computational Disaster Mitigation and Reduction Research Team

17.1 Members

Satoru Oishi (Team Leader)

Muneo Hori (Senior Visiting Scientist)

Hideyuki O-tani (Research Scientist)

Jian Chen (Research Scientist)

Kazuki Yamanoi (Postdosctoral Researcher)

Tsuyoshi Ichimura (Visiting Scientist)

Lalith Maddegedara (Visiting Scientist)

Kohei Fujita (Visiting Scientist)

Hiroki Motoyama (Visiting Scientist)

Yasuyuki Nagano (Visiting Scientist)

Tomohide Takeyama(Visiting Scientist)

17.2 Research Activities

Computational Disaster Mitigation and Reduction Research Team is aimed at developing advanced large-scale numerical simulation of natural disasters such as earthquake, tsunami, flood and inundation, for Kobe City and other urban areas in Hyogo Prefecture. Besides for the construction of a sophisticated urban area model and the development of new numerical codes, the team seeks to be a bridge between Science and Local Government for the disaster mitigation and reduction.

From FY2017, Computational Disaster Mitigation and Reduction Research Team started to integrate all kinds of geo hazards, water hazards and related hazards. Demand for natural disaster simulations became increasing because disasters frequently take place. Therefore, we are developing appropriate sets of programs which meet the demand of calculations. Computational Disaster Mitigation and Reduction Research Team is dealing with the following three kinds of research topics.

Urban model development: Research for urban hazards requires urban models which represent structure and shape of cities in numerical form. However, it takes very long time to develop urban models consisting of buildings, foundations and infrastructures like bridges ports and roads. Therefore, it is indispensable to invent methods which automatically construct urban models from exiting data that is basically ill-structured. Computational Disaster Mitigation and Reduction Research Team developed Data Processing Platform (DPP) for

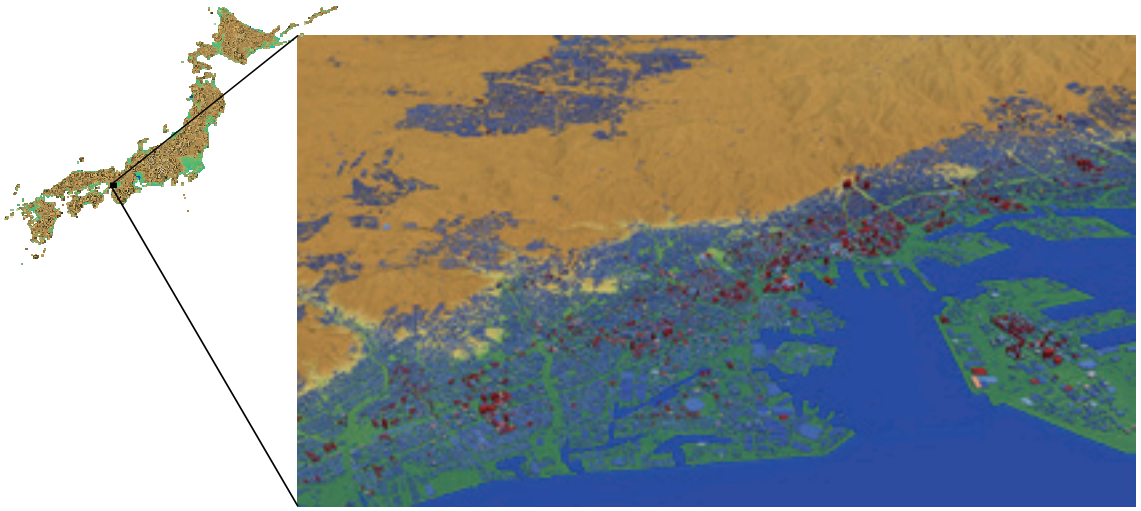

Figure 17.1: The whole Japan model including abount 60,000,000 buildings.

such purpose. By using DPP, construction of a national-wide urban model and 3D model construction from engineering drawings are achieved.
Liquefaction hazard assessment: To rigorously evaluate the quality of liquefaction simulations, and simulations with incremental elasto-plastic models in general, we have developed the method of numerically manufactured solutions (MNMS). This method provides developers and users a quantitative way to examine the accuracy of simulation codes which have implemented elasto-plasticity models for materials. To extend our current liquefaction hazard assessment framework, we have implemented Monte-Carlo (MC) simulations for each single site within a target urban area. This extension allows a prediction with error-bars of liquefaction hazard for urban areas rather than a collection of binary results of deterministic nature. The feasibility of such a prediction for an urban area of target site of the order of 10^4 has been tested.
Water related disaster: Frequency of water disaster has increased. Not only water itself but also sediment cause damage to residents and their assets. Understanding possible hazards is necessary for a measure of precaution and making less damage. Therefore, Computational Disaster Mitigation and Reduction Research Team started to deal with water and sediment related disasters by making numerical simulation model for river basins in Kobe city and Hyogo prefecture.

17.3 Research Results and Achievements

17.3.1 Construction of a National-Wide Urban Model

Large-scale disaster simulations for the purpose of comprehensive disaster mitigation and reduction requires an automation tool which can be used to construct the detailed urban models for target cities. We have been developing such an automation tool, named Data Processing Platform (DPP), so that it can deal with multiple numerical simulations including tsunami inundation and evacuation, and seismic response analysis of ground and buildings [1]. In this fiscal year, we have implemented a MPI-based parallelization of DPP, and have constructed an urban models for the whole Japan which includes about 60,000,000 buildings as shown in Figure 1. This is a first step to realize a national-wide real-time disaster simulation. Now, once given a certain appropriate ground property and motion, a simulation-based assessment of disasters can be achieved for the whole Japan. In addition, we have developed an automation functionality of DPP to conduct pre-ordered disaster simulations. This is also important for a national-wide real-time disaster simulation.

17.3.2 Trial of 3D Model Construction from Engineering Drawings

In the collaborative research project with Hanshin Expressway, we seek to develop a module of DPP to automatically construct a certain 3D model from paper-based engineering drawings so that we can simulate the seismic response of the entire network with high fidelity models. Since paper-based engineering drawings include errors

and lack of information, it is hopeless to perform a robust model construction by merely extracting information from engineering drawings. To tackle with this problem, we have developed a template-based methodology, where a prescribed template of high fidelity models with appropriate internal structures is to be selected and the selected template is to be modified to fit the input engineering drawings. As a trial, we succeeded to construct a 3D shape from a three-view drawing by selecting an appropriate template and fitting it to the three-view drawing.

17.3.3 Improvement of liquefaction hazard assessment

For predicting earthquake-induced hazards, numerical simulations of physical processes are regarded as promising alternatives for conventional empirical correlation based approaches. However, the trustworthy of numerical simulations relies on an assumption that a simulation code in use solves the target mathematical problems correctly with sufficient accuracy. Objective evaluation of a simulation code in a quantitative manner, the so-called code verification, is thus needed. Such evaluation is seldom performed for simulation of liquefaction, either due to the importance and necessity of code verification not yet well-recognized or due to the lack of suitable methodology for soil simulations in general. For verifying the quality of the code we have been using for liquefaction assessment, we proposed and implemented the method of numerically manufactured solutions (MNMS), see Fig. 17.2. Our MNMS is featured by manufacturing numerically a load term used as an input for code verification, which is difficult for conventional methods. Since the manufactured solutions can be specified arbitrarily, as long as they are smooth enough for the target differential equations, this method enable users to access a large number of "benchmark solutions". More details about MNMS refers to our publication [2]. And we are now preparing a manuscript on the application of MNMS for IES-DACSAR-I, the code we used for simulation of liquefaction.

In recent years, we have been developing and improving a numerical simulation based liquefaction hazard assessment code for urban areas[1]. In FY2016, we started to investigate the effect of uncertainties soil properties on the liquefaction assessment using Monte-Carlo (MC) simulations for a single site [2]. In FY2017, we extended the urban-wide liquefaction assessment framework with MC simulations. With this enhancement, it is possible to predict liquefaction hazard with "error-bars" while conventional predictions are only a collection of binary assessment of deterministic nature. As a trail run, for a target urban region with 11151 sites, we constructed 100 models for each site. These models are with different permeability parameters, k, the orders of the value of which follows a normal distribution, see Fig. 17.3 (a). The statistics of the most and the least occurrence of liquefaction are summarized in Fig. 17.3 (b) from the trial run. From the simulation results, it is clear that the variation is large in the the prediction for liquefaction under the same input earthquake wave when taking into account the uncertainties in one kind of soil property. The research results will be presented in the coming ICCM2018 in Rome, Italy as a keynote speech at one of its mini-symposiums.

17.3.4 Development of Distributed Rainfall-Sediment Runoff/Inundation Simulator

In order to evaluate a risk of flood disaster under the influence of sediment production/supply due to landslide disaster, integrated simulator considering both water and sediment runoff and their inundation is required. However, existing 2D rainfall runoff and inundation simulators do not basically consider the sediment transport. On the contrary, existing sediment runoff simulators mainly focus on the small-scale sediment transport such as soil erosion and fine particle transport. Therefore, these simulators are not suitable for evaluating the flood risk under the large scale sediment supply due to landslide. For this reason, we have been started to develop Distributed Rainfall and Sediment Runoff/Inundation Simulator (DRSRIS).

DRSRIS can be characterized as an integrated simulator considering the series of phenomena which occurs in a river catchment related to rainfall runoff and sediment transport shown in Fig. 17.4. In this calculation, 2D underground flow, 2D overland flow, and 2D sediment transport are calculated employing Finite Volume method on orthogonal staggered grid from rainfall distribution, DEM, land use, distribution of sediment supply volumes, and sediment characteristics (e.g. porosity, grain size distribution). To take the different flow characteristics depending on the land use into account, land use is divided into 3 categories (i.e. forest, channel, and city).

[1] Chen, J., Takeyama, T., O-tani, H., Fujita, K. and Hori, M. (2016). "Framework for Assessing Liquefaction Hazard for Urban Areas Based on Soil Dynamics", International Journal of Computational Methods, 13(4), 1641011.

[2] Chen, J., Takeyama, T., O-tani, H., Fujita, K., Motoyama, H. and Hori, M. (2018). "Using High Performance Computing for Liquefaction Hazard Assessment with Statistical Soil Models", International Journal of Computational Methods, Online, 15(2),1840005.

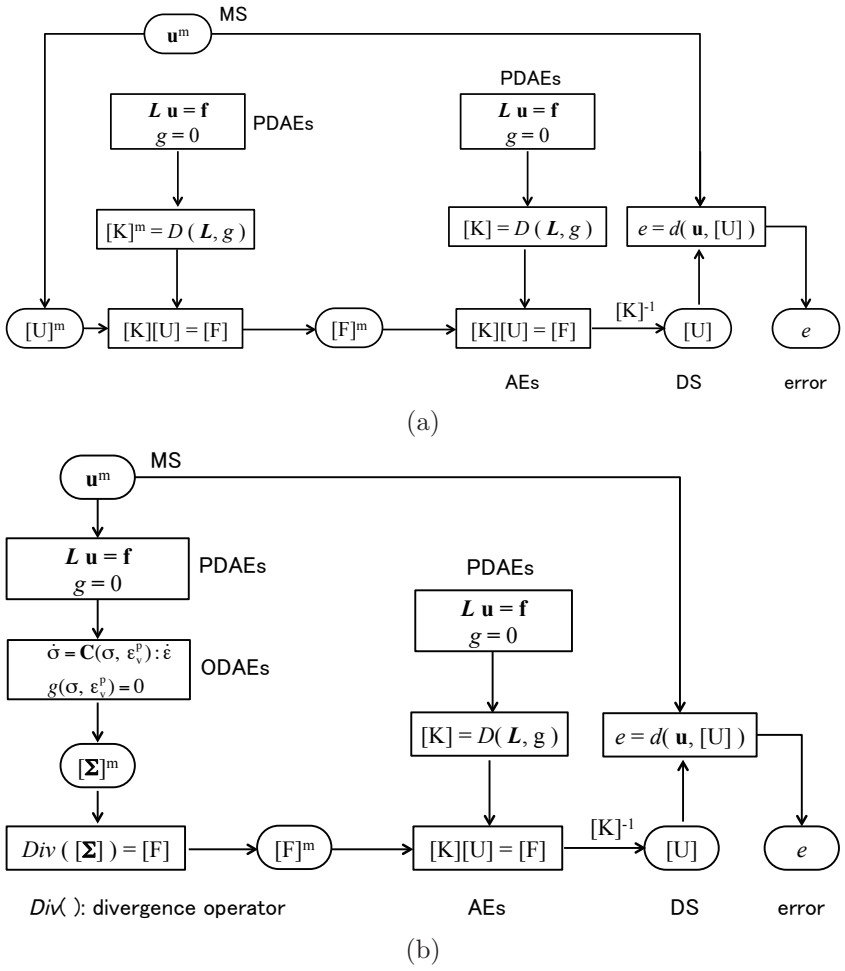

Figure 17.2: The flowcharts of two alternatives of the Method of Numerically Manufacture Solutions (MNMS) we proposed [2]: (a) For a target set of partial differential algebraic equations (PDAEs), MNMS-I manufactures a load term numerically based on the discretized algebraic equations (AEs) from a given manufactured solution (MS), which is compared with the discrete solution (DS) for error measurement. (b) With a given MS, the target PDAEs is converted to a set of ordinary differential algebraic equations (ODAE) which is solved numerically to manufacture a load term for code verification.

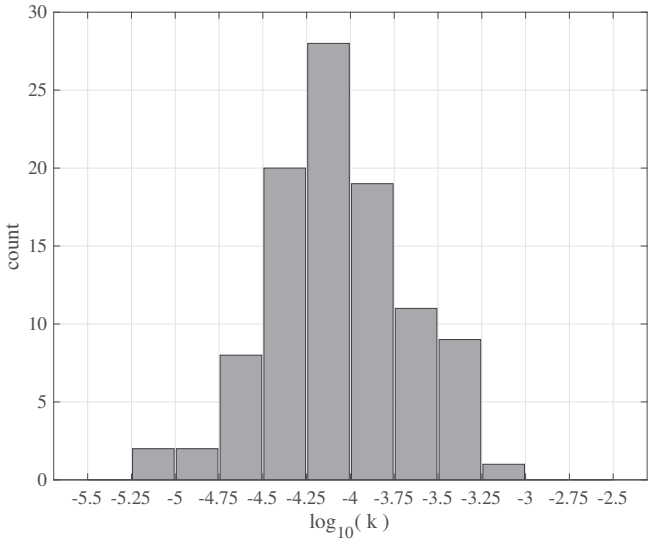

(a)

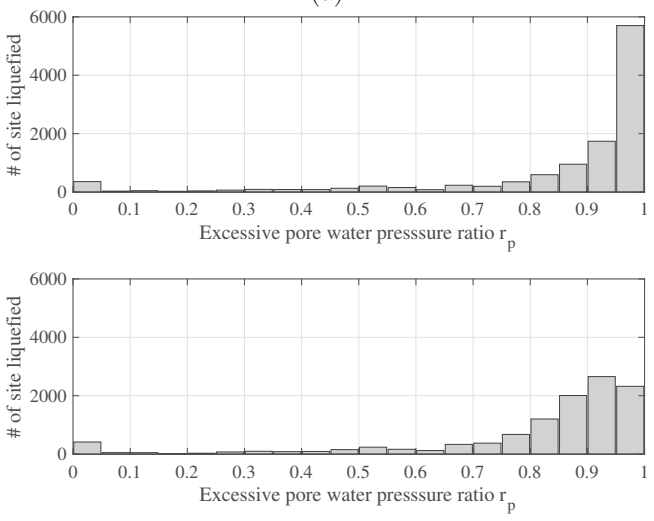

(b)

Figure 17.3: Monte-Carlo simulations for liquefaction hazard assessment of an urban area: (a) A normal distribution for the order of the value of soil permeability parameter, $k = 1 \times 10^n$ m/s where n follows $f(n| -4, 0.5^2)$. (b) The number of sites assessed as liquefied in the most occurrence of liquefaction is more than twice of the number in the least case when considering statistical soil models (liquefaction criterion $r_{\mathrm{p}} > 0.95$).

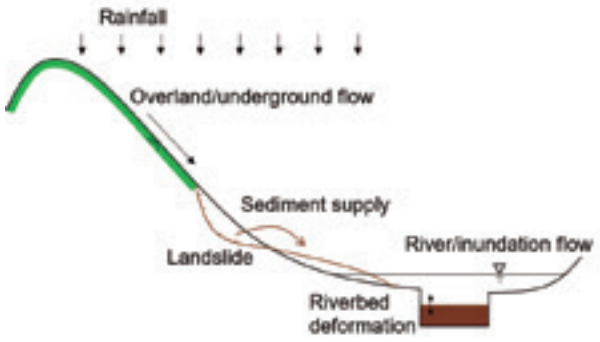

Figure 17.4: Overview of the phenomena simulated in DRSRIS

DRSRIS calculates underground flow only in the forest area considering lateral saturated flow based on Darcy's law and overland/inundation flow in all of land use employing Saint-Venant equations. Also, 2D sediment transport calculation is contained in the DRSRIS considering bed load and suspended load transportation. Currently, DRSRIS requires the assumed distribution data of sediment deposition, which means that it is difficult to apply besides already-happened landslide disaster. To solve this problem, we will combine DRSRIS and a landslide simulator to consider the dynamic movement of landslide mass and its deposition and improve the applicability and validity of the DRSRIS in the next fiscal year.

As a trial, we applied the DRSRIS to simulate Akatani river watershed in Asakura city, Fukuoka prefecture, where actually damaged by the heavy rainfall event occurred in Northern Kyushu Island in July, 2017. In this calculation, input condition of sediment supply volume was estimated by actual landslide distribution data and topography assuming that the deposition angle of sediment is constant. Figure 17.5 shows the one of the trial results of the water level during the heavy rainfall event, which roughly agreed with the observed inundated area.

17.4 Schedule and Future Plan

[1] Developing a national-wide real-time disaster simulation: We will enhance the automation of DPP to collect real-time seismic information and to perform an automated disaster simulation in a certain target area. This will reveal the extent to which speeding up is required for real-time characteristics.

[2] Construction of templates for high fidelity models of highway network: In the template-based methodology, we need to ready the templates in beforehand, and the quality and quantity of templates will be critical to the output model.

[3] Extend current Monte-Carlo simulations for multiple types of soil properties with uncertainties: it is clear that not only the permeability parameter, which is currently studied with statically models, but also other types of soil property, such as the so called N values, has significant effect on liquefaction occurrence. The current code will be extended for Monte-Carlo simulations with multivariate statistical models.

[4] Introduce the "big data" and AI techniques for fast liquefaction prediction: From our numerical simulations, a large number of samples are ready for AIs as training data. We will look for further opportunities to take advantage of the simulation data accumulated for fast liquefaction prediction.

[5] Extend soil dynamics-based simulations for liquefaction assessment to the other type of geo-disaster, landslides: we will start to develop simulation based assessment code for landslide hazards.

[6] Quantitative verification of DRSRIS: We will continue application to an actual flood disaster and evaluate the validity of the calculation. Also, we will apply it to the well-gauged catchment in Rokko mountain area, Hyogo, Japan to make a quantitative verification of sediment transport.

[7] Establishing a method of evaluating flood risk change due to the earthquake-induced landslide disaster by connecting the landslide simulator and DRSRIS: By connecting them, sediment supply volume, one of the required data of DRSRIS, will be obtained directly from the ground condition.

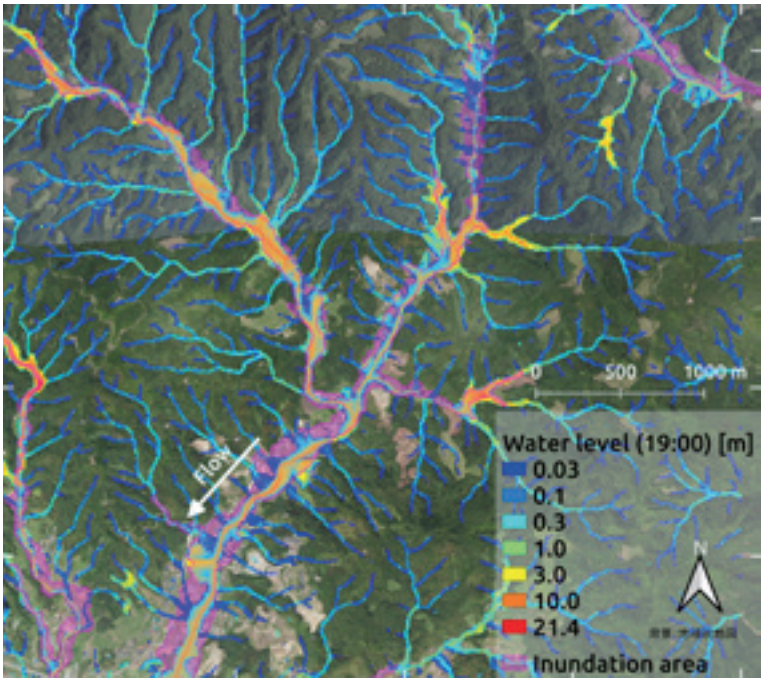

Figure 17.5: A trial results of the comparison between calculated water level (19:00) and the observed inundated area during the sediment-related disaster happened in northern Kyushu island. Note that this result is only for testing the simulator under development.

[8] Applying to a larger river catchment: Urban area is often located in a great river catchment. To estimate the flood risk change due to sediment supply in such areas, we will challenge to expand a calculation area to $100-1000\text{km}^2$ in order. To establish it, parallelization rate will be improved by introducing 2D domain decomposition.

[9] Developing FDPS based landslide simulation: Landslide simulation is one of the difficult target for numerical simulation because sediment particles consisting a slope move largely when land slide takes place. By using FDPS framework made by Makino Team, large scale land slide simulation can be developed. We are developing FDPS based landslide simulation program that simulates a slope with size of original scale rather than laboratory scale.

17.5 Publications

17.5.1 Articles

[1] Hori, M., Ichimura, T., Lalith, M., Ohtani, H., Chen, J., Fujita, K., Motoyama, H. (2018). "Application of High Performance Computing to Earthquake Hazard and Disaster Estimation in Urban Area." Frontiers in Built Environment. 4. 1. 10.3389/fbuil.2018.00001.
[2] Chen, J., Hori, M., O-tani, H., Oishi, S., Fujita, K. and Motoyama, H. (2017). "Proposal of Method of Numerically Manufactured Solutions for Code Verification of Elasto-Plastic Problems", Journal of Japan Society of Civil Engineers, Ser. A2 (Applied Mechanics), Vol.73(2).

17.5.2 Oral Talks

[3] O-tani, H., Chen, J., Fujita, K. and Hori, M. (2017). "A Data Integration Framework for Urban Area Disaster Simulations." 6th International Conference on Computational Methods in Structural Dynamics and Earthquake Engineering (COMPDYN2017), Rhodes Island, Greece, June 2017. (KEYNOTE)
[4] Chen, J., O-tani, H., Fujita, K., Motoyama, H., Takeyama, T. and Hori, M. (2017). "High Performance Computing for Hazard Assessment of Soil Liquefaction in Urban Regions", 15th International Conference of

the International Association for Computer Methods and Advances in Geomechanics (IACMAG), Wuhan, Oct. 2017
[5] Chen, J., O-tani, H., Oishi, S. and Hori, M. (2017). "Application of HPC boosted liquefaction assessment for urban regions", 2nd International Conference on Computational Engineering and Science for Safety and Environmental Problems (CompSafe), Chengdu, Oct. 2017.

Chapter 18

Computational Structural Biology Research Team

18.1 Members

Florence Tama (Team Leader)

Miki Nakano (Postdosctoral Researcher)

Sandhya Tiwari (Postdosctoral Researcher)

Yumeno Kusuhara (Assistant)

18.2 Research Activities

18.2.1 Introduction

Biological molecular complexes of such as proteins and RNAs are of great interest in the area of molecular biology, as they are involved in cell replication, gene transcription, protein synthesis, regulation of cellular transport and other core biological functions. Those systems undergo large conformational transitions to achieve functional processes. Therefore characterization of dynamical structures of these macromolecular complexes is crucial to understand their functional mechanisms and play an important role in the development of new drugs to treat human disease.

Experimentally, X-ray crystallography has been the primary tool to study protein structures, providing high-resolution structures. In recent years, cryo electron microscopy (EM) is also becoming a vital approach, due to rapid developments in technology and data processing software. It can be used to observe large macromolecules without the necessity of crystallization and has revealed a wealth of critical information on structure and dynamics of important large biological molecules. More recently, X-ray free-electron laser (XFEL) light sources offer a new possibility to image single biological macromolecules. RIKEN/SACLA is one of a few facilities that currently exist and several more being constructed in the world. It can produce photon pulses significantly stronger than previous facilities and enables instant "single shot imaging" of biological systems. Since crystallization is not necessary for such measurements, it would be possible to investigate the structure of biomolecules under various physiological conditions or to observe elementary steps of a biochemical function. However, in the current experimental condition, it cannot achieve atomic level resolution such as obtained by X-ray crystallography.

Computationally, algorithms to process experimental data play critical roles to obtain the structural models of biological molecules, because biological molecules are exceedingly complex, consisting of thousands to millions of atoms. Even without experimental data, atomic models could be predicted using homology modeling and ab initio prediction methods. Algorithms to analyze protein/proteins interactions also have shown successes in predicting proteins complexes. While such ab initio predictions, based solely on computation, succeed in predictions for small proteins, it still remains difficult for large proteins. Therefore, in the studies of biologically important large macromolecular complexes, it is essential to integrate computational modeling approaches with experimental data.

The ultimate line of our interdisciplinary research is to bring experimental data as obtained from X-ray, cryo-EM, and XFEL with development and applications of computational tools, through K computer, to acquire knowledge on the structures of physiologically important protein complexes that are unattainable with existing experimental techniques. We have been working on the development of data analysis algorithms, with the emphasis on the integration of molecular mechanics simulation and experimental data processing, and applying the developed algorithms to experimental data through collaborations.

18.2.2 Computational tools for XFEL experimental data

The recent development of intense X-ray free-electron laser (XFEL) light sources offers a possibility to obtain new structural information of biological macromolecules. Strong X-ray pulse allows measurement of X-ray diffractions from microcrystals, and furthermore, enables the imaging of single biological macromolecules. Measurements using such a strong pulse also has advantages, enabling time-resolved measurements at femtoseconds resolution as well as the measurements at the ambient temperature. SPring-8/SACLA is one of a handful of XFEL facilities in the world. However, with current experimental conditions, atomic level resolution such as obtained by X-ray crystallography cannot yet be achieved. As XFEL experiments are very recent and still undergoing further development for routine applications to biological molecules, computational algorithms and tools to analyze experimental data also need to be developed simultaneously. One focus of our research is the development of such computational tools from multiple angles summarized below.

18.2.2.1 3D structure reconstruction from 2D diffractions data

Three-dimensional (3D) structural analysis for single particles using X-ray free electron laser (XFEL) enables us to observe hard-to-crystallize biomolecules in a state close to nature. To restore the 3D structure of the molecule from the diffraction patterns obtained by XFEL experiments, computational algorithms are necessary as one needs to estimate the angles of incident laser beams to the molecule for each of 2D diffraction patterns and assemble them into 3D volumetric structural information.

We have demonstrated the 3D structure reconstruction of a large biological molecule, ribosome, from diffraction data created by computer simulation. We proposed a sequence of algorithms that allow accurate angle estimations and 3D reconstructions. In addition, we showed the experimental conditions that are required (the number of diffraction images and the intensity of the laser beam) to restore the molecular structure at a certain resolution (Figure 18.1) (Nakano et al, J. Sync Radiat. 2018). Following this work, we are developing data processing protocols to apply such reconstruction algorithms to actual experimental data. Experimental data contains noise and uncontrollable fluctuation of samples and measurement conditions, unlike synthetic data. Therefore, we are developing algorithms for filtering high-quality diffraction patterns that contain signals useful to reconstructions

These data analysis tools are being developed using XMIPP, which is commonly used for image processing of single-particle 3D cryo EM. Since XMIPP is designed to work with 2D data in real space, some of the routines were modified to deal with 2D diffraction patterns in Fourier space. The programs for the reconstructions are ported to K-computer and being customized to improve performance.

18.2.2.2 "Idea generator" from 2D data of biological systems

Data analysis for XFEL data remains challenging. XFEL diffraction pattern is an unintuitive representation of the projection image of the sample in reciprocal space. For biological systems, the current standard approach to reconstruct a real-space image of the sample, phase recovery, often fails due to the low diffraction power of biological samples. Therefore, we are developing a new hybrid approach to interpret diffraction patterns that utilizes image analysis with database search. In this approach, for an obtained XFEL diffraction pattern, the algorithm proposes a few low-resolution 3D models that are consistent with the data using a database of known or hypothetical shapes of biological systems (Figure 18.2).

We previously demonstrated the feasibility of such an approach using cryo EM images, which are in "real space". We generated a database of shape, utilizing the existing EM database and developed a protocol to identify 3D models that match a set of inquiry 2D images (submitted). Following this, we have been adopting this approach for the application to XFEL diffraction patterns, which is in "Fourier space". From the database of shapes, expected diffraction patterns in all possible beam orientations are precomputed, and inquiry XFEL diffraction patterns are compared against this database. We are refining the similarity detection procedures to increase the accuracy of diffraction pattern comparisons.

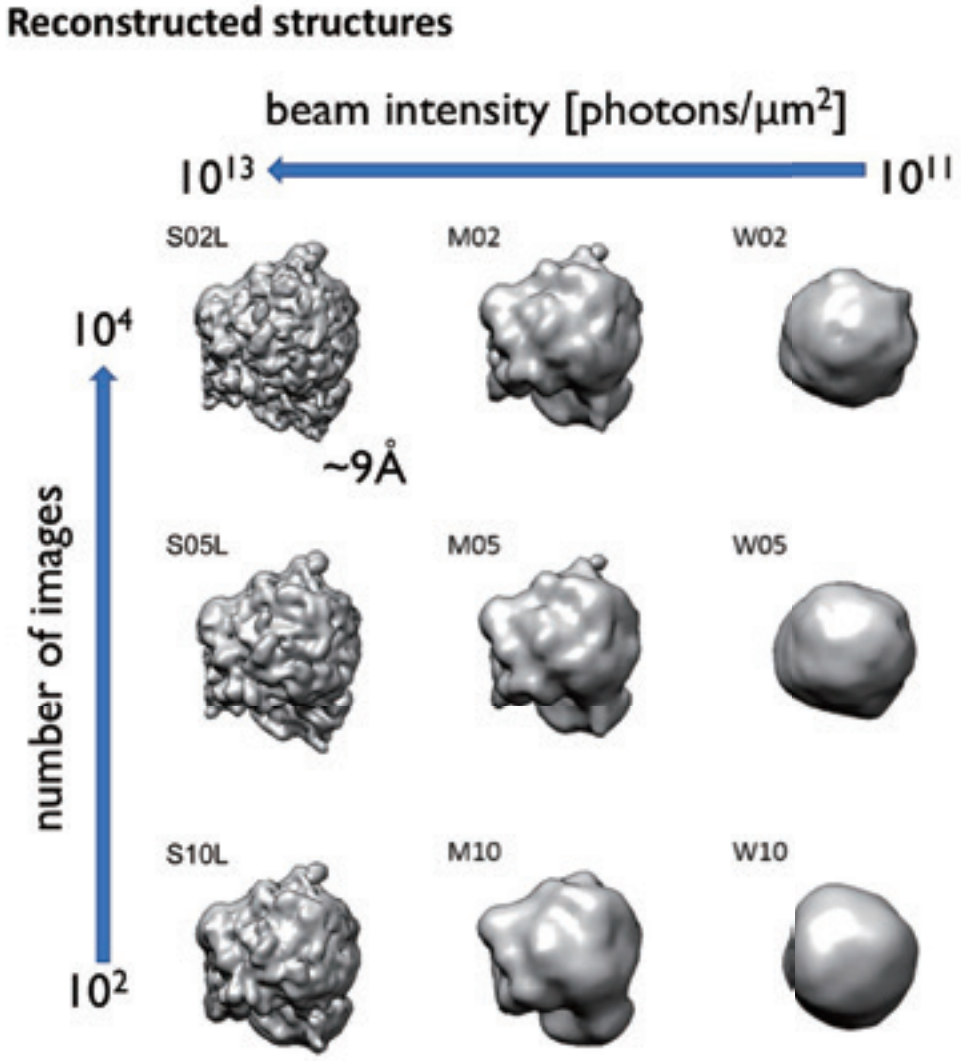

Figure 18.1: Examples of 3D reconstructions of a ribosome from synthetic diffraction patterns. With stronger beam intensity and a large number of diffraction patterns, the structure of a ribosome can be reconstructed at 9Åresolution. The strength of beam intensity has large effect on the resolution of reconstructed models.

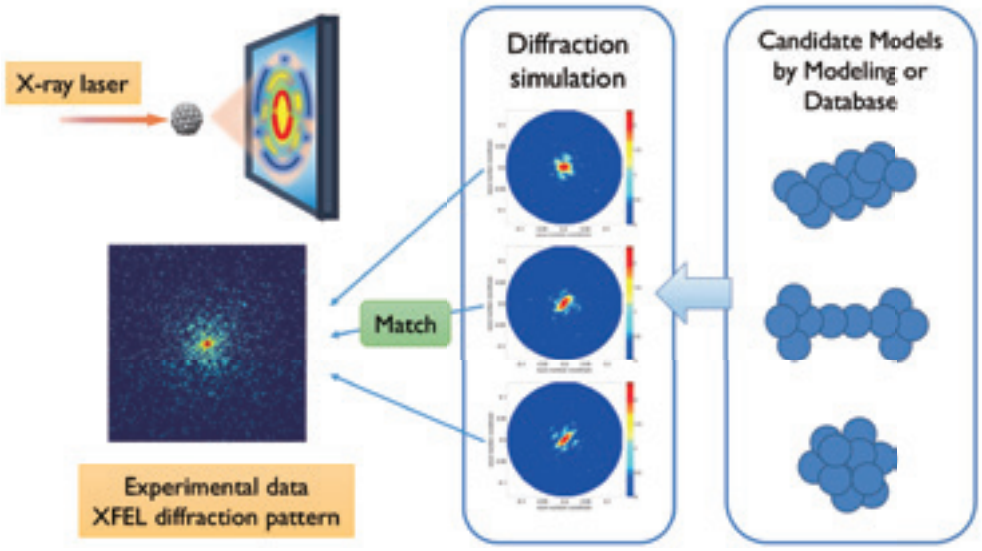

Figure 18.2: Scheme of structure model reconstruction from a few experimental diffraction patterns. A large number of possible structure models are generated using the database that assembles known biological shapes, or sampling techniques using coarse-grained models. For each candidate model, expected diffraction patterns are calculated and compared against the target experimental diffraction pattern to identify the structure that is most consistent with the data.

18.2.2.3 Coarse-grained structure representation for XFEL data analysis

In parallel to the above database approach, we are also exploring ab initio approaches, where the structural models that match experimental data are generated through optimization procedures (Figure 2). We are examining the use of Gaussian mixture model (GMM), which approximates a biomolecular shape by the superposition of Gaussian distributions. As the Fourier transformation of GMM can be quickly performed, GMM can be used to efficiently simulate XFEL diffraction patterns from approximated sample structures. We have shown that with a sufficient number of GMMs, diffraction patterns that are highly consistent with the ones simulated from atomic models can be obtained using a fraction of CPU time (Figure 18.3). These results demonstrate that GMM serve as a useful coarse-grained models, in the context of hybrid modeling approach, in XFEL single particle experiments (submitted).

18.2.3 Refinement of cryo-EM structure models using X-ray structures

Recent advances in cryo-EM experiments and data processing have produced high-resolution structures of biomolecules. Nevertheless, in many cases, the obtained resolution still remains in the 6-12 Årange, which requires computational techniques to build reliable atomic models. In an approach, “flexible fitting”, known X-ray structures are optimally deformed to match experimental data using molecular mechanics simulations. In collaboration with Dr. Sugita’s laboratory in Wako, we have been implementing such type of approaches in GENESIS. Taking advantage of the generalized ensemble algorithms embedded in GENESIS to maximize conformational sampling, increase in reliability of the atomic models was achieved. Fitting subroutines are fully parallelized in the latest implementation and allow the modeling of large macromolecules.

We have been further improving the flexible fitting approaches to improve its applicability to real experimental data. 3D volume from cryo-EM reconstruction contains strong noise and there are large uncertainties in the data. In recent applications, we are examining the protocols to calibrate the parameters for flexible fitting to ensure the quality of the resulting models. The result strongly indicates that the noise in the data can easily cause “overfitting”, where the resulting model is distorted by noise. We also examined the procedure to calibrate the size parameter of pixels in the microscopy data, which may contain some error (Figure 18.4).

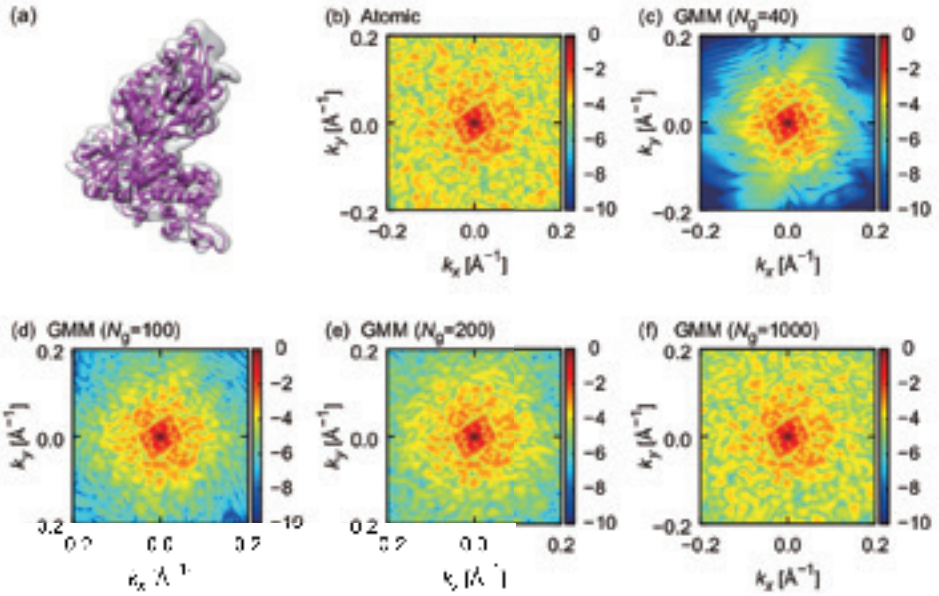

Figure 18.3: Demonstration of fast diffraction pattern simulation using GMM. (a) The original atomic model of a protein, EF2. (b) A diffraction pattern that is simulated from the atomic model. (c-f) The diffraction patterns simulated using GMM. As the number of Gaussians that are used to approximate the volume of original protein increases, the simulated diffraction patterns agrees better with the one from the atomic model. With 100 Gaussians, diffraction patterns can be simulated up to 0.1 Å^{-1}, which is sufficient for the modeling of large macromolecules.

18.3 Schedule and Future Plan

Cryo-EM experiments are quickly becoming an essential tool for studying biomolecular complexes. New XFEL facilities are getting into operation every year in the world, providing opportunities for new experiments. The amount of data from such experiments will continue to grow in numbers and analysis of such big datasets will increase the necessity of high performance computing. We aim to utilize K and post-K to break the limitation of current processing power and to obtain a new level of structural information of biological complexes from EM and XFEL data. For this goal, we plan to develop algorithms and software to analyze large dataset to obtain not only structural models but also dynamical information that can utilize computers in different sizes such as cluster and supercomputer. By sharing the software and results from structural modeling with other research institutes, we aim to contribute to the structural biology community.

XFEL facility SACLA started its operation in 2012. Other XFEL facilities are gradually established in the world and the number is still limited, but data for 亮 m systems, such as viruses and organelle, are being obtained. We have been developing algorithms to obtain structural models of biological systems by using XFEL data from two aspects.

In one approach, we aim to predict structural models from a limited amount of XFEL data. Such an approach is necessary since XFEL data collection is still a challenge and, moreover, the biological samples are intrinsically not uniform and it is difficult to obtain a large number of diffraction patterns from the samples in an identical conformation. We have developed a series of algorithms for coarse-grained representation of the structures, matching the model against experimental data. At the next step, we plan to establish sampling and optimization procedures to generate models that match experimental data.

In another approach, we aim to reconstruct structural models from a large number of XFEL data. With the advancement of experimental techniques, more than 10,000 XFEL diffraction images could be soon obtained, and furthermore, theoretical studies suggest that 1 million images are necessary to obtain high resolution models. In the near future, we will need to utilize such a large amount of dataset to reconstruct detailed 3D models from XFEL data. Thus, we have been developing algorithms to efficiently construct 3D models from XFEL diffraction patterns. We are aiming to apply the algorithm to new experimental data, and for this purpose, we

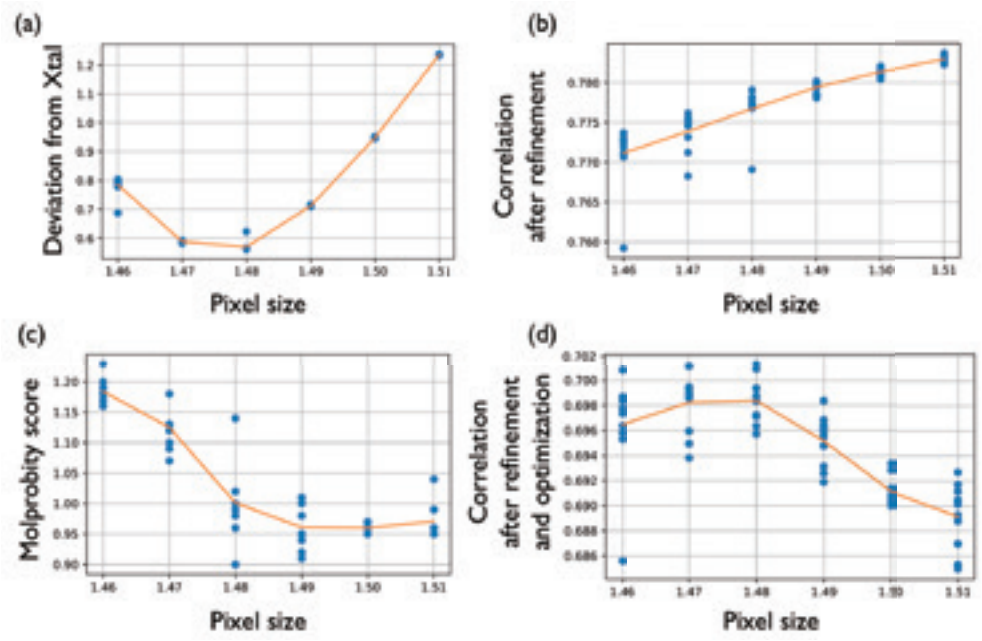

Figure 18.4: A various indicators were tested to find an indicator that can be used for calibration of the pixel size of cryo-EM density map during structure refinement procedures for a protein molecule. (a) The deviation of protein structure from the original conformation during refinement. At pixel size of 1.48, the struct is least deviated. (b) The value of CC (correlation coefficient), which is commonly used to assess the match between cryo-EM maps and protein structures. This indicator is not appropriate since it can be higher even with wrongly large pixel sizes. (c) Another commonly used indicator, Molprobity score. This indicator also cannot detect the error from wrongly large pixel size. (d) CC value after structure optimization. This indicator can identify the correct pixel value.

are developing data processing protocols to filter the data with good signals for reconstruction. These programs need to be improved further to allow the analysis of the anticipated large dataset, utilizing HPC.

We also plan to continue to improve the software for structure modeling from cryo-EM data. With the improvement of technology and algorithms, structural models with higher resolutions are being obtained. The current challenge in computation is how we ensure the quality and reliability of the resulting models. We plan to add new approaches to the current flexible fitting algorithm so that it can be applied to experimental data in a variety of qualities.

From these projects, new techniques for data analysis will become available, which will provide new structural information on biomolecules. Using the developed programs, we will work with experimental groups to obtain revolutionary structural information and contribute to the understanding of mechanisms of biological functions. We will maintain the new software and also provide usage support so that it is easily accessible to experimental groups from other institutions.

18.4 Publications

18.4.1 Journal Articles

1. M. Nakano, O. Miyashita, S. Jonic, A. Tokuhisa, F. Tama. Single-particle XFEL 3D Reconstruction of Ribosome-size Particles based on Fourier Slice Matching: Requirements to Reach Subnanometer Resolution. *J. Synchrotron Rad.* 2018 25:1010-1021

2. A. Srivastava, T. Hirota, S. Irle and F. Tama. Conformational dynamics of human Protein Kinase CK2 留 and its effect on function and inhibition. *Proteins.* 2018 86: 344-3

3. S.P. Tiwari, N. Reuter, Conservation of intrinsic dynamics in proteins-what have computational models taught us? *Curr Opin Struct Biol.* 2018 50:75-81

Part II

Operations and Computer Technologies Division

Operation status and research activities of Operations and Computer Technologies Division are presented in this part. Operation and Computer Technologies Division are responsible for operation and enhancement of the K computer and the facilities. Operation and support of High Performance Computing Infrastructure (HPCI) system are also a part of our missions. Our division consists of four teams. The missions and members of the teams are shown as follows:

- Facility Operations and Development Team (Team Head: Toshiyuki Tsukamoto)
  Missions: Operation and Enhancement of the facility for the K computer
  Members: Technical Staff(7)

- System Operations and Development Team (Team Head: Atsuya Uno)
  Missions: Operation and Enhancement of the K computer
  Members: R&D Scientist(4), Technical Staff(2)

- Application Tuning Development Team (Team Head: Kazuo Minami)
  Missions: Application tuning and enhancement of software developed by R-CCS
  Members: R&D Scientist(3)

- HPC Usability Development Team (Team Head: Fumiyoshi Shoji)
  Missions: Enhancement of usability of the K computer and Operation and Enhancement of HPCI shared storage system
  Members: R&D Scientist(6), Senior Visiting Scientist(2), Visiting Scientist(1), Technical Staff(1)

The detail of the operational improvements and research activities are reported in the following chapters. We hope readers find our experiences and lessons learned informative.

Chapter 19

Facility Operations and Development Team

19.1 Members

Toshiyuki Tsukamoto (Team Head)

Mitsuru Tanaka (Technical Staff)

Hiroyuki Takitsuka (Technical Staff)

Satoshi Matsushita (Technical Staff)

Katsuyuki Tanaka (Technical Staff)

Fumio Tsuda (Technical Staff)

Hajime Naemura (Technical Staff)

Makoto Igasaki (Technical Staff)

Hiroshi Shibata (Technical Staff)

19.2 Research Activities

The K computer facilities possess multiple features not found at other supercomputer sites. These features include an expansive and pillar-free computer room, a power supply system that consists of a co-generation system (CGS) and a high-speed current-limiting circuit breaker without uninterruptible power supply (UPS), distribution boards installed not on the computer-room walls but under a raised floor, extremely quiet and high-efficiency air conditioners, and a water-cooling system for the CPUs featuring precise temperature control.

To ensure stable operation of the K computer and its peripherals, the facility operations and development team (FODT) of the operations and computer technologies division, RIKEN AICS, is responsible for the operation and enhancement of the facilities. Furthermore, FODT conducts research on the advanced management and operations of the AICS facilities.

One of the most serious problems is the rapid and substantial increase in the electricity prices since 2011. Therefore, we are investigating the most suitable driving conditions to allow the AICS facilities to achieve effective cost reductions.

Another problem is the increased power consumption by AICS. The use of electricity by AICS is strictly limited by a contract between AICS and the local electric supply company. However, in the early stage of operation, the facility's power consumption exceeded the contract limit. This is important because the company requires us to accept an increase in the upper/lower power limit, which amounts to an increase in the electricity cost. To prevent this, we have investigated methods to control the power consumption of the K computer using emergency job stopping together with the system operations and development team and the application tuning development team of the operations and computer technologies division, RIKEN AICS.

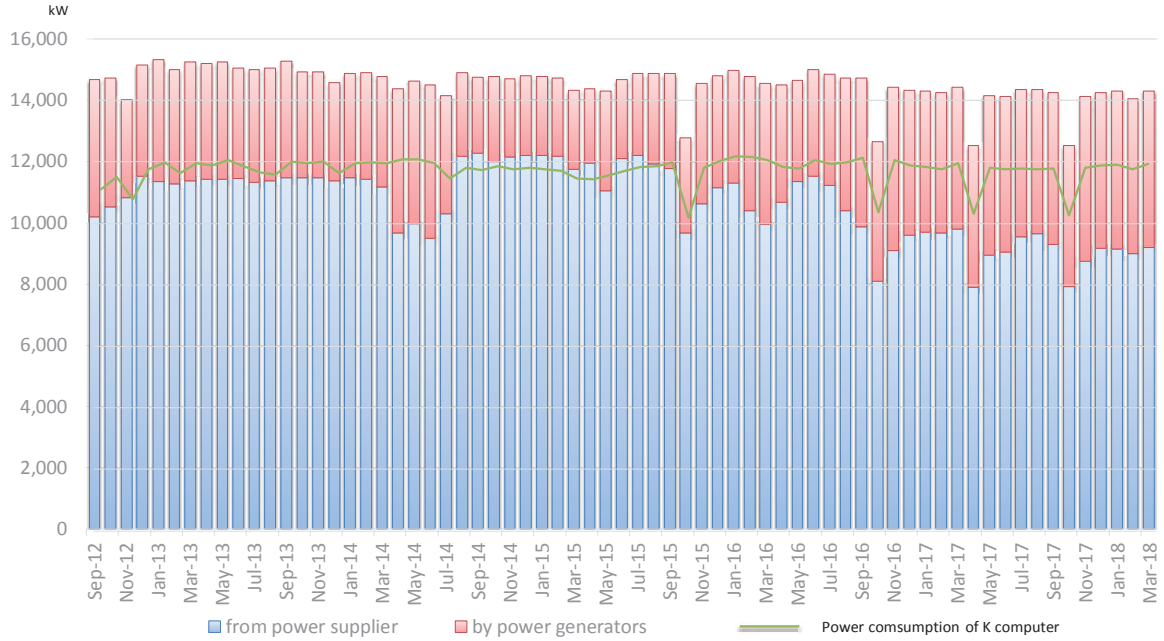

Figure 19.1: Monthly power supply and K computer power consumption.

19.3 Research Results and Achievements

19.3.1 Optimum operation of electric power

Figure 19.1 shows the monthly total power supply and power consumption of the K computer from September 2012 to March 2018. The power supply consists of commercial power purchased from a supply company and power generated by CGS.

The AICS power consumption is nearly synchronized with that of the K computer. The power consumption of AICS is nearly 15,000 kW on average, and the power consumption of the K computer accounts for approximately 80% (12,000 kW) of the total consumption of AICS.

As shown in Figure 19.1, the electric power supply of AICS consists of commercial and CGS power. There are two CGS systems at AICS, and they are used in turn for two weeks at a time. Therefore, at least one CGS is always in use. Commercial electric power is contractually set at approximately 12,500 kW, and the power consumption was approximately 12,000 kW (annual average), which corresponds to approximately a 90% load factor.

To minimize the cost, we try to optimize the ratio of the commercial and CGS electricity. To investigate the optimized conditions that minimize the sum of the electricity and gas cost, we determined the costs of several ratios of commercial electricity to CGS electricity. We also constructed a model to describe the energy flow of the electric power supply and the cooling system. Then, we performed computer simulations using the model and the actual operating data. In the near future, we intend to identify the cost-optimized conditions that contribute to reducing costs.

19.3.2 Improvements to the power usage effectiveness (PUE)

We have continued to work on improvements for the effective use of electricity. PUE is a well-known indicator of the effectiveness of electricity use.

To improve the PUE, we have attempted to optimize the operation of the cooling equipment (e.g., chillers and air-handlers) since FY2013.

Figure 19.2 indicates the change in the annual average power consumption of the K computer (including the peripheral devices) and the cooling equipment. Since FY2013, the power consumption of the K computer has been nearly flat at approximately 11,800 kW; however, the power consumption of the equipment decreased gradually from FY2013 to FY2017. Accordingly, the PUE of AICS improved to 1.299 in FY2017 from 1.447 in FY2012, contributing to the reduction in the electricity cost.

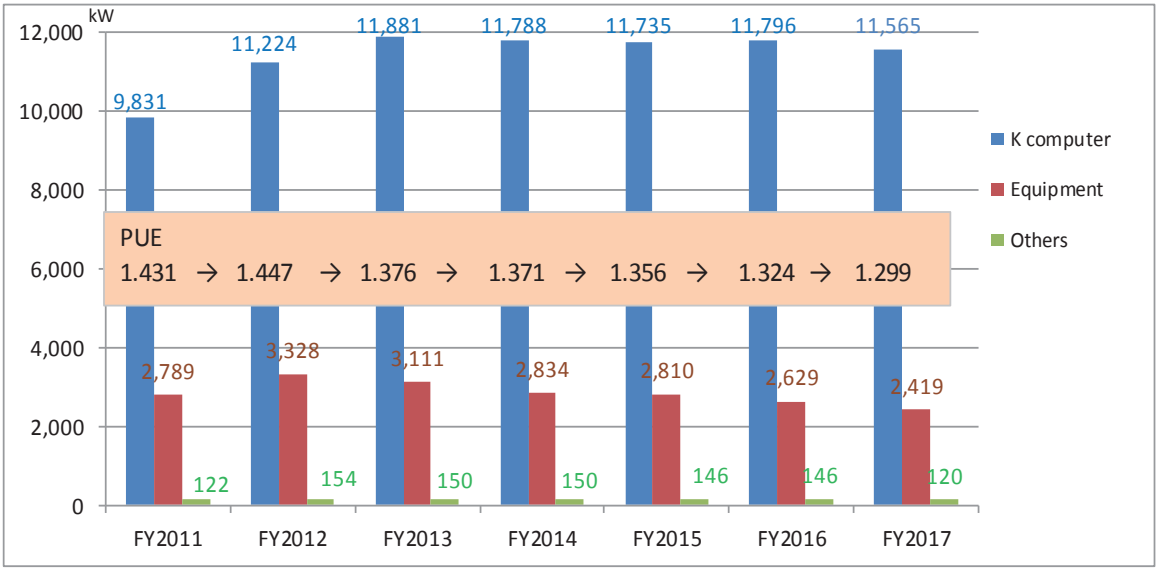

Figure 19.2: Trend in the annual average electric power consumption.

In FY2013, we reduced the electricity cost of the air conditioners by reducing the number of working air conditioners. The total cooling performance was maintained by lowering the air temperature. We achieved a reduction in the power consumption of 217 kW.

In FY2014, we focused on the fault-tolerance feature of the air-conditioning equipment. Each air conditioner has two motors for fault tolerance. We found that if one of the two motors could be stopped, the airflow could be maintained at approximately 60%. Therefore, we reduced the power consumption by a further 277 kW in FY2014 and by 24 kW in FY2015.

In FY2016, we worked on improving the efficiency of the cooling tower. As a result, we achieved a reduction of 181 kW in the power consumption.

In FY2017, we focused on optimizing the operation control of the refrigerator using a heat storage tank. This reduced the power consumption by 210 kW.

19.4 Schedule and Future Plan

We will continue to improve the advanced management and operation of the AICS facilities and contribute to the user service of the K computer. We will work on reducing costs by investigating and applying the most suitable driving conditions to all the electric power supply and cooling equipment. Further, we will improve the electric power control of the entire AICS facility with the system operations and development team to prevent overshooting of the contracted power demand.

19.5 Publication, Presentation, and Deliverables

19.5.1 Journal Papers

[1] Keiji Yamamoto, Atsuya Uno, Katsufumi Sugeta, Toshiyuki Tsukamoto, Fumiyoshi Shoji, “スーパーコンピュータ「京」の運用状況,” IPSJ Magazine Vo.55 No.8 pp.786-793, 2014. (In Japanese)

[2] Keiji Yamamoto, Atsuya Uno, Hitoshi Murai, Toshiyuki Tsukamoto, Fumiyoshi Shoji, Shuji Matsui, Ryuichi Sekizawa, Fumichika Sueyasu, Hiroshi Uchiyama, Mitsuo Okamoto, Nobuo Ohgushi, Katsutoshi Takashina, Daisuke Wakabayashi, Yuki Taguchi, and Mitsuo Yokokawa. “The K computer operations: Experiences and statistics.” In Proceedings of the International Conference on Computational Science, ICCS 2014, Cairns, Queensland, Australia, 10-12 June, 2014, pages 576-585, 2014.

[3] Fumiyoshi Shoji, Shuji Matsui, Mitsuo Okamoto, Fumichika Sueyasu, Toshiyuki Tsukamoto, Atsuya Uno, and Keiji Yamamoto. “Long term failure analysis of 10 peta-scale supercomputer.” In HPC in Asia session at ISC2015, Frankfurt, Germany, July 12-16, 2015.

19.5.2 Conference Papers

[4] Atsuya Uno, Hajime Hida, Fumio Inoue, Naoki Ikeda,Toshiyuki Tsukamoto, Fumichika Sueyasu, Satoshi Matsushita, Fumiyoshi Shoji, “Operation of the K computer Focusing on System Power Consumption,” HPCS2015, 2015, Japan. (In Japanese)
[5] Lili Jin, Kouji Yutani, Hiroyuki Yamano, Hiroyuki Takitsuka, Satoshi Matsusita, Toshiyuki Tsukamoto, “計算科学研究機構における設備最適運転条件の検討その２,” Proceedings of the 49th Japanese Joint Conference on Air-conditioning and Refrigeration(Tokyo). (In Japanese)
[6] Satoshi Matsushita, Hiroyuki Takitsuka, Toshiyuki Tsukamoto, “スーパーコンピュータ施設における低騒音空調機の省エネ運用,” Proceedings of the 49th Japanese Joint Conference on Air-conditioning and Refrigeration(Tokyo). (In Japanese)
[7] Hiroyuki Takitsuka, Toshiyuki Tsukamoto, “冷却塔の効率改善その２,” Proceedings of the 51th Japanese Joint Conference on Air-conditioning and Refrigeration(Tokyo). (In Japanese)
[8] Kouji Yutani, Hiroyuki Yamano, Lili Jin, Masanori Toi, Tatsuo Takahashi, Makoto Yamada, Toshiyuki Tsukamoto, Satoshi Matsushita, Keiji Yamamoto, “New power supply system by direct current compensation demonstrative test report of power fluctuation mitigation in K-computer facility”, 電気学会 B 部門大会,2017,Japan. (In Japanese)

19.5.3 Invited Talks

None

19.5.4 Posters and presentations

[9] Fumio Inoue, Atsuya Uno, Toshiyuki Tsukamoto, Satoshi Matsushita, Fumichika Sueyasu, Naoki Ikeda, Hajime Hida, Fumiyoshi Shoji, “電力消費量の上限を考慮した「京」の運用,” IPSJ-SIGHPC 2014-HPC-146 No.4, 2014. (In Japanese)
[10] Atsuya Uno, Hajime Hida, Naoki Ikeda, Fumio Inoue, Toshiyuki Tsukamoto, Fumichika Sueyasu, Fumiyoshi Shoji, “「京」におけるジョブ単位の消費電力推定の検討,” IPSJ-SIGHPC 2014-HPC-147 No.20, 2014. (In Japanese)

19.5.5 Patents and Deliverables

None

Chapter 20

System Operations and Development Team

20.1 Members

Atsuya Uno (Team Head)

Hitoshi Murai (Research & Development Scientist)

Motoyoshi Kurokawa (Research & Development Scientist)

Keiji Yamamoto (Research & Development Scientist)

Fumio Inoue (Research & Development Scientist)

Yuichi Tsujita (Research & Development Scientist)

Mitsuo Iwamoto (Technical Staff)

Katsufumi Sugeta (Technical Staff)

20.2 Research Activities

K computer, a distributed-memory parallel computer comprising 82,944 computing nodes, has played a central role in the High Performance Computing Infrastructure (HPCI) initiative funded by the Ministry of Education, Culture, Sports, Science and Technology. The HPCI has achieved an integrated operation of the K computer with other supercomputer centers in Japan. Furthermore, it has enabled a seamless access for user machines to a cluster of supercomputers that includes the K computer. Moreover, the HPCI has provided large-scale storage systems that are accessible from all over Japan.

The system operations and development team (SODT) has conducted research and development for the advanced management and operation of the K computer. While analyzing operational statistics collected during its shared use, the SODT has improved the system configuration, including aspects involving job scheduling, the file system, and user environments.

In the fiscal year 2017 (FY2017), we primarily implemented improvements to the following operational issues:

- Alleviation of MDS performance degradation
- InfiniBand network monitoring
- Topology-aware enhancement of MPI-IO
- Log collection, analysis, and visualization
- Introduction of long-term jobs
- Improvement of information provision to users

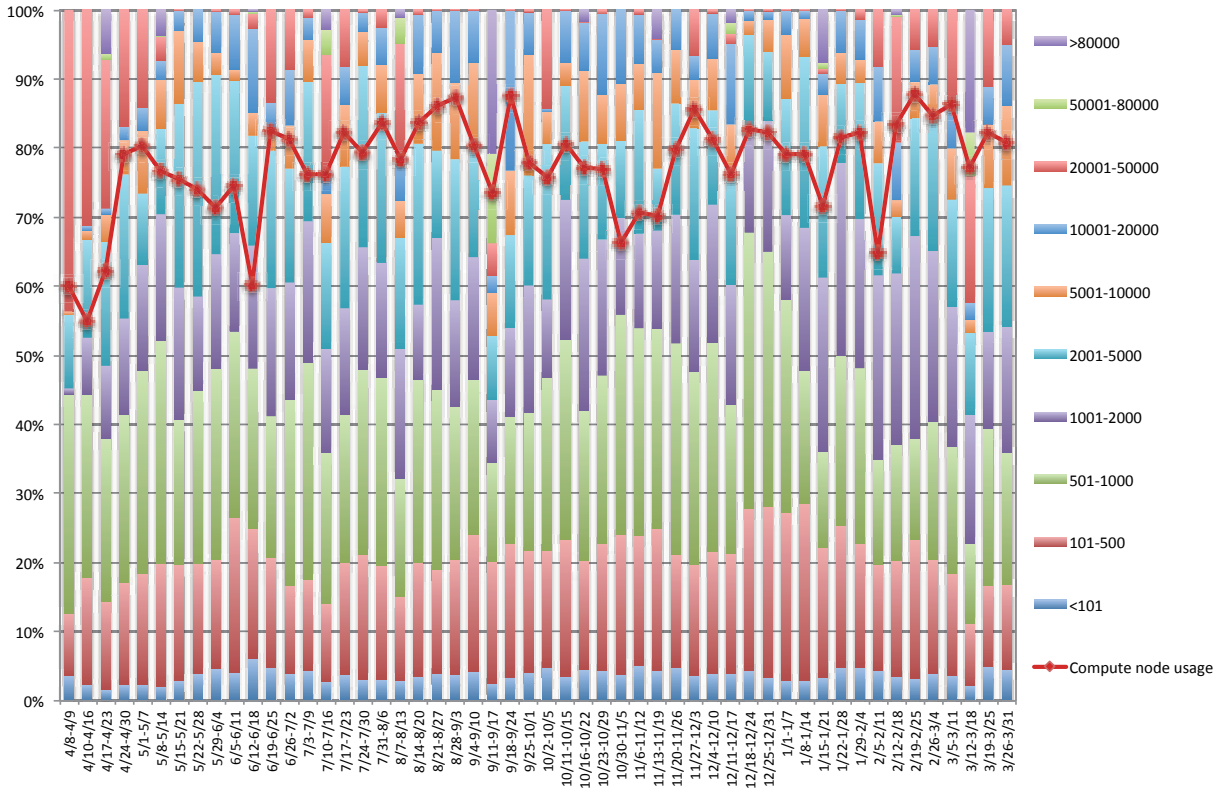

Figure 20.1: Resource usage in FY2017

- Optimization of maintenance operations
- Estimation of power consumed by jobs

20.3 Research Results and Achievements

Figure 20.1 shows the resource usage details for FY2017. As usual, the resource usage is low at the beginning of the fiscal year. In addition, a system software malfunction, which took almost 2 days to resolve, resulted in very low usage in April. In June, usage was low due to a local file system error. The resource usage was low in February because the co-generation system (CGS) that provides a part of the electric power required for the K computer was not functioning, the K computer itself was down at that time. Apart from those incidents, we maintained a high utilization rate, approximately 78%, which is nearly equal to that achieved in FY2016 (79%).

20.3.1 Alleviation of MDS Performance Degradation

A high load or a slow response of the Metadata Server (MDS) at the local file system (LFS) alleviated file I/O performance. Figure 20.2 shows the effect of these two distinct MDS activities on low file I/O performance: (1) high MDS load and (2) quite slow response from the MDS. Both a high MDS load and a slow MDS response are harmful not only for file I/O performance of user jobs but also for job scheduling including data staging.

To investigate the root cause of such MDS performance degradation, we performed MDTEST benchmark runs. Figure 20.3 shows the benchmark results of the MDTEST for 768 and 1,536 processes on 192 ($4 \times 6 \times 8$) nodes with various stripe counts including the default count (12). Every process accessed 100 files per iteration in each individual directory within the shared space of the LFS. Mean performance values were obtained from six iterations in addition to the maximum and minimum values, indicated by bars in each case.

The results imply that an increase in stripe count reduces performance. This is because of congestion in the operations between the MDS and the associated Object Storage Servers (OSSes) that delays metadata flow. In the Lustre configuration, an increase in the stripe count increases the number of requests traversing from an

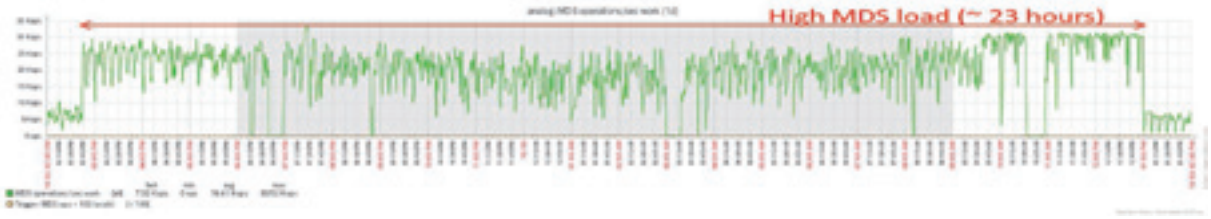

(a) high MDS load for 23 hours

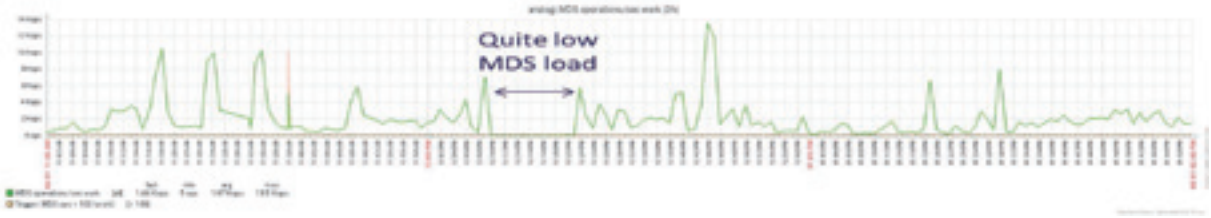

(b) very slow MDS response

Figure 20.2: MDS activities under (a) high load for 23 hours and (b) very slow MDS response due to a large number of files and stripe count

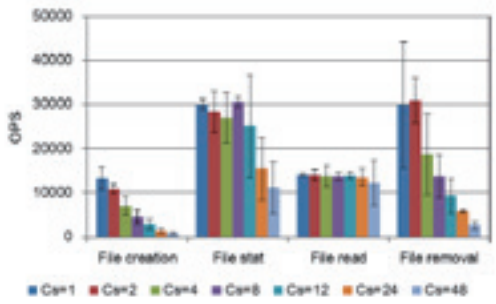

(a) 768 processes on 192($4 \times 6 \times 8$) nodes

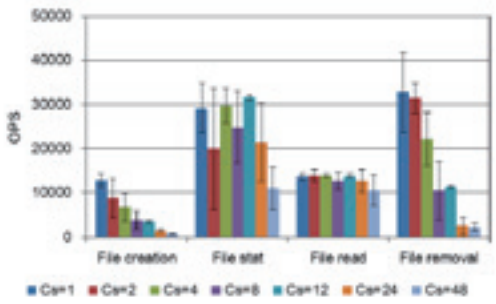

(b) 1,536 processes on 192($4 \times 6 \times 8$) nodes

Figure 20.3: MDTEST evaluation results for various stripe counts, where C_S denotes the stripe count.

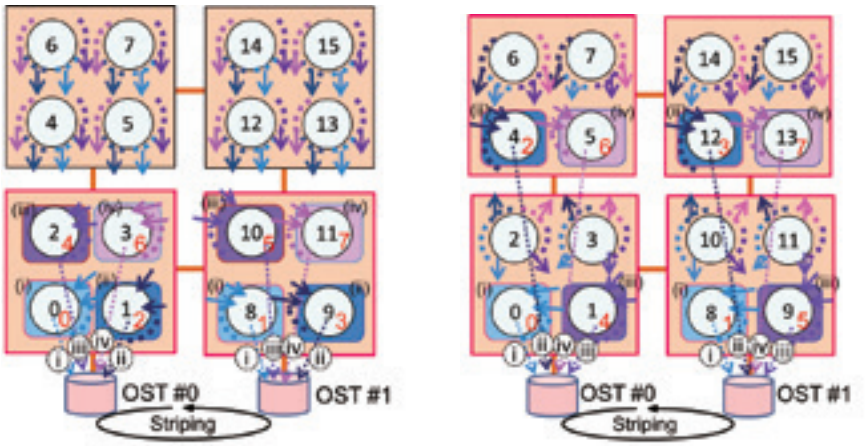

(a) (b)

Figure 20.4: Aggregator layout in (a) the blocked-layout case and (b) the newly proposed round-robin-layout case

MDS to the corresponding OSSes. The MDS remains idle until it receives a response from the OSSes. Therefore, an increase in the number of files and processes leads to slow MDS response.

Based on the results, we asked users to specify "-1" as the stripe count to change the request to the appropriate one. Meanwhile, we will examine the alleviation effect of a quality of service (QoS) function of the Fujitsu Exabyte File System (FEFS) against such MDS performance problems.

20.3.2 InfiniBand Network Monitoring

InfiniBand connections are important components not only for data staging but also for accessing files in the Global File System (GFS). We have observed failures in data staging due to network link failures and even node failures due to restart of compute nodes and I/O nodes originated by the link failure. To prevent these failures, we monitor error counters of InfiniBand links using the system log, and we replace failed links according to the monitoring and throughput performance evaluations. Through this activity, we have minimized the number of problems in GFS accesses including data staging.

20.3.3 Topology-aware enhancement of MPI-IO

We have enhanced the MPI-IO library named Effective Aggregation Rounds with Throttling (EARTH) and improved its implementation at the K computer, named as "EARTH on K." Important features of the EARTH are (1) aggregator layout optimization, (2) I/O throttling, and (3) stepwise data aggregation. Based on these features, we have focused performance optimization for multiple aggregators per compute node.

When multiple processes play as aggregators, we may face high contention in data aggregation and file I/O on the same compute node. By considering the process layout, we have implemented topology-aware placement for aggregators, where we deployed aggregators in a round-robin manner among the compute nodes. Figure 20.4 depicts the aggregator layout in the original case and in the round-robin layout case. These figures depict MPI-IO write operations using 16 processes on 4 compute nodes. The circles denote processes, and the numbers inside the circles represent MPI ranks. It is assumed that half of the processes work as aggregators. In the blocked layout of the previous case, the aggregators were localized in the lower two nodes. That layout led to contention in the two nodes during file I/O and data aggregation. On the other hand, the proposed round-robin layout alleviates such contention.

Figure 20.5 shows collective I/O performance results using HPIO benchmark. The evaluated configurations are summarized in Table 1. The evaluated configurations are summarized in Table 20.1. From the performance results, the full-set optimization with the newly implemented round-robin aggregator layout outperformed other layout cases, including the original implementation indicated as "original." Such an aggregator layout using I/O throttling and stepwise data aggregation with four or two requests (E, agg, rr, req = 4 or E, agg, rr, req = 2) showed the best performance for 12,288 and 24,576 processes, respectively. For better usability, the self-tuning function for the number of requests in I/O throttling and stepwise data aggregation will be considered in the

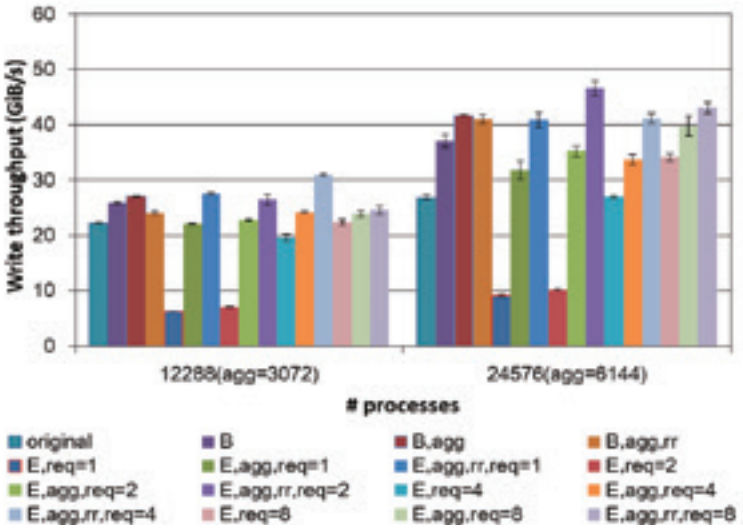

Figure 20.5: I/O performance of collective write using 12,288 and 24,576 processes on 3,072 and 6,144 compute nodes, respectively

Table 20.1: Evaluated configurations in HPIO benchmark runs. "✓" means that the corresponding function is available.

Notation	Striping-aware aggregation	Aggregator layout		I/O throttling & stepwise exchange
		Striping-aware	Round-robin	
original				
B	✓			
B,agg	✓	✓		
B,agg,rr	✓	✓	✓	
E,req={1,2,4,8}	✓			✓
E,agg,req={1,2,4,8}	✓	✓		✓
E,agg,rr,req={1,2,4,8}	✓	✓	✓	✓

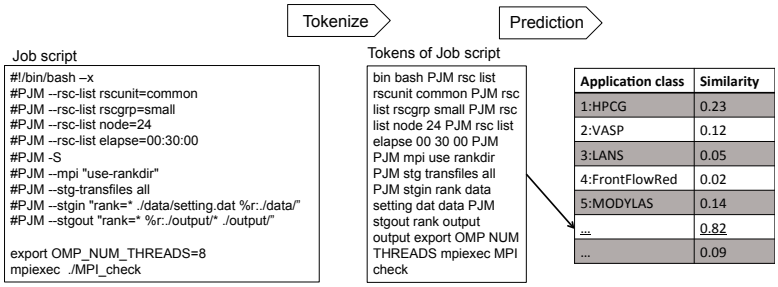

Figure 20.6: Overview of estimating application from job script

future. Evaluation of the EARTH with some I/O intensive applications is also our future work.

20.3.4 Log collection, analysis, and visualization

Continuing from the last fiscal year, we collected various log outputs from different servers in the database, and examined and implemented the visualization of data that will aid analysis. In FY2017, we introduced the database visualization tool "redash." With this tool, job performance information, billing-related information, and power consumption information can be easily analyzed. We also provide this tool to the user support desk.

20.3.5 Introduction of long-term jobs

In FY2016, because some users requested job execution exceeding 24 hours, we considered the introduction of long-term jobs up to 72 hours. We investigated the influence of this move on the waiting time of normal jobs and on node failure. In FY2017, we introduced this long-term job into actual operation. We analyzed the statistics of long-term job execution for one year and confirmed that it had almost no effect on normal jobs in the resource group "small" using the same area. Therefore, we will continue to look at the operation status and investigate optimization of various parameters next year.

20.3.6 Improvement of information provision to users

We provide operation information to users mainly via e-mails or user portal announcements. In addition to these, we implemented a mechanism that displays the latest information when logging in with ssh. The method of displaying the information of the user portal has also been improved. Information that requires itself to be displayed up to a specific date such as maintenance information can be continuously displayed on the higher level. The function of displaying the usage status of the node now provides information in two dimensions, but we are investigating whether it can be displayed in three dimensions.

20.3.7 Optimization of maintenance operations

We have a large-scale execution period once a month, and hardware maintenance is performed before the execution of large-scale jobs every time. Maintenance routinely lasts about 6 hours, depending on the content. By analyzing the maintenance content and optimizing the execution order, this time was reduced by about 1 hour.

20.3.8 Estimation of power consumed by jobs

Since FY2015, we have attempted to predict the jobs' power consumption. In FY2017, we studied job scheduling considering power consumption per job. According to the currently implemented method, the power consumption for each job is estimated at the time of the job submission. As shown in Figure 20.6, the submitted job script is analyzed, and we estimate its characteristics from information on the same job executed in the past. Thus, it is possible to specify the application with an accuracy of about 90% using job information actually executed on the K computer. In the future, we would like to improve the estimation method and perform job scheduling considering power consumption.

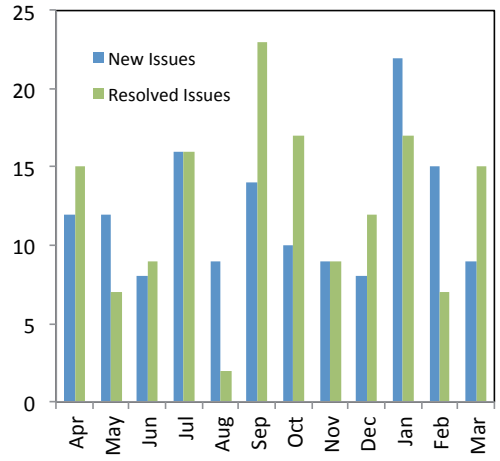

Figure 20.7: Number of issues addressed in FY2017

20.4 User Support

The K computer executed approximately 210 projects in FY2017. The number of active daily users was approximately 120. We supported users through the K support desk and provided them with technical information regarding the K computer, including information regarding its system environment, system tools, and software libraries. In addition, we performed user registrations, failures investigation, software installation, etc. We offered our consulting services together with the HPC Usability Development Team and Application Tuning Development Team. Figure 20.7 presents the number of issues addressed in FY2017, showing the number of new issues in FY2017 to be approximately 140. The number of resolved issues was approximately 150. The number of new issues in FY2016 was approximately 160.

20.5 Schedule and Future Plan

In this past fiscal year, we continued to analyze the operation situation and improve the operation from the previous year. Regarding power consumption, we investigated job scheduling considering the power consumption per job. We think that analyzing various logs and metrics from the system would allow for an early detection of the problem. To tackle a detection of problems before they become serious problems, we plan to continue the analyses of logs. Moreover, we will continue trying to improve the user environment and provide user support.

20.6 Publications

20.6.1 Articles

[1] Yuichi Tsujita, Tatsuhiko Yoshizaki, Keiji Yamamoto, Fumichika Sueyasu, Ryoji Miyazaki, and Atsuya Uno, "Alleviating I/O Interference Through Workload-Aware Striping and Load-Balancing on Parallel File Systems," Proceedings of ISC ' 17, Lecture Notes in Computer Science, Vol. 10266, pp. 315-333, Springer, 2017
[2] Yuichi Tsujita, Atsushi Hori, Toyohisa Kameyama, Atsuya Uno, Fumiyoshi Shoji, and Yutaka Ishikawa, "Improving Collective MPI-IO Using Topology-Aware Stepwise Data Aggregation with I/O Throttling," Proceedings of HPC Asia 2018, pp. 12-23, ACM, 2018

20.6.2 Oral Talks

[3] Yuichi Tsujita, "High Availability Operation of Parallel File Systems at the K computer," HPC-IODC 2017, June 22, 2017, Frankfurt, Germany
[4] Yuichi Tsujita, "Stable and Scalable Operation of Parallel File Systems at the K computer," Japan Lustre User Group 2017, November 2, 2017, Akihabara, Chiyoda-ku, Tokyo, Japan
[5] Atsuya Uno, "Approaches to the Power Consumption Problem on the K computer", SIAM Conference on Parallel Processing for Scientific Computing, March 7, 2018, Tokyo, Japan

20.6.3 Software

[6] EARTH on K (Version 1.1), AICS software

Chapter 21

Application Tuning Development Team

21.1 Members

Kazuo Minami (Team Head)

Akiyoshi Kuroda (Research & Development Scientist)

Kiyoshi Kumahata (Research & Development Scientist)

Kengo Miyamoto (Research & Development Scientist)

21.2 Research Activities

The application tuning development team has been conducting performance evaluation and enhancement aimed at popularizing the applications developed by the RIKEN Advanced Institute for Computational Science (AICS) research team (i.e., AICS software) from applications on the K computer. By improving and enhancing the software, we expect industries and communities that have not used the AICS software to start using it. Furthermore, along with above activities, we are also trying to systemize performance optimization technology. Improving application performance will lead to a shortening of the elapsed time, which makes it possible to use more computational resources. This will help in the more effective utilization of resources. We kept these factors in mind while carrying out the following tasks.

21.2.1 Enhancement of the AICS software

The AICS software was developed by the AICS research team. The use of this software leads not only to the effective utilization of the K computer, but it also contributes to the development of computational science. In the fiscal year (FY) 2017, we supported the enhancement of the AICS software. In this paper, we will describe the support activities performed on the AICS software GENESIS, NTChem, SCALE, OACIS, and EigenExa.

21.2.1.1 Enhancement of the AICS software (GENESIS)

GENESIS is a massively parallel molecular dynamics software developed by RIKEN AICS. This application has been provided for the analysis of biological phenomena such as drug discovery. GENESIS can also be used to investigate the dynamic properties of large molecules such as proteins. The molecular dynamics method is employed for calculations in this software. A number of functions, such as various force fields and acceleration algorithms, have been implemented, and we can calculate the general molecular dynamics method, replica exchange method, energy optimization, and so on.

To enhance the software functions, we supported the upgrade of the GENESIS code on the GPGPU machine that was published by cooperating with a software vendor. To obtain basic data for improving performance, we measured the profile data by using several GPGPU machines for the current GENESIS CUDA implementation. As a result of the analysis, variables using the asynchronous transfer were found therefore, all the variables allocated with pageable memory in GENESIS were changed to pinned memory. We also divided the communication task aimed at concealing the communication time and performed bitization of the mask array for interaction calculation aimed at reducing the communication data amount for transfer to the GPGPU. Another problem

remaining was that the bitization needed time because the SIMD operation was not used. However, the SIMD operation was applied by changing the algorithm; as a result, its duration could be shortened to approximately 60%. By shortening the communication and the bitization time for the mask array, this time could be hidden behind other calculation time. To conceal the communication time and reduce the communication data amount for transfer to the GPGPU, we divided the communication and performed bitization of the mask array used for calculating interactions. The speedup for making the pairlist procedure increased by 3 to 10 times, and the whole application improved approximately 20%, with these improvements.

In addition, further performance improvement was considered. In this program, there was no imbalance in the host processing; therefore, the entire host processes tried to reserve CUDA cores at the same time. This conflict about CUDA cores disturbed high-performance calculations. We propose that there is a possibility of performing high-performance calculation by making the imbalance host processing on conscious perception.

21.2.1.2 Enhancement of the AICS software (NTChem)

NTChem is the molecular chemistry software developed by RIKEN AICS. This application has been provided for the analysis of life science and material science, and it can be used for examining the electronic state of a material. The molecular orbital method and the density functional method are employed in this software. We implemented a number of functions such as the various basis functions and many algorithms for acceleration of calculation. This application is good for calculating the density functional theory including the relativistic effect.

To enhance the NTChem software, we performed the parallelization of linear response type time-dependent density functional method calculation section (KAIN method) by making calculations using memory without I/O (i.e., In-Core); we did this by cooperating with a software vendor. The data for the calculation of the KAIN method was treated by using I/O because of the memory limit until now. As a result of this improvement, we could reduce the I/O value to approximately 1/35, and the memory consumption could be suppressed approximately 30% more despite the In-Core. By these improvements, the elapsed time of the KAIN method was significant improved.

Furthermore, we also investigated other regions of the KAIN method. As a result, we found a possibility of performance improvement by changing the algorithm for the region of the four-center integral. In future studies, to improve parallel scalability, we need to perform a more detailed analysis.

21.2.1.3 Enhancement of the AICS software (SCALE)

Scalable Computing for Advanced Library and Environment (SCALE) is a basic library for the next generation research of weather and climate science. It was developed at RIKEN AICS. It has numerous functions that help in making weather and climate calculations. This includes processes management, I/O, dynamical calculations, and physical calculations. SCALE was developed to execute with high performance on a wide range of computers from small PC cluster to supercomputer.

For enhancing the software, the Application Tuning Development Team supported an improvement in which famous visualization tools, such as GrADS, NCView, and Paraview, would accept the parallel output files from SCALE. The contents of the improvement were mainly an expansion of the input file reading parts of those tools to obtain the ability of reading the NetCDF format distributed files from SCALE that was running in parallel. Each distributed file contains the calculated result of the decomposition domain.

For GrADS, it expanded the control file reading part. A new keyword of the control file was created. This specifies the numbers of the decomposition domain in two directions (east-west and south-north) and the file name basis of distributed files from SCALE. From giving numbers and file name basis, GrADS automatically read the distributed files to be read. After this modification, GrADS can visualize, such as contour, velocity vector, and so on, about multiple region calculated by domain decomposition method.

For NCView, it expanded a command line option reading part. Similar to the new keyword of the GrADS control file, the new option species the numbers of decomposition domains and the file name basis. NCView treats each file as a different time state of the same domain when inputting multiple files. Therefore, it was necessary to make modifications such that NCView would simultaneously treat the multiple files meant for different domain state of the same time. Therefore, we performed the modification.

For Paraview, there was a problem that was the lack of drawing of a common region the of neighboring domains (HALO region) because of the specifications of the distributed files from SCALE. Therefore, it was necessary to improve to draw the common region by interpolation. Since Paraview provides APIs for Python to

control the Paraview behavior, the Python script to realize this function was implemented instead of modifying the Paraview core.

These efforts were performed based on the budget about the AICS software center in cooperated with a software vendor.

21.2.1.4 Enhancement of the AICS software (OACIS)

Organizing Assistant for Comprehensive and Interactive Simulations (OACIS) is a tool that assists the exploring parameter space frequently during computer simulation. OACIS helps the user to control the parameter and input file generation corresponding to the given condition. It also helps to submit jobs and manage many results by a web interface it is easy to use. OACIS itself is not an application; it is a tool for the improving application convenience. Therefore, it is necessary to make an effort for several application areas to appeal the convenience by using OACIS.

In FY2017, the Application Tuning Development Team supported an improvement GUI of the web interface. In particular, the web structure modifying to improve the consistency of operation, database refinements to perform manage more parameter sets were performed. And, to improve usability when managing a lot of parameter sets, we performed the asynchronization of the communications between the web browser and the web server, the modification of the list view of the parameter sets, and filter functions that provided the search and select of the parameter sets corresponding to the specified conditions.

Furthermore, employing “boostwatch/yeti” as CSS that controls appearance of the web helped improved the visibility. Although it employed Rails4 as the framework, Rails5 was employed for the implementation of the web application.

These efforts were performed based on the budget about the AICS software center in cooperated with a software vendor.

21.2.1.5 Enhancement of the AICS software (EigenExa)

The EigenExa library is a high-performance eigenvalue solver developed by RIKEN AICS; it is a versatile diagonalization library with excellent parallel performance. This library has already been introduced in various applications that require diagonalization calculation such as material science and global environment. We have collected and evaluated the basic data in the large-scale simulation of the problem of diagonalization calculation used in the real-space density functional theory (RSDFT) program.

The size to be evaluated was 221,184 bases equivalent to the number of bands used in the RSDFT program. The maximum number of nodes was $96 \times 96 = 9,216$ processes, and the performance of each module in EigenExa was measured using various versions of EigenExa, process sizes, and process geometries. Our measurements showed that the elapsed time improved in speed up to 9,216 processes with the latest EigenExa for diagonalization of this matrix size. By comparing this elapsed time with the measurement at the time of receiving the Gordon-Bell Award in 2011, it was possible to improve the elapsed time to approximately 100 s from 283-380 s because of the tuning effect of the communication aggregation in the tridiagonalization module. In addition, we evaluated the case where EigenExa (9,216 processes) was called from the actual application RSDFT kernel. As a result, it was found that to change the data division format by using Basic Linear Algebra Communication Subprograms (BLACS) service routine requires a lot of time. Therefore, we thought it necessary for performance tuning of the method changing the data division format.

21.2.2 Activities for AICS software center

The activity is to publicize the functions and the usability of the software developed by AICS research teams for users and potential users of the K computer. In particular, as a survey about the web site of the AICS software center, two works were performed. One was the comparison of the functions of AICS software and other popular software. And another was the investigation of the providing information on the web site of the AICS software center.

For comparing the functions, each software was compared with other popular software in same field. The molecular dynamics software GENESIS was compared with GROMACS. The ab-initio quantum chemistry calculations software NTChem was compared with GAMESS. The library for weather and climate science SACLE was compared with WRF. And the job management assist tool OACIS was compared with HPC/PF.

For the investigation of the providing information web site, it was necessary to determine what information should be needed for offer. Therefore, we gathered information by performing typical tutorials of some software,

and surveyed the web site of the popular software such as OpenFOAM and ANSYS. The evaluated tutorials were GENESIS and NTChem from the AICS software and WRF from not AICS software. It clarified that it would be difficult for beginners to install additional software for data conversion, visualization, and so on. Based on our survey results, we proposed a model in which users were separated into three layers, (1) users who were still considering using the AICS software, (2) users who had already started using the AICS software, and (3) users who wanted use the AICS software extensively. This provides suitable information for each layer. Information that we provide for the first kind of users contains a purpose of the software, an overview of functions of the software, examples of calculations, an overview of accepted file types, and actual results on the K computer. This information would help the users easily determine whether or not this soft would be suitable for their use. Information the second category of users contains a list of all the functions, required external tools, and how to install them, and all of tutorials. This information enables to users to troubleshoot problems. Information provided to the third category of users contains a table that describe which functions the software could use simultaneously, tips for making correct calculation about user's problems, detailed information about the file format of the original file type of the software, and ways to add user's original functions. This information helps users who want to perform difficult calculations that cannot be performed by the expansion of tutorials. The above model has not been used for current AICS website for GENESIS, OACIS, and SCALE in deference to the developer's wishes. The pages of the software have not been change.

21.2.3 Survey for the systematization of application performance optimization technology

21.2.3.1 Analysis of published MPI performance data

In FY2017, we evaluated the validity of the performance of the major communication functions of the MPI library in the previous year. The performance of FY2015 has already been measured. The communication performance can be evaluated by using two parameters: the bandwidth and latency. The bandwidth becomes dominant for lengthy messages, and the latency becomes dominant in short messages. The bandwidth and latency can be calculated from the peak performance and the half-performance length of the measured throughput. The estimation formula of the communication time was derived theoretically from the model of communication behavior. Then we compared the communication bandwidth and latency with the estimated value obtained from the measured data in a wide range of message sizes. As a result, the communication bandwidth was up to approximately 20% different, and the latency was up to approximately 50% different, but the measurement results had the same trend as the estimation results [1][4].

21.3 Schedule and Future Plan

In FY2017, we evaluated the performance and enhanced the functions of applications (AICS software) developed by the AICS research team on the K computer. In the same year, we proposed new ideas for the AICS software to enhance its functions. In FY2018, we aim to realize these proposals for the enhancement of new functions. For NTChem, we will consider how to reduce the amount of computation required for four center integrals for integration with a high load by storing some necessary data on the disk. For SCALE, the characteristics of the physical process do not provide good performance although it has a number of calculations and its data are stored in cache memory. To solve this problem, we try to improve performance by the simultaneous calculation of loops of different characteristics for each thread. For OACIS, the expansion and dissemination of users is the main problem. To solve this problem, we plan to develop an environment in which users can easily try OACIS. In addition, we will expand the usage scene of OACIS such as include the measurement of scalability in performance evaluation at tuning and include resource management.

In the past, we proposed a model in which software kernels were classified into six types corresponding to the calculation characteristics such as busy time of cache, memory, and calculation unit. This model is useful for estimation and for improving performance. This model is based on the information from the precision PA function of Fujitsu. To use this model not only the K computer and FX100 but also for other architecture, such as ARM, Intel, GPU, and the Vector machine, it is necessary to investigate ways to obtain busy time similar to FX100. Therefore, we will expand this model to other architectures in our future studies.

21.4 Publications

21.4.1 Articles

[1] Y. Kitazawa, A. Kuroda, N. Shida, T. Adachi and K. Minami, “Evaluation of MPI Communication Performance Using Throughput on the K computer (in Japanese)”, IPSJ Transactions on Advanced Computing System, Vol.10 , No.3, pp1-11 (2017.11).

21.4.2 Invited Talks

[2] 南一生, ポスト「京」, 第 1 回 HPC ものづくり統合ワークショップ, (September 12, 2017).

[3] 熊畑清, スーパーコンピュータ「京」上での FrontFlow/blue の性能チューニング, 第 1 回 HPC ものづくり統合ワークショップ, (September 12, 2017).

21.4.3 Oral Talks

[4] Y. Kitazawa, A. Kuroda, N. Shida, T. Adachi and K. Minami, “Evaluation of MPI communication performance using throughput on the K computer (in Japanese)”, IPSJ High Performance Computing Symposium (IPSJ HPCS2017), Vol.2017, pp17-25, (Kobe, Jun. 5-6，2017).

[5] A. Kuroda, S. Inoue, R. Sekizawa and K. Minami, “Analysis of the Load of Local Meta Data Server Access from the Job I/O on the K computer (in Japanese)”, IPSJ SIG Technical Reports (SWoPP2017), Vol.2017-HPC-160, NO.27, pp.1-6 (Akita, July 26-28, 2017).

[6] A. Kuroda, S. Inoue, R. Sekizawa and K. Minami, “Analysis of the Load of Local Meta Data Server Access from the Job I/O on the K computer”, Academic eXchange for Information Environment and Strategy (AXIES2017), WC2-4, pp.1-8 (Hiroshima, Dec. 13-15, 2017).

[7] K. Minami, “Expectation to Supercomputer Benchmarks from the Viewpoint of Performance Optimization”, SIAM PP, pp.198 (Tokyo, March 7-10, 2018).

[8] K. Kumahata, Y. Yamade, C. Kato, K. Minami, “Performance improvement of the general-purpose CFD code FrontFlow/blue on the K computer”, HPC Asia 2018, pp.171-182 (Tokyo, Jan. 28-31, 2018)

21.4.4 Poster

[9] A. Kuroda, S. Inoue, K. Koyama, R. Sekizawa and K. Minami, “Analysis of the Load of Local Meta Data Server Access from the Job I/O on the K computerr (in Japanese)”, The 8th AICS International Symposium, P-28, p.31 (Kobe, Feb. 7-8, 2018).

21.4.5 Patents and Deliverables

[10] 下司雅章, 南一生, 高橋大介, 尾崎泰助, 安藤嘉倫, 小林正人, 成瀬彰, 黒澤一平, “計算科学のための HPC 技術 2”, 大阪大学出版会, 2017.

21.4.6 Software

None.

Chapter 22

HPC Usability Development Team

22.1 Members

Fumiyoshi Shoji (Team Leader)

Hiroshi Harada (Research & Development Scientist)

Shun Ito (Research & Development Scientist)

Masaaki Terai (Research & Development Scientist)

Jorji Nonaka (Research & Development Scientist)

Motoshiko Matsuda (Research & Development Scientist)

Tomohiro Kawanabe (Technical Staff)

22.2 Research Activities

The HPC Usability Development Team has newly started its activities this FY2017 and has aimed to improve the overall software environment of the K computer (hereinafter referred as "K-computer" or "K"). The team's mission covers a wide range of software-related topics in the K operational environment, and in this fiscal year, we mainly focused on the following topics: Installation and maintenance of some OSS (Open-Source Software); Preparation of a large data visualization environment; Seeking for some evidence-based operational issues via log-analysis technique; Development of a workflow management software; Preparation of a data analysis environment using the OpenStack virtualization technology. In addition, we also dedicated to a commissioned project funded by the MEXT (Ministry of Education, Culture, Sports, Science and Technology) by operating the HPCI shared storage, located in Kobe. Furthermore, we have other activities that have been conducted in collaboration with universities and research institutes, in various fields of science and technology (e.g., econophysics, software engineering, materials informatics), and what they have in common is the investigation and exploration on how to enhance the usability and to improve the productivity of the K environment.

The summary of our activities are listed below.

- In the K operational environment, the main software maintenance contractors (Fujitsu and Intel) have provided their proprietary compilers and numerical libraries, which are periodically updated to the latest version (at least once a year). On the other hand, most of the OSS installed on the K have not been maintained to provide the latest versions because of the costly update/upgrade process. Most of the OSS have been developed to the x86 architecture environment, while K employs the SPARC architecture, and as a result, a lot of time and effort are usually required in the install/update process on the K. In FY2017, trying to fulfill some of the software requests from the users, we selected thirty-three OSS for trying its installation on the K.
- Visualization has traditionally used a variety of hardware and software platforms, and as the size of the simulation results increases, the execution of the visualization processing in the HPC environment side

becomes attractive, since it can minimize the costly data movement problem. Therefore, we focused on preparing a large data visualization environment on the K by utilizing the PPS (Pre/Post processing Servers) as well as the K itself.

- In these past few years, the Operations and Computer Technologies Division has developed a logging database system that collects several operational and facility related logs and event information from the K environment. We have worked on this collected data sets seeking for valuable pieces of information, to serve as the feedback, in improving the operation.
- We have worked on a workflow management software, called WHEEL and developed by the Advanced Visualization Research Team, looking for more efficient use of the "Micro" class jobs on the K. In FY2017, we added some functionality to the WHEEL in order to efficiently perform capacity computing, and integrated with some production-level applications, ABINIT-MP and NTChem, for the initial test and evaluation.
- Data analysis has become an important topic in the field of HPC/Data Centers. However, the existing data analysis servers in the K environment are disproportionately small compared to the K compute nodes. The virtualization technology has matured, and can nowadays provide an ideal software environment for the users. Therefore, to accelerate the data analysis without compromising the usability, we have investigated an OpenStack-based virtualization technology for data analysis and planned to install an experimental cluster using the technology.
- In the commissioned project for the HPCI shared storage, we need to consider the collaboration between the K and other nationwide HPC facilities. In FY2017, we replaced the existing storage system to meet the ever-increasing user demands for storage capacity and to replace some of the aged systems in operation.

Although we have a wide variety of missions, our common objective is to improve the usability of K environment as well as of the HPCI shared storage. Under this main goal, we have investigated and explored new usage for the K, and for the HPCI storage, trying to embrace not only the traditional HPC users but especially new users from various other fields. In the rest of this section, we will detail these aforementioned research and development projects carried out in FY2017.

22.2.1 Installing/Updating some Open-Source Software

In the K operational environment, Fujitsu and Intel proprietary compilers are available to the users for building their optimized codes to be run on the K compute nodes (SPARC) and PPS (x86) respectively. These compilers along with some proprietary numerical libraries are maintained by the software vendors and are periodically updated (at least once a year). Unfortunately, Open-Source Software (OSS) on the K environment has not been maintained at the same pace, and most of them were rarely updated. This was because most of the OSS have been developed for the x86 architecture while K employs the SPARC architecture, and as a result, the install/update process usually requires a lot of time and effort. Sometimes the amount of required work may nearly be equal to a pure porting case.

Following some user requests, in FY2017, we selected thirty-three OSS for the install/update on the K operational environment. Most of the requests were for updating to newer versions, while some of them were for new installing, and it is worth noting that these requested OSS are not officially supported on the SPARC platform. Among the thirty-three OSS, we successfully installed/updated twenty OSS, and the complete list of these OSS, released for the users in FY2017, is shown in the Tab. 22.1. During this work, we prepared some patches that convert the original source codes, usually designed for the traditional x86 architecture, to the specific environment of K, and part of the developed patches were released via the AICS (currently R-CCS) official GitHub repository [9].

It is worth noting that during the porting work on the "HDF5" and "Boost", we faced some problems on the K system software, which were immediately reported to the developer (Fujitsu), and as a result, this work has unexpectedly contributed to bug fix and improving the K system software environment. Due to these non-planned things, the porting work took much time than expected and was not possible to finish in time, and we will continue to work on these OSS in the following fiscal year.

22.2.2 Large Data Visualization Environment

Visualization has been widely recognized as an important and powerful approach to explore and comprehend large and complex data produced from large-scale numerical simulations. As the size and complexity of these

Table 22.1: List of the newly installed/updated OSS in FY2017.

Name	Version	Hardware Environment	Utilized Compiler Suite
Chainer	3.0.0	K compute node	Fujitsu
NetCDF	C: 4.5.0 Fortran: 4.4.4 C++: 4.3.0	PPS (Pre/Post Server) node	GCC
Parallel-NetCDF	1.8.1	PPS (Pre/Post Server) node	GCC
HDF5	1.10.1	PPS (Pre/Post Server) node	GCC
FFTW	3.3.6-pl2	K compute node	Fujitsu
MUMPS	5.1.1	K compute node	Fujitsu
GSL	2.4	K compute node	Fujitsu
Lis (MPI)	2.0.6	K compute node	Fujitsu
Lis (Non-MPI)	2.0.6	K compute node	Fujitsu
Git	2.14.3	Login node	GCC
OpenMPI	3.0.0	PPS (Pre/Post Server) node	GCC
OpenMPI	3.0.0	PPS (Pre/Post Server) node	Intel
MPICH	3.2	PPS (Pre/Post Server) node	GCC
MPICH	3.2	PPS (Pre/Post Server) node	Intel
Python2.7	2.7.14	K compute node	Fujitsu
Python3	3.5.4	K compute node	Fujitsu
CMake	3.9.2	Login node	GCC
GCC	6.3.0	Login node (Cross compiler for K compute node)	GCC
GCC	6.3.0	K compute node	GCC
GCC	6.3.0	Login node	GCC

data sets increase, the execution of visualization processing in the HPC environment becomes attractive, since it can minimize the costly data movement problem when transferring to a remote site. In this FY2017, we focused on preparing a large data visualization environment on the K environment utilizing the PPS (Pre/Post processing Servers) as well as the K itself.

On the PPS side, we focused on providing a well-known general-purpose visualization application named ParaView. The hardware architecture of the PPS is based on Intel x86, and there is no GPU with hardware graphics acceleration capability. Therefore, in addition to the visualization application itself, there was a need to prepare an off-screen rendering environment via Mesa 3D graphics library. This work was done in strict combination with the OSS preparation and release taskforce since new OSS compilers, tools, and libraries were required. The Intel OpenSWR (Open Software Rasterizer for OpenGL) was built to take advantage of the Intel AVX available on the PPS. Although we could successfully install the ParaView on top of the OpenSWR, the most recent ray-tracing based rendering functionality was not able to be installed due to some software dependencies that were not possible to solve in time. We expect to work further on this issue to provide a fully capable visualization environment on the PPS.

On the K side, the main issue for providing a visualization environment was the lack of a fully functional Mesa 3D environment to enable the use of OpenGL based large data visualization applications directly on K. Currently, there exist four Mesa 3D drivers (swrast, softpipe, llvmpipe, swr), and excluding the swr driver, which has x86 hardware dependency, only three others can be used in K as shown in the Fig. 22.1. Among them, the "llvmpipe" driver is the most recent one and can use the GLSL (OpenGL Shading Language) code and multithreading function, but it requires the JIT (Just-in-Time) compiler function of the LLVM (Low-Level Virtual Machine) compiler suite. In this fiscal year, we could successfully prepare the "swrast" and "softpipe" drivers [2], thanks to the effort on providing more recent versions of the OSS compilers, tools, and libraries also for the K compute nodes. It is worth noting that although it was not possible to prepare in time, there is still an ongoing effort for providing the "llvmpipe" driver on the K compute node.

The Mesa 3D drivers just provide a graphics environment for enabling the use of OpenGL based visualization applications. Therefore, the next step will be to work on the main visualization tools and applications for enabling their use on the K environment. In this fiscal year, we have worked on the parallel PBVR (Particle-based Volume Rendering), over the Mesa 3D driver, in collaboration with Kobe University [8]. There is also another collaborative work with Kobe University, which uses some log data from the logging database system, for visual failure analysis [7]. The right side of the Fig. 22.1 shows an overview of the GUI prototype of this visual analysis system. We also have a collaborative work with the Federal University of Santa Catarina, in Brazil, focusing on the flexible data loading mechanism of simulation results via xDMlib, a data management library being developed at the Advanced Visualization Research Team [1].

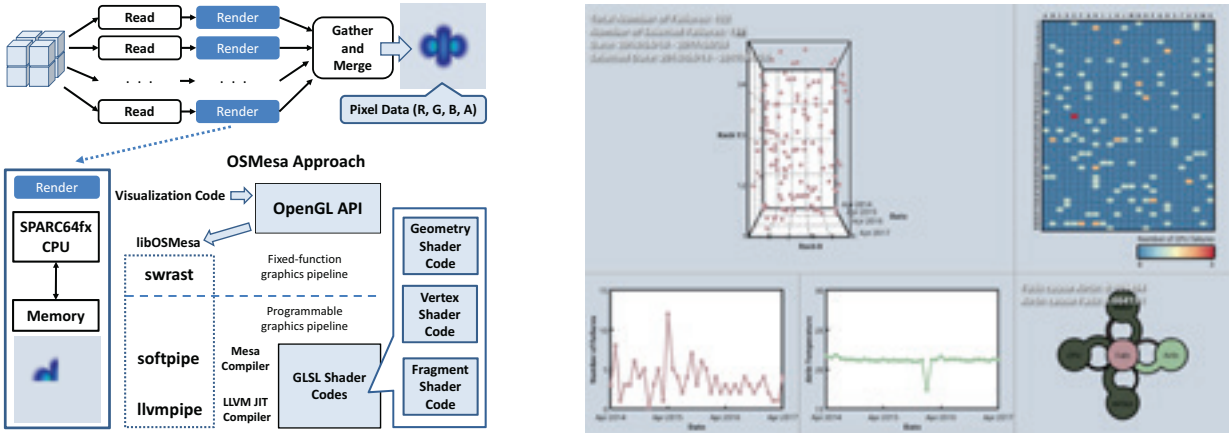

Figure 22.1: An overview of the Mesa 3D drivers for the K compute nodes, and a GUI prototype of the visual failure analysis using log data from the logging database system.

22.2.3 Development of a Job Retrieval System for Performance Improvement

In these past few years, the Operations and Computer Technologies Division has developed a logging database system that collects the logs and event information from some components of the K, and store them into the database system. Our team inherited this system, which employs the hardware counters of the SPARC64VIIIfx chip, and can achieve profiler-level accuracy without any additional overhead. Currently, other information, regarding jobs/workloads, has also been accumulated in the databases. However, this database system was not systematically designed, and most of the information has been stored in the databases as unorganized text files. Due to the database design, this system has caused some difficulties for cross-searching over databases.

In FY2017, the databases were aggregated in collaboration with the System Operations and Development Team. In addition, the system has new features to perform query-based job retrieval, and a handy visualization interface via web browser. To extract a user project which is required to check workload behavior in more detail, we developed a new feature on top of the new system. This feature is able to summarize the job performance information for each user project. Furthermore, to narrow down the result of the screening process and choose a candidate job that needs to improve the performance, we developed a feature to summarize performance information for each load-module in a single project. The development of these features was conducted in collaboration with the RIST (Research Organization for Information Science and Technology.) Eventually, our work has contributed to widening the user support service.

22.2.4 Workload Classification and Performance Analysis using Job Metrics

The job manager and the peripheral tools in the K environment collect various metrics for each job and store them into the databases. At the moment, this information has been accumulated and has reached more than nearly million jobs/workloads, which makes difficult to comprehend them at a glance. In FY2017, as an early study, to get the picture of workloads behavior with modern method, we classified the workloads using k-means clustering and DBSCAN (Density-Based Spatial Clustering of Applications with Noise) after a feature selection process with PCA (Principal Component Analysis) and some other statistical techniques as the pre-processing. Furthermore, we have analyzed their performance characteristics on a group-by-group basis. Base on the nearly million records in the original database, we found some candidates to be checked in more detail, regarding arithmetic, memory access, and I/O intensiveness. In addition to those, to verify the metrics behavior, we compared the metrics with typical HPC benchmarks. Part of the results was reported in [3] and [4]. Also, this work was conducted under the internship program contracted with the University of Hyogo.

22.2.5 Workflow Management Software (WHEEL)

In the fields of drug discovery and material research, there is an increasing demand for so-called capacity computing, which involves massively executing small- and medium-scale analytical calculations simultaneously for searching for candidate substances. By using the workflow management software called WHEEL, which

has been developed by the Advanced Visualization Research Team, the execution of parameter survey can be automated facilitating the capacity computing. In FY2017, to efficiently perform the capacity computing, we added some functionality to the WHEEL, and prepared some practical examples of capacity computing, using the "Micro" class jobs of the K-computer, for the following production-level applications.

ABINIT-MP
ABINIT-MP is an application for quantum chemical calculation based on the FMO (Fragment Molecular Orbital) method. We created an example workflow of capacity computing that calculates the interaction parameter between fragments of 3 types of combination of the molecule as hexane-hexane, hexane-nitrobenzene, and nitrobenzene-nitrobenzene. For the practical use, there is a need to calculate using several thousand cases of each combination, but for evaluating the newly added functionality, we evaluated by calculating 300 cases for each combination and confirmed that this size of the workflow can successfully be automated.

NTChem
NTChem is an application for molecular science simulation. We created an example workflow of capacity computing that calculates 300 samples, which were selected from trajectories of water molecules obtained by classical molecular dynamics method, and energy gradients and physical property values were calculated using NTChem.

In addition, to verify that this approach can be applied to fluid analysis, we also created some examples for small parameter studies using OpenFOAM, and summarized its procedure and the obtained result in the tutorial document released to the users.

22.2.6 Data Analysis Server using Virtualization Technology

To enhance the data processing and visualization feature on the K, there exist subsidiary x86-based data-analysis servers, known as PPS (Pre/Post processing Servers), where the users are allowed to submit jobs using larger memory and longer duration than compared to those allowed on the K. It is well-known that most of the OSS are developed for the x86 architecture. Therefore, the data analysis servers employ the x86 architecture instead of the SPARC architecture to facilitate the installation and use of OSS. Meanwhile, even though data analysis is one of the significant topics in HPC/Data Centers, these data analysis servers have small scale compared to the K compute nodes. To accelerate the data analysis, the strengthening of the hardware and software resources was readily required.

In terms of the usability, modern analysis environments have been used various OSS tools and libraries to quickly assemble their customized environment. It is worth noting that the versions of the tools and libraries are one of the important conditions for the reproducibility. However, it is widely known that most of the OSS are frequently updated, thus the analysis environment should ideally be created independently for each of the users, and allow the users to fully control the versions in the software stack. Unfortunately, traditional HPC environment did not provide such kind of flexibility to the users.

Nowadays, the virtualization technology, such as the OpenStack framework, has matured and can provide an ideal software environment for the users. The users are allowed to install and uninstall any software on their own virtualized environment, including not only the OSS but also the operating system they want to use. In addition, the users can generate an image of the virtualized server for sharing with their community. In this FY2017, we conducted a procurement process for a new data analysis system, with the OpenStack framework, in order to enhance the data analysis capability on the K environment.

22.2.7 HPCI Shared Storage

In FY2017, we introduced a new storage system to overcome two main problems: the ever-increasing user demands for storage capacity and the aging of our existing facility. We initially installed six new login nodes at the beginning of August. As shown in the Fig. 22.2, half of the login nodes are connected to the global file system of the K. Once a user starts to exchange the data between the K and the HPCI shared storage, all the login nodes will start the service. In the same month, we also installed other hardware devices: Two meta-data servers; three storage controllers; four management nodes; some management network switches; and some backbone network switches. After some operational tests, involving the practical use, all equipment of this new the HPCI shared storage system has become operational on Oct. 12. After that, an additional eight storage controllers were installed at the end of the month, and a new 51PB storage system was finally started its

operation on Jan. 17. We have also installed a 7.6PB high-performance storage system as the primary storage on the RIKEN AICS side.

During the replacement of the storage system, we transferred the user data from the existing storage to the new storage. The data transferring has done by using the automatic data replication function provided by the Gfarm. Furthermore, to enhance the robustness of the user data, we also implemented a disaster recovery feature. As a result, the new storage system automatically duplicates the user data between two sites, that is, RIKEN AICS and the University of Tokyo. On Feb. 17, we completed to carry out the data synchronization without interrupting (shutting down) the service.

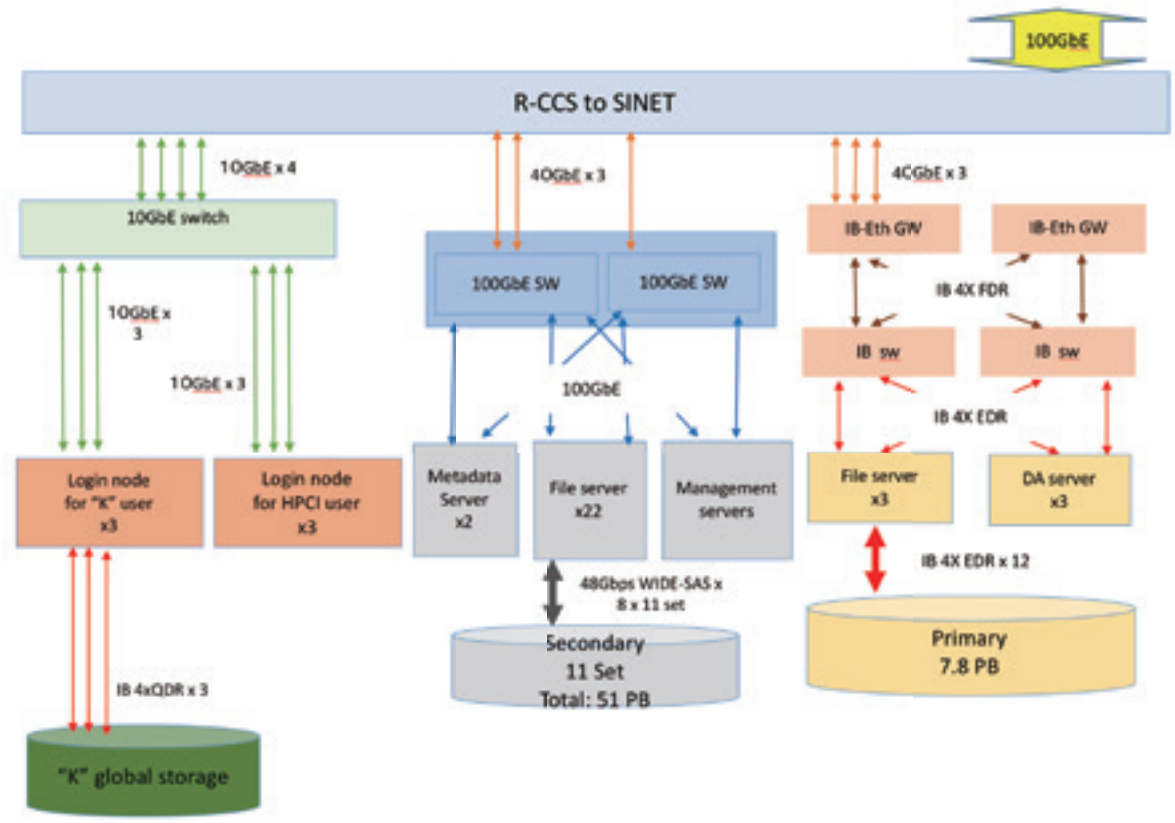

Figure 22.2: An overview of the new HPCI shared storage system.

22.2.8 Other Activities

In addition to those activities detailed in the previous section, we also contributed to the following projects, which produced some publications:

- Graph-based Economic Simulation under the Exploratory Challenges on Post-K computer (Studies of Multi-level Spatiotemporal Simulation of Socioeconomic Phenomena, Macroeconomic Simulations)[3]
- Evidenced-based Performance Tuning in collaboration with the Software Technology and Artificial Intelligence Research Laboratory (STAIR), the Chiba Institute of Technology[6,10]
- Materials informatics using the micro resource group in collaboration with the National Institute for Materials Science

22.3 Schedule and Future Plan

In FY2017, we worked on a variety of projects, mainly focusing on the improvements of the software environment of the K, and on maximizing the utilization of the K computing resources via “Micro” resource group. We also

dedicated to the commissioned project funded by MEXT by operating the HPCI shared storage, located in Kobe. Our team has newly started its activities this fiscal year, and most of the research/development projects are still at an early stage. In the next fiscal year, we are planning to continue working on these projects by continuously striving to improve the usability of the K environment as well as the HPCI shared storage system. In addition, we will continue trying our best to investigate and explore new usages for both facilities seeking not the traditional HPC users, but especially the potential new users from different fields.

22.4 Publications

22.4.1 Articles

[1] Jorji Nonaka, Eduardo Camilo Inacio, Kenji Ono, Mario Antonio Ribeiro Dantas, Yasuhiro Kawashima, Tomohiro Kawanabe, Fumiyoshi Shoji, "Data I/O Management Approach for the Post-hoc Visualization of Big Simulation Data Results," International Journal of Modeling, Simulation, and Scientific Computing, https://doi.org/10.1142/S1793962318400068 (Onlilne Ready).

22.4.2 Oral Talks

[2] Jorji Nonaka, Motohiko Matsuda, Takashi Shimizu, Naohisa Sakamoto, Masahiro Fujita, Keiji Onishi, Eduardo C. Inacio, Shun Ito, Fumiyoshi Shoji, and Kenji Ono, "A Study on Open Source Software for Large-Scale Data Visualization on SPARC64fx based HPC Systems," International Conference on High Performance Computing in Asia-Pacific Region (HPC Asia 2018), Tokyo, Japan, pp. 278-288, (2018).
[3] Yoshiyuki Arata, Abhijit Chakraborty, Yoshi Fujiwara, Hiroyasu Inoue, Hazem Krichene, Masaaki Terai, "Shock Propagation through Customer-Supplier Relationships: An Application of the Stochastic Actor-Oriented Model," The 6th International Conference on Complex Networks and Their Applications (Complex Network 2017), Studies in Computational Intelligence (Springer), 689, pp. 1100-1110, https://doi.org/10.1007/978-3-319-72150-7_89, (2017).
[4] Masaaki Terai, Riku Kashiwaki, Fumiyoshi Shoji, "Workload Classification and Performance Analysis using Job Metrics in the K computer," IPSJ, HPC-162, (2017).

22.4.3 Posters

[5] Masaaki Terai, Riku Kashiwaki, Fumiyoshi Shoji, "Performance Classification of the K-Computer Workloads using Hierarchical Clustering and K-Means," HPC Asia 2018, (2018).
[6] Masatomo Hashimoto, Masaaki Terai, Toshiyuki Maeda, Kazuo Minami, "CCA/EBT: Code Comprehension Assistance Tool for Evidence-Based Performance Tuning," HPC Asia 2018, (2018).
[7] Kazuki Koiso, Naohisa Sakamoto, Jorji Nonaka, Fumiyoshi Shoji, "Development of a Visual System for Failure Analysis using HPC Log Data (Poster)," *VSJ (Visualization Society of Japan) 1st Visualization Workshop*, Yokohama, Japan (2018).
[8] Yoshiaki Yamaoka, Kengo Hayashi, Naohisa Sakamoto, Jorji Nonaka, "Parallel Particle Based Volume Rendering using 234Compositor (Poster)," *VSJ (Visualization Society of Japan) 1st Visualization Workshop*, Yokohama, Japan (2018).

22.4.4 Software

[9] The Official GitHub Repository for RIKEN AICS OSS (AICS was reorganized in FY2018, and renamed as R-CCS), https://github.com/RIKEN-RCCS/.
[10] CCA/EBT: Code Comprehension Assistance for Evidence-Based Performance Tuning, https://github.com/ebt-hpc/cca.

Part III

Flagship 2020 Project

Chapter 23

Flagship 2020 Project

23.1 Members

Primary members are only listed.

23.1.1 System Software Development Team

Yutaka Ishikawa (Team Leader)

Masamichi Takagi (Senior Scientist)

Atsushi Hori (Research Scientist)

Balazs Gerofi (Research Scientist)

Masayuki Hatanaka (Research & Development Scientist)

Takahiro Ogura (Research & Development Scientist)

Tatiana Martsinkevich (Postdoctoral Researcher)

Fumiyoshi Shoji (Research & Development Scientist)

Atsuya Uno (Research & Development Scientist)

Toshiyuki Tsukamoto (Research & Development Scientist)

23.1.2 Architecture Development

Mitsuhisa Sato (Team Leader)

Yuetsu Kodama (Senior Scientist)

Miwako Tsuji (Research Scientist)

Jinpil Lee (Postdoctoral Researcher)

Tetsuya Odajima (Postdoctoral Researcher)

Hitoshi Murai (Research Scientist)

Toshiyuki Imamura (Research Scientist)

Kentaro Sano (Research Scientist)

23.1.3 Application Development

Hirofumi Tomita (Team Leader)

Yoshifumi Nakamura (Research Scientist)

Hisashi Yashiro (Research Scientist)

Seiya Nishizawa (Research Scientist)

Yukio Kawashima (Research Scientist)

Soichiro Suzuki (Research & Development Scientist)

Kazunori Mikami (Research & Development Scientist)

Kiyoshi Kumahata (Research & Development Scientist)

Kengo Miyamoto (Research & Development Scientist)

Mamiko Hata (Technical Staff I)

Kazuto Ando (Technical Staff I)

Hiroshi Ueda (Research Scientist)

Naoki Yoshioka (Research Scientist)

Yiyu Tan (Research Scientist)

23.1.4 Co-Design

Junichiro Makino (Team Leader)

Keigo Nitadori (Research Scientist)

Yutaka Maruyama (Research Scientist)

Masaki Iwasawa (Research Scientist)

Takayuki Muranushi (Postdoctoral Researcher)

Daisuke Namekata (Postdoctoral Researcher)

Long Wang (Postdoctoral Researcher)

Kentaro Nomura (Research Associate)

Miyuki Tsubouchi (Technical Staff)

23.2 Project Overview

The Japanese government launched the FLAGPSHIP 2020 project [1] in FY 2014 whose missions are defined as follows:

- Building the Japanese national flagship supercomputer, the successor to the K computer, which is tentatively named the post K computer, and
- developing wide range of HPC applications that will run on the post K computer in order to solve the pressing societal and scientific issues facing our country.

Table 23.1: Development Teams

Team Name	Team Leader
Architecture Development	Mitsuhisa Sato
System Software Development	Yutaka Ishikawa
Co-Design	Junichiro Makino
Application Development	Hirofumi Tomita

RIKEN is in charge of co-design of the post K computer and development of application codes in collaboration with the Priority Issue institutes selected by Japanese government, as well as research aimed at facilitating the efficient utilization of the post K computer by a broad community of users. Under the co-design concept, RIKEN and the selected institutions are expected to collaborate closely.

As shown in Table 23.1, four development teams are working on post K computer system development with the FLAGSHIP 2020 Planning and Coordination Office that supports development activities. The primary members are listed in Section 23.1.

The Architecture Development team designs the architecture of the post K computer in cooperation with Fujitsu and designs and develops a productive programming language, called XcalableMP (XMP), and its tuning tools. The team also specifies requirements of standard languages such as Fortran and C/C++ and mathematical libraries provided by Fujitsu.

The System Software Development team designs and specifies a system software stack such as Linux, MPI and File I/O middleware for the post K computer in cooperation with Fujitsu and designs and develops multi-kernel for manycore architectures, Linux with light-weight kernel (McKernel), that provides a noise-less runtime environment, extendability and adaptability for future application demands. The team also designs and develops a low-level communication layer to provide scalable, efficient and portability for runtime libraries and applications.

The Co-Design team leads to optimize architectural features and application codes together in cooperation with RIKEN teams and Fujitsu. It also designs and develops an application framework, FDPS (Framework for Developing Particle Simulator), to help HPC users implement advanced algorithms.

The Application Development team is a representative of nine institutions aimed at solving Priority Issues. The team figures out weakness of target application codes in terms of performance and utilization of hardware resources and discusses them with RIKEN teams and Fujitsu to find out best solutions of architectural features and improvement of application codes. Published papers, presentation and posters are summerized in the final subsecton in this chapter.

23.3 Target of System Development and Achievements in FY2017

The post K's design targets are as follows:

- A one hundred times speed improvement over the K computer is achieved in maximum case of some target applications. This will be accomplished through co-design of system development and target applications for the nine Priority Issues.
- The maximum electric power consumption should be between 30 and 40 MW.

In FY2016, the second phase of the detailed design was completed. The major components of system software are summarized as follows:

- Highly productive programming language, XcalableMP
  XcalableMP (XMP) is a directive-based PGAS language for large scale distributed memory systems that combines HPF-like concept and OpenMP-like description with directives. Two memory models are supported: global view and local view. The global view is supported by the PGAS feature, i.e., large array is distributed to partial ones in nodes. The local view is provided by MPI-like + Coarray notation. In 2017, we finished the front-end for Fortran 2008 Standard for Omni XcalableMP compiler, and are still working on C++ Front-end based on LLVM clang. We are currently working on XcalableMP 2.0 which newly supports task-parallelism and the integration of PGAS models for distributed memory environment.

[1]FLAGSHIP is an acronym for Future LAtency core-based General-purpose Supercomputer with HIgh Productivity.

- Domain specific library/language, FDPS
  FDPS is a framework for the development of massively parallel particle simulations. Users only need to program particle interactions and do not need to parallelize the code using the MPI library. The FDPS adopts highly optimized communication algorithms and its scalability has been confirmed using the K computer.

- MPI + OpenMP programming environment
  The current de facto standard programming environment, i.e., MPI + OpenMP environment, is supported. Two MPI implementations are being developed. Fujitsu continues to support own MPI implementation based on the OpenMPI. RIKEN is collaborating with ANL (Argonne National Laboratory) to develop MPICH, mainly developed at ANL, for post K computer. Achievements of our MPI implementation have been described in Section 1.3.1.

- New file I/O middleware
  The post K computer does not employ the file staging technology for the layered storage system. The users do not need to specify which files must be staging-in and staging-out in their job scripts in the post K computer environment. The LLIO midleware, employing asynchronous I/O and caching technologies, has been being designed by Fujitsu in order to provide transparent file access with better performance. The implementation of LLIO started in FY2017 and will be completed in FY2018.

- Application-oriented file I/O middleware
  In scientific Big-Data applications, such as real-time weather prediction using observed meteorological data, a rapid data transfer mechanism between two jobs, ensemble simulations and data assimilation, is required to meet their deadlines. In FY2016, a framework called Data Transfer Framework (DTF), based on PnetCDF file I/O library, that silently replaces file I/O with sending the data directly from one component to another over network was designed and its prototype system was implemented and evaluated. The detailed achievement has been described in Section 1.3.2.

- Process-in-Process
  "Process-in-Process" or "PiP" in short is a user-level runtime system for sharing an address space among processes. Unlike the Linux process model, a group of processes shares the address space and thus the process context switch among those processes does not involve hardware TLB flushing. It was implemented in FY2016, and its applicability to a communication mechanism has been tested. The detailed achievement has been described in Section 1.3.3.

- Multi-Kernel for manycore architectures
  Multi-Kernel, Linux with light-weight Kernel (McKernel) is being designed and implemented. It provides: i) a noiseless execution environment for bulk-synchronous applications, ii) ability to easily adapt to new/future system architectures, e.g., manycore CPUs, a new process/thread management, a memory management, heterogeneous core architectures, deep memory hierarchy, etc., and iii) ability to adapt to new/future application demands, such as Big-Data and in-situ applications that require optimization of data movement. In FY2016, McKernel was improved for NUMA CPU architectures. The detailed improvements have been described in Section 1.3.4.

It should be noted that these components are not only for post K computer, but also for other manycore-based supercomputer, such as Intel Xeon Phi.

The architecture development team is also working on the researches on co-design tools as well as the design of the post K supercomputer:

GEM5 processor simulator for the post-K processor
We are developing a cycle-level processor simulator for the Post-K processor based on GEM-5, which is a general-purpose processor simulator commonly used for the processor architecture research. ARM provided us the source code of GEM-5 Atomic-model processor simulator for ARM v8 with Scalable Vector Extension (SVE). The Atomic model enables an instruction-level simulation. We deployed and tested it, and extend it for the cycle-level Out-Of-Order(O3) model processor simulator with the post-K hardware parameters. It enables the cycle-level performance evaluation of application kernels. Currently, we are working on the adjustment of parameters and performance with Fujitsu-in-house processor simulator for more accurate performance evaluation. In 2017, we started the service to provide "post-K performance

evaluation environment" including this simulator for performance evaluation and tuning by potential post-K users. And, we presented the preliminary study on the performance of multiple vector lengths by SVE vector-length agnostic feature [2].

Performance estimation tools for co-design study
We have tools for co-design study for future huge-scale parallel systems. The MPI application replay tool is a system to investigate a performance and behavior of parallel applications on a single node using MPI traces. SCAMP (SCAlable Mpi Profiler) is other system to simulate a large scale network from a small number of profiling results.

Study on performance metrics
We have been developing a new metric, called Simplified Sustained System Performance (SSSP) metric, based on a suite of simple benchmarks, which enables performance projection that correlates with applications. In 2017, we presented the preliminary results in the conference [3].

In addition to co-design tools, we are working on the evaluation of compilers for ARM SVE. There are two kinds of compiler for ARM SVE: Fujitsu Compiler and ARM compiler. The Fujitsu compiler is a proprietary compiler supporting C/C++ and Fortran. The ARM compiler is developed by ARM based on LLVM. Initially, LLVM only supports C and C++, and supports Fortran recently by flang. We are evaluating the quality of code generated by both of the compilers with collaboration of Kyoto University. Since these compilers are still immature, we give several feedbacks by examining the generated code. And our team is carrying out several collaborations with ARM compiler team on LLVM. In 2017, we have proposed the extension of OpenMP SIMD directive for SVE in the collaboration with Arm's researchers [4].

23.4 International Collaborations

23.4.1 DOE/MEXT Collaboration

The following research topics were performed under the DOE/MEXT collaboration MOU.

- Optimized Memory Management
  This research collaboration explores OS supports for deep memory hierarchies. In FY2016, the movepages system call was parallelized in McKernel and its applicability for a manycore processor with two memory hierarchies, KNL, was evaluated using a simple stencil code.

- Efficient MPI for exascale
  In this research collaboration, the next version of MPICH MPI implementation, mainly developed by Argonne National Laboratory (ANL), has been cooperatively developed. The FY2016 achievements have been described in the previous section.

- Dynamic Execution Runtime
  This research collaboration shares designs for asynchronous and dynamic runtime systems. In FY2016,

- Metadata and active storage
  This research collaboration, run by the University of Tsukuba as contract, studies metadata management and active storage.

- Storage as a Service
  This research collaboration explores APIs for delivering specific storage service models. This is also run by the University of Tsukuba.

- Parallel I/O Libraries
  This research collaboration is to improve parallel netCDF I/O software for extreme-scale computing facilities at both DOE and MEXT. To do that, the RIKEN side has designed DTF as described in the previous section.

- OpenMP/XMP Runtime
  This research collaboration explores interaction of Argobots/MPI with XscalableMP and PGAS models.

Figure 23.1: Schedule

- Exascale co-design and performance modeling tools
  This collaborates on an application performance modeling tools for extreme-scale applications, and shared catalog of US/JP mini-apps.
- LLVM for vectorization
  This research collaboration explores compiler techniques for vectorization on LLVM.
- Power Monitoring and Control, and Power Steering
  This research collaboration explores APIs for monitoring, analyzing, and managing power from the node to the global machine, and power steering techniques for over-provisioned systems are evaluated.

23.4.2 CEA

RIKEN and CEA, Commissariat *à* l'*é*nergie atomique et aux *é*nergies alternatives, signed MOU in the fields of computational science and computer science concerning high performance computing and computational science in January 2017. The following collaboration topics are now taken into account:

- Programming Language Environment
- Runtime Environment
- Energy-aware batch job scheduler
- Large DFT calculations and QM/MM
- Application of High Performance Computing to Earthquake Related Issues of Nuclear Power Plant Facilities
- Key Performance Indicators (KPIs)
- Human Resource and Training

23.5 Schedule and Future Plan

As shown in Figure 23.1, the design and prototype implementations will be done before the end of 2019, and the system will be deployed after this phase. The service is expected to start public operation at the range from 2021 to 2022.

23.6 Publications

23.6.1 presentation and poster

[1] Hisashi Yashiro, Koji Terasaki, Takemasa Miyoshi, and Hirofumi Tomita: "Towards an extreme scale global data assimilation on the post-K supercomputer: development of a throughput-aware framework for ensemble data assimilation", The 1st JpGU-AGU joint meeting, Makuhari, Japan, May 2017.

[2] Hisashi Yashiro: "Recent Extreme-Scale Simulation Efforts for NICAM in BoF "Cloud Resolving Global Earth-System Models: HPC at its Extreme" ISC High Performance 2017. Frankfurt, Germany, Jun. 2017.
[3] Yoshifumi Nakamura, Y. Kuramashi, S. Takeda: "Critical endline of the finite temperature phase transition for $2+1$ flavor QCD away from the SU(3)-flavor symmetric point" Lattice 2017, Granada, Spain, Jun. 2017.
[4] Yoshifumi Nakamura: "Lattice QCD with pseudo-fermionparallelization" 7th JLESC Workshop, Urbana, USA, Jul. 2017.
[5] Yukio Kawashima: "Toward path integral molecular dynamics simulation of biomolecules" 3rd Japan-Thai workshop on Theoretical and Computational Chemistry 2017, Yokohama, Japan, Jul. 2017.
[6] Kiyoshi Kumahata, Kazuo Minami, Yoshinobu Yamade, Chisachi Kato: "Performance improvement of the general-purpose CFD code FrontFlow/blue on the K computer" HPC Asia 2018, Tokyo, Japan, Jan. 2018.
[7] Y. Nakamura: "Investigating Columbia plot with clover fermions" XQCD 2017, Pisa, Italy, Jun. 2017.
[8] Y. Kawashima, K. Hirao: "Long-Range Corrected Density Functional Theory with Periodic Boundary Condition", The 11th Annual Meeting of Japan Society for Molecular Science, Sendai, Japan, Sep. 2017.

23.6.2 Articles and Technical Paper

[1] Y. Kawashima, K. Hirao: ""Singularity Correction for Long-Range-Corrected Density Functional Theory with Plane-Wave Basis Sets" The Journal of Physical Chemistry A, Vol. 121, No. 9, P. 2035-2045, 2017
[2] Yuetsu Kodama, Tetsuya Odajima, Motohiko Matsuda, Miwako Tsuji, Jinpil Lee, Mitsuhisa Sato. "Preliminary Performance Evaluation of Application Kernels using ARM SVE with Multiple Vector Lengths," Re-Emergence of Vector Architectures Workshop (Rev-A), HI, USA, Sep. 2017.
[3] Miwako Tsuji, William Kramer, Mitsuhisa Sato. "A Performance Projection of mini-Applications onto Benchmarks toward the Performance Projection of real-Applications," Workshop on Representative Applications (WRAp), HI, USA, Sep. 2017.
[4] Jinpil Lee, Francesco Petrogalli, Graham Hunter, Mitsuhisa Sato. "Extending OpenMP SIMD support for target specific code and application to ARM SVE," 13th International Workshop on OpenMP, NY, USA, Sep. 2017.

RIKEN
Center for
Computational Science

RIKEN Center for Computational Science

ANNUAL REPORT

FY2017

7-1-26, Minatojima-minami-machi, Chuo-ku, Kobe, Hyogo 650-0047 Japan

https://www.r-ccs.riken.jp/en/

RIKEN 2018-076